

A CHARACTERIZATION OF THE IMPACT OF CLOUDS ON  
REMOTELY SENSED WATER QUALITY

by

Ronald R. Fairbanks

A dissertation submitted in partial fulfillment of the  
requirements for the degree of Ph.D. in the Chester F. Carlson  
Center for Imaging Science, College of Science, Rochester  
Institute of Technology

July 1999

Signature of Author Ronald R. Fairbanks

Accepted by Henry E. Rhoady 24 Aug 99  
Coordinator, Ph.D. Degree Program Date

CHESTER R. CARLSON  
CENTER FOR IMAGING SCIENCE  
COLLEGE OF SCIENCE  
ROCHESTER INSTITUTE OF TECHNOLOGY  
ROCHESTER, NEW YORK

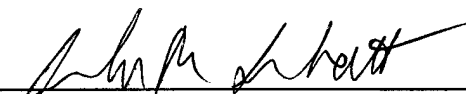
CERTIFICATE OF APPROVAL

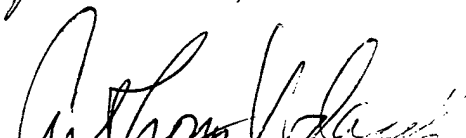
---

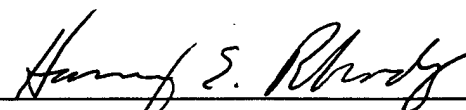
Ph. D. DEGREE DISSERTATION

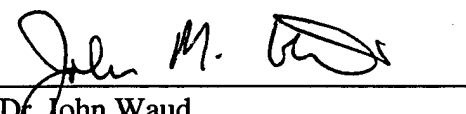
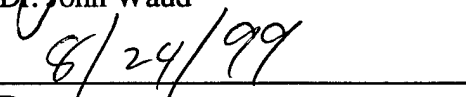
---

The Ph.D. Degree Dissertation of Ronald R. Fairbanks  
has been examined and approved by the  
dissertation committee as satisfactory for the  
dissertation requirement for the  
Ph.D. degree in Imaging Science

  
Dr. John R. Schott, Thesis Advisor

  
Dr. Anthony Vodacek

  
Dr. Harvey Rhody

  
Dr. John Waud  
  
Date

DISSERTATION RELEASE PERMISSION  
ROCHESTER INSTITUTE OF TECHNOLOGY  
COLLEGE OF SCIENCE  
CHESTER F. CARLSON CENTER FOR IMAGING SCIENCE

Title of Dissertation: A Characterization of the impact of clouds on remotely sensed water quality

I, Ronald R. Fairbanks, hereby grant permission to the Wallace Memorial Library at R.I.T. to reproduce my thesis in whole or in part. Any reproduction will not be for commercial use or profit.

Signature: Ronald R Fairbanks

Date: 24 August 1999

REPORT DOCUMENTATION PAGE			Form Approved OMB No. 0704-0188	
Public reporting burden for this collection of information is estimated to average 1 hour per response, including the time for reviewing instructions, searching existing data sources, gathering and maintaining the data needed, and completing and reviewing the collection of information. Send comments regarding this burden estimate or any other aspect of this collection of information, including suggestions for reducing this burden, to Washington Headquarters Services, Directorate for Information Operations and Reports, 1215 Jefferson Davis Highway, Suite 1204, Arlington, VA 22202-4302, and to the Office of Management and Budget, Paperwork Reduction Project (0704-0188), Washington, DC 20503.				
1. AGENCY USE ONLY (Leave blank)	2. REPORT DATE 17.Sep.99	3. REPORT TYPE AND DATES COVERED DISSERTATION		
4. TITLE AND SUBTITLE A CHARACTERIZATION OF THE IMPACT OF CLOUDS ON REMOTELY SENSED WATER QUALITY		5. FUNDING NUMBERS		
6. AUTHOR(S) MAJ FAIRBANKS RONALD R				
7. PERFORMING ORGANIZATION NAME(S) AND ADDRESS(ES) RÖCHESTER INSTITUTE OF TECHNOLOGY		8. PERFORMING ORGANIZATION REPORT NUMBER		
9. SPONSORING/MONITORING AGENCY NAME(S) AND ADDRESS(ES) THE DEPARTMENT OF THE AIR FORCE AFIT/CIA, BLDG 125 2950 P STREET WPAFB OH 45433		10. SPONSORING/MONITORING AGENCY REPORT NUMBER  FY99-296		
11. SUPPLEMENTARY NOTES				
12a. DISTRIBUTION AVAILABILITY STATEMENT Unlimited distribution In Accordance With AFI 35-205/AFIT Sup 1		12b. DISTRIBUTION CODE		
13. ABSTRACT (Maximum 200 words)		<b>DISTRIBUTION STATEMENT A</b> Approved for Public Release Distribution Unlimited		
14. SUBJECT TERMS		15. NUMBER OF PAGES 236		
		16. PRICE CODE		
17. SECURITY CLASSIFICATION OF REPORT	18. SECURITY CLASSIFICATION OF THIS PAGE	19. SECURITY CLASSIFICATION OF ABSTRACT	20. LIMITATION OF ABSTRACT	



Date 25 July 1999

Rochester Institute of Technology

Abstract

A CHARACTERIZATION OF THE IMPACT OF  
CLOUDS ON REMOTELY SENSED WATER QUALITY

by Ronald R. Fairbanks

Atmospheric correction and subsequent chlorophyll detection algorithms via remote sensing means were designed for use over the world's oceans. The algorithms seem to fail when used on data taken over the Laurentian Great Lakes. Two primary reasons for the failure have been identified as higher suspended minerals in the Great Lakes than in the oceans and normally higher cloud cover over the Great Lakes. A characterization of the impact of clouds on the radiance reaching remote sensing platforms has been performed. From this characterization, the impact on the calculated chlorophyll content determined by current algorithms is derived. The work presented here describes the creation of an end-to-end radiative transfer model for the complete sun-air-water-air-detector system and the application of that model to perform the cloud impact characterization. The radiative transfer model is modular; the modules relate to each propagation/scattering regime. Existing radiative transfer

computer codes were used when the required accuracy and resolution could be met. The cloud module in particular represents an advance in the radiative transfer methods found in the literature.

## ACKNOWLEDGEMENTS

I wish to acknowledge the tremendous contributions that helped me complete this body of work. Specifically, Dr. John Schott is my principal advisor and the driving source behind the creation of both the end to end radiative transfer model and the cloud characterization. Both were his ideas and it was under his direction that the work took shape. Dr. Anthony Vodacek supplied many comments, goals, and advice for radiative transfer under water. Dr. Vodacek also supplied the original Hydrolight 3.0 code that I started with. The rest of my dissertation committee, Dr. Harvey Rhody and Dr. John Waud, also supplied several meaningful comments and advice along the way.

Scott Brown supplied several MODTRAN tips and tricks and generously allowed me to bounce ideas and thoughts off of him before I implemented them. Capt Erich Hernandez-Baquero was a tremendous help in the code validation process. Erich always seemed to have the right question for me to attack and he helped exercise HydroMod in the early stages. 1Lt Niki Wilson and Mary Ellen Miller were also early participants and helped by asking challenging questions and probing for clarity and understanding.

It is safe to assert that I may not have finished this program had it not been for the efforts of Capt Charles Daly, Ph.D., in helping to prepare me for the comprehensive exams. Capt Daly went well above and beyond normal measures to tutor, lecture, and quiz me and I am in his debt.

I wish to thank Dr. Ian Gatley and the RIT Center for Imaging Science faculty for the excellent education and for allowing me to pursue the doctoral degree.

I wish to thank the United States Air Force for paying for the degree and generously allowing me the required time.

I also wish to thank Dr. Curtis Mobley for making Hydrolight 3.0 available for educational purposes.

The support and love from my wife, Tina, and my children, Alex and Joshua, were indispensable. The working weekends, long days, and many evenings take their toll. Families as loving and as strong as mine help each other survive and thrive and I am truly blessed.

Dedicated to Tina, Alexandra, and Joshua

## TABLE OF CONTENTS

<b>Table Of Contents</b> .....	iii
List Of Figures.....	v
Glossary .....	ix
<b>Introduction</b> .....	1
<b>Defining The Problem</b> .....	9
GEOMETRY USED .....	14
RADIATION IN THE AIR.....	16
Sun Source Radiance .....	17
Sky Source Radiance.....	20
Radiance From Clouds .....	23
An Elegant And Simple Method.....	30
TRANSITION FROM AIR TO WATER.....	35
Some Anomalous Cases .....	45
UNDER WATER REFLECTION MODELS.....	51
What Is In The Water .....	55
TRANSITION FROM WATER TO AIR.....	65
PROPAGATION TO THE SENSOR .....	65
RADIATIVE TRANSFER MODEL SUMMARY .....	66
<b>SeaWiFS Derived Chlorophyll Content</b> .....	69
<b>SeaWiFS Cloud Study Scope</b> .....	79
<b>Results And Analysis</b> .....	87
Single Step-By-Step Analysis .....	87
Affect On The SeaWiFS Calculations .....	98
Cloud Location Affects .....	102
Introducing A Cloudbank.....	103
Cloud Density Level Impact .....	108
The Wind Speed Impact.....	111
The Impact With Respect To Water Quality .....	116
The Impact With Respect To Atmosphere Model.....	120
SM Or Clouds .....	125
Summary Of Results.....	128
Operational Impact Of Results.....	131
<b>CONCLUSIONS</b> .....	135
Summary Of Contributions .....	135
Recommendations .....	137
Appendix I.....	141
Appendix II .....	203
<b>Bibliography</b> .....	231



## LIST OF FIGURES

<i>Number</i>	<i>Page</i>
Figure 1: Apparent Reflectance As Measured By At Select Locations.....	5
Figure 2: Light Pathways In The Atmosphere .....	11
Figure 3: Radiative Transfer Model Regimes.....	13
Figure 4: Angle Definitions For The Geometry Used.....	15
Figure 5: Standard Polar View.....	16
Figure 6: Example Possible Output. ....	18
Figure 7 Exo-Atmospheric Solar Spectral Irradiance. ....	21
Figure 8: Radiance To And From Clouds.....	25
Figure 9: Cloud Spectral Response Curves.....	32
Figure 10: Measured Cloud Spectral Data. ....	34
Figure 11: Geometry For A Wave Facet Defined By $\beta$ And $\zeta$ . ....	38
Figure 12: Geometry Of Reflection Off A Wave Facet.....	40
Figure 13: Geometry Of Refraction Through A Wave Facet.....	40
Figure 14: Refractive Index For Fresh Water .....	46
Figure 15: Facet-To-Facet Shadowing And Multiple Reflection.....	48
Figure 16: Scattering Cross Sections .....	62
Figure 17: Absorption Cross Sections. ....	63
Figure 18: Absorption Coefficient For Water.....	64
Figure 19: Scattering Coefficient For Water.....	64

Figure 20: Two Sample Empirical Relationships Scanned From Gordon (1994). .....	71
Figure 21: Affect Of Changing The Reflectance Ratio On The Calculated Chlorophyll Content. ....	77
Figure 22: Fresnel Reflection Coefficients At The Air/Water Interface. ....	80
Figure 23: Two Quantized Spheres .....	84
Figure 24: Two Input Sky Radiance Data Sets. ....	88
Figure 25: The Direct Sun Radiance Term .....	89
Figure 26: Surface Reflected And Total Water Leaving Radiance .....	90
Figure 27: Two Nearly Identical Upwelled Radiance Data Sets. ....	91
Figure 28: Total Sensor Reaching Radiance For The Clear Sky Case .....	92
Figure 29: Total Sensor Reaching Radiance For The Single Cloud Case .....	93
Figure 30: Error Caused By A Single Cloud In An Otherwise Clear Sky.....	95
Figure 31: A 3-D View Of Figure 30 (D).....	96
Figure 32: A Diameter Slice Through The Center Of Figure 30 (D) .....	97
Figure 33: The Error In The Ratio Between $\rho_T(765)$ And $\rho_T(865)$ (A) And Between $\rho_W(490)$ And $\rho_W(555)$ (B).....	100
Figure 34: Change In Peak Percent Error For Varying Cloud Brightness Levels ....	101
Figure 35: Effect Of Changing The Cloud Declination Angle.....	102
Figure 36: Cloud Bank Input Sky Data.. ....	104
Figure 37: Percent Error For The Two Main Quality Parameters.....	105
Figure 38: Peak Percent Error On The Chlorophyll. ....	106
Figure 39: Calculated Chlorophyll Levels.....	107



Figure 40: Calculated Chlorophyll Differences Between The Cloud Case And The No Cloud Case .....	108
Figure 41: Peak Error In The Sensor Reaching Reflectance Band 7/8 Ratio V .....	109
Figure 42: Peak Error In The Water Leaving Band 3/5 Ratio.....	110
Figure 43: Changes In The Chlorophyll Level For The Varying Cloud Brightness For Different Cloud Densities. ....	111
Figure 44: Changes In The Chlorophyll Level For The Varying Cloud Brightness For Different Cloud Densities. ....	112
Figure 45: Percent Error In Band 7/8 Ratio With Respect To Wind Speed For Different Brightness Factor Levels. ....	113
Figure 46: Percent Error In The Band 3/5 Ratio As A Function Of Wind Speed At Different Cloud Brightness Factor Levels .....	114
Figure 47: Normalized Error Width Ratio.....	115
Figure 48: Calculated Chlorophyll Levels.....	116
Figure 49: Percent Error Both The Sensor Reaching Band 7/8 Ratio And The Water Leaving Band 3/5 Ratio For Pure Water, Semi-Clean Water, And More Turbid Water. ....	117
Figure 50: Calculated Chlorophyll Content For The Three Water Cases Used In Figure 49.....	119
Figure 51: Percent Error For The Band 7/8 Ratio (At The Sensor) And The Band 3/5 Ratio (At The Water Surface.). ....	120

Figure 52: Calculated Chlorophyll Content Using The Original (A) And The New (B) SeaWiFS Algorithms.....	121
Figure 53: The Sensor Reaching Band 7/8 Ratio Error And Water Leaving Band 3/5 Ratio Error.....	122
Figure 54: The Calculated Chlorophyll Content With Varying Atmospheres. ....	124
Figure 55: SM And Cloud Changes At A Chlorophyll Level Of 1.0/L .....	124

## GLOSSARY

- $\alpha$ ..... Spherical declination angle ranging from 0 to  $\pi$  radians
- $\beta$  ..... Wave facet slope which is equal to the declination angle of the normal to the wave facet
- $\gamma$ ..... Spherical azimuthal angle ranging from 0 to  $2\pi$  radians
- $\zeta$ ..... Azimuthal angle from the wind speed direction,  $\omega$ , to the direction of steepest slope,  $\beta$ , for a wave facet. The angle is measured counter clockwise looking down on a "flat" water surface.
- $\eta$ .....
- $\theta$ ..... Hemispherical declination angle normally ranging from 0 to  $\pi/2$  radians; angles outside that range are handled as special cases
- $^+\theta$ ..... Hemispherical declination angle above (+) the water's surface ranging from 0 to  $\pi/2$  radians measured from the +z axis
- $^-\theta$ ..... Hemispherical declination angle below (-) the water's surface ranging from 0 to  $\pi/2$  radians measured from the -z axis
- $\theta_i$ ..... A specific hemispherical declination angle. This variable could be superscripted with a + or - to indicate above or below the water surface. The subscript, i, may be replaced with a prime, ', in some cases to indicate specific  $\theta$ 's
- $\theta_d$ ..... Specific declination angle between the pixel of interest and the detector
- $\lambda$ ..... Wavelength. Subscripted  $\lambda$ 's indicate a particular wavelength
- $^+v_i$ ..... Angle between a wave facet normal and an incoming or reflected radiance vector above the water surface
- $^-v_i$ ..... Angle between a wave facet normal and a refracted radiance vector below the water surface
- $\rho$ ..... Reflection coefficient which is a function of wave facet orientation, incoming radiance direction, wavelength, and index of refraction
- $\sigma$ ..... Specific sun hemispherical declination angle
- $\sigma_c$ ..... Cross Wind RMS slope component =  $(0.003+0.00192W)^{1/2}$
- $\sigma_u$ ..... Upwind RMS slope component =  $0.056214W^{1/2}$
- $\tau$ ..... Transmission coefficient equal to  $1-\rho$  with zero absorption

$\phi$ .....	Hemispherical azimuthal angle ranging from 0 to $2\pi$ radians; may be subscripted ( $\phi_i$ ) or primed ( $\phi'$ ) to indicate specific azimuthal angles or superscripted with a + or - to indicate above or below the water surface or a combination.
$\phi_d$ .....	Specific azimuthal angle indicating the direction of the detector
$\phi_s$ .....	Specific azimuthal angle indicating the direction of the sun
$\omega$ .....	Azimuthal angle of the wind direction measured from due north positively west
$\epsilon$ .....	Ratio between the single scattering aerosol reflectance at 765nm and the single scattering aerosol reflectance at 865nm; the ratio is assumed constant when an arbitrary $\lambda$ is substituted for 765nm
$\epsilon_{Peak}$ .....	Peak of the error whether a minimum or a maximum
$\epsilon_{WR}$ .....	Normalized Error Width Ratio defined by dividing the full solid angle with error values at or above half the maximum error value (analogous to a full width at half max parameter) by the solid angle of the cloud that caused the error.
CZCS .....	Coastal Zone Color Scanner
$E_{Sun}$ .....	Exoatmospheric Solar Irradiance
${}^+L_{\lambda}^{\downarrow}(\theta, \phi)$ .....	Radiance with a wavelength dependence above the water surface heading down as a function of the $\theta, \phi$ direction angles. The $\theta, \phi$ angles may be subscripted to indicated a specific direction for a specific vector radiance.
${}^+L_{\lambda}^{\uparrow}(\theta_d, \phi_d)$ .....	Radiance with a wavelength dependence above the water surface heading up in the specific $\theta_d, \phi_d$ direction. An absence of the "d" subscript would indicate that the radiance is a function of the $\theta, \phi$ direction angles.
${}^-L_{\lambda}^{\downarrow}(\theta, \phi)$ .....	Radiance with a wavelength dependence below the water surface heading down as a function of the $\theta, \phi$ direction angles. The $\theta, \phi$ angles may be subscripted to indicated a specific direction for a specific vector radiance.
${}^-L_{\lambda}^{\uparrow}(\theta, \phi)$ .....	Radiance with a wavelength dependence below the water surface heading up as a function of the $\theta, \phi$ direction angles. The $\theta, \phi$ angles may be subscripted to indicated a specific direction for a specific vector radiance.
$n$ .....	Index of refraction usually subscripted to indicate which medium it relates to ( $n_{water}$ or $n_{air}$ or $n_{1...}$ )

$p(\beta, \zeta)$ ..... Probability Density Function for a wave facet with slope  $\beta$  in the  $\zeta$  direction  
 $R(a, b; c, d)$  .... Bi-directional Reflectance Factor from (a, b) direction to (c, d) direction  
 SeaWiFS ..... Sea Viewing Wide Field-of-view Sensor  
 $W$  ..... Wind Speed



## *Chapter 1*

### **INTRODUCTION**

The importance of the world's oceans combined with their vastness has prompted their study via remote sensing. Many orbiting sensors view the earth's oceans, but two in particular were specifically design for that purpose: the Coastal Zone Color Scanner (CZCS) and the Sea-viewing Wide Field of View Sensor (SeaWiFS).

Both the CZCS and SeaWiFS systems address remote sensing difficulties that are intrinsic to large bodies of water. Specifically, differences in the optical properties of land based versus aquatic phenomenon create challenging problems when attempting to remotely sense water properties. Two obvious differences are the penetrability of water and the temporally and spatially varying nature of surface waves. Not so obvious differences include the more difficult acquisition of ground truth and the relative importance for atmospheric subtraction. These challenges and others are frequently addressed in the literature and were specifically addressed for both CZCS and SeaWiFS. (Gordon, 1994 and Bukata, 1995)

However, the CZCS and SeaWiFS solutions are optimized for the world's open oceans (and specifically for Case I waters) (Gordon, 1994) and are not always applicable to the coastal ocean regions and other large bodies of water such as the

Laurentian Great Lakes. The atmospheric correction algorithms used for the CZCS data relied on three main assumptions: the water was clear (except for a small amount of phytoplankton-pigment less than 0.25  $\mu\text{g/l}$ ); the atmospheric aerosols absorbed and scattered the same at all wavelengths; and multiple scattering within the atmosphere was negligible (Gordon, 1994). The CZCS atmospheric correction algorithms were based on "knowing" the top-of-the-atmosphere reflectance<sup>1</sup> component due to the atmosphere for at least two wavelengths ( $\rho_{a1}$  and  $\rho_{a2}$  for  $\lambda_1$  and  $\lambda_2$  respectively). A constant,  $n$ , was obtained by assuming a power law relationship:  $(\rho_{a1}/\rho_{a2}) = (\lambda_1/\lambda_2)^n$ . The atmospheric reflectance component,  $\rho_{a3}$  at some other  $\lambda_3$  is simply a matter of extrapolating the same power law to the unknown reflectance at  $\lambda_3$ .

For many open ocean scenes, these assumptions produced reasonable results. However, in areas with spectrally variant aerosols, clouds, and/or non-clear waters the atmospheric correction algorithms used for the CZCS data were far from accurate (Gordon, 1994). Better solutions were developed for SeaWiFS.

The SeaWiFS atmospheric subtraction routines are improved over the CZCS due to the introduction of additional data acquisition bands and the abandonment of the CZCS based power-law-reflectance extrapolation. In particular, the SeaWiFS sensor includes two infrared wavelengths that were not included in the CZCS sensor. These were included to make the "clear water" assumption more accurate.

---

<sup>1</sup> Top-of-the-atmosphere reflectance values,  $\rho$ , are favored in the CZCS and SeaWiFS literature over the top-of-the-atmosphere radiance,  $L$ . The two are related by  $\rho = \pi L / E_0 \cos(\sigma)$  where  $E_0$  is the exo-atmospheric irradiance and  $\sigma$  is the solar declination angle.



Atmospheric models were introduced to bound the aerosol response for the two known wavelengths ( $\lambda_1=765$  nm and  $\lambda_2=865$  nm) and assume that the response in the same ratio would apply for the reflectance at wavelengths in the visible region. A more precise description of the SeaWiFS algorithms will appear later in this report.

With the atmosphere corrected (and a few additional adjustments for masked or flagged data due to ice, direct-path clouds, coccolithophores, etc., as described by McClain, 1995) chlorophyll content and dissolved organic carbon (DOC) are derived from the reflectance values calculated in the visible wavelengths. Yet two anomalies remain: the affect of clouds in the vicinity is unknown and suspended minerals tend to amplify the derived chlorophyll content (Bukata, 1995). Therefore, the SeaWiFS algorithms tend to work well for Case I waters (open ocean and clear) and moderately well for Case II waters (oceanic and higher levels of DOC and chlorophyll) but fail with Case III<sup>2</sup> waters and for waters where cloud cover predominates.

Unfortunately, the Laurentian Great Lakes are primarily Case II and III waters with a high probability of cloud contamination. Robert Bukata and colleagues at Canada's National Water Research Institute, NWRI, in Ontario have characterized the failures for Case III waters (Bukata, 1995, 1997, and 1998 and Jerome, 1996) and are involved with working toward algorithm adjustments. However, the effect of nearby clouds has not been well characterized until now.

---

<sup>2</sup> The term "Case III" applies to contaminated oceanic waters as defined by Jerlov 1976 or, more meaningfully here, as any waters with suspended minerals and/or suspended inorganic matter as defined by Bukata, 1998.

Nearby clouds may contaminate the data in two ways: by changing the magnitude of the spectral radiance into and reflected from the water from the direction of the cloud and by changing the spectral shape of the radiance into and reflected from the water from the direction of the cloud.

Figure 1 is used as motivation to indicate that clouds may indeed be a major source of error in current data and algorithms. This figure shows simulated spectral data of the apparent reflectance that may be measured just below the water surface (3), just above the water surface (2) and in orbit (1) for both a clear sky (solid lines) and single cloud bank sky (----dashed lines). Just below the water surface, the "measurement" uses the hemisphere above the sensor but below the water surface as the source radiance. The calculations integrated these values to get the total irradiance below the water surface heading down. With this total and the radiance from the direction that will exit the water in the cloud specular direction, the apparent reflectance is easily determined. The n-squared law is also used to equate the above and below water data sets. The two plotted lines below the surface (3) in Figure 1 show that including a cloud will reduce the measured apparent reflectance due to the increased source radiance. As the light exits the water at (2) the cloudless sky apparent reflectance increases slightly over the same measurement below the surface. However, introducing the cloudbank greatly increases the apparent reflectance in the specular direction (2a). The same is true at a sensor in orbit (1). The final plot in the figure (2b) is not measurable and is used for analysis only. It shows the component

arriving at the orbiting sensor due to the water leaving component after atmospheric transmittance is accounted for but without the upwelling radiance.

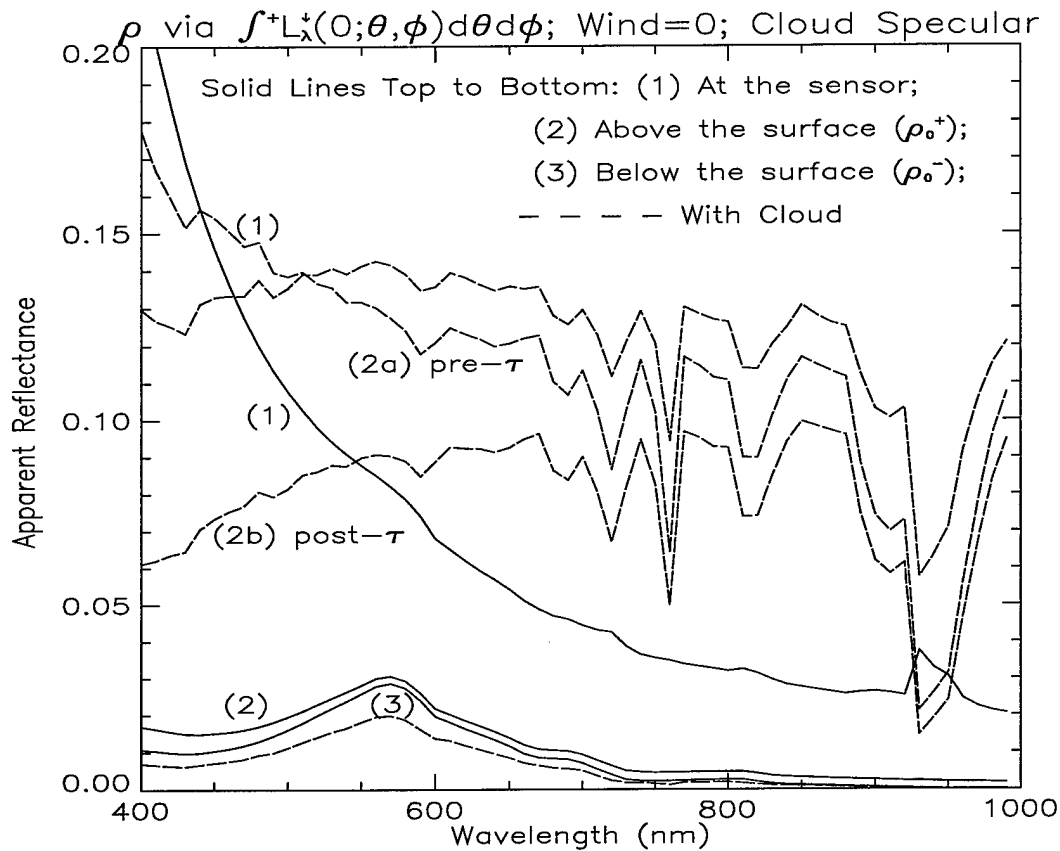


Figure 1: Apparent Reflectance as Measured by at Select Locations. This figure shows simulated spectral data of the apparent reflectance that may be measured just below the water surface (3), just above the water surface (2) and in orbit (1) for both a clear sky (solid lines) and single cloud bank sky (-----dashed lines). Just below the water surface, the "measurement" uses the hemisphere above the sensor but below the water surface as the source radiance and the radiance from the direction that will exit the water in the cloud specular direction to determine the apparent reflectance. The n-squared law is also used to equate the above and below water data sets. The two plotted lines below the surface (3) show that including a cloud will reduce the measured apparent reflectance due to the increased source radiance. As the light exits the water at (2) the cloudless sky apparent reflectance increases slightly over the same measurement below the surface. However, introducing the cloudbank greatly increases the apparent reflectance in the specular direction (2a). The same is true at a sensor in orbit (1). The final plot in the figure (2b) is not measurable and is used for analysis only. It shows the component arriving at the orbiting sensor due to the water leaving component after atmospheric transmittance is accounted for but without the upwelling radiance. The simulation used a zero wind speed and the cloud's specular direction.

The first step in determining the impact of each of these contamination methods is to build a computer model capable of accurately predicting the radiance

reaching an orbiting sensor. Key elements of the model include accurate predictions of radiance transfer in the atmosphere (including clouds), between the atmosphere and water, and in the water. Such a radiance transfer solution program was created as part of this effort. The computer code is called HydroMod and a full description of the program and its use can be found in Appendix I of this report.

Chapter 2 covers the important radiative transfer regimes and describes the solution methods used in the cloud impact study. Included in Chapter 2 is the separation of the problem into modules that provide natural impact analysis areas, creation of the geometrical equations to be used, and descriptions of most of the key elements that are modeled in HydroMod. As the problem is broken into manageable modules, a review of the key literature concerning that module and associated radiative transfer is also included.

The derivation of the error in SeaWiFS derived chlorophyll-a content is covered in Chapter 3. Specifically, the methods of atmospheric correction and the empirically derived formulas pertaining to atmospheric correction and chlorophyll-a concentrations are reviewed.

A discussion of the specific parameters used in the SeaWiFS/Great Lakes cloud impact study is contained in Chapter 4. The actual values that were used and the reasons for using them are provided in Chapter 4.

The results of the study are reported in Chapter 5. Discussions of the data and the expectations and surprises are also included there. However, much of the study was concerned with validating the operation of HydroMod through a series of data acquisitions designed to confirm expected results. This "confirmation of expectations" analysis is not presented in the body of this report. Most of the confirmation of expectations can be found in Appendix II.

Finally, the conclusions and recommendations are included as Chapter 6.



## *Chapter 2*

### **DEFINING THE PROBLEM**

This chapter describes the key elements of an end-to-end hyperspectral radiative transfer model that incorporates all pertinent aspects of a realistic water scene with a broad range of sensitivity parameters. One goal for the creation of the model is that it is flexible enough to be used for many water remote-sensing applications beyond the cloud impact characterization. The problem is defined with this in mind (although the primary concern of this effort is to characterize the affect of circuitous clouds on the radiance at the sensor and the impact to the derived chlorophyll content for the SeaWiFS system.) The specific model parameters used and the cloud impact characterization are covered in later chapters. The path used for the creation of the end-to-end radiative transfer model is also followed in this chapter:

- (1) separation of the radiative transfer into manageable regimes;
- (2) review of the pertinent literature and established solutions for those regimes;
- (3) selection of methods and/or solutions of choice;
- (4) creation of missing components; and

(5) linking the components together.

Radiative transfer through the multiple scattering regimes in a realistic water scene has many challenges (see Figure 2). Including clouds in the vicinity only serves to further complicate the challenges. The individual components (atmosphere, clouds, air-water interface, water, wind roughened surface,...) have been studied to varying degrees and the literature contains several examples of possible individual and partial solutions to the some of the challenges.

At times, the problems are mitigated by assuming a smooth surface (Gordon, 1975), a clear or homogeneous sky (Gordon, 1997), or similar simplifications within the water. At other times, one or more of the problems are directly considered and solutions are sought as the thrust of the research. For instance, several models have been generated for propagation of light in the underwater light field (Gordon, 1975; Kirk, 1984; Kirk, 1991; Morel, 1993; Bukata, 1981; Mobley, 1994; and Jerome, 1988) or for modeling more complex atmospheric phenomenon (Plass, 1968 and Plass, 1969).

Yet even those studies have only pursued one or two parts of the overall water remote-sensing problem. The challenge is to construct a comprehensive model utilizing the best available methods to date in each of the problem areas.

Specifically, a comprehensive model will incorporate a standard radiative transfer code (such as MODTRAN) that allows for user modifications of the



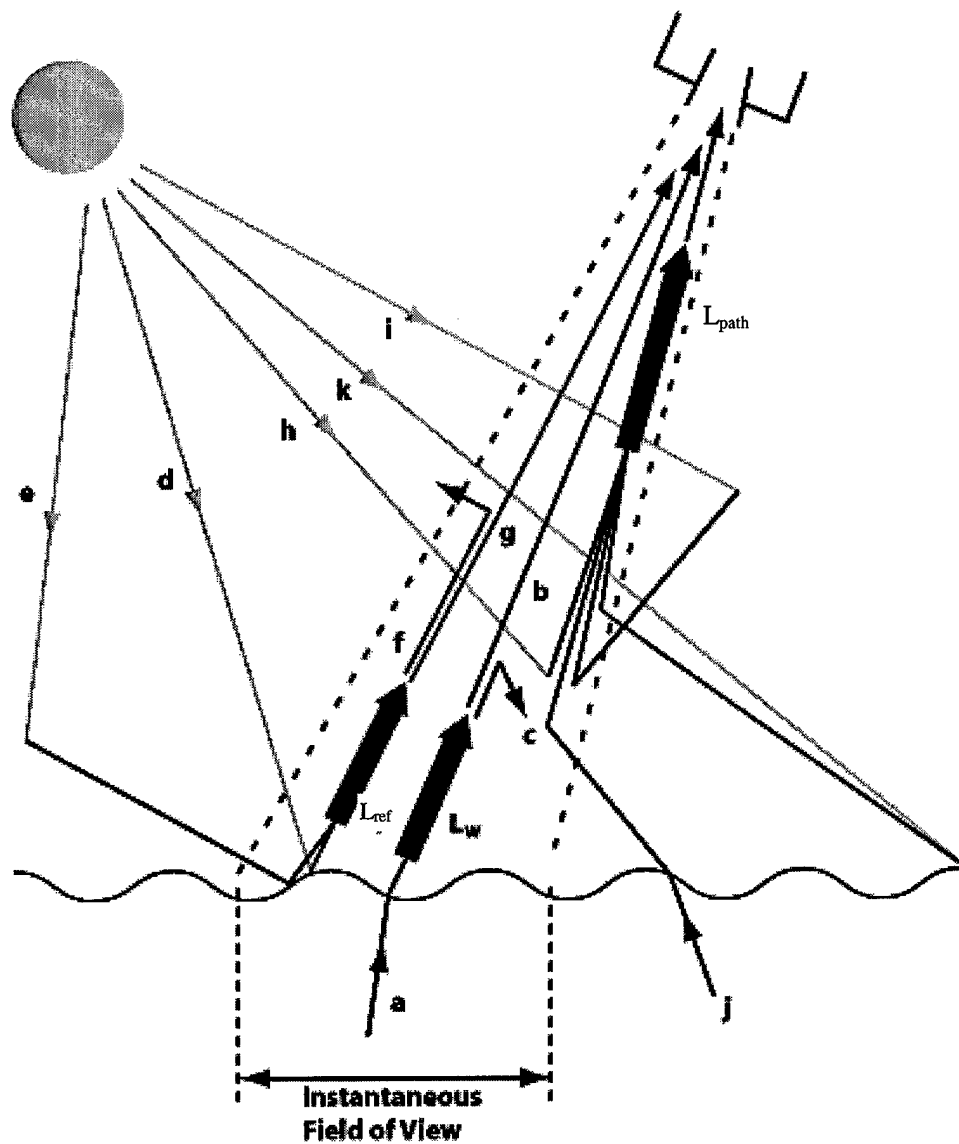


Figure 2: Light Pathways in the Atmosphere: a) The light path of the water-leaving radiance. b) Shows the attenuation of the water-leaving radiance. c) Scattering of the water-leaving radiance out of the sensor's FOV. d) Sun glint (reflection from the water surface). e) Sky glint (scattered light reflecting from the surface). f) Scattering of reflected light out of the sensor's FOV. g) Reflected light is also attenuated towards the sensor. h) Scattered light from the sun which is directed toward the sensor. i) Light which has already been scattered by the atmosphere which is then scattered toward the sensor. j) Water-leaving radiance originating out of the sensor FOV, but scattered toward the sensor. k) Surface reflection out of the sensor FOV which is then scattered toward the sensor.  $L_w$  = Total water-leaving radiance.  $L_{ref}$  = Radiance above the sea surface due to all surface reflection effects within the IFOV.  $L_{path}$  = Atmospheric path radiance. (This figure is adapted from Robinson, I.S., 1983: Satellite observations of ocean colour, Philo. Trans. Royal Soc. of London, Series A, Volume 309, 338-347 and obtained from URL [http://phyvax.ir.miami.edu:8001/chris/envr\\_optics.html](http://phyvax.ir.miami.edu:8001/chris/envr_optics.html))

atmospheric constituents. It will allow the introduction of clouds (varying type, location, and percent coverage) to the standard atmospheres. At the air water interface an accurate wind roughened surface will form the boundary. Below the water, the radiative transfer must include the absorption and scattering of the water constituents as well as the water itself. Many existing methods discussed by Bukata (1995) and Mobley (1994) allow for changing the materials within the water to generate the volume spectral reflectance. Mobley's HYDROLIGHT (Mobley 1995) code in particular, also generates three dimensional radiance distributions within and exiting the water. Most other codes, including the Monte Carlo codes discussed and used by Bukata, require modifications to obtain a three dimensional radiance distribution exiting the water.

To obtain radiance at the sensor, the end-to-end model will propagate the underwater-scattered field back through the wind roughened air/water interface, add the radiance reflected off the water surface, and propagate the sum back through the atmosphere to the sensor.

To facilitate impact analyses, a method by which the radiative field can be viewed and studied is also required. Preferably, the radiative field in each regime can be viewed and studied and separated to allow in-depth impact analyses.

In the discussion to follow, I refer to any photons that reach the target (i.e. the water's surface) as source photons. If they enter the water and end up exiting the water toward the sensor, they become the "a" type photons in **Figure 2**; if they exit in

another direction, they are the “j” type photons. If they never exit they are still important, but they are not included in **Figure 2**.

The following sections are separated into a geometrical overview and the radiative transfer regimes: air, air/water interface, water, water/air interface, and air again. These regimes are illustrated in **Figure 3**.

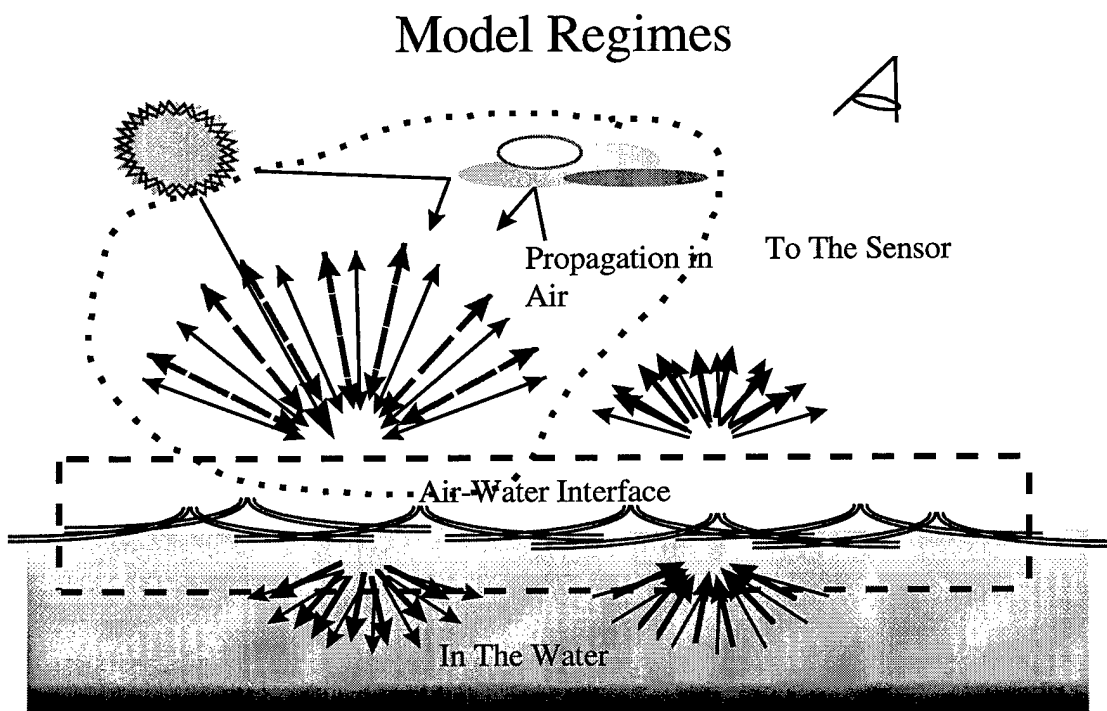


Figure 3: Radiative Transfer Model Regimes. The radiative transfer model will incorporate sections from each of the four regimes shown here. Further, each regime may contain subsections such as a cloud model for the propagation in air regime.

## GEOMETRY USED

I used the world coordinate system geometry found in *Remote Sensing The Image Chain Approach* (Schott, 1997) with one modification. Referring to Figure 4, the X, Y, and Z axes are North, West, and vertical respectively. The declination angle between the sun and the normal to the earth,  $\sigma$ ; and the declination angle between the sensor and the normal to the earth<sup>3</sup>,  $\theta_d$ , are bounded by  $0^\circ$  and  $90^\circ$ ; the sun directly vertical has a declination angle of  $\sigma = 0^\circ$ . The azimuthal angles between the X-axis (North) and the projection of the sun,  $\phi_s$ , and the detector,  $\phi_d$ , are positive counter-clockwise looking down. These are the fixed coordinates. Wave orientation, wind direction, and cloud positions, will be referenced to the fixed coordinates of Figure 4.

The geometry defined in Figure 4 is used in calculations and the identification of directional information associated with incoming and outgoing radiance. However, for viewing the magnitude of the radiance in all (hemispherical) directions simultaneously, other means are required. The method used in this work is a polar view representing the directional information and a gray scale that represents the magnitude information. The polar view is demonstrated in Figure 5. With this view, the center of the circular section would be straight up (or down as the case may be)

---

<sup>3</sup> This is the aforementioned modification; Schott uses  $\theta$  for the detector angle. I will use the more generic  $\theta$  to represent an arbitrary declination angle in describing the hemisphere in terms of  $\theta$  and  $\phi$ .

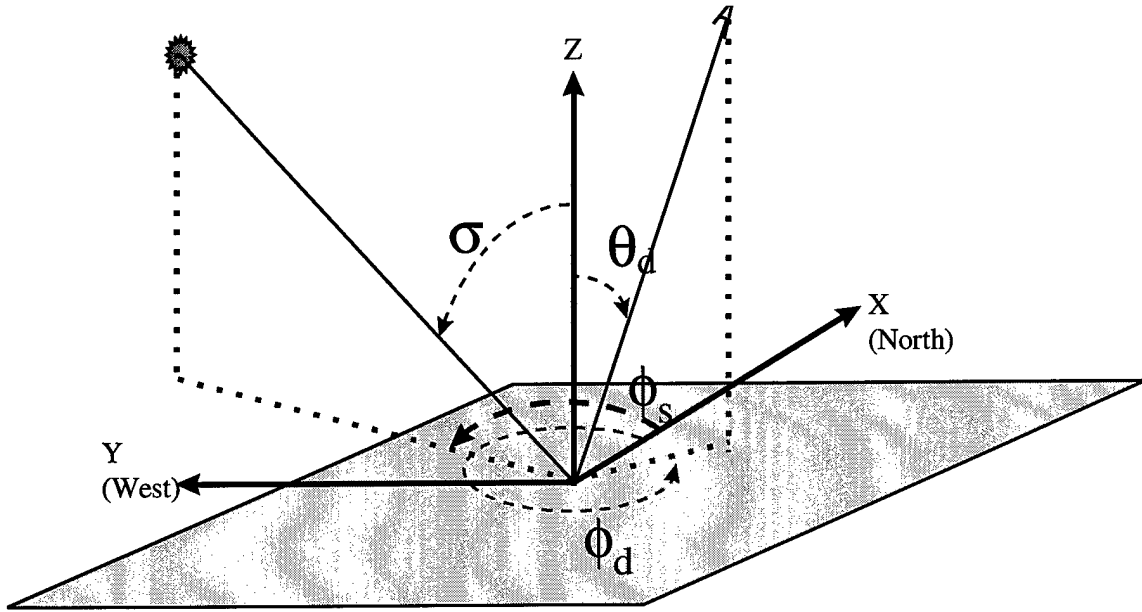


Figure 4: Angle Definitions For The Geometry Used. The X, Y, and Z axes are North, West, and vertical respectively. The declination angle between the sun and the normal to the earth,  $\sigma$ , and the declination angle between the sensor and the normal to the earth,  $\theta_d$ , are bounded by  $0^\circ$  and  $90^\circ$ ; the sun directly vertical has a declination angle of  $\sigma = 0^\circ$ . The azimuthal angles between the X axis (North) and the projection of the sun,  $\phi_s$ , and the detector,  $\phi_d$ , are positive counter-clockwise looking down

and the outer edges of the outer-most circle is the horizon. The declination angle,  $\theta$ , increases from  $0^\circ$  at the center to  $90^\circ$  around the outer edge. I define the azimuth angle,  $\phi$ , to be North =  $0^\circ$  at the top of the graph and positive West of North. However, an advantage of these polar plots is that the azimuthal angle reference perspective is completely arbitrary as long as it remains consistent. (That is, having North as the top or not and positive East or West of North is completely arbitrary as long as we are consistent once defined. I will refer to my defined reference of North =  $0^\circ$  at the top and positive West of North throughout this report.)

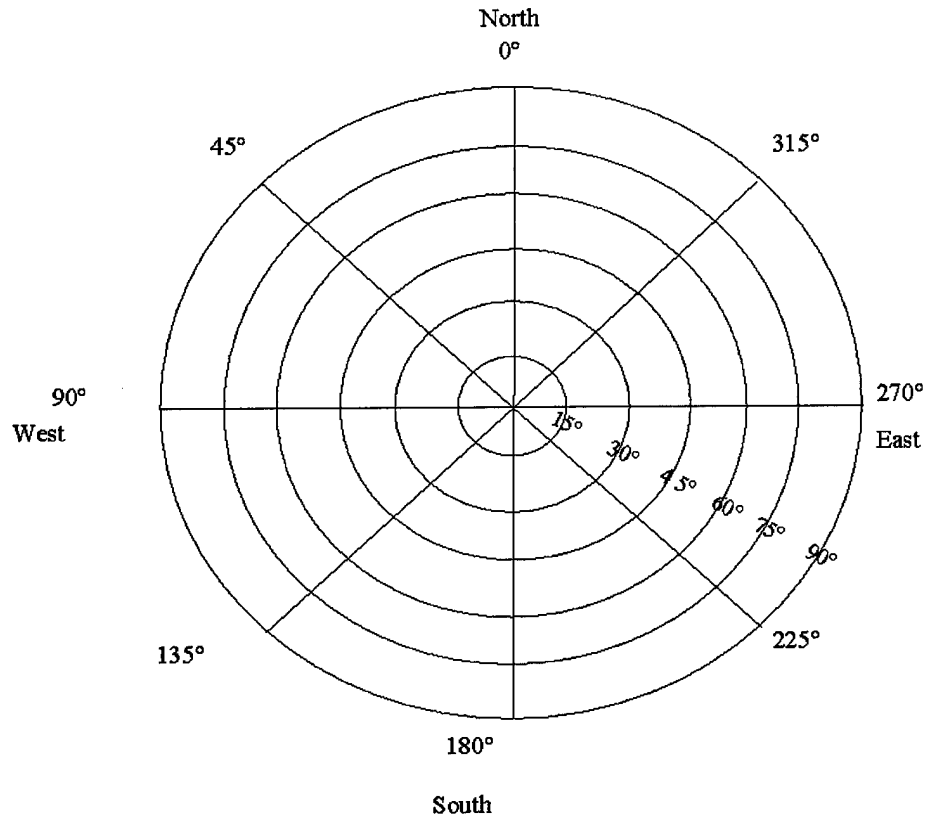


Figure 5: Standard Polar View. With this view, the center of the circular section would be straight up (or down as the case may be) and the outer edges of the outer-most circle is the horizon. The declination angle,  $\theta$ , increases from  $0^\circ$  at the center to  $90^\circ$  around the outer edge. Reference Figure 4 for the geometry definitions and Figure 6 for an example of the polar plot style with radiance levels inserted using gray scale values.

## RADIATION IN THE AIR

The source radiation propagation is the direct sunlight source irradiance, the downwelled radiance from a clear sky (Rayleigh scattered), downwelled radiance from aerosols and water vapor, and the affect of clouds. Each of these are considered to be a radiance source to the surface of the water and they sum to  $L_a(\theta, \phi)$ :

$$L_{\lambda}(\theta, \phi) = L_{\lambda}(\sigma, \phi_s) + L_{\lambda R}(\theta, \phi) + L_{\lambda a}(\theta, \phi) + L_{\lambda C}(\theta, \phi)$$

EQ 1

Where  $L_{\lambda}(\sigma, \phi_s)$  = Radiance directly from the sun

$L_{\lambda R}(\theta, \phi)$  = Rayleigh scattered radiance

$L_{\lambda a}(\theta, \phi)$  = Aerosol/water vapor scattered radiance (including Rayleigh/Aerosol Interaction)

$L_{\lambda C}(\theta, \phi)$  = Radiance scattered from clouds

Light scattering in the atmosphere and off the surface of the water ( $L_{\text{path}}$  and  $L_{\text{ref}}$  in **Figure 2**) will also reach the sensor and contaminate the data.

The standard output from this stage is a two-dimensional radiance magnitude and direction for a point on the sea surface at each wavelength of interest. For instance, combining a large source irradiance from the sun with typical atmospheric scatter (Schott, 1997 and Bukata, 1995 derived from Moon, 1942) and a cloud reflection component with the geometry found in Figure 5 may produce the distribution found in Figure 6. Though this section seems to be straight forward, the task is large when the full radiation pattern at each wavelength is considered. Note that Figure 6 is only a sample of one possible output. By using the Interactive Data Language (IDL) from Research Systems Incorporated, multiple surface and plotting routines are available.

### Sun Source Radiance

Sun source radiation in remote sensing is normally viewed as an exo-atmospheric irradiance,  $E_{\text{sun}}$ , attenuated by the atmosphere and impinging on a point on the earth's surface. However, irradiance does not provide the directional

information of the sun,  $\sigma$  and  $\phi_s$ , nor can it provide  $L_\lambda(\theta, \phi)$  for the hemisphere above the water's surface. A radiative transfer code such as MODTRAN can be used to obtain the required hemispherical radiance (see the next section), but the direct solar radiance must come from some other means. A less spectrally accurate, but

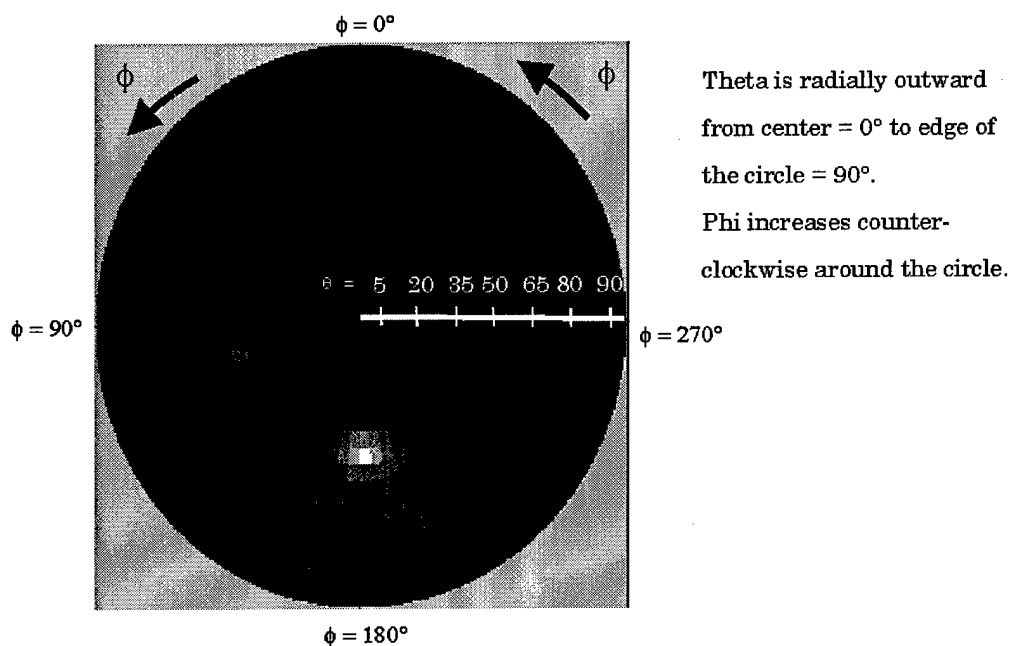


Figure 6: Example Possible Output. One hardcopy output style is illustrated here. The declination angle,  $\theta$ , runs radially outward from the center of the plotted circle. The azimuthal angle,  $\phi$ , runs counter-clockwise around the circle. The bright spot just below and left of center would represent, here, the input radiance from a cloud at roughly  $\theta = 35^\circ$  and  $\phi = 110^\circ$ . The brightest spot below the center of the circle represents the sun forward scattering. Most of the sky radiance is diffuse with the non-uniform illumination of the source radiation clearly visible.



intuitively pleasing remedy is found following the developments of Schott (1997) and Maul (1985) by assuming the sun is a blackbody radiator between 5800 Kelvin (Schott, 1997) and 5900 Kelvin (Maul, 1985). Using Planck's radiation equation for radiant exitance,  $M_\lambda$ , and then noting that  $L_\lambda$ , is essentially zero for directions other than  $(\sigma, \phi_s)$ , we can obtain an equation for  $L_\lambda(\sigma, \phi_s)$ . The blackbody radiant exitance is given as

$$M_\lambda = \frac{2\pi hc^2}{\left[ e^{\frac{hc}{\lambda kT}} - 1 \right] \lambda^5}$$

EQ 2

with

$$\begin{aligned} h &= \text{Planck's Constant} \\ &= 6.6256 \times 10^{-34} \text{ Joule} \cdot \text{Sec} \\ c &= \text{Speed of Light} \\ &= 3 \times 10^8 \text{ m/sec} \\ k &= \text{Boltzman's Constant} \\ &= 1.38 \times 10^{-23} \text{ Joules/Kelvin} \\ T &= \text{Temperature (Kelvin)} \\ \lambda &= \text{Wavelength} \end{aligned}$$

With the sun radiating the same in all directions (at  $T=5800\text{K}$  or  $5900\text{K}$ ), the sun's source radiance can be calculated as  $L_\lambda(\sigma, \phi_s) = M_\lambda/\pi$ . Relating the earth's exo-atmospheric sun source irradiance,  $E_{\text{sun}\lambda}$ , to  $L_\lambda(\sigma, \phi_s)$  is simply a matter of integrating a constant  $L_\lambda(\sigma, \phi_s)$  over the solid angle subtended by the sun at the earth. Using the

mean sun-earth distance of  $1.497 \times 10^{11}$  meters and a sun radius of  $6.96 \times 10^8$  meters gives a solid angle of  $6.791 \times 10^{-5}$  sr which means that  $E_{\text{sun}\lambda} = L_{\lambda}(\sigma, \phi_s)(6.791 \times 10^{-5} \text{ sr})$ .

At the eight specific wavelengths detected by SeaWiFS this approximation may be adequate. However, the sun is not a true blackbody and the exo-atmospheric irradiance has more spectral variation than predicted by the Planck blackbody radiation (EQ 2). This development for  $L_{\lambda}(\sigma, \phi_s)$  can be used for relative reference to the true exo-atmospheric solar irradiance as in Figure 7. In Figure 7, the measured exo-atmospheric solar irradiance (obtained from the Air Force Research Laboratory) is compared to the Planck blackbody calculated radiance from the above analysis. The two smooth curves in Figure 7 are for a 5900 Kelvin (upper curve) and a 5800 Kelvin (lower curve) blackbody sun. We may conclude from Figure 7 that a more accurate  $L_{\lambda}(\sigma, \phi_s)$  than that found using the above development is obtained by attenuating the measured  $E_{\text{sun}\lambda}$  with the atmospheric transmission coefficient,  $\tau$ , (to get the irradiance at the water surface) and dividing by the solid angle subtended by the sun,  $6.791 \times 10^{-5}$  sr. It is also reasonable to assume a constant radiance over that solid angle.

### **Sky Source Radiance**

The direct solar irradiance is by far the largest contributor to the source illumination. As such, some of the early work in underwater illumination studies (including some of the Monte Carlo codes previously mentioned) considered only a

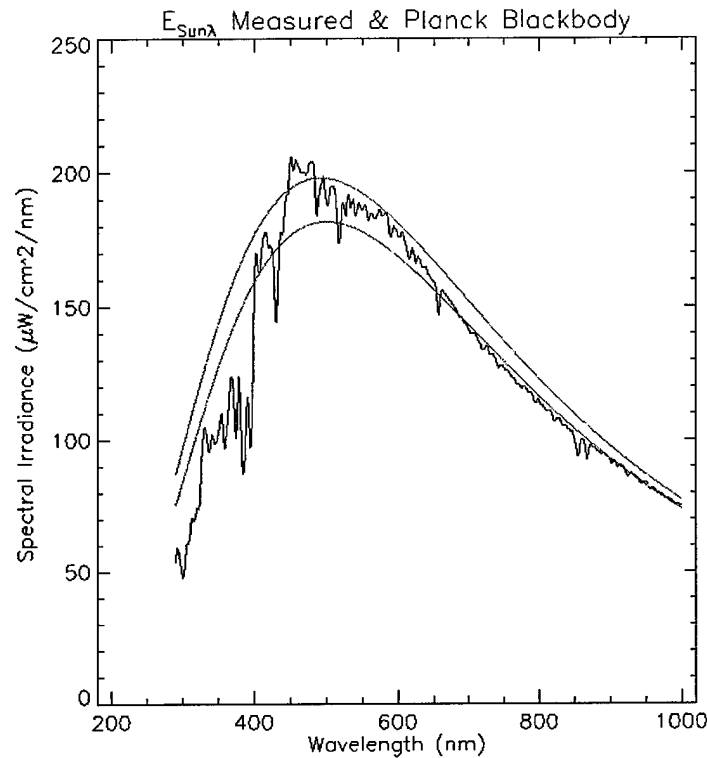


Figure 7 Exo-atmospheric Solar Spectral Irradiance for measured data and calculated from Planck's radiation law using the sun as a blackbody disk at 5800 Kelvin (lower smooth curve) and 5900 Kelvin (upper smooth curve).

single source (Bukata, 1995 and Kirk, 1991). (To be fair, all of the Monte Carlo codes could be employed using several runs of a single source and their output combined using superposition. This would give the same result as a multiple source input run would produce.) The single source method loses credibility when the water leaving radiance in all directions is the primary objective.

Since the water leaving radiance in all directions is indeed one of the primary objectives of this work, accurate source radiance  $L_\lambda(\theta, \phi)$  from all  $(\theta, \phi)$  directions is required. There are several avenues available to determine  $L_\lambda(\theta, \phi)$  from all  $(\theta, \phi)$

directions. An obvious next approximation is to use uniform sky illumination. However, even in the early 1940's, uniform sky illumination models were replaced with measurement derived cardioidal illumination formulas (Moon and Spencer, 1942). The sky illumination models continued to improve and become more and more complex. The Air Force released the low-resolution atmospheric transmission model, LOWTRAN 2 in 1972 (Selby, 1972). The sole purpose of LOWTRAN 2 was to compute the transmittance through a user-defined atmosphere. Calculation of radiance was added to LOWTRAN 4 in 1978 (Kneizys, 1980). LOWTRAN eventually gave way to MODTRAN (moderate resolution atmospheric transmission code) and the current version is MODTRAN 4.0 (Acharya, 1998).

Though promisingly accurate, the LOWTRAN and MODTRAN family of codes were considered cumbersome to use and somewhat time consuming in the calculations (Gregg, 1990). Closed form type solutions along the lines of the original Moon and Spencer (1942) work were and are still being pursued. One promising line of development progressed from Leckner (1978) through Bird and Riordan (1986) to Gregg and Carder (1990). The Gregg and Carder model is specifically for clear maritime atmospheres and compares quite well to measured irradiance values (Gregg, 1990); the previous versions were only intended for use over non-maritime conditions (Bird, 1986).

However easy these models are, they have neither the flexibility nor the industry acceptance of MODTRAN (not to mention the endorsement by the United

States Air Force). Combine those advantages with the MODTRAN experience level at RIT (which minimizes the “cumbersome” argument previously stated) and MODTRAN is a very attractive method for computing the sky components of  $L_\lambda(\theta, \phi)$  from all  $(\theta, \phi)$  directions. Another MODTRAN advantage is that atmospheric attenuation of the  $L_\lambda$  component from the  $\sigma, \phi_s$  direction can also be obtained in addition to both the Rayleigh scatter component,  $L_{\lambda R}(\theta, \phi)$ , and the aerosol/water vapor component,  $L_{\lambda a}(\theta, \phi)$ . Using repeated runs of MODTRAN with the “sensor” located at the water surface can produce  $L_{\lambda R}(\theta, \phi) + L_{\lambda a}(\theta, \phi)$  for the entire hemisphere above the water surface.

Yet another MODTRAN advantage is that the amount and type of atmospheric constituents can be variable and may come from standard aerosol models built in to MODTRAN, radiosonde data, or tabular self-generated form. Virtually any atmosphere can be modeled using MODTRAN and  $L_\lambda(\theta, \phi)$  from any and all  $(\theta, \phi)$  directions can be calculated. This functionality means that the atmosphere for a given day can be modeled very accurately. In fact, algorithms that rely on inverting radiance at the sensor by correcting for the atmosphere can be tested with “ground-truth” measured data.

### **Radiance from Clouds**

To build realistic atmospheres, we need the ability to add variable clouds at select locations that would, in turn, modify the  $L_\lambda(\theta, \phi)$  from the pertinent  $(\theta, \phi)$  directions to give  $L_{\lambda C}(\theta, \phi)$ . The literature has many cloud models that range from a built-in module in MODTRAN to stand alone Monte Carlo style codes that calculate

bi-directional reflectance factors (BDRF) for a given cloud with variable extinction coefficient,  $\beta$ , in three dimensions. One of the latter models was written and used by the University of Arizona's Institute of Atmospheric Physics (Várnai, 1998). The Monte Carlo code was specifically designed to compute the BDRF using the sun as an input source and multiple directions as the output reflectance angles. If this or similar Monte Carlo based codes were used in this effort, a geometry inversion would be required along with the use of reciprocity to speed the computations. That is, we would use the  $(\theta, \phi)$  direction as the single source input and calculate BDRF. The true multiple source input to the cloud (direct sun plus scattered skylight) would then be used, assuming reciprocity holds, to calculate  $L_{\lambda C}(\theta, \phi)$ . The process is illustrated in Figure 8.

In the next few paragraphs I will derive a method for calculating the radiance into the point of interest on the water surface due to a cloud,  $L_{\lambda C}(\theta, \phi)$ , in the  $(\theta, \phi)$  direction. In the quest of accuracy in the development, more and more uncertainty is added until the final calculated  $L_{\lambda C}(\theta, \phi)$  is quite questionable. That high uncertainty will lead to an elegant and simple solution for determining  $L_{\lambda C}(\theta, \phi)$  that applies quite well to almost any atmosphere. The first step is to derive a method of calculating  $L_{\lambda C}(\theta, \phi)$ .

The contribution to  $L_{\lambda}(\theta, \phi)$  from clouds,  $L_{\lambda C}(\theta, \phi)$ , in EQ 1 is fairly complex if the full impact is used. Referring to Figure 8, the cloud contribution to  $L_{\lambda}(\theta, \phi)$  can be calculated as

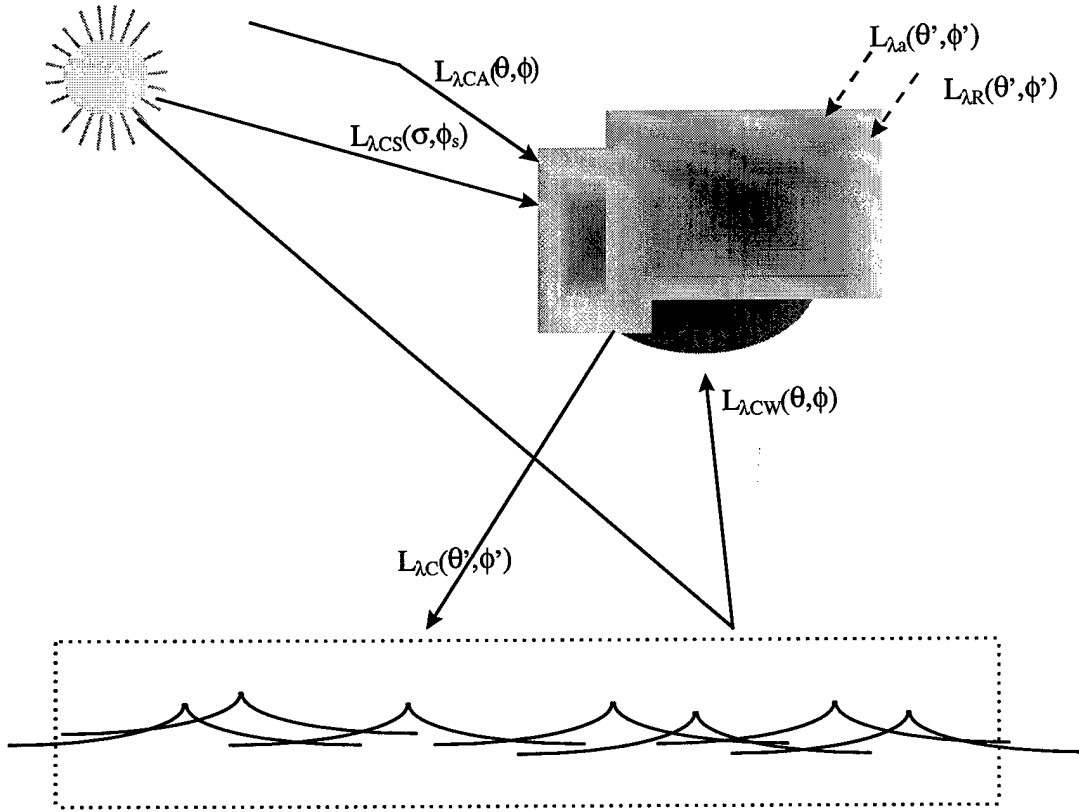


Figure 8: Radiance To and From Clouds. Obtaining the cloud contribution,  $L_{\lambda C}(\theta', \phi')$  to the total input radiance term,  $L_{\lambda}(\theta, \phi)$ , requires knowing the radiance from the sun to the cloud,  $L_{\lambda CS}(\sigma, \phi_s)$ ; the radiance reflected off the water to the cloud,  $L_{\lambda CW}(\theta, \phi)$ ; the radiance from the atmosphere to the cloud,  $L_{\lambda CA}(\theta, \phi)$ ; and the removal of the Rayleigh and aerosol/water vapor components from the  $(\theta', \phi')$  direction. The last step is required because the  $L_{\lambda CA}(\theta, \phi)R(\alpha, \gamma; \theta', \phi')$  term in EQ 3 includes the Rayleigh and aerosol components attenuated by the cloud EQ 1 also includes the terms un-attenuated by the cloud.

$$L_{\lambda C}(\theta, \phi) = L_{\lambda C}(\theta', \phi') = [L_{\lambda CS}(\sigma, \phi_s)R(\sigma, \phi_s; \theta', \phi') + L_{\lambda CW}(\alpha, \gamma)R(\alpha, \gamma; \theta', \phi') + L_{\lambda CA}(\alpha, \gamma)R(\alpha, \gamma; \theta', \phi')] \tau_c - L_{\lambda R}(\theta', \phi') - L_{\lambda a}(\theta', \phi') \quad \text{EQ 3}$$

where

$L_{\lambda C}(\theta', \phi')$  = Cloud contribution from the specific  $\theta', \phi'$  direction

$L_{\lambda CS}(\sigma, \phi_s)$  = Radiance Input to the cloud from the sun

$R(a, b; c, d)$  = Bi-directional Reflectance Factor from (a, b) direction to (c, d) direction

$L_{\lambda CW}(\alpha, \gamma)$  = Radiance Reflected off the water to the cloud

$L_{\lambda CA}(\alpha, \gamma)$  = Combined Rayleigh and aerosol scattering to the cloud  
 $\tau_c$  = transmission coefficient from the cloud to the point on the water  
 $(\alpha, \gamma)$  = input angles for radiance to the cloud over the entire input sphere

EQ 3 would need to be solved for each set of  $(\theta', \phi')$  for which a cloud would impact the  $L_{\lambda}(\theta, \phi)$  input radiance. Some of the components of  $L_{\lambda C}(\theta', \phi')$  are straightforward:  $L_{\lambda CS}(\sigma, \phi_s) = L_{\lambda}(\sigma, \phi_s)$  with, perhaps, a different attenuation factor due to atmospheric propagation for instance. However, the sky radiance term,  $L_{\lambda CA}(\alpha, \gamma)$ , is much more difficult and the water radiance term,  $L_{\lambda CW}(\alpha, \gamma)$  is even worse. (Subtracting out  $L_{\lambda R}$  and  $L_{\lambda a}$  in the  $(\theta', \phi')$  direction is straightforward and those components already are calculated with MODTRAN.)

The largest expected input radiance component to the cloud is the direct sunlight component,  $L_{\lambda CS}(\sigma, \phi_s)$ . With some preliminary analysis, it may be sufficient to neglect the other components. (Certainly if nearby clouds are found to greatly affect the SeaWiFS algorithms using only the  $L_{\lambda CS}(\sigma, \phi_s)$  term as input to the clouds, then using the rest of the components would only add to the impact.)

The radiance component coming from the atmosphere,  $L_{\lambda CA}(\alpha, \gamma)$ , may require many more runs of MODTRAN for the "sensor" located at the cloud position and varying  $\alpha$  and  $\gamma$ . This method would assume, for input purposes only, that the cloud is a point located at the "sensor" location. Other possibilities are to simplify  $L_{\lambda CA}(\alpha, \gamma)$  somehow with, perhaps, averaging or with the models previously discussed (Moon and Spencer, 1942; Gregg, 1990; and Bird, 1986).



The input to the clouds coming from the water surface is another challenge. Radiance coming from the water's surface is either reflected sun light or sky light or light that penetrates the surface, scatters off of something below the surface, and exits again. Further complications come from the spatial extent of both the water and the cloud so that radiance from the input angles,  $\alpha$  and  $\gamma$ , direction arrive at each spatial location on the cloud which means that cloud shadowing may be important. Two simplifications are possible: one is to only use the reflected component from the water's surface and the other is to treat the cloud as a point.

Using only the reflected component would simplify the problem, but it would slightly underestimate  $L_{\lambda cw}(\alpha, \gamma)$ . Since the goal is to look into the water we would tend towards times when the reflected component is minimized. Water has high penetrability at sun zenith angles of  $\sigma < 70^\circ$  or so (Bukata, 1995). Only these small sun zenith angles would be used which would lower the sun-water-cloud reflected component.

Treating the cloud as a point has some advantages in that the spatial extent of the cloud is ignored. That means that no shading occurs on the water surface and only one set of radiances from the  $(\alpha, \gamma)$  directions,  $L_{\lambda cw}(\alpha, \gamma)$ , is needed. Proceeding with this method, the water leaving radiance in all directions would be calculated assuming a cloudless sky ( $L_{\lambda c}(\theta, \phi) = 0$ ) and set equal to  $L_{\lambda cw}(\alpha, \gamma)$ . The water leaving radiance would then be re-calculated with the new input  $L_{\lambda}(\theta, \phi)$  (in which  $L_{\lambda c}(\theta, \phi) \neq 0$ ) and only the component toward the sensor is used. Obviously, this method requires

many more computations than simply using the reflected component or ignoring the water component altogether. We must also keep in mind the accuracy obtained by the extra calculations with respect to the accuracy of the reflectance from the cloud.

The above discussion and all of the associated uncertainty provides only one portion of the calculation of  $L_{\lambda c}(\theta, \phi)$ . We also need to define the cloud itself and that is where most of the uncertainty lies (Várnai, 1996).

It is difficult to define what is a cloud and what is not a cloud (Várnai, 1996). Determining the bi-directional reflectance from this ill-defined phenomenon is even more difficult. There are large uncertainties in the actual cloud definition which somewhat alleviates the accuracy requirements of the input radiance to the cloud itself. Therefore, ignoring the radiance from the water as an input to the cloud should not greatly affect the overall uncertainty. I'll use this same simplification later in the aforementioned elegant and simple  $L_{\lambda c}(\theta, \phi)$  determination method.

Several models can be found in the literature that can help determine  $L_{\lambda c}(\theta, \phi)$  once the cloud is defined and the radiance into the cloud is known. One promising existing and available code called *Streamer* was written by Jeffery Key at Boston University (Key, 1998). An advantage of *Streamer* is its mirror to MODTRAN for several input parameters including the surrounding atmospheric makeup and the geometry. (That is an advantage to those who use MODTRAN extensively; it may be a disadvantage to some.) However, a disadvantage of using *Streamer* is the complexity of running the code and of the actual code itself.

The Institute of Atmospheric Physics' cloud model previously mentioned is a Monte Carlo based code that calculates the bi-directional reflectance factor for a given input direction and a defined set of output directions. The data set that constitutes the cloud is a three-dimensional set of extinction coefficients and a three dimensional scattering phase function. The code can use simple model geometry (such as plain parallel clouds) to complex inhomogeneous 3-D varying models. (Várnai, 1998)

As previously stated, if the Monte Carlo based code is used, the "input" direction for the bi-directional reflectance factor calculations will be the reciprocal to the  $(\theta', \phi')$  direction and  $R(\theta', \phi'; \alpha, \gamma)$  is set equal to  $R(\alpha, \gamma; \theta', \phi')$  via reciprocity. The  $L_{\lambda C}(\theta', \phi')$  component to  $L_{\lambda}(\theta, \phi)$  is then found by summing the radiance reflected by the cloud to the point on the water surface from each cloud input direction.

$$L_{\lambda C}(\theta', \phi') = \left[ \sum_i \sum_j L_{\lambda CS/A}(\alpha_i, \gamma_j) R(\alpha_i, \gamma_j; \theta', \phi') \right] \tau_c - L_{\lambda a}(\theta', \phi') - L_{\lambda R}(\theta', \phi') \quad \text{EQ 4}$$

That is a lot of work with a lot of uncertainty in the cloud definition and a lot of uncertainty in the radiance into the cloud which equates to even more uncertainty in  $L_{\lambda C}(\theta', \phi')$ . Further, all of these calculations are for that one cloud in that one location and that one moment in time (since the atmosphere and the cloud will change as a function of time).

## **An Elegant and Simple Method**

A few paragraphs back we concluded that since the uncertainties in the cloud definition were expected to be large, ignoring the water leaving radiance component should not appreciably impact the total radiance coming from the direction of the cloud. This same argument may be taken further: since large uncertainties exist for ANY cloud size, shape, elemental particles, scattering functions,..., why not simply use representative radiances for  $L_{\lambda C}(\theta', \phi')$  and let that define the cloud? The impact analysis could surely be performed using radiance values. This greatly simplified and elegant method would rely solely on finding representative radiance values to use for  $L_{\lambda C}(\theta', \phi')$  in the impact analysis. Four methods jump immediately to mind for finding the representative radiances: we could use the two codes and the associated methods previously discussed; we could use values gleaned from the literature; we could use the cloud models built in to MODTRAN; or we could use measured data from representative clouds.

Literature reviews yielded little help below  $1\mu\text{m}$  for either reflectance values or cloud leaving radiance values. Both of the cloud prediction codes were highly dependent on the cloud definition data and virtually any spectral response can be generated with the "right" cloud definitions. The MODTRAN method and measurements both produced better results.

Using MODTRAN provided excellent results easily and quickly. I set up MODTRAN by putting my sensor just above the clouds and looked down at several

different look angles and an earth surface of zero reflectance. I used several clouds built in to MODTRAN. I ran the same scenario with the sensor just below the clouds and looking up at several angles. With the output from these runs I was able to generate a family of curves for the spectral radiance exiting the MODTRAN modeled clouds.

The family of cloud spectral response curves generated with this method all had very similar spectral shapes. The relative magnitudes, however, varied by more than a factor of 15 from the brightest clouds to the darkest clouds that I was able to generate. Figure 9 shows some of the cloud spectral response data. The shape of the cloud spectral response was found by averaging representative bright, medium, and dark cloud spectral responses. In Figure 9(a) the cloud spectral response in radiance ( $\mu\text{W}/\text{cm}^2 \cdot \text{sr} \cdot \text{nm}$ ) is plotted along with the sun's forward scattering radiance after equating the total integrated radiance of the two spectral files. This is the cloud reference spectral radiance data used in most of the study. The third plot in Figure 9(a) is the cloud reference spectral radiance scaled by a factor of 0.3 and represents one of the brightest clouds found using the MODTRAN method discussed. In Figure 9(b), the cloud spectral response from Figure 9(a) was scaled by a factor of 0.065 and plotted along with the average sky radiance using the entire hemisphere. In both Figure 9(a) and Figure 9(b) the cloud spectral response is certainly less blue and more green and red (which yields a visually white cloud) than either the sun forward scatter or the average sky component.

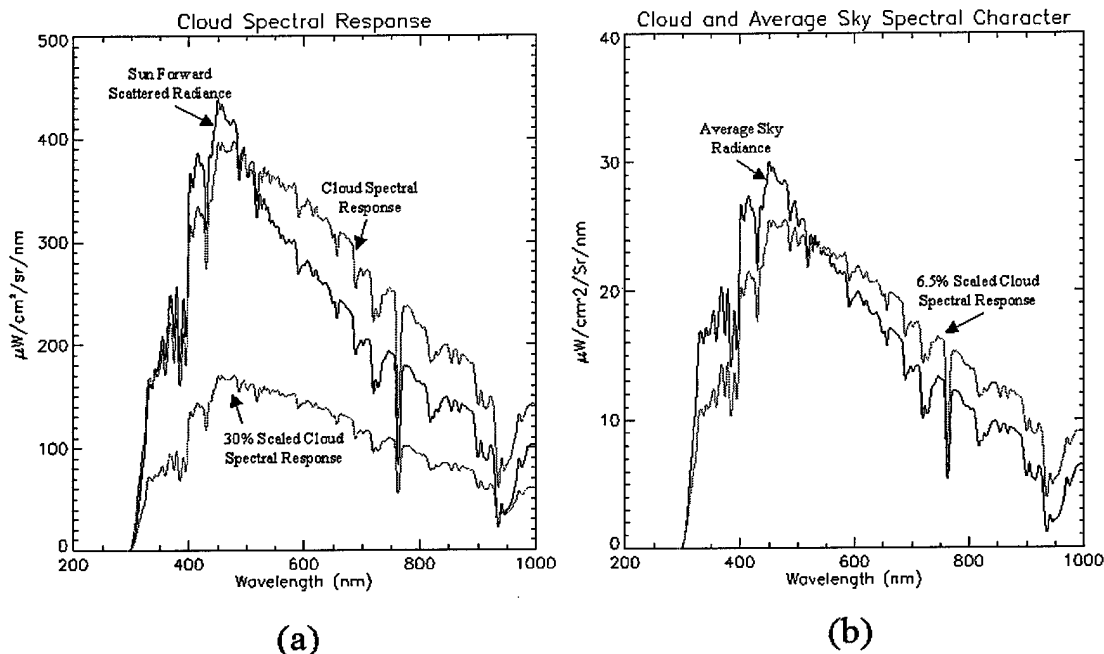


Figure 9: Cloud Spectral Response Curves compared to (a) the sun forward scattering term and (b) the average sky term. In (a) the cloud spectral response in radiance ( $\mu\text{W}/\text{cm}^2\cdot\text{sr}\cdot\text{nm}$ ) is plotted along with the sun's forward scattering radiance after equating the total integrated radiance of the two spectral files. The third plot is the cloud spectral radiance scaled by a factor of 0.3 and represents one of the brightest clouds found using the MODTRAN method discussed. In (b), the cloud spectral response from (a) was scaled by a factor of 0.065 and plotted along with the average sky radiance using the entire hemisphere. In both (a) and (b) the cloud spectral response is certainly less blue and more green and red than either the sun forward scatter or the average sky component.

The family of cloud spectral curves generated with the MODTRAN method also provides the range of representative values for "bright" clouds to "dark" clouds. Using the larger cloud spectral response from Figure 9(a) as the normalizing curve, the cloud family ranged from scale factors of 0.35 to 0.015 with a very bright cloud having a scale factor above 0.25 and a very dark cloud having a scale factor below 0.03.

Similar data were obtained by spectrally measuring the radiance from representative clouds using an Analytical Spectral Devices, Incorporated, (ASD) Full Range (FR) Spectroradiometer. Some of these data are shown in Figure 10. The

spectral radiance from several clouds is plotted in Figure 10(a); obviously, the spectral character of these real clouds is not as well behaved as the MODTRAN family of clouds. Some of the clouds show a flatter spectrum and some show a less flat spectrum. The average of 70 cloud data sets is plotted along with the average of 40 blue sky data sets in Figure 10(b). These data show many similarities with the data in Figure 9. The biggest differences between the ASD measurements and the MODTRAN predictions include the variability in the measured cloud spectral data (from cloud to cloud as shown in Figure 10) and the overall flatness of the measured data is less than the MODTRAN data. That is, the measured clouds and the measured sky were both more blue and less red than the MODTRAN predictions. The ratios of sky to cloud, however, were very similar.

The data in Figure 10 are all normalized to have the same total integrated radiance from 350nm to 1000nm. Some clouds obviously have much more blue content and much less red content than other clouds. This variability between clouds is much more than the MODTRAN method would lead us to believe. However, spectral character similar to the MODTRAN predictions does seem to exist in real clouds. Therefore, it is reasonable to use the MODTRAN predictions as the cloud spectral response data.

This simple and elegant method has a minor flaw in that there is no accounting for the cloud's impact to its surroundings. That is, a true cloud would actually shadow a portion of the atmosphere from direct sunlight and I do not account

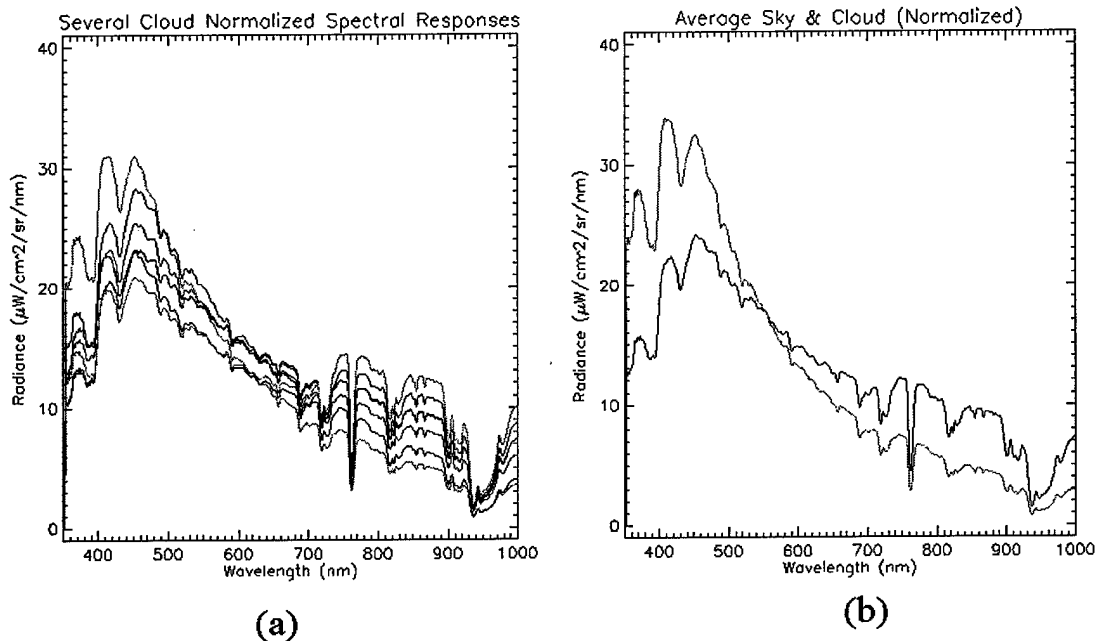


Figure 10: Measured Cloud Spectral Data. These data show several cloud spectral responses (a) and the average cloud along with an average sky spectral response (b). An Analytical Spectral Devices, Incorporated, Full Range Spectroradiometer was used to collect the data. In (a) we can see that the spectral character of clouds has much more variability than the MODTRAN predictions would imply. The data were normalized to have the same integrated radiance in both (a) and (b) which means that some clouds in (a) have less blue and more red than other clouds and vice versa. Averaging all of these yields the darker curve in (b) the represents the average spectral character from the measured clouds.

for that. Also, true clouds would reflect light to the atmosphere causing it to be brighter. I do not account for that either. Finally, the light reflected off of clouds and then off of the atmosphere increases the upwelled radiance as well.

Fortunately, this last interaction may not be a problem. If clouds are far from the line between the sensor and the point on the water surface, they will not attenuate the water leaving radiance nor greatly enhance it (i.e. the "i" type photons in **Figure 2** reflecting off of clouds are negligible). Further, if clouds are in between the point on the surface and the sensor, then the radiance exiting the point may not be important



at all because the cloud contamination is too large and even the current SeaWiFS algorithms flag the data with direct path clouds (Barnes, 1994). However, if a highly reflecting cloud is close to the line between the detector and the point on the water surface then the upwelling radiance along that line *may* be augmented significantly. However, a quick review of the results section will show that the clouds tend to contaminate the remotely sensed data due primarily to reflected light off the water surface. That means that the sensor's line of sight for most of the contaminated data is far from the actual cloud itself.

Summarizing the **RADIATION IN AIR** section, the input radiance to the water's surface,  $L_\lambda(\theta, \phi)$ , is calculated using the measured exo-atmospheric solar irradiance along with the MODTRAN generated atmospheric transmittance for the direct sun ( $L_\lambda(\sigma, \phi_s)$ ) and MODTRAN for Rayleigh and aerosol components ( $L_{\lambda R}(\theta, \phi)$  and  $L_{\lambda a}(\theta, \phi)$  respectively). The cloud component,  $L_{\lambda c}(\theta, \phi)$ , comes from scaling the MODTRAN generated cloud spectral response by a factor representative of the particular cloud we're trying to model. (If we're modeling a bright cloud, the scale factor would be above 0.25 and if we're modeling a very dark cloud it would be below 0.03.)

## TRANSITION FROM AIR TO WATER

The input to the air-water interface is the magnitude of the radiance entering the water in all directions,  $L_\lambda(\theta, \phi)$ , at the point of interest on the surface. To maintain

consistency with the rest of the development,  $L_{\lambda}(\theta, \phi)$  will be renamed to  ${}^+L_{\lambda}^{\downarrow}(\theta, \phi)$  to indicate above the surface (+) heading down ( $\downarrow$ ) at many angles  $(\theta, \phi)$  with a wavelength dependence ( $\lambda$ ). The output will be the magnitude of the down directed radiance just below the surface in all directions,  ${}^-L_{\lambda}^{\downarrow}(\theta, \phi)$ . The transition through the water relies on the shape of the surface waves and the refractive index of the water. Multiple reflections in the water (between waves) are also considered. Visualizing the output from this module will be a key component to understanding the underwater light field. Methods similar to Figure 6 will be used.

The work of Cox and Munk (1954, 1955, 1956) provides a model of the sea surface for varying wind speeds that is the consistent choice used in the literature. A more recent study by Khristoforov (1992) using a laser inclinometer agrees with the classical Cox and Munk work.

The Cox and Munk work was completed in open ocean waters. A review of the literature to search for a similar model for surface roughness of large lakes and for near shore conditions was not productive. One small study performed by Duntley around the same time as the original Cox and Munk work indicates good agreement with their findings (Duntley, 1954). The other works that were found all refer to the original work by Cox and Munk.

Due to the continuously varying nature of the surface, the underwater light field,  ${}^-L_{\lambda}^{\downarrow}(\theta, \phi)$ , and the reflected light field,  ${}^+L_{\lambda}^{\uparrow}(\theta, \phi)$ , are scaled probability density functions (PDFs) in two dimensions. These 2-D PDFs are the result of passing each

input vector,  ${}^+L_{\lambda}^{\downarrow}(\theta_i, \phi_i)$ , through the faceted wave surfaces with orientation and slope defined by the Cox and Munk equations (EQ 5). The probability distribution function for a surface wave to have a slope  $\beta$  with a direction of steepest descent  $\zeta$  (from the downwind direction) was empirically derived by Cox and Munk to be given by EQ 5.

$$p(\beta, \zeta) = (2\pi\sigma_c\sigma_u)^{-1} e^{-\frac{1}{2}(a^2+b^2)} \left[ 1 - \frac{1}{2}c_{21}(a^2-1)b - \frac{1}{6}c_{03}(b^3-3b) + \frac{1}{60}(a^4-6a^2+3) + 0.03(a^2-1)(b^2-1) + \frac{23}{2400}(b^4-6b^2+3) + \dots \right]$$

EQ 5

where  $\sigma_c$  = Cross Wind RMS slope component =  $(0.003 + 0.00192W)^{1/2}$   
 $\sigma_u$  = Upwind RMS slope component =  $0.056214W^{1/2}$   
 $W$  = Wind speed  
 $a = -\tan(\beta)\sin(\zeta)/\sigma_c$   
 $b = -\tan(\beta)\cos(\zeta)/\sigma_u$   
 $C_{21} = 0.01 - 0.0086W$   
 $C_{03} = 0.04 - 0.033W$

To get the probability for a specific wave orientation, EQ 5 is quantized in equal  $d\beta$  and  $d\zeta$  steps so that an approximate probability is easily obtained. A full set of  $\beta, \zeta$  orientations combined with the input radiance distribution,  ${}^+L_{\lambda}^{\downarrow}(\theta, \phi)$  and Snell's law,

$$n_1 \sin(\theta_1) = n_2 \sin(\theta_2)$$

EQ 6

yields the PDF of the radiance below the surface heading down,  ${}^-L_{\lambda}^{\downarrow}(\theta, \phi)$ ; replacing Snell's Law with the law of reflection yields the reflected radiance above the surface heading up,  ${}^+L_{\text{ref}}^{\uparrow}(\theta, \phi)$ . However, we must be careful in applying the laws of refraction and reflection for the three dimensional geometry under consideration.

Referring to Figure 11 which illustrates a wave facet defined by  $\beta, \zeta$  oriented within the geometry

defined by Figure 4, the objective is to find the distribution angles above and below

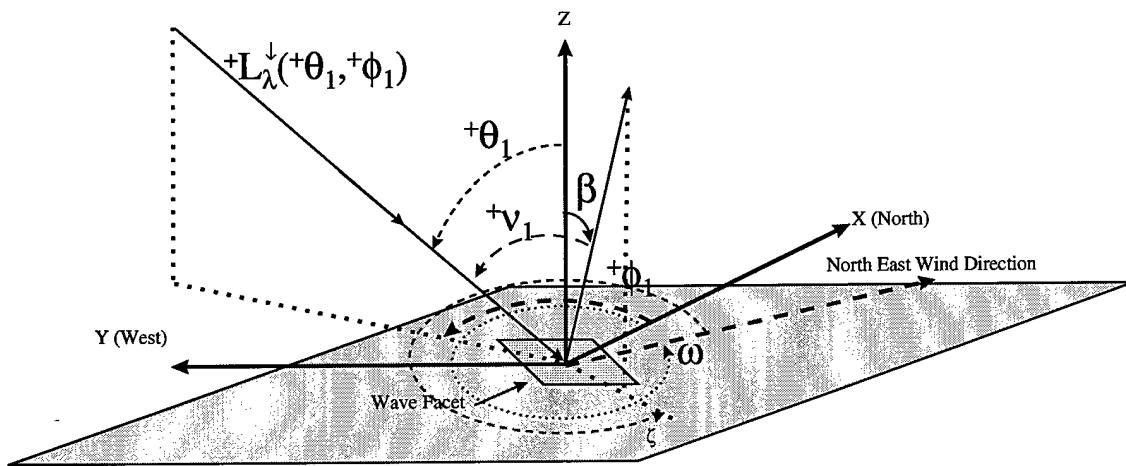


Figure 11: Geometry For A Wave Facet Defined By  $\beta$  And  $\zeta$ . The wind direction from North is defined here as  $\omega$ . A particular input radiance at  $+\theta_1$  and  $+\phi_1$  is illustrated. The objective is to find  $L_{\lambda}^{\downarrow}(-\theta_1, -\phi_1)$  and  $L_{\lambda}^{\uparrow}(+\theta_{1ref}, +\phi_{1ref})$  or more directly,  $-\theta_1, -\phi_1, +\theta_{1ref}$ , and  $+\phi_{1ref}$ . Refer to the next two figures.

the surface,  $(+\theta_{1ref}, +\phi_{1ref})$  and  $(-\theta_1, -\phi_1)$ , corresponding to the input radiance angles above the surface  $(+\theta_1, +\phi_1)$  (see Figure 12 and Figure 13). If we define the wind direction from due North as  $\omega$  and the angle between facet normal and the input radiance  $+L_{\lambda}^{\downarrow}(+\theta_1, +\phi_1)$  as  $+v_1$ , then  $+v_1$  and  $-v_1$  can be found using spherical trigonometry and Snell's Law from

$${}^+v_1 = \cos^{-1} \left\{ (\cos({}^+\theta_1) \cos(\beta) + \sin({}^+\theta_1) \sin(\beta) \cos({}^+\phi_1 - \omega - \zeta)) \right\}$$

EQ 7

$${}^-v_1 = \sin^{-1} \left( \frac{n_{air}}{n_{water}} \sin({}^+v_1) \right)$$

EQ 8

To derive the equations for reflection in three dimensions I use the fact that the vector difference between the incident radiance and the reflected radiance must lie on the surface normal with a magnitude given by the law of reflection as  $2\cos(v)$ . This yields three equations (for the three dimensions) and two unknowns ( $\theta_{ref}$  and  $\phi_{ref}$ ) with the angle ambiguity removed using the third equation. Specifically, the reflected declination angle is given by

$${}^+\theta_{1ref} = \cos^{-1} \{ 2 \cos({}^+v_1) \cos(\beta) - \cos({}^+\theta_1) \}$$

EQ 9

and the reflected azimuthal angle is given by either

$${}^+\phi_{1ref} = \cos^{-1} \left\{ \frac{2 \cos({}^+v_1) \sin(\beta) \cos(\zeta + \omega) + \sin({}^+\theta_1) \cos(180^\circ + {}^+\phi_1)}{\sin({}^+\theta_{1ref})} \right\}$$

EQ 10

or

$${}^+\phi_{1ref} = \sin^{-1} \left\{ \frac{2 \cos({}^+v_1) \sin(\beta) \sin(\zeta + \omega) + \sin({}^+\theta_1) \sin(180^\circ + {}^+\phi_1)}{\sin({}^+\theta_{1ref})} \right\}$$

EQ 11

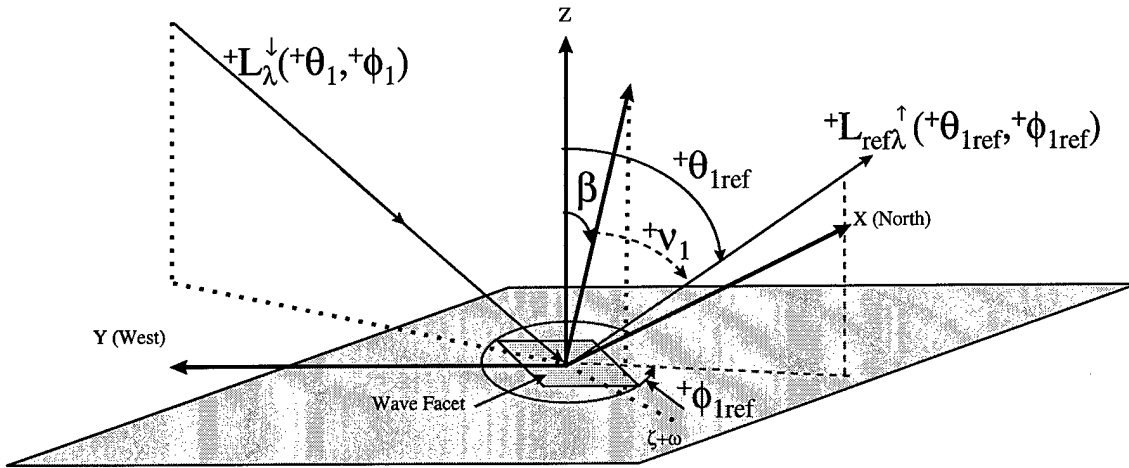


Figure 12: Geometry of Reflection off a Wave Facet. Here the reflection angles,  $+\theta_{1ref}$  and  $+\phi_{1ref}$ , correspond to the specific input angles,  $+\theta_1$  and  $+\phi_1$ , and the wave facet slope and direction angles,  $\beta$  and  $\omega + \zeta$  according to the development in the text. The magnitude of the reflected radiance,  $+L_{ref\lambda}^{\uparrow}(+\theta_{1ref}, +\phi_{1ref})$ , is obtained by multiplying the input radiance magnitude by the reflection coefficient to get  $|+L_{ref\lambda}^{\uparrow}(+\theta_{1ref}, +\phi_{1ref})| = \rho |+L_{\lambda}^{\downarrow}(+\theta_1, +\phi_1)|$  where  $\rho$  is a function of  $+v_1$ .

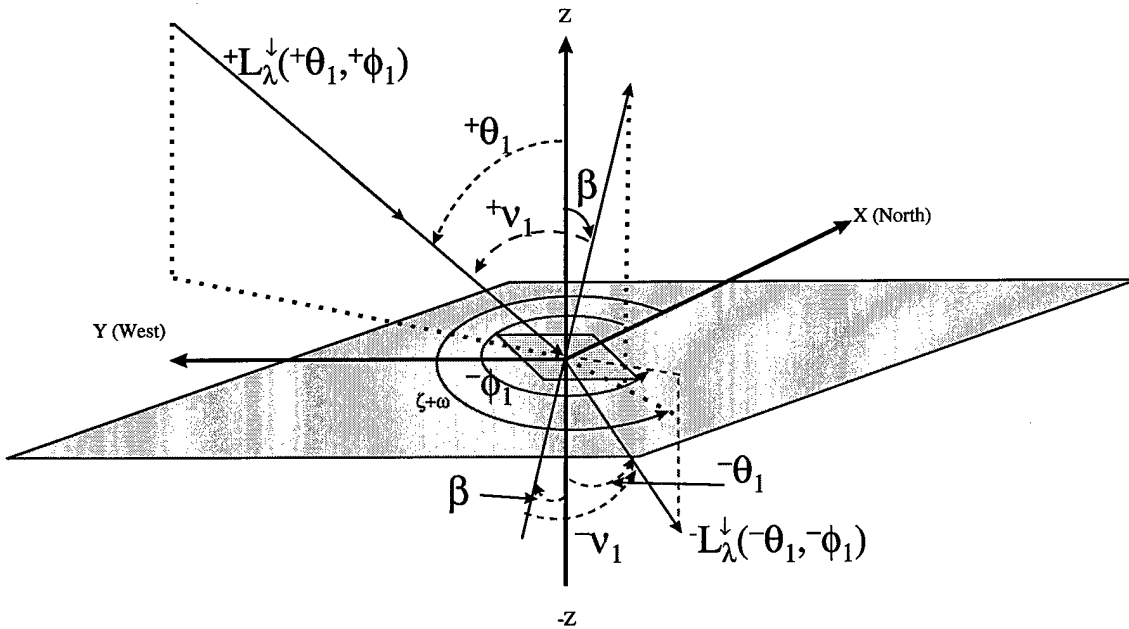


Figure 13: Geometry Of Refraction Through A Wave Facet. Here the refraction angles,  $-\theta_1$  and  $-\phi_1$ , correspond to the specific input angles,  $+\theta_1$  and  $+\phi_1$ , and the wave facet slope and direction angles,  $\beta$  and  $\zeta + \omega$  according to the development in the text. The magnitude of the refracted radiance,  $-L_{\lambda}^{\downarrow}(-\theta_1, -\phi_1)$ , is obtained by multiplying the input radiance magnitude by one minus the reflection coefficient to get  $-L_{\lambda}^{\downarrow}(-\theta_1, -\phi_1) = (1 - \rho) +L_{\lambda}^{\downarrow}(+\theta_1, +\phi_1)$  where  $\rho$  is a function of  $+v_1$ .

Due to the ambiguity associated with the arccosine and arcsine, both EQ 10 and EQ 11 are used to determine the particular  $+\phi_{1\text{ref}}$  required. (By using the arguments of EQ 10 and EQ 11 the correct quadrant can be easily determined. Given the correct quadrant, the ambiguity is removed.)

The magnitude of the reflected radiance is simply a matter of multiplying the magnitude of the input radiance by the reflection coefficient in the  $+v_1$  direction. The reflectance of the air/water interface can be readily computed from the Fresnel Reflectance formulae

$$\rho_{\perp} = \frac{\sin^2(\theta_i - \theta_r)}{\sin^2(\theta_i + \theta_r)} \quad \text{EQ 12}$$

$$\rho_{\parallel} = \frac{\tan^2(\theta_i - \theta_r)}{\tan^2(\theta_i + \theta_r)} \quad \text{EQ 13}$$

and

$$\rho = 0.5 \frac{\sin^2(\theta_i - \theta_r)}{\sin^2(\theta_i + \theta_r)} + 0.5 \frac{\tan^2(\theta_i - \theta_r)}{\tan^2(\theta_i + \theta_r)} \quad \text{EQ 14}$$

The three reflection coefficients represent perpendicular polarization ( $\rho_{\perp}$ ), parallel polarization ( $\rho_{\parallel}$ ), and random polarization ( $\rho$ ). Random polarization is assumed throughout the development of the model. The angles in EQ 12 through EQ

14 are for the incident ( $\theta_i$ ) and refracted ( $\theta_r$ ) angles, which correspond to  ${}^+v_1$  and  ${}^-v_1$  respectively.

With the above development, we can compute the magnitude and the direction of the reflected radiance from the air/water interface for each input radiance vector and for each input wave facet. Further, we can compute the probability of each wave facet orientation with the added input of wind speed and direction. Therefore, each input radiance vector will produce a probability distribution of reflected radiance vectors. Summing the distributed reflected radiance vectors derived from each input radiance vector and each wave facet will yield the total reflected radiance vector distribution. A similar development is required for the refracted radiance.

The magnitude of the refracted radiance through a given wave facet is found using  $(1-\rho)$  times the magnitude of the input radiance for the  ${}^+v_1$  incident angle. That is the easy part. I derived the refraction angles,  ${}^-\theta_1$  and  ${}^-\phi_1$ , using a three-dimensional form of the law of refraction and similar logic as with the reflection equations. Specifically, using the fact that the vector difference between the incident radiance and the product of the index of refraction and the refracted radiance must lie on the facet normal, I derived the following relationships:

$${}^-\theta_1 = \cos^{-1} \left\{ \frac{k_w \cos(\beta) - \cos({}^+\theta_1)}{-n_w} \right\}$$

EQ 15

and



$$^{-}\phi_1 = \cos^{-1} \left\{ \frac{k_w \sin(\beta) \cos(\zeta + \omega) + \sin(^+\theta_1) \cos(180^\circ + ^+\phi_1)}{n_w \sin(^-\theta_1)} \right\} \quad \text{EQ 16}$$

and to again remove the ambiguity,

$$^{-}\phi_1 = \sin^{-1} \left\{ \frac{k_w \sin(\beta) \sin(\zeta + \omega) + \sin(^+\theta_1) \sin(180^\circ + ^+\phi_1)}{n_w \sin(^-\theta_1)} \right\} \quad \text{EQ 17}$$

In the above equations,  $n_w$  is the index of refraction in the water normalized to the index of refraction of the air (which is assumed to be 1) and  $k_w$  is the magnitude of the unitized difference vector along the facet normal and is found from

$$k_w = \cos(^+\nu_1) - n_w \cos \left( \sin^{-1} \left( \frac{\sin(^+\nu_1)}{n_w} \right) \right) \quad \text{EQ 18}$$

Similar to the reflected radiance distribution,  $^{+}\text{L}_{\text{ref}}^{\uparrow}(\theta, \phi)$ , the below the surface downward radiance distribution,  $^{-}\text{L}_{\lambda}^{\downarrow}(\theta, \phi)$ , becomes a matter of summing all contribution combinations from the above water downward distribution,  $^{+}\text{L}_{\lambda}^{\downarrow}(\theta, \phi)$ , and the probability of wave orientation,  $p(\beta, \zeta)$  scaled by one minus the reflection coefficient

(refracted) or by the reflection coefficient (reflected) and the square of the index of refraction<sup>4</sup>:

$$^{-}L_{\lambda}^{\downarrow}(\theta, \phi) \Big|_{\text{binned}} = \sum_i \sum_j \sum_k \sum_l {}^{+}L_{\lambda}^{\downarrow}(\theta_i, \phi_j) p(\beta_k, \zeta_l) (1 - \rho_{ijkl}) n_w^2$$

EQ 19

and

$$^{+}L_{\text{ref } \lambda}^{\uparrow}(\theta, \phi) \Big|_{\text{binned}} = \sum_i \sum_j \sum_k \sum_l {}^{+}L_{\lambda}^{\downarrow}(\theta_i, \phi_j) p(\beta_k, \zeta_l) (\rho_{ijkl})$$

EQ 20

Note that each set of i, j, k, and l will correspond to a particular ( $^{-}\theta$ ,  $^{-}\phi$ ) and ( $^{+}\theta_{\text{ref}}$ ,  $^{+}\phi_{\text{ref}}$ ) but the total contribution to each ( $^{-}\theta$ ,  $^{-}\phi$ ) and ( $^{+}\theta_{\text{ref}}$ ,  $^{+}\phi_{\text{ref}}$ ) direction will come from several sets of i, j, k, and l combinations. The  $|_{\text{binned}}$  nomenclature results. Note also that EQ 19 and EQ 20 refer only to the source radiance to the water coming from the sky, sun, and clouds and hitting the water surface. (The full radiative transfer equations are discussed later.)

For this development, the wind speed and direction are the only inputs that effect the facet model. One tacit assumption in the literature is that the surface wave distribution is the same temporally and spatially. In fact, the Cox and Munk work would not apply if the ergodic assumption is not true; however, the assumption is

---

<sup>4</sup> The  $n^2$  comes from the fundamental theorem of radiometry: "the radiance divided by the square of the index of refraction is constant along any path". See Wyatt (1978) or Mobley (1994).

most likely correct. In Duntley's measurements that agree with Cox and Munk, he used an electrical measurement system of closely spaced wires to directly measure the wave slopes versus wind speed over time (Duntley, 1954). Agreement between Duntley's measurements and Cox and Munk makes the ergodic assumptions very plausible.

The index of refraction could also be a variable input to the model. I do not expect the index of refraction to greatly affect the overall radiance reaching the sensor for "normal" values of  $\sim 1.33$  or so. Though the index of refraction for natural waters is both known and a function of wavelength as in Figure 12, the affects of added chlorophyll, suspended minerals and dissolved organic material is unknown. Therefore, a nominal value of  $n=1.33$  is used in the simulations performed here.

### **Some Anomalous Cases**

Now that the geometry is defined for both reflected and refracted radiance, shadowing and multiple reflections can be addressed. These cases can best be visualized using the defined and derived geometry while highlighting some anomalous points.

For instance, when the reflection declination angle,  $\theta_{\text{ref}}$ , is greater than  $90^\circ$ , the reflected radiance MUST reflect back into the air/water interface. The reflected radiance in that case is added to the input radiance at  $\theta = (\theta_{\text{ref}} - 90^\circ)$  and  $\phi = \phi_{\text{ref}}$  to arrive at a new input radiance from that direction.

# Water Refractive Index

No Salt; T = 0 to 30 C

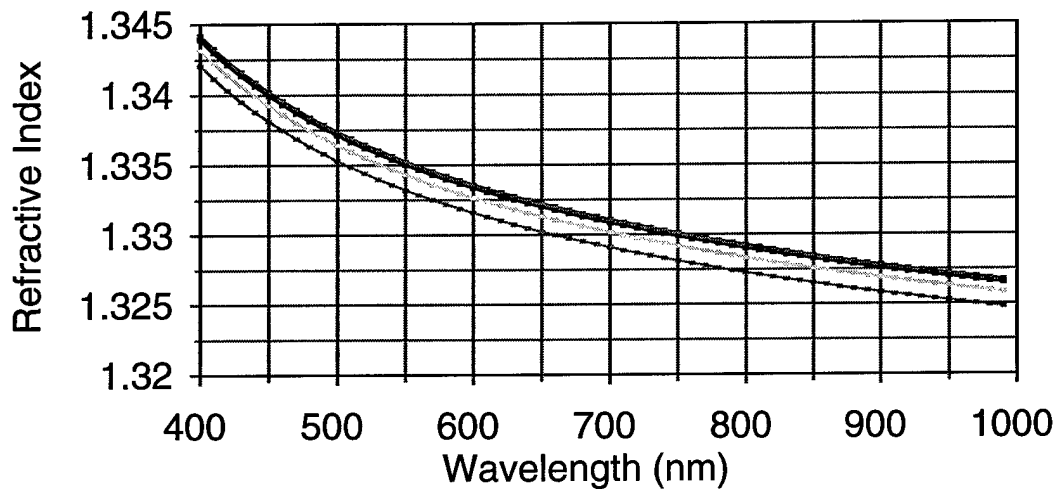


Figure 14: Refractive index for fresh water as a function of wavelength for temperatures ranging between 0°C and 30°C. Data generated using Quattro Pro 7 with equations of Quan and Fry (1995).

Another anomaly occurs when  $\theta_{v1}$  is greater than  $90^\circ$ . For  $\theta_{v1} > 90^\circ$ , the input radiance is more than  $90^\circ$  away from the normal to the wave facet for the radiance and wave facet under question. In other words, the wave facet is shadowed to that radiance vector. For that case, the input radiance vector is not used.

The next anomaly occurs when  $\theta_1$  is greater than  $90^\circ$ . This is an extremely rare condition. In words,  $\theta_1 > 90^\circ$  means that the refracted radiance enters that water at an angle that greatly increases the probability of exiting the water. This brings some difficult choices: the photons enter the water, travel some distance, and, if they don't scatter off anything, exit the water, but how far do they travel and what are the orientations of the exit facets? The distance and orientation of the exit facet require more information than provided by EQ 5.

One possible solution is to assume that all photons that produce  $\theta_1 > 90^\circ$  immediately impinge on the water/air interface (from the water side) for facets oriented with the same probabilities as given by EQ 5. This solution is reasonable considering the small number of photons for which it would apply. Note that to get  $\theta_1 > 90^\circ$  we need to have  $\beta > 90^\circ$  which immediately eliminates at least  $\frac{1}{2}$  the geometry due to shadowing alone. The probability of having a wave facet with  $\beta > 90^\circ$  is also very small (Cox and Munk, 1956) and, finally, the act of refraction further reduces the number of photons that would produce  $\theta_1 > 90^\circ$ . With all the caveats and reduced probabilities, it is safe to assert that the number of photons producing  $\theta_1 > 90^\circ$  is vanishingly small.

Two other anomalies occur that would normally be difficult to track. They are:

- (1) photons that fail to reach a wave facet due to shadowing by another wave facet and
- (2) reflected photons with  $\theta_{1ref} < 90^\circ$  that re-enter the air/water interface due to localized geometry (See Figure 15). For both of these cases, the number of photons

under consideration is relatively small. (Note that the geometry indicated in Figure 15 is greatly exaggerated to illustrate the anomalous conditions. In reality, such peaks do not normally exist in surface waves per Cox and Munk, 1956.)

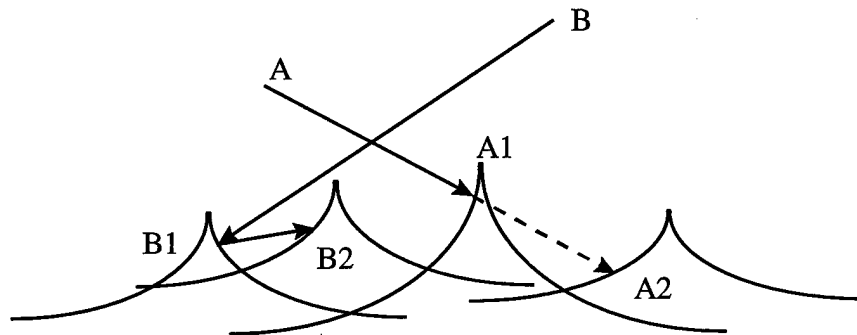


Figure 15: Facet-to-facet Shadowing and Multiple Reflection. Photons coming from direction of "A" fail to impinge on point A2 due to shadowing at A1 and photons that come from direction of "B" reflect at B1 and re-enter the water at B2 even though the reflection declination angle is less than  $90^\circ$ . The sea surface wave geometry is greatly exaggerated for illustration purposes.

The probability for wave orientation given in EQ 5 does not give the entire wave shapes, nor can the shapes be derived from the original Cox and Munk work (Cox and Munk, 1956). To accurately assess the numbers of photons that are facet-to-facet shadowed or reflected requires knowledge of the overall wave shape that we do not possess. We have a method empirically derived by Neumann and reported by Preisendorfer (1976, Vol. 4) to relate the wave elevation probabilities to wind speed, but we do not have any correlation data for the wave slopes. North (1990) provides a way (via multiple assumptions and simplifications) to estimate the shape of the

surface waves. However, North's purposes did not require the accuracy needed for radiance transfer and using his results would simply trade one set of unknown information for another.

If we examine the effects of ignoring facet-to-facet shadowing, we find that the resulting radiance at the sensor would be slightly over estimated because the radiance reaching point A2 in Figure 15 would be slightly over estimated. Further, we note that most of the facet-to-facet shadowing will occur for input radiance coming from very high declination angles ( $\theta_1$  approaching  $90^\circ$ ). (Remember that self-shadowing is already addressed.) EQ 5 tells us that most of the surface waves have fairly low slopes (almost all are less than  $45^\circ$ ) which pushes the  $\theta_1$  even closer to  $90^\circ$  for facet-to-facet shadowing. Combining this with the Fresnel reflectance formula we find that most of the radiance we neglect by neglecting facet-to-facet shadowing is reflected radiance and the reflection angles would be near the horizon. Therefore, I conclude that neglecting facet-to-facet shadowing slightly overestimates the radiance reaching the sensor, but the overestimate is extremely small for sensor angles away from the horizon.

Using the same development, we find that omitting photons that are facet-to-facet reflected with  $\theta_{1ref} < 90^\circ$  will slightly underestimate and rearrange the radiance reaching the sensor. Not addressing this facet-to-facet reflection would give a reflected radiance in the  $\theta_{1ref}$  that is slightly too large and slightly underestimate the radiance in some other  $\theta_{ref}$  direction due to the double reflection at point B2 in Figure

15. The radiance entering the water at point B2 would also be underestimated and, therefore, so is the radiance exiting the water. The directional information is difficult to even localize without more knowledge than is given in the studies by Cox and Munk, but it appears as though the underestimated radiance is most likely spread over a large angular sector that would tend to reduce the error in any one direction. The anomaly also occurs very rarely so the uncertainty is further reduced. Yet, the affect remains unknown and (via mental methods) seems to reach a maximum for mid-level incidence angles.

That conclusion seems to agree with a study completed by Preisendorfer and Mobley (1986). Their numerical study via Monte Carlo methods indicated that multiple reflections occur between 5 and 10 percent of the time for incident angles between about  $50^\circ$  and  $80^\circ$  and wind speeds above 10 m/sec. These multiple reflections act to redistribute the radiance (Mobley, 1994). However, the study did not delineate between  $+\theta_{1ref} > 90^\circ$  and  $+\theta_{1ref} < 90^\circ$ . Nor did it give probability distributions for reflection angles; it only gave probabilities for multiple reflections.

Repeating their work would get one step closer to the actual radiance distributions above and below the water. However, Preisendorfer and Mobley did not have any correlation data for wave slopes and they assumed complete randomness. Correlation data for wave slopes is not found in the literature to date. The completely random assumptions will certainly provide data, but the data may not be accurate.



Even so, the inaccuracies seem to be limited for the anomalous cases discussed above. Therefore, the work of Preisendorfer and Mobley (1986) as repeated and coded by Mobley (1995) as part of the Hydrolight computer code is used here to pass the light through the air/water interface.

## UNDER WATER REFLECTION MODELS

Several underwater reflection models have been reported in the literature including the works that were previously cited (Gordon, 1975; Kirk, 1984; Kirk, 1991; Morel, 1993; Bukata, 1981; Mobley, 1994; and Jerome, 1988). Bukata (1995) summarizes most of the referenced work and explains the problems and advantages associated with each. He goes further to address several areas of concern specifically related to the Laurentian Great Lakes. One Monte Carlo based code used by Jerome (1996) was seriously considered for the main underwater module in this study for two reasons. The reasons are: (1) it was used by Jerome and Bukata to help derive the suspended materials (SM) impact results previously discussed; and (2) it applies an easily understood method (Monte Carlo) in a straightforward manner. One drawback to Jerome's code is that it was designed for light entering the water from only one direction. I would have had to modify the code to take advantage of the three-dimensional radiance field below the water surface.

A second concern comes from the lack of good quality measurements in the literature for optical cross sections of suspended minerals, chlorophyll-a, and/or dissolved organic matter (DOM) for wavelengths outside the 400nm-750nm region.

Bukata (1981, #1) defines these three groups as generic components of natural waters and he and Jerome build their models using the three groups. At the May 1998 International Association of Great Lakes Research conference, one of the main points in the remote sensing unit was the lack of good optical cross sections (Bukata, 1998). Others in the field echo these statements (Pegau, 1995; Maffione, 1997).

A third concern comes from the fact that at each point (or "cell") the input light is traveling in all directions. The size of the "point", or cell, will depend on the eventual sensor in question (1.13 km x 1.13 km for SeaWiFS; Barnes, 1994). Adjacent cells will certainly impact the light under each cell; there will be more impact at the edges and deeper beneath the cells. For large cells such as SeaWiFS, the effect is probably negligible; for smaller cells such as our in-house MISI sensor (with spatial resolution on the order of a few feet) the effect could be major in a cell by cell basis. Since most remote sensing systems have resolutions much larger than a few feet, ignoring the adjacent cell effect should not be a problem. Also, even for small MISI type cells, we could assume that the radiance scattered in would be the same as the radiance scattered out and, thereby, ignore the cell size.

The essence of the underwater model is that light travels through the water until it reflects off of materials within the water or until it is totally absorbed. The further the light travels, the more it is absorbed. Reflection off of material will alter the direction of the light. Sometimes multiple reflections are required before the light exits the water; often the light does not exit the water before being totally absorbed.

With all of the reflecting and direction changes occurring, Monte Carlo methods certainly lend themselves to this environment and they are easy to understand.

Another promising technique (and the one eventually adopted) is the method of invariant imbedding detailed in Preisendorfer, 1976, (Vol. 4) and explained by Mobley (1994). Invariant imbedding's greatest assets are that the entire radiance field,  $L_{\lambda}^{\uparrow}(\theta, \phi)$ , can be calculated with one sweep using matrix methods and that statistical residual errors normally found with Monte Carlo methods are non-existent.

The invariant imbedding technique used in the Hydrolight code by Mobley (1995) is not as easy to understand as Monte Carlo methods. In fact, Mobley's textbook, "Light and Water", (1994) is almost entirely devoted to setting up and describing the invariant imbedding solution method for the radiative transfer equations under water. I will not repeat that here. The Hydrolight code is enough of an industry standard and its mathematical techniques are documented well enough to use it, with slight modifications, for the underwater module (Schott, 1998). The modifications that were required are covered in the appendices. Hydrolight numerically solves the radiance transfer equations given in EQ 21 through EQ 24 below.

$$\begin{aligned}
 {}^+L_{\lambda}^{\uparrow}(\theta, \phi) = & \int_{\Xi_+} {}^-L_{\lambda}^{\uparrow}(\theta', \phi') r((\theta', \phi') \rightarrow (\theta, \phi)) d\Omega(\theta', \phi') \\
 & + \int_{\Xi_-} {}^+L_{\lambda}^{\downarrow}(\theta', \phi') r((\theta', \phi') \rightarrow (\theta, \phi)) d\Omega(\theta', \phi') \quad \text{for } (\theta, \phi) \text{ in } \Xi_+
 \end{aligned}$$

EQ 21

$$\begin{aligned}
^{-}L_{\lambda}^{\downarrow}(\theta, \phi) &= \int_{\Xi_{-}} ^{-}L_{\lambda}^{\uparrow}(\theta', \phi') r((\theta', \phi') \rightarrow (\theta, \phi)) d\Omega(\theta', \phi') \\
&\quad + \int_{\Xi_{+}} ^{+}L_{\lambda}^{\downarrow}(\theta', \phi') r((\theta', \phi') \rightarrow (\theta, \phi)) d\Omega(\theta', \phi') \quad \text{for } (\theta, \phi) \text{ in } \Xi_{-}
\end{aligned}$$

EQ 22

$$\begin{aligned}
\cos(\theta) \frac{d^{-}L_{\lambda}^{\downarrow}(z; \theta, \phi)}{dz} &= -^{-}L_{\lambda}^{\downarrow}(z; \theta, \phi) + \tilde{S}(z; \theta, \phi) + \\
&\quad \varpi_o(z) \int_{\Xi_{\pm}} ^{-}L_{\lambda}^{\downarrow}(z; \theta', \phi') \tilde{\beta}(z; (\theta', \phi') \rightarrow (\theta, \phi)) d\Omega(\theta', \phi') \\
&\quad \text{for } (\theta, \phi) \text{ in } \Xi_{\pm}
\end{aligned}$$

EQ 23

$$\begin{aligned}
^{-}L_{\lambda}^{\uparrow}(bottom; \theta, \phi) &= \int_{\Xi_{-}} ^{-}L_{\lambda}^{\downarrow}(\theta', \phi') r_{bottom}((\theta', \phi') \rightarrow (\theta, \phi)) d\Omega(\theta', \phi') \\
&\quad \text{for } (\theta, \phi) \text{ in } \Xi_{+}
\end{aligned}$$

EQ 24

With a little explanation, EQ 21 through EQ 24 seem obvious. EQ 21 and EQ 22 refer to the radiance at the water surface. In EQ 21, the spectral radiance above the surface heading up in all directions is equal to the radiance transmitted through the surface from below plus the radiance reflected off of the surface from above. EQ 22 refers to the radiance just below the water surface heading down. It says that the spectral radiance below the water surface heading down in all directions is equal to the radiance reflected off of the surface from below plus the radiance transmitted through the surface from above. The two integrals in each of EQ 21 and EQ 22 are over the associated hemispheres. The second integral in EQ 21 is analogous to EQ 20

and the second integral in EQ 22 is analogous to EQ 19. However, here they are included as part of the complete radiance transfer equations.

More nomenclature is required for EQ 23. It refers to the spectral radiance in all directions at a particular optical depth,  $z$ , below the water surface. EQ 23 equates the change in radiance at depth  $z$  with the total radiance into the depth plus the radiance generated at the depth from internal sources  $\tilde{S}$  less the radiance exiting the depth. Here all directions and both hemispheres  $\uparrow\downarrow$  (upward and downward) are used.

Finally, EQ 24 refers to the radiance coming from the bottom and equates the spectral radiance heading up in all directions to the radiance reflected off of the bottom. We assume that there are no sources at or below the bottom.

Hydrolight solves these equations numerically without the statistical residual left from Monte Carlo methods. As previously stated, Hydrolight is used in this study for the underwater module. Hydrolight also performs the radiance transfer through the water surface for both into and out of the water. However, Hydrolight employs a wind direction invariant form of Cox and Munk's probability distribution function found in EQ 5.

### **What is in the Water**

With the decision to use Hydrolight and its invariant imbedding technique for the underwater radiative transfer solution method, the next step is to determine what is in the water to absorb and scatter light. The following sections will describe the

substances found in many natural water bodies and give the concentrations reported in the literature. Together with the absorption and scattering cross sections, the concentrations will provide the absorption coefficient,  $a(\lambda)$ , and scattering coefficient,  $b(\lambda)$  via<sup>5</sup>

$$a(\lambda) = \sum_{i=1}^n C_i a_i(\lambda) = \text{Absorption Coefficient}$$

$$b(\lambda) = \sum_{i=1}^n C_i b_i(\lambda) = \text{Scattering Coefficient}$$

EQ 25

where the  $C_i$  are the concentration levels, the  $a_i$  are the absorption cross sections and the  $b_i$  are the scattering cross sections.

Natural water bodies are comprised of an innumerable amount of substances. Knowing how these substances absorb and scatter electromagnetic energy is paramount to solving radiative transfer within water bodies. Yet the sheer number of aquatic constituents requires a simplification. Bukata (and many others) categorize these substances into five groups: pure water, dissolved salts and gases, dissolved organic matter, chlorophyll-a, and suspended matter.

---

<sup>5</sup> In practice the absorption and scattering coefficients are actually measured along with the concentrations to derive the specific cross sections. Modeling changes in the absorption and scattering coefficients, however, is often done via changes in concentrations while maintaining the fixed specific cross sections.

Dissolved salts and gases most significantly absorb or scatter light in the ultraviolet region and are normally omitted from simulations at longer wavelengths. Thus, "n" in EQ 25 is simply 4.

Excluding pure water, we're left with three groups of substances: Dissolved Organic Matter; Suspended Matter; and Chlorophyll-a. Most of the following information (and all the numeric values) comes from Bukata (1995) or sources referenced there.

### **Dissolved Organic Matter**

Dissolved organic matter (DOM) comes from two primary sources: within the water and from outside the water. The indigenous DOM is primarily the byproduct of photosynthesis by phytoplankton and the remains of decomposing (or decomposed) phytoplankton. The decomposition of the aquatic life also results in humic and fulvic acids, which create a yellowish hue. This is sometimes referred to as gelbstoff or simply "yellow substance" in the literature. DOM in open oceans is primarily the indigenous variety. (Bukata, 1995)

Nearer to shore or for lakes, another source of DOM comes from the land. Surface run-off and river discharges introduce a wide variety of DOM into the water. Further, near shore and in lakes the nutrient levels tend to be higher which, in turn, increases the indigenous DOM due to higher metabolic rates for the phytoplankton. Both sources result in higher DOM concentrations in lakes and near shore than they are in the open ocean. For instance, the literature reports various concentrations in

different inland lakes from ~1-2 gC/m<sup>3</sup> to as high as 20-25 gC/m<sup>3</sup> while open ocean levels tend to be ~0.001-0.005 gC/m<sup>3</sup> (Bukata, 1995). (The DOM concentration is reported in grams of Carbon per volume; Carbon normally makes up approximately half the DOM by weight.) Lake Ontario levels have been determined by Bukata (1980) to be around 2 gC/m<sup>3</sup>.

Even these concentration levels are still much lower than dissolved salts. However, the DOM affects light in the visible spectrum and is, therefore, important. DOM absorbs light, but the scattering coefficient is generally accepted to be small enough to ignore. Studies have shown that the absorption coefficient follows an exponential decay with increasing wavelength with a decay slope,  $s$ , between 0.011 and 0.021 (Carder, 1989 via Bukata, 1995). (The decay is from a reference point generally at 400nm or 440nm.)

### **Suspended Matter**

Suspended matter is a mix of many types of organic and inorganic material. It ranges from living and dead phytoplankton, zooplankton, and other aquatic organisms to clay, sand, and silt from land-based sources. Also included are human wastes and byproducts (including pollution); precipitated atmospheric aerosols (including volcanic ash); and specific elements, usually in the form of oxides, hydroxide, or carbonates, such as iron, magnesium, silicon, calcium, and aluminum. (The hydroxides and carbonates tend to be localized phenomenon that only exist under specific circumstances.) (Bukata, 1995)



The specific form and composition of suspended matter is spatially, temporally, and geographically variable. We can simplify the variability somewhat by removing some of the components. In fact, to get Bukata's five groups, he already has essentially removed phytoplankton (and all algae) to form the chlorophyll-a group (see below).

It is believed that zooplankton do not contribute much to the overall absorption and scattering coefficients of the water volume due to their low concentrations. Also, since zooplankton consume phytoplankton, they may have absorption and scattering characteristics very similar to phytoplankton. It seems safe to ignore the zooplankton as a special category and account for their absorption and scattering contributions via phytoplankton (chlorophyll-a) or suspended minerals. (Bukata, 1995)

Bacterioplankton cannot be ignored. Bacterioplankton can be subdivided into two groups: those with color and those without color. The colorless bacterioplankton do not absorb visible energy, but they most likely scatter visible energy. The colored subgroup, however, are referred to as bacterial chlorophylls a, b, c, and d due to their resemblance to the pigments in phytoplankton (Bukata, 1995).

The suspended minerals (sand, silt, clay...) are the most important and most troublesome of the constituents in suspended matter. (The two terms are sometimes interchanged because of this.) They can range from (3-4)  $\mu\text{m}$  in diameter (clay) to (130-250)  $\mu\text{m}$  (sand) (Adamenko via Bukata, 1995). Concentrations range from (0.02-0.17)  $\text{g/m}^3$  in the open ocean (Jerlov, 1976) to as high as (0.1-12.0) $\text{g/m}^3$  in some lakes

(Bukata, 1995). Lake Ontario concentrations have been reported at  $(0.2-8.9)\text{g/m}^3$  (Bukata, 1981 #1) They are the most troublesome because of the high scattering coefficients for these particles.

### **Chlorophyll-a**

Chlorophylls, carotenoids, and phycobilins are the three basic types of photosynthesizing agents. They are present in varying degrees in all species of phytoplankton and, therefore, algae. (Algae can be seaweed or pond scum or any of several species in between.) They are also primary ocean color constituents.

Chlorophyll itself is separated into four varieties designated a, b, c, and d. Of these, chlorophyll-a is by far the most prominent. (All green algae contain chlorophyll-a, but not all contain b and c. Of those that do contain b or c, the a to b and a to c ratios are ~3:1.) Knowing the location and concentration of chlorophyll-a would lead to locations and concentrations of phytoplankton.

Knowing those concentrations over a wide scale could lead to more accurate worldwide energy budgets for tracking global warming and/or climate and seasonal changes. In a less global sense, we could also extrapolate fish school locations with the phytoplankton knowledge. For these reasons, chlorophyll-a concentrations and locations are some of the primary reasons for water quality measurements on a large scale. (Bukata, 1995)

Unfortunately, absorption and scattering cross-sections of chlorophyll-a vary along with the alga species in the region as well as the age and cell structure and even the previous amount of light absorbed by the algae. Fortunately, the spectral shape of the various species, ages, structure, and history absorption and scattering cross-sections tends to stay roughly the same with peaks at ~440nm and ~675nm. That means that we may be able to determine that chlorophyll-a is present, but we may error on the exact concentration. Data for the Great Lakes seems to point to slightly higher than average absorption cross-sections for algae species found there. (Bukata, 1995)

Now that we've covered the four main components of natural waters (Pure Water, DOM, SM, and Chlorophyll-a) and their typical concentration levels, EQ 25 can be re-written and simplified to

$$a(\lambda) = a_w(\lambda) + C_{DOM}a_{DOM}(\lambda) + C_{SM}a_{SM}(\lambda) + C_{chl}a_{chl}(\lambda)$$

$$b(\lambda) = b_w(\lambda) + C_{SM}b_{SM}(\lambda) + C_{chl}b_{chl}(\lambda)$$

EQ 26

The final step is to determine the optical cross sections,  $a_{DOM}(\lambda)$ ,  $a_{SM}(\lambda)$ ,  $a_{chl}(\lambda)$ ,  $b_{SM}(\lambda)$ , and  $b_{chl}(\lambda)$ . The literature contains several examples. The particular water body in question tends to have its own variety of chlorophyll-a and suspended matter so the optical cross sections tend to be different. Further, the values reported in the literature tend to range in wavelength from 400nm to 700nm because that is

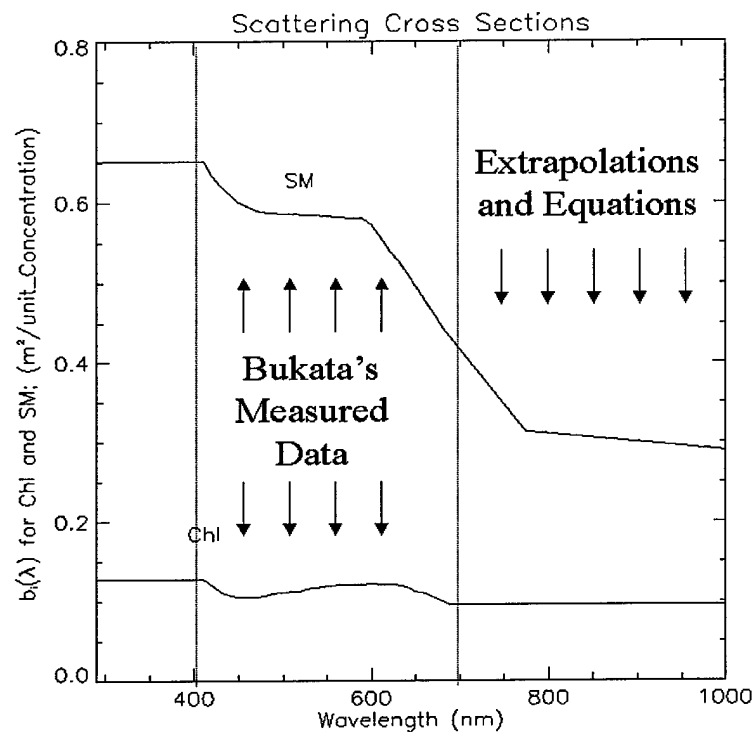


Figure 16: Scattering Cross Sections for Chlorophyll-a content and Suspended Mineral content. Curves are from Bukata (1995) using measured data (400nm to 690nm) and analytical equations (290nm to 400nm and 700nm to 1000nm)

typically where water-viewing sensors operate. For my purposes, I need data above 700nm and would like the range to run from 290nm to 1000nm. Bukata (1995) reports cross section curves for Lake Ontario waters in the 400nm to 690nm range and provides numerical equations for the key cross sections outside of that region. I used Bukata's cross section data in this study. The cross sectional curves used are given in Figure 16 through Figure 19.

These data comprise most of the input to the Hydrolight code to describe the water body. Other water parameters include internal sources such as

bioluminescence, fluorescence, and Raman scattering. These sources are modeled in Hydrolight (and modified in my version of Hydrolight), but they did not play a major role in the cloud impact analysis.

The output from the underwater module will be the upward traveling radiance in all directions,  $\bar{L}_\lambda^\uparrow(\theta, \phi)$ , at the point of interest re-entering the water/air interface. (Note that Jerome's code currently provides a volume reflectance factor for a single input angle and would need several changes to provide the  $\bar{L}_\lambda^\uparrow(\theta, \phi)$  required.) This output is then the input to the light traveling back through the water/air interface.

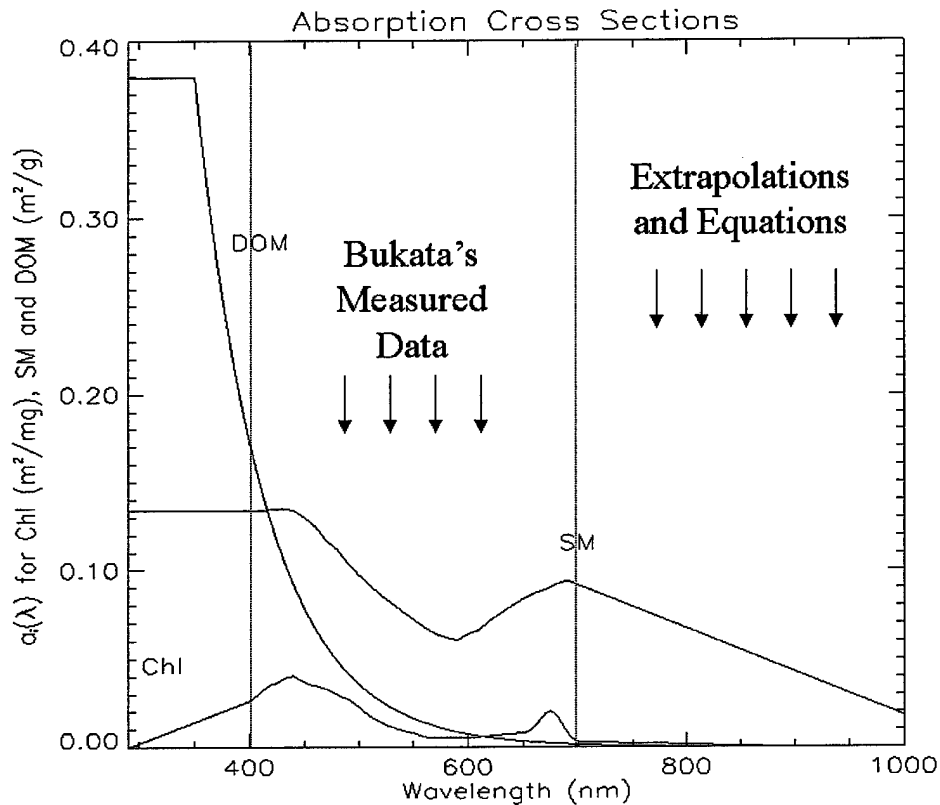


Figure 17: Absorption Cross Section curves from Bukata (1995) data (400nm to 690nm) and analytical equations (below 400nm and 700nm to 1000nm).

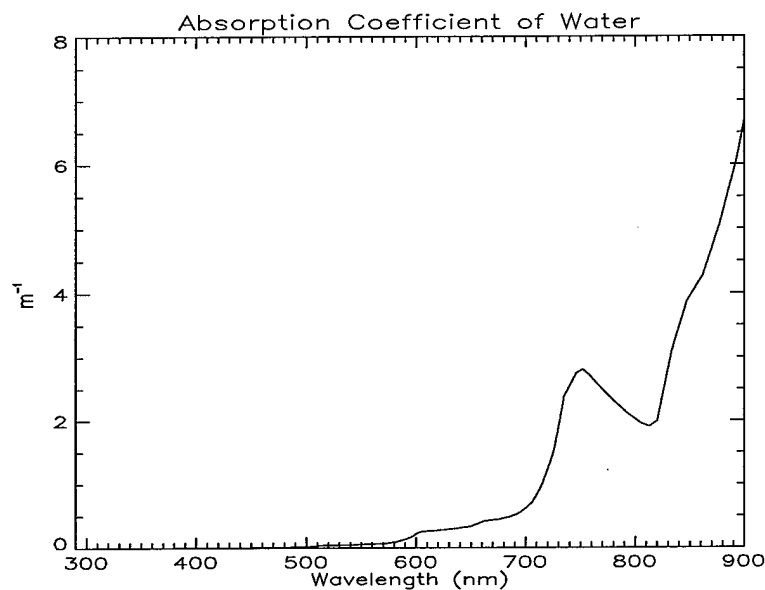


Figure 18: Absorption Coefficient for water. Note that the wavelength range is truncated at 900nm due to a peak in absorption near 914nm that would render the rest of the data non-viewable. However, we can still see large absorption coefficients above 700nm. Data from Pope (1997).

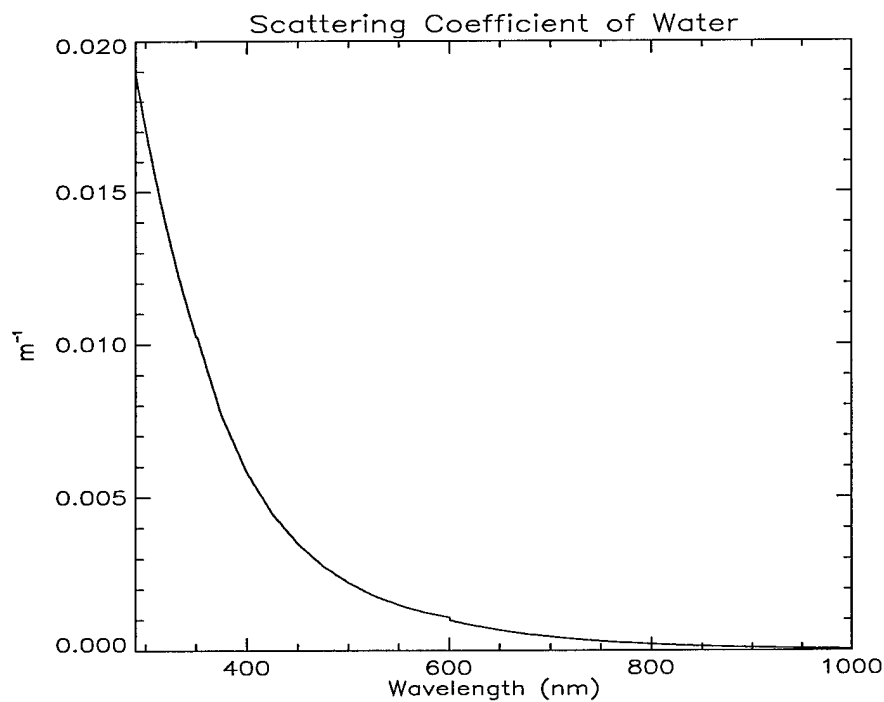


Figure 19: Scattering Coefficient for water.

## TRANSITION FROM WATER TO AIR

The model for this module is simply a reverse of the previous **Air/Water Interface** section; finding  $+L_{\lambda}^{\uparrow}(\theta, \phi)$  from the radiance distribution  $-L_{\lambda}^{\uparrow}(\theta, \phi)$  is a matter of applying the Cox and Munk probability distribution equations (EQ 5) and Snell's Law (EQ 6) to  $-L_{\lambda}^{\uparrow}(\theta, \phi)$ . Only the angles toward the detector,  $\theta_d$  and  $\phi_d$ , are of interest, so only  $+L_{\lambda}^{\uparrow}(\theta_d, \phi_d)$  is required. However, obtaining  $+L_{\lambda}^{\uparrow}(\theta, \phi)$  for several angles is a simple matter at this point. Therefore, the radiance distribution above the water surface in all directions,  $+L_{\lambda}^{\uparrow}(\theta, \phi)$  is calculated. The module is further simplified by the previous selection of Hydrolight as the underwater code. Hydrolight performs this calculation and provides the radiance above the water surface heading up in all directions,  $+L_{\lambda}^{\uparrow}(\theta, \phi)$ .

One complication arises due to possible self-shadowing or self-hiding of the wave. If the wave is oriented such that it physically blocks part of itself from the detector, then a portion of  $+L_{\lambda}^{\uparrow}(\theta_d, \phi_d)$  is lost. In fact, a *particular* portion of  $+L_{\lambda}^{\uparrow}(\theta_d, \phi_d)$  is lost that comes from the particular portion of the wave that is blocked. Determining the  $\beta_{\text{block}}$  and  $\zeta_{\text{block}}$  again requires the wave slope correlation data that is not found in the Cox and Munk probability distribution given in EQ 5. Fortunately, for small sensor declination angles the shadowing is negligible (Preisendorfer, 1986)

## PROPAGATION TO THE SENSOR

The final module in the model is propagation from the water surface, through the atmosphere, to the sensor. The radiance exiting the water is combined with the radiance reflected off the water ( $L_{ref}$  in **Figure 2** found in EQ 20) and the upwelled radiance ( $L_{path}$  in **Figure 2** and  $+L_{\uparrow R}^{\uparrow}(\theta, \phi) + +L_{\uparrow a}^{\uparrow}(\theta, \phi)$  in our current nomenclature) found from another series of MODTRAN runs. The radiance leaving the surface must be propagated to the sensor through the attenuating atmosphere.

The attenuation of the radiance between the water surface and the sensor comes from the transmission coefficient,  $\tau$ , and can be obtained in the original MODTRAN runs that produced  $L_{\lambda}(\sigma, \phi_s)$ ,  $L_{\lambda R}(\theta, \phi)$  and  $L_{\lambda a}(\theta, \phi)$  or on the upwelled radiance series. Though both sets of transmission coefficient values are equal for a space based sensor, the appropriate  $\tau$  to use comes from the upwelled radiance series of MODTRAN runs. Obviously,  $\tau$  is a function of orientation angle and is more appropriately termed  $\tau(\theta, \phi)$ . For a given atmospheric mix of water vapor, aerosols, ..., the  $\tau(\theta, \phi)$  is invariant as a function of  $\phi$ . Therefore,  $\tau$  is only a function of the declination angle and is termed  $\tau(\theta)$ .

## RADIATIVE TRANSFER MODEL SUMMARY

The end-to-end radiative transfer model has five major modules for the five regions of radiance transfer: air, air-to-water, water, water-to-air, and air again. The first module, air, has two sub-modules for the radiance due to the sun and sky (from MODTRAN) and for the radiance due to local clouds. The inputs to this module are



the properties of the air (aerosols and water vapor present and their concentrations and distributions); the cloud location, size, and extinction coefficient distributions and scattering phase functions; and the sun location. The output from the first module is  $^+L_{\lambda}^{\downarrow}(\theta, \phi)$  which is the input to the subsequent modules.

A modified form of Hydrolight accomplishes all transitioning through the air/water interface and radiance transfer within the water. The input to these sections includes the radiance distribution above the water surface,  $^+L_{\lambda}^{\downarrow}(\theta, \phi)$ , the wind speed, and the properties of the DOM, SM, and Chlorophyll-a in the water. These properties include the concentrations, optical cross sections, and changes in concentration levels as a function of water depth. Other parameters for the water module include internal sources such as Raman scattering, DOM fluorescence, bioluminescence, and chlorophyll fluorescence.

The final propagation to the detector uses transmission coefficients and upwelling radiance calculated in another set of MODTRAN runs using the same atmospheric inputs.

The total inputs required are the sun and detector locations, the properties of the atmosphere, the type and location of the clouds, the properties of the water, and the wind speed. The final output is the radiance at the detector for the location of interest on the water surface. However, the radiance distribution at (above) the water surface and below the water surface is also available. With this modular approach,

the radiance at these locations due to each individual module is also available for study.

### Chapter 3

#### SEAWIFS DERIVED CHLOROPHYLL CONTENT

Let's begin with a quick look at the SeaWiFS algorithms. The sensor senses a total radiance,  $L_{t\lambda}$ , in each of the 8 bands. The algorithms first turn this radiance into a reflectance,  $\rho_t(\lambda)$ , defined as (McClain, 1995)

$$\rho_t(\lambda) = \pi L_{t\lambda} / E_0 \cos(\sigma) \quad \text{EQ 27}$$

where  $E_0$  is the exoatmospheric solar irradiance and  $\sigma$  is the pixel centered solar zenith angle. The total reflectance is made up of several parts:

$$\rho_t(\lambda) = \rho_r(\lambda) + \rho_a(\lambda) + \rho_{ra}(\lambda) + \tau\rho_{wc}(\lambda) + T\rho_g(\lambda) + \tau\rho_w(\lambda) \quad \text{EQ 28}$$

which are the Rayleigh, Aerosol, Rayleigh/Aerosol interaction, white cap, sun glint, and water leaving components respectively. The Rayleigh and white cap components are removed via estimates of the wind speed and the surface atmospheric pressure (McClain, 1995). The sun glint component is neglected by looking away from locations that have a high sun glint (the SeaWiFS sensor tilts  $\pm 20^\circ$  to avoid sun glint). We are left with

$$\rho_t(\lambda) - \rho_r(\lambda) - \tau\rho_{wc}(\lambda) = [\rho_a(\lambda) + \rho_{ra}(\lambda)] + \tau\rho_w(\lambda)$$

EQ 29

The absorption coefficient for pure water is so high at NIR wavelengths (see Figure 18 ) that we can normally set  $\rho_w(\text{NIR})=0$ . The SeaWiFS algorithms use this to find  $\rho_a(\lambda)+\rho_{ra}(\lambda)$  at two different NIR wavelengths (765nm and 865 nm) and then use these two values with several (N) atmospheric predictions to determine the single scattering aerosol components,  $\rho_{as}(765\text{nm})$  and  $\rho_{as}(865\text{nm})$  (Gordon, 1994). There is a linear relationship, found empirically, between  $\rho_{as}$  and  $\rho_a+\rho_{ra}$ , but the linear relationship is different for each type of atmospheric makeup and each angle of observation and each wavelength (Wang, 1994). The single scattering aerosol component is needed to find

$$\varepsilon(\lambda_1, \lambda_2) = \frac{\rho_{as}(\lambda_1)}{\rho_{as}(\lambda_2)}; \quad \varepsilon(765\text{nm}, 865\text{nm}) = \frac{\rho_{as}(765\text{nm})}{\rho_{as}(865\text{nm})}$$

EQ 30

The value of  $\varepsilon(765\text{nm}, 865\text{nm})$  is used to find  $\varepsilon(\lambda, 865\text{nm})$  via another empirically derived linear relationship (Gordon, 1994), and then  $\rho_{as}(\lambda)$  is determined. Also, the value of  $\varepsilon(765\text{nm}, 865\text{nm})$  found above will fall in between two of the  $\varepsilon(765\text{nm}, 865\text{nm})$ s determined from the N atmospheres used in the predictions. These two atmospheres (in the same ratios) are used to find  $\rho_a(\lambda)+\rho_{ra}(\lambda)$  once  $\rho_{as}(\lambda)$  is known. Now, finally, we can subtract out  $\rho_a(\lambda)+\rho_{ra}(\lambda)$  and divide by the transmittance,  $\tau$ , to find  $\rho_w(\lambda)$ . Samples of the empirically derived curves are found in Figure 20.

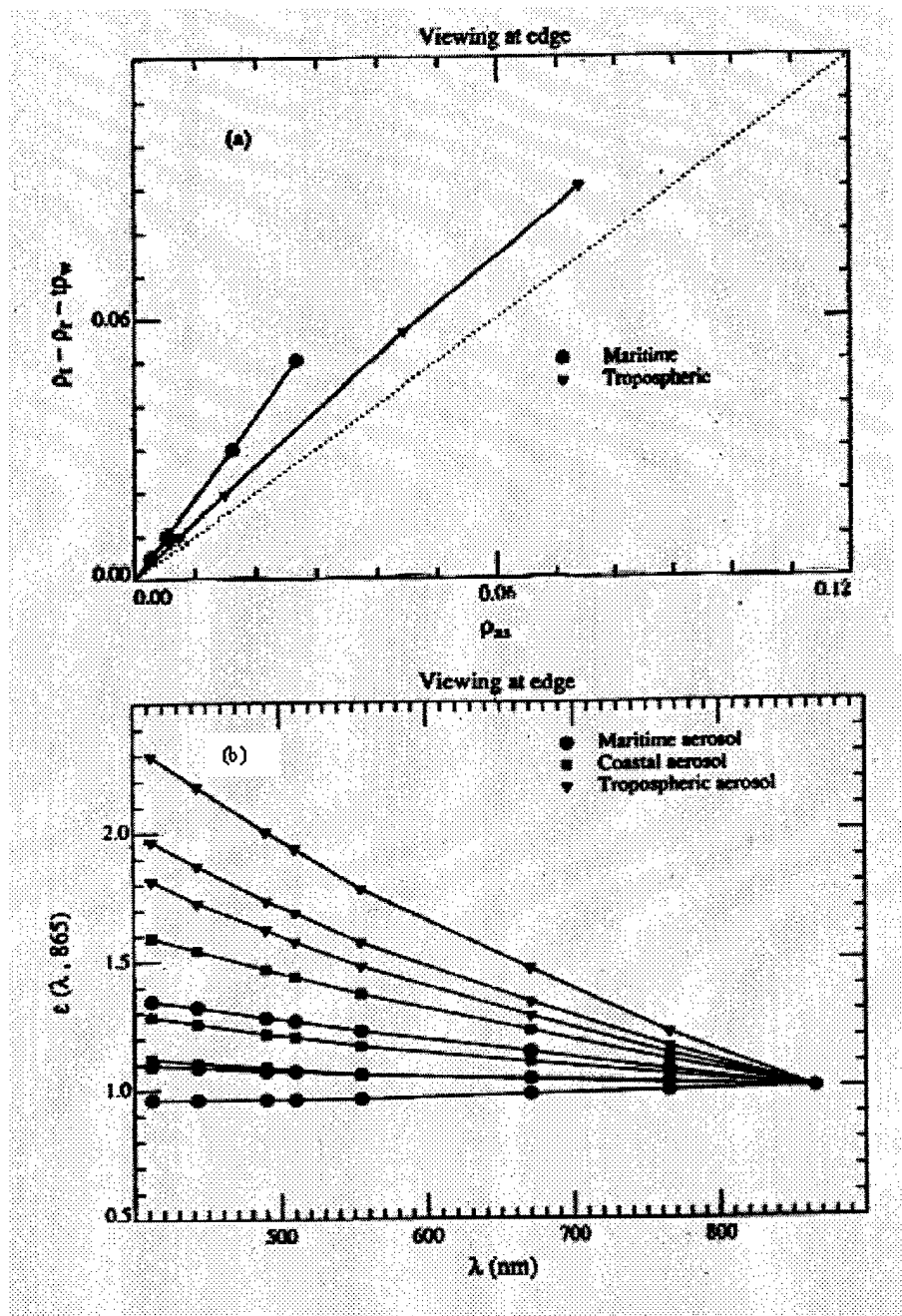


Figure 20: Two Sample Empirical Relationships Scanned from Gordon (1994). In (a) the relationship between  $\rho_a(443\text{nm}) + \rho_{Ra}(443\text{nm})$  and  $\rho_{as}(443\text{nm})$  at the edge of the SeaWiFS scan is presented for two different atmospheres. The relative humidity level for the tropospheric atmosphere was set at 70% and for the Maritime atmosphere it was set at 98%. Each SeaWiFS view angle, wavelength and atmosphere would use a different curve such as the two found in (a). In (b),  $\epsilon(\lambda, 865\text{nm})$  is plotted as function of  $\lambda$  for 9 specific atmospheres (the three listed with RH of 70%, 90%, and 98%) at the edge of the SeaWiFS scan. A separate relationship is used for each atmosphere and each look angle. Few examples such as these are found in the literature.

The chlorophyll-a content is determined from the reflectance for bands 3 and 5 (centered at 490nm and 555nm respectively) using another empirically derived formula. McClain (1995) terms the formula "Ocean Color 2" or simply OC2 and gives the chlorophyll-a content as

$$Chlor\_a = 10^{(0.3410 - 3.001R + 2.811R^2 - 2.041R^3)} - 0.40 \quad (\mu g / l) \quad \text{EQ 31}$$

$$\text{where } R = \text{Log}_{10} \left( \frac{\rho_w(\lambda = 490nm)}{\rho_w(\lambda = 555nm)} \right) \quad \text{EQ 32}$$

However, Acker (1998) reports that the SeaWiFS algorithm for chlorophyll-a content has changed. Though the exact coefficients are not published, recent correspondence indicates that the algorithm will remain the same and the coefficients in the algorithm changed to yield (Hooker and Firestone, 1999)

$$Chlor\_a = 10^{(0.2974 - 2.2429R + 0.8358R^2 - 0.0077R^3)} - 0.0929 \quad (\mu g / l) \quad \text{EQ 33}$$

We may expect that both the algorithm and the coefficients used in EQ 32 and EQ 33 will be periodically updated to reflect new ground truth data results.

Notwithstanding the uncertainties in the empirical algorithms, we note three additional possible problems with this process:

- (1) We assumed that we could look away from highly reflecting areas when we set  $\rho_g=0$ . Therefore, glint from clouds,  $\rho_{cg}$ , is not included.
- (2) We assumed that the water's high absorption coefficient for NIR overshadowed the scattering coefficient(s) of material in the water and from the surface reflection component.
- (3) The empirically derived equations do not account for source radiance spectrum flattening which may result from large "white" clouds reflecting energy to the water.

Problems (1) and (2) will most likely have the largest impact on the chlorophyll-a determination. The flatter spectral response from the clouds, however, is a very real phenomenon that must be considered. The average ratio between  $+L_{\lambda=765nm}^{\downarrow}(\theta,\phi)$  and  $+L_{\lambda=865nm}^{\downarrow}(\theta,\phi)$  for the input cloudless sky ranges from 1.23 for rural atmospheres to 1.3 for very clear tropospheric atmospheres, while the same cloud ratio is very close to 1.0. The  $+L_{\lambda=490nm}^{\downarrow}(\theta,\phi)$  and  $+L_{\lambda=555nm}^{\downarrow}(\theta,\phi)$  ratio is even worse. It ranges from 1.24 to 1.5 for the input cloudless skies and is still very close to 1.0 for the cloud spectral response. (These data are based on several MODTRAN runs and include the averages over the bands as defined by SeaWiFS.)

Problem (2) above is highly suspended matter dependent. The suspended matter problem is not studied as part of this effort. Dr. Robert Bukata and colleagues are attacking the issue directly for Lake Ontario waters. Concisely,  $\rho_w(765nm) \neq 0$

$\neq \rho_w(865\text{nm})$  as is assumed in the algorithm because substantial concentrations of suspended minerals combined with the scattering cross section cause some light to exit the water even in the NIR. Obviously, higher concentrations of suspended matter (as found in the Laurentian Great Lakes) will produce even higher scattering coefficients, which, in turn, deviates  $\rho_w$  further from 0. Until the Bukata work is complete or another study is performed, we can only speculate as to the impact of the suspended matter on  $\rho_w(765\text{nm}) \neq 0 \neq \rho_w(865\text{nm})$  and the associated atmospheric subtraction.

It is reasonable to assume that the water leaving reflectance ratio for  $\lambda=765\text{nm}$  and  $\lambda=865\text{nm}$ ,  $\rho_w(765)/\rho_w(865)$ , is greater than the atmospheric ratio,  $(\rho_a(765\text{nm})+\rho_{ra}(765\text{nm})) / (\rho_a(865\text{nm})+\rho_{ra}(865\text{nm}))$ , when suspended matter is present. That is because the spectral absorption coefficient of water increases for increasing wavelength while the spectral scattering coefficient for suspended matter tends to decrease with increasing wavelength. That means that the error in finding  $\rho_a(765\text{nm})+\rho_{ra}(765\text{nm})$  is larger than the error in finding  $\rho_a(865\text{nm})+\rho_{ra}(865\text{nm})$  by an unknown amount (due to  $\rho_w(765) > \rho_w(865)$ ). Using the SeaWiFS algorithms, the errors propagate to  $\rho_{as}(765\text{nm})$  and  $\rho_{as}(865\text{nm})$  and then to  $\epsilon(765\text{nm},865\text{nm})$ . (The error in  $\rho_{as}(765\text{nm})$  is greater than the error in  $\rho_{as}(865\text{nm})$  and both are too large. Unfortunately, it is not possible to determine whether  $\epsilon(765\text{nm},865\text{nm})$  is too large or too small.) With an inflated  $\epsilon$ , the determined atmospheric contribution for bands 3 and 5,  $\rho_a(490\text{nm})+\rho_{ra}(490\text{nm})$  and  $\rho_a(555\text{nm})+\rho_{ra}(555\text{nm})$ , will be inflated with band 3



error greater than band 5 error. This translates to calculating  $\rho_w(490\text{nm})$  and  $\rho_w(555\text{nm})$  that are too small with  $\rho_w(490\text{nm})$  having the most error. Again, unfortunately, we cannot speculate on the affect this error has on the ratio between  $\rho_w(490\text{nm})$  and  $\rho_w(555\text{nm})$  without more knowledge about both the error and the original ratio. We can say that if the ratio between  $\rho_w(490\text{nm})$  and  $\rho_w(555\text{nm})$  is reduced, then the SeaWiFS algorithms would predict more chlorophyll-a in the water than it would without the suspended matter and if the ratio is increased the opposite would occur. (See Figure 21). This speculation can be confirmed with the same computer model used in the cloud study.

Obviously, adding suspended matter to the water will not appreciably change the atmospheric contamination to the data, but the SeaWiFS algorithms will have an error in the aerosol determination due to the non-zero water leaving radiance at NIR. It is ultimately the non-zero NIR water leaving radiance that causes most of that error and we see the same error caused by clouds. Additional contributions come from the increased scattering in the visible region due to the suspended matter.

For clouds, we have two problems to worry about. The biggest expected impact is from cloud glint. SeaWiFS tilts to avoid the sun glint so that  $\rho_g = 0$ . However, it is possible for clouds to reflect sun light in non-predictable (a priori) directions, producing cloud glint that SeaWiFS does not avoid. Clouds will make  $\rho_{cg} > 0$ . In this case, the questions to be asked are: "When is  $\rho_{cg}$  increased enough to impact SeaWiFS derived volume reflectance and chlorophyll-a levels? What cloud locations,

concentrations, and distributions affect the data and by how much? How “bright” do they need to be?”

Answering these questions by varying the types, locations, concentrations, distributions, and “brightness” of clouds in a controlled way is the essence of this study. In each case, the model calculates the radiance at the sensor and the water leaving radiance in each band. From there, the SeaWiFS algorithms are employed to determine the impact of the clouds on the SeaWiFS derived products.

The sources of the impact to the SeaWiFS products are the non-zero  $\rho_{cg}$  and the flatter or “white” cloud spectral response. Both sources of error will affect both the 765nm/865nm atmospheric subtraction algorithm and the 490nm/555nm chlorophyll-a determination algorithm. In fact, for the atmospheric subtraction algorithm, the chain of events leading to errors in the SeaWiFS derived chlorophyll-a content is exactly the same as those previously discussed for the suspended matter case with one exception: the  $\rho_w(765nm)/\rho_w(865nm)$  ratio (due to clouds and the non-zero  $\rho_{cg}$ ) is often less than the atmospheric ratio. (Recall that the discussion for the suspended matter case started with a greater water leaving radiance ratio due to the suspended matter.)

The empirically derived chlorophyll-a formula (EQ 32) is affected similarly by the flattened spectrum. If we assume, for the moment, that we can find the true volume reflectance values,  $\rho_w(490nm)$  and  $\rho_w(555nm)$  then we can determine the expected impact of the clouds on the chlorophyll-a content while ignoring the affect of the atmosphere. In fact, it becomes a simple matter.

Clouds have a flatter spectrum (essentially a 1:1 ratio between 490nm and 555nm) so at lower true chlorophyll levels (when the water leaving 490nm to 555nm ratio is greater than 1:1), the ratio in EQ 32 would be smaller with clouds present then it would be without clouds present. For instance, with minimal chlorophyll and very blue water,  $\rho_w(490)/\rho_w(555)$  may be something like 1.5. Adding in a cloud to the scene with its flatter 1.0 ratio would reduce  $\rho_w(490)/\rho_w(555)$  to, say 1.45. A smaller ratio yields a higher calculation for chlorophyll content.

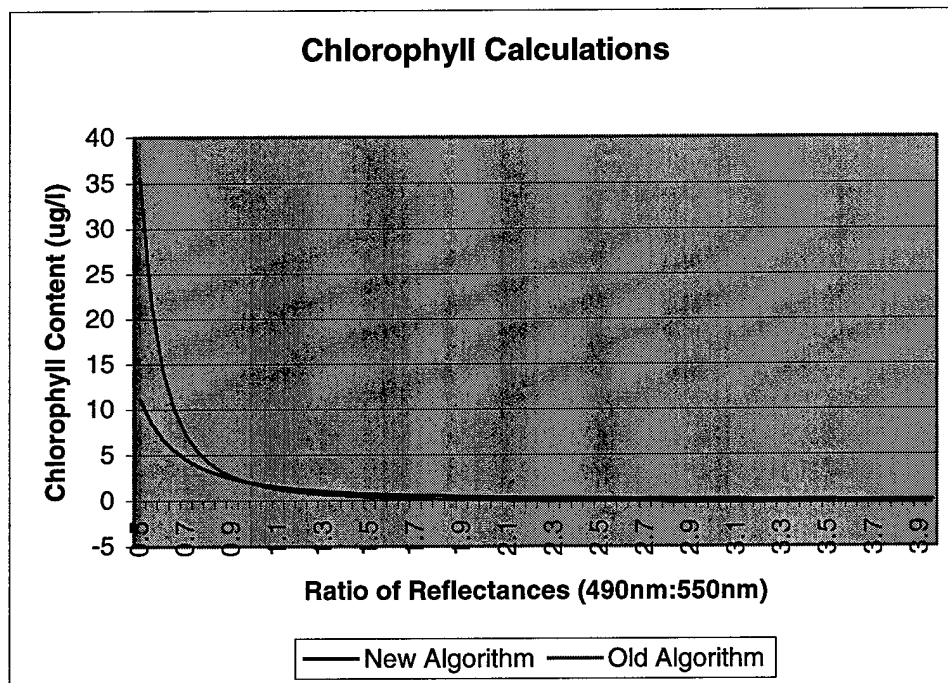


Figure 21: Affect of changing the reflectance ratio on the calculated chlorophyll content. For waters that are more blue than green, the  $\rho_w(490nm) : \rho_w(555nm)$  ratio is greater than one. For waters that are more green than blue, the ratio is less than one

At higher true chlorophyll levels (green water and  $\rho_w(490)/\rho_w(555)$  around 0.8 for instance), the flatter spectrum caused by the clouds would tend to increase the  $\rho_w(490\text{nm})$  to  $\rho_w(555\text{nm})$  ratio (to, say, 0.83) and an underestimate of the chlorophyll content results. These conclusions apply using both EQ 31 and EQ 33 as illustrated in Figure 18.

## Chapter 4

### SEAWIFS CLOUD STUDY SCOPE

HydroMod is the radiative transfer code created for this effort by combining MODTRAN and Hydrolight together with other capabilities previously discussed (see Appendix I and II). The flexibility built into HydroMod makes it applicable to any water body for any wind speed and atmosphere and any sun location or any detector at any wavelength (from 290nm to 1000nm). The cloud impact characterization problem, however, can be scoped by only considering the input parameters that apply for the Laurentian Great Lakes and the SeaWiFS sensor. Physical laws also apply to further limit the scope of the study.

The reflectance of the air/water interface can be readily computed from the Fresnel Reflectance formulae repeated here

$$\rho_{\perp} = \frac{\sin^2(\theta_i - \theta_r)}{\sin^2(\theta_i + \theta_r)} \quad \text{EQ 34}$$

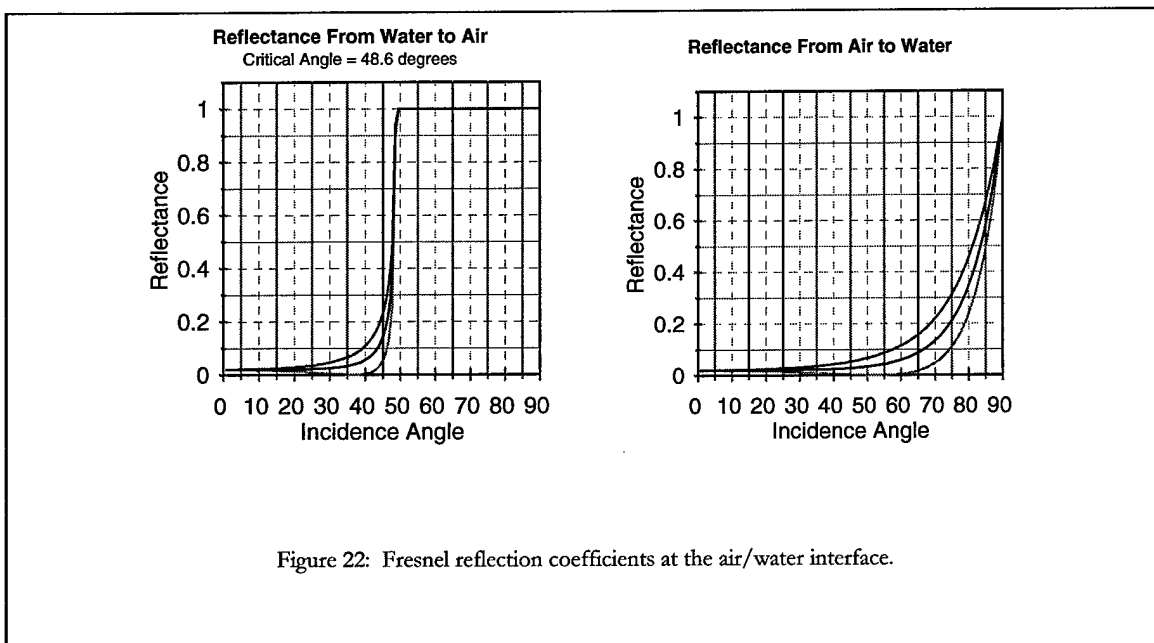
$$\rho_{\parallel} = \frac{\tan^2(\theta_i - \theta_r)}{\tan^2(\theta_i + \theta_r)} \quad \text{EQ 35}$$

and

$$\rho = 0.5 \frac{\sin^2(\theta_i - \theta_r)}{\sin^2(\theta_i + \theta_r)} + 0.5 \frac{\tan^2(\theta_i - \theta_r)}{\tan^2(\theta_i + \theta_r)}$$

EQ 36

which yield the graphs found in Figure 22. The three reflection coefficients represent perpendicular polarization ( $\rho_{\perp}$ ), parallel polarization ( $\rho_{\parallel}$ ), and random polarization ( $\rho$ ).



For light hitting the air/water interface from above ( $+L_{\lambda}^{\downarrow}(\theta, \phi)$ ) the reflectance coefficient is very high (20%) for incidence angle above  $\theta = 75^{\circ}$  or so. Thus, a good upper limit for the sun location,  $\sigma$ , would be  $\sigma \leq 75^{\circ}$ .

Noting the location of the Laurentian Great Lakes relative to the earth/sun system, we see that the highest  $\sigma$  would be found at local noon at the summer solstice at or near the southern most point of the lakes. The Tropic of Cancer is at  $23^{\circ} 27'$

north latitude and the southern end of Lake Erie is at  $41^{\circ}22'$  north latitude. Ignoring the radius of the earth with respect to the sun-earth distance yields an absolute minimum  $\sigma$  of  $17^{\circ}55'$  (including the full geometry would increase  $\sigma_{\min}$  slightly). Therefore, the sun input angles are limited to  $18^{\circ} \leq \sigma \leq 75^{\circ}$ . Using an even more limited range may be prudent; for most of the time over most of the Great Lakes,  $\sigma_{\min}$  is considerably greater than  $18^{\circ}$ . The sun's azimuth angle,  $\phi_s$ , is similarly limited and is a function of location of the point of interest and the declination angle.

The atmospheric aerosol models will be limited to only those applicable over the Great Lakes region. Specifically, the Maritime, Urban and Rural atmospheres with varying visibility will be used. The "standard" atmosphere for the cloud study is the MODTRAN standard Maritime atmosphere with 23 Km visibility and a sun location at  $41^{\circ}$  declination. The Maritime atmosphere is chosen so that the results found here will apply to world-wide coastal zones in addition to the Great Lakes.

Similarly, the water quality models (including optical cross sections and concentrations) used by Bukata and Jerome (1995 through 1998) are used since they are characteristic of the Great Lakes. These data and the extensions above 700nm and below 400nm wavelengths are given in Figure 16 through Figure 19.

Nominal prevailing winds in the Great Lakes region tend toward 5 to 15 knots (2.57 to 7.72 m/sec) in an east-northeast direction (various web based sources). Wind speeds in excess of 18 knots (9.27 m/sec) introduce enough whitecaps that they impact the water's reflectance values too much (Gordon, 1997). Since the objective is to

characterize the affect of clouds, it is reasonable to minimize the expected white caps. Therefore, wind speeds are limited to 0 m/sec through 9 m/sec. This limitation has the added affect of eliminating most of the facet-to-facet scattering that occurs when the light first enters the water (Preisendorfer and Mobley, 1986).

The SeaWiFS sensor has a maximum scan angle of  $58.3^\circ$  and can tilt  $\pm 20^\circ$  from nadir to avoid the direct sun glint (Barnes, 1994). For a flat earth, this would limit  $\theta_d$  to less than  $60.4^\circ$ . Using an earth mean radius of 6371km, the limit on  $\theta_d$  for a spherical earth is  $74.95^\circ$ . The azimuth angle,  $\phi_d$ , is not limited ( $0^\circ \leq \phi_d < 360^\circ$ ).

The cloud models used in the study are described in *Radiance from Clouds* and Figure 9. The MODTRAN derived cloud family of spectral response curves condensed to the one cloud spectral response curve in Figure 9 is used. The brightness, size and shape, location, and cloud:(cloud+sky) ratio are also variable. The brightness values associated with the cloud spectral curve vary from 0.30 for the bright clouds down to 0.0001 for the darkest clouds. These brightness values range outside the observed range in both the MODTRAN calculations and the ASD spectroradiometer measurements and should cover all possible clouds from a magnitude perspective.

The size and shape of the clouds vary from a single cloud to a large cloudbank to a nearly fully cloudy sky. Most of the analysis is performed using the single clouds and the single cloud bank.



Cloud locations vary anywhere within the hemisphere. Specific series of data acquisitions for clouds that vary in declination angle and azimuth angle are accomplished.

Finally, clouds that are very thin (low density) to very thick (high density) are used. Specifically, a 25% cloud and 75% sky spectral set of data acquisitions and 50% cloud and 50% sky set and a 75% cloud and 25% sky set are accomplished. Most of the clouds are built using 100% cloud and 0% sky.

Of all the internal water sources, Raman scattering was the only one enabled in all of the data runs. Bioluminescence and DOM and chlorophyll fluorescence are species and activity dependent and were not included. However, Raman scattering is only dependent on the excitation wavelength and can be included without requiring specific species or agitation levels (Bartlett, 1998 and Mobley, 1994).

Another constraint is the level of spatial resolution required. Most of the equations presented thus far (actually, all except for EQ 19 and EQ 20) represent continuously varying functions. To digitally perform the calculations, we need to quantize the three dimensional space. I use the same method as Mobley (1994, 1995) to enable a smooth transition to the Hydrolight code. The unit sphere (see Figure 23) defined by  $(\theta, \phi)$  heading up and down (i.e. the two hemispheres previously discussed) is quantized into 36 elevation and 72 azimuthal "quads" (roughly  $5^\circ \times 5^\circ$  sectors with the endcaps treated separately). The Hydrolight 3.0 standard is to partition the sphere into  $20 \times 24$  quads which equates to roughly  $9^\circ \times 15^\circ$  sectors. Both quad

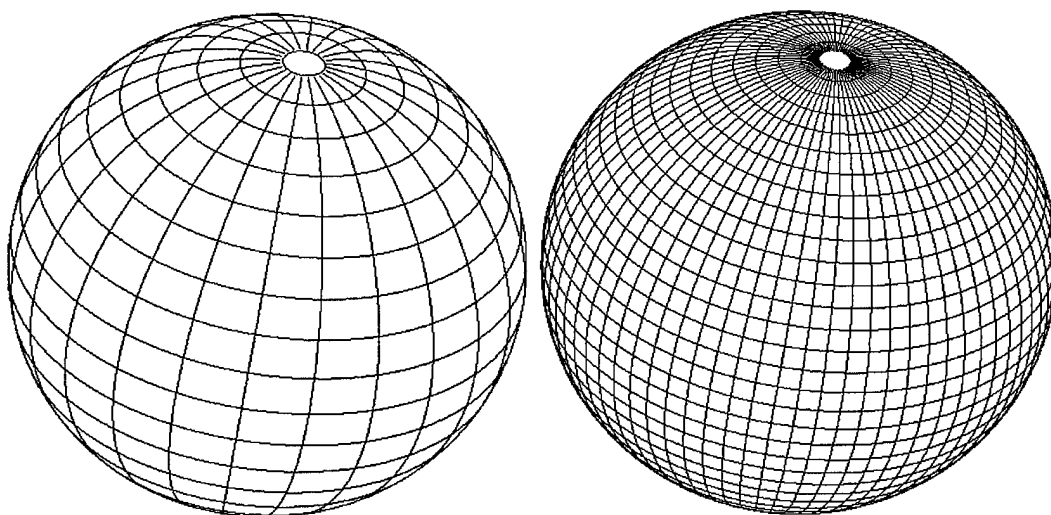


Figure 23: Two quantized spheres representing the Hydrolight 3.0 spatial resolution standardized of 20 x 24 partitions and the new higher resolution HydroMod 36 x 72 partition standard.

partitioned unit spheres are shown in Figure 23. The HydroMod standard 36 x 72 quantized unit sphere then becomes the accounting method used in the numerical solutions for the directional information. It is important to point out that the remote sensing platform will view the point in question on the water surface from one of those  $34 \times 72 + 2 = 2450$  directions. In fact, since the remote sensing platform is above the surface, we're only concerned with the upper hemisphere and one of the 1225 directions.

The final constraint is the wavelengths of interest. SeaWiFS uses 8 bands centered at 412nm, 443nm, 490nm, 510nm, 555nm, 670nm, 765nm, and 865nm with bandwidths of 20nm each except for bands 7 and 8 (765nm and 865nm) which have bandwidths of 40nm each (Barnes, 1994). These are my operating bands as well.

However, to included internal sources such as Raman Scattering, one additional band is added so that HydroMod accounts for the shorter wavelength inducing internal source radiation within the water column. The additional band is 50nm wide centered at 325nm.

These are the parameters I vary to characterize the impact of clouds to the SeaWiFS chlorophyll detection algorithms over the Laurentian Great Lakes. HydroMod is not necessarily limited to the scope provided here.



## *Chapter 5*

### **RESULTS AND ANALYSIS**

Approximately 350 HydroMod data acquisition runs were accomplished for this effort. I will not present them all here. Instead, I will walk through one set of calculations and then show the final results for several runs at once.

#### **Single Step-by-Step Analysis**

To begin, consider the two input sky radiance files in Figure 24. The data sets are displayed in decibel log format for viewing purposes. (The units on the scales are given as “dBr” for “decibels relative to a single radiance unit where, here, the radiance units are  $\mu\text{W}/\text{cm}^2 \cdot \text{sr} \cdot \text{nm}$ . For instance, the 24.9328dBr as the maximum value on the scale given in Figure 24(a) and(b) represents  $10^{2.49328} = 311.37 \mu\text{W}/\text{cm}^2 \cdot \text{sr} \cdot \text{nm}$  and the 43.1135dBr in Figure 25 represents  $10^{4.31135} = 20480.95 \mu\text{W}/\text{cm}^2 \cdot \text{sr} \cdot \text{nm}$ . The “relative to 1 radiance unit” is required because, mathematically, a logarithm’s argument must be unitless.) The geometry is the same as given previously with the center of the circle representing zenith and the edges representing the horizon with  $0^\circ$  and North at the top. Two sky inputs are shown with Figure 24(a) representing a clear sky and Figure 24 (b) representing the same sky with a single cloud at  $41^\circ$  declination angle and  $100^\circ$  azimuthal angle. The direct sun term is removed from these data so that the radiance distribution across the sky can be viewed. If we add

the direct sun radiance term to the input, data similar to that displayed in Figure 25 results and the sky distribution is not as easy to view.

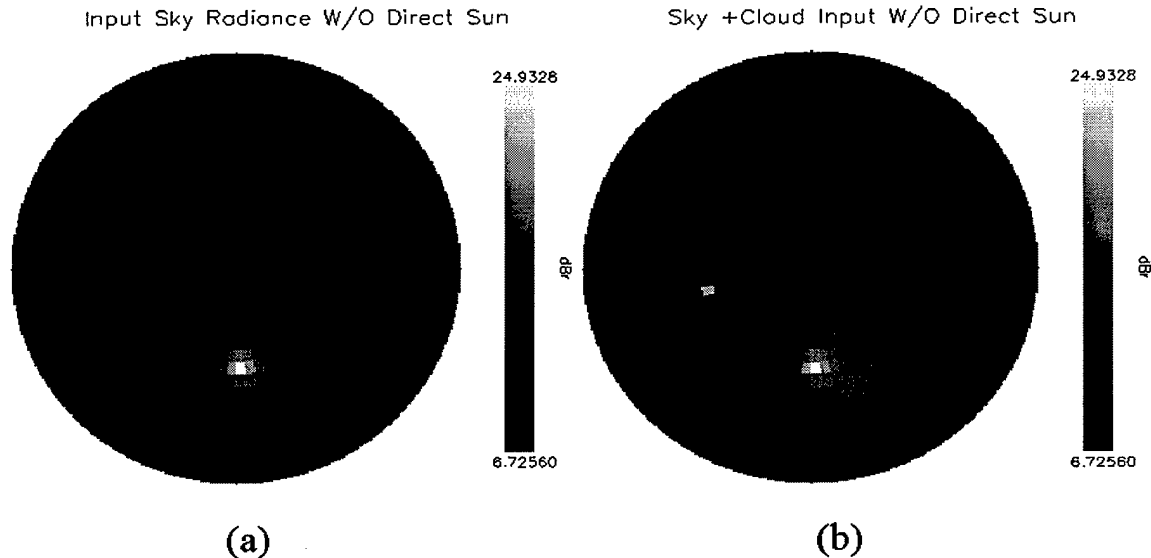


Figure 24: Two input sky radiance data sets. (a) represents a clear sky with no clouds and (b) is the same sky with one single cloud at 40° declination angle and 100° azimuth angle. The data are displayed in log format (decibels relative to a radiance unit of  $\mu\text{W}/\text{cm}^2 \cdot \text{sr} \cdot \text{nm}$ ) with the scales for each of the displays given to the right of the display. The circular region represents a hemisphere; the center is nadar (or zenith as the case may be) and the outside edges are the horizon. North is at the top. For these images, the sun is located due South at a declination angle of 41°. The data are for  $\lambda=555\text{nm}$ .

All of the data displayed in Figure 24 through Figure 32 were generated using HydroMod and nominal Lake Ontario waters of 10 $\mu\text{g}/\text{l}$  of chlorophyll, 2 $\text{g}/\text{m}^3$  dissolved organic carbon, and 6 $\text{g}/\text{m}^3$  of suspended minerals. The MODTRAN generated atmosphere is for a maritime 23Km visibility, mid-latitude summer with the sun due south in the quad centered at 41.143°. Two HydroMod sky files were used: a specially generated "direct sun term only" sky and a sky only file with no direct sun term. This

allows separating out the sky and sun as in Figure 24 and Figure 25. The output files were combined using superposition. Raman scattering was enabled starting at 300nm. Most of the data are for SeaWiFS Band 5 (centered at 555nm) with Bands 3 (centered at 490nm), 7 (centered at 765nm) and 8 (centered at 865nm) also used as noted in the individual figures.

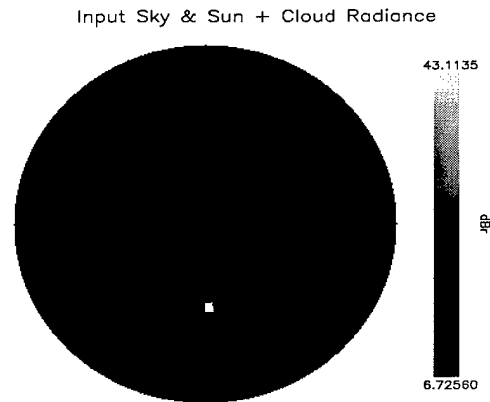


Figure 25: The direct sun radiance term has been added to Figure 24(b). Even when displayed on a decibel scale, the radiance distribution across the sky is not viewable.

Adding a 5m/sec (9.7knots) wind to roughen the surface yields the radiance reflected at the water surface,  $L_{ref}(\theta, \phi)$ , is displayed in Figure 26 (a) and (b). The total water leaving radiance,  $+L_{\lambda=555nm}^{\uparrow}(0; \theta, \phi)$ , (which includes the reflected radiance) is displayed in Figure 26 (c) and (d). The two sky input files from Figure 24 with the direct sun term included as in Figure 25 were used to generate these data. The upwelled radiance distribution for each of these cases is displayed in

Figure 27 . The only difference in the two displays is, again, the single cloud at 41° declination and 100° azimuth. Note that upwelled radiances for declination angles

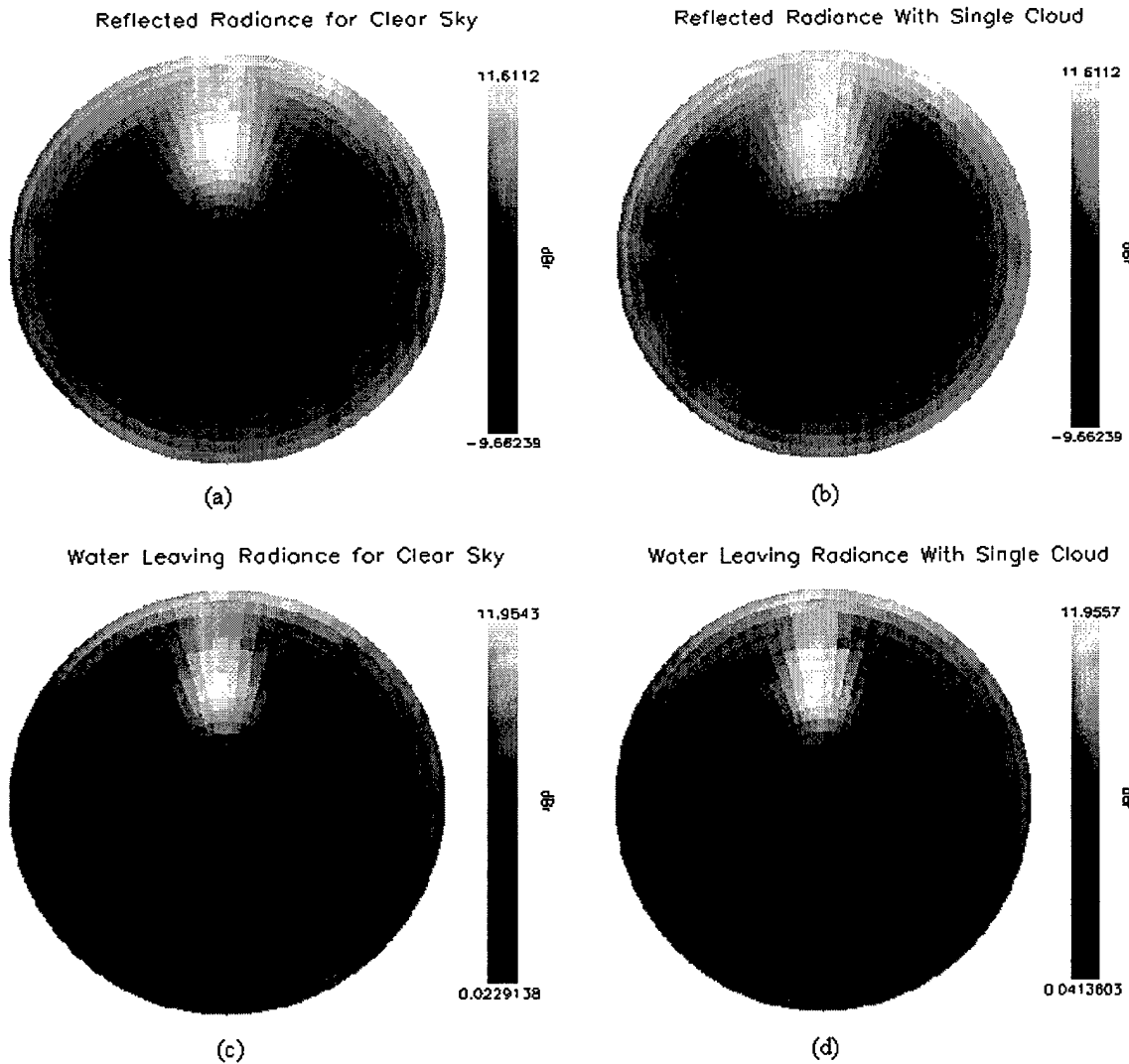


Figure 26: Surface Reflected (a and b) and total water leaving (c and d) radiance for the two input files given in Figure 24. (a) and (c) are for the clear sky only and (b) and (d) are for the single cloud in that clear sky. All four plots are for  $\lambda=555\text{nm}$  and are displayed in decibels relative to  $1 \mu\text{W}/\text{cm}^2\cdot\text{sr}\cdot\text{nm}$ . Note very little noticeable difference in the two cases. (The atmospheric and water parameters used for these data are described at the beginning of the section.)



greater than  $75^\circ$  do not reach the SeaWiFS sensor and are not calculated or used.

The black “no data” ring remains in the displays to highlight the pre-horizon cutoff.

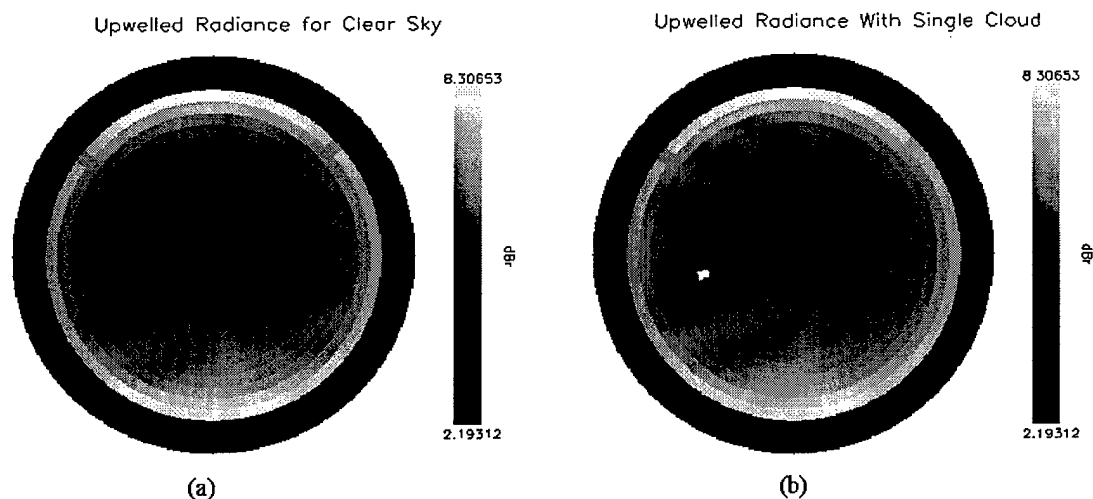


Figure 27: Two nearly identical upwelled radiance data sets. The only difference between (a) and (b) is the single quad that contains a cloud. The upwelled radiance data do not extend to the horizon because of the limited look angles for orbiting sensors. The SeaWiFS maximum pixel centered declination angle for upwelled radiance is  $74.95^\circ$ . Therefore, upwelled radiance is neither calculated nor used beyond that point. However, the black “no data” ring remains in the data displays to prevent angular confusion. (The atmospheric and water parameters used for these data are described at the beginning of the section.)

We can combine all of these data (Figure 24 through Figure 27) along with the transmission coefficient for the water leaving component propagating through the atmosphere to get the total radiance at the sensor. Figure 28 and Figure 29 show the total radiance at the sensor for the four SeaWiFS bands of interest: 490nm, 555nm, 765nm, and 865nm for these two cases. Together with the total water leaving radiance, these are the bands and the data sets that I'll use throughout the rest of the analysis.

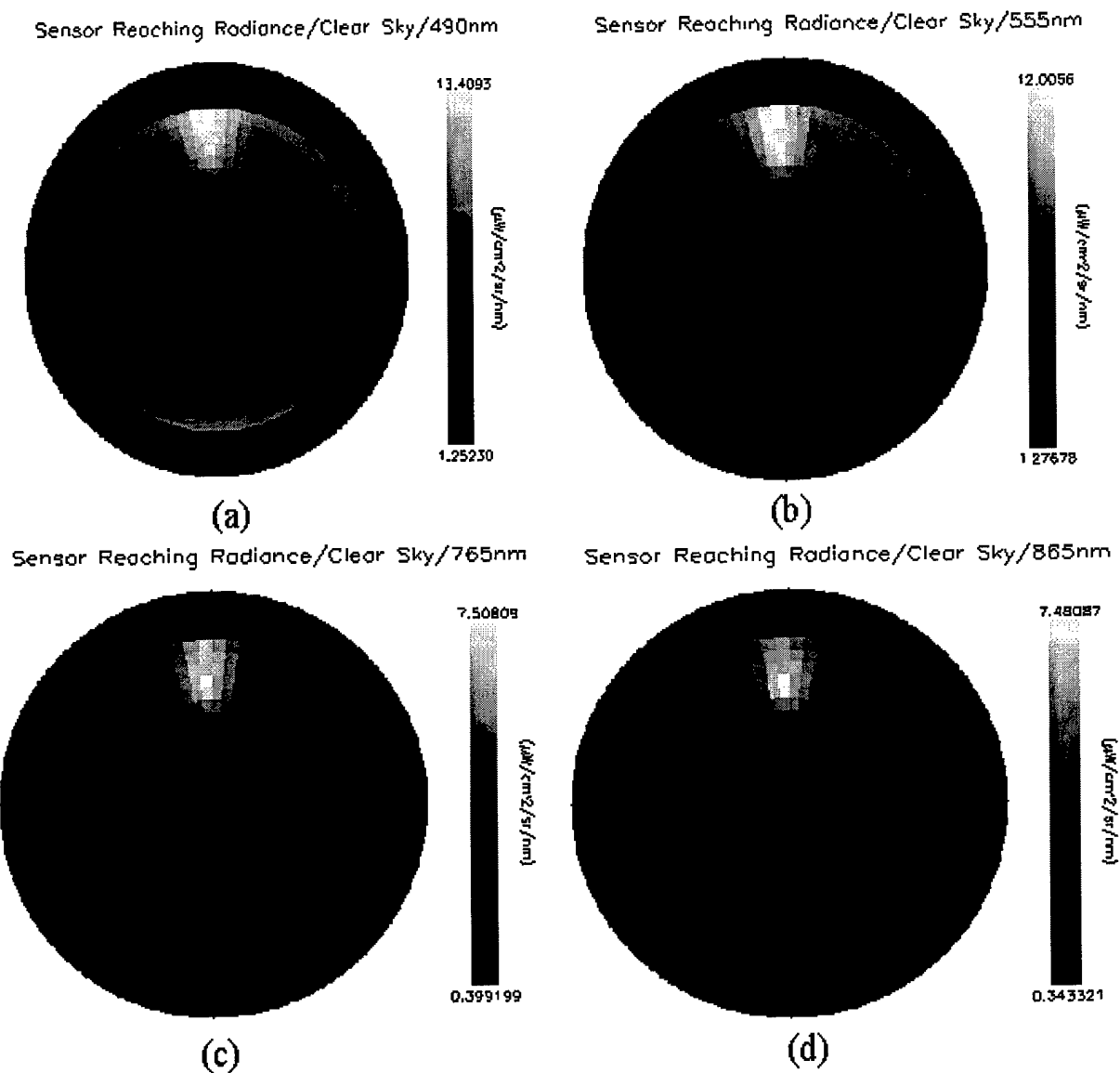


Figure 28: Total Sensor reaching radiance for the clear sky case at SeaWiFS bands 3 (a,  $\lambda=490\text{nm}$ ); 5 (b,  $\lambda=555\text{nm}$ ); 7(c,  $\lambda=765\text{nm}$ ) and 8 (d,  $\lambda=865\text{nm}$ ). The sun glint is very apparent. Also note less radiance reaching the sensor in the near IR. The blank "no data" zone from the upwelled radiance is also enabled here. (The atmospheric and water parameters used for these data are described at the beginning of the section.)

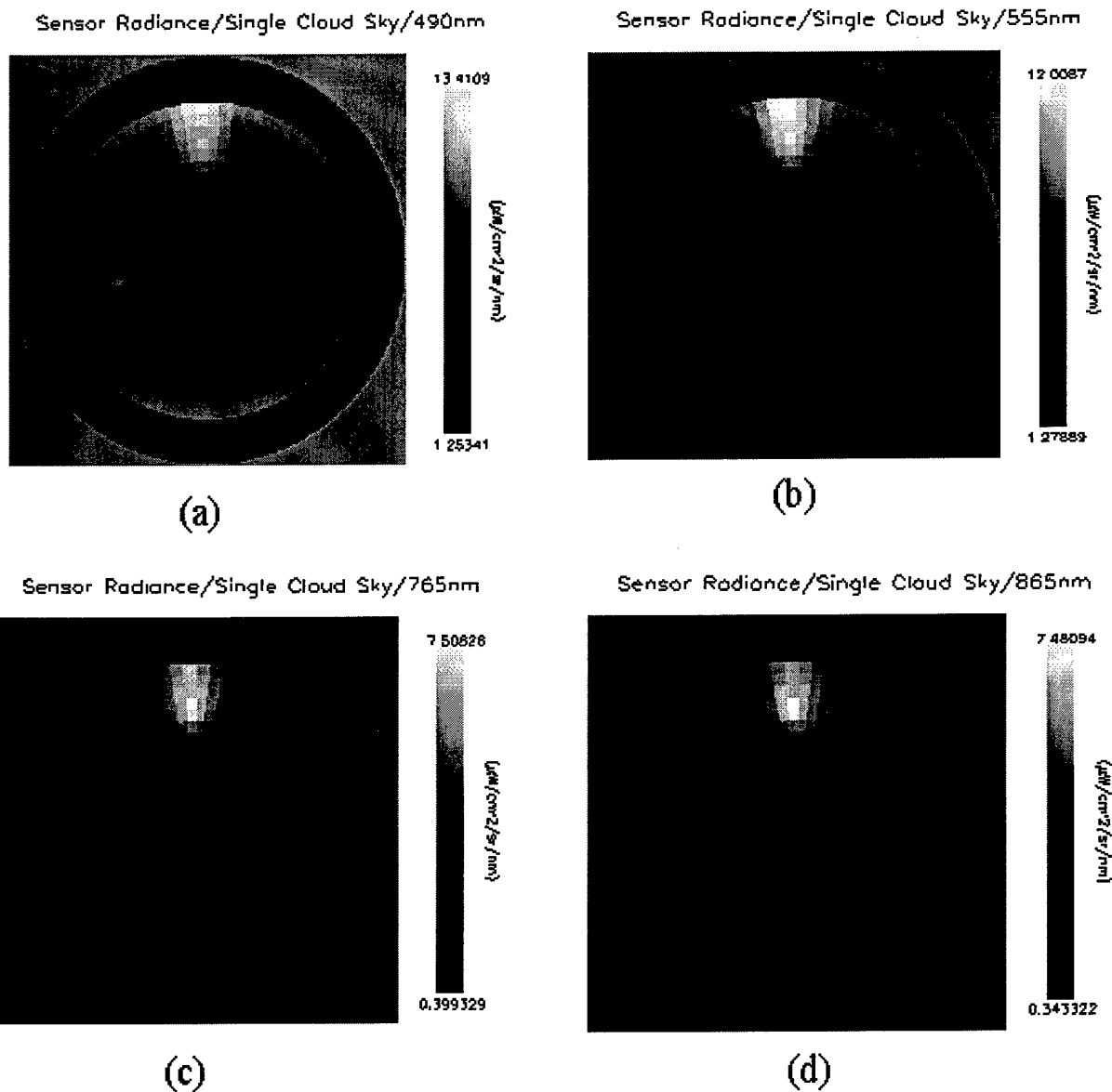


Figure 29: Total sensor reaching radiance for the single cloud case at SeaWiFS bands 3 (a,  $\lambda=490\text{nm}$ ); 5 (b,  $\lambda=555\text{nm}$ ); 7(c,  $\lambda=765\text{nm}$ ) and 8 (d,  $\lambda=865\text{nm}$ ). The sun glint is very apparent. Also note less radiance reaching the sensor in the near IR. (The atmospheric and water parameters used for these data are described at the beginning of the section.)

Looking close at Figure 26 (a) and (b) the cloud induced reflection component may be just barely noticeable. However, by the time the total water leaving radiance is calculated as in Figure 26 (c) and (d), any visual differences that may have been discernable with only the reflected component are gone. Obviously, propagating the water leaving radiance to the sensor and adding the upwelled radiance further obliterates any visual differences caused by the cloud (outside of the single quad that contains the cloud).

We can, however, calculate the differences in the total radiance at the sensor and determine a percentage error using

$$\%error = \frac{L_1 - L_2}{L_2} \bullet 100\%$$

EQ 37

where the  $L_1$  and  $L_2$  represent the single cloud and clear sky cases for each wavelength, and  $(\theta, \phi)$  direction at any location (although the two primary locations are at the sensor and at the water surface). Calculating the error at the sensor for the four bands of interest in the SeaWiFS chlorophyll determination algorithms yields the data displayed in Figure 30.

From these data, it appears as though most of the error comes from the reflected component of the water leaving radiance and that the peak error tapers to zero following a near Gaussian pattern. This conclusion is reinforced by viewing the

data in other manners such as that found in the three dimensional view of Figure 31 or the radial slice through the center and peak as in Figure 32. Both of these data sets are for the error in Band 8 as displayed in Figure 30(d).

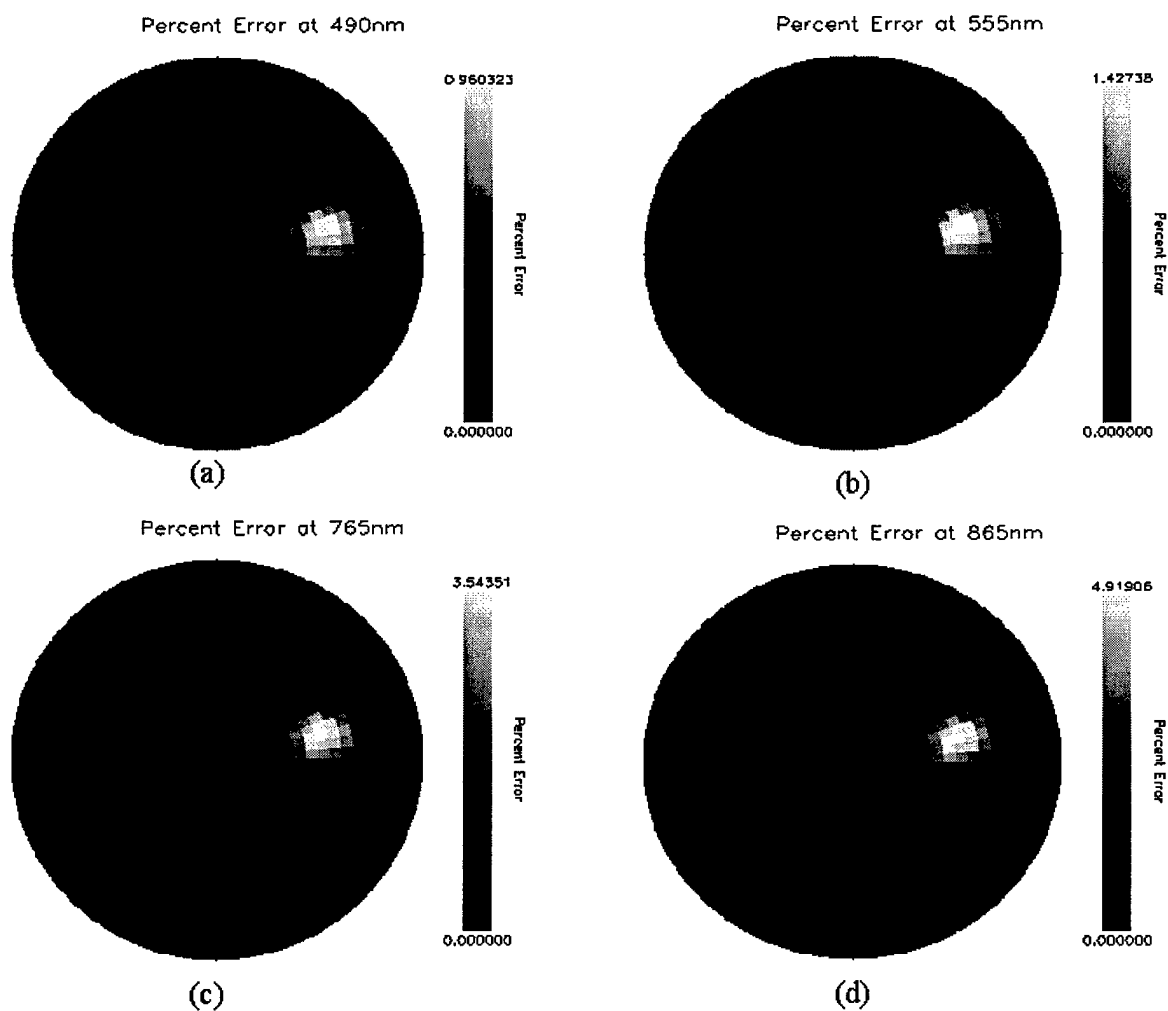


Figure 30: Error caused by a single cloud in an otherwise clear sky. The peak error ranges from less than 1% in (a) for Band 3 (490nm) to almost 5% in (d) for Band 8 (865nm). The other two percent errors displayed are for SeaWiFS Band 5

(b) and Band 7 (c). (The atmospheric and water parameters used for these data are described at the beginning of the section.)

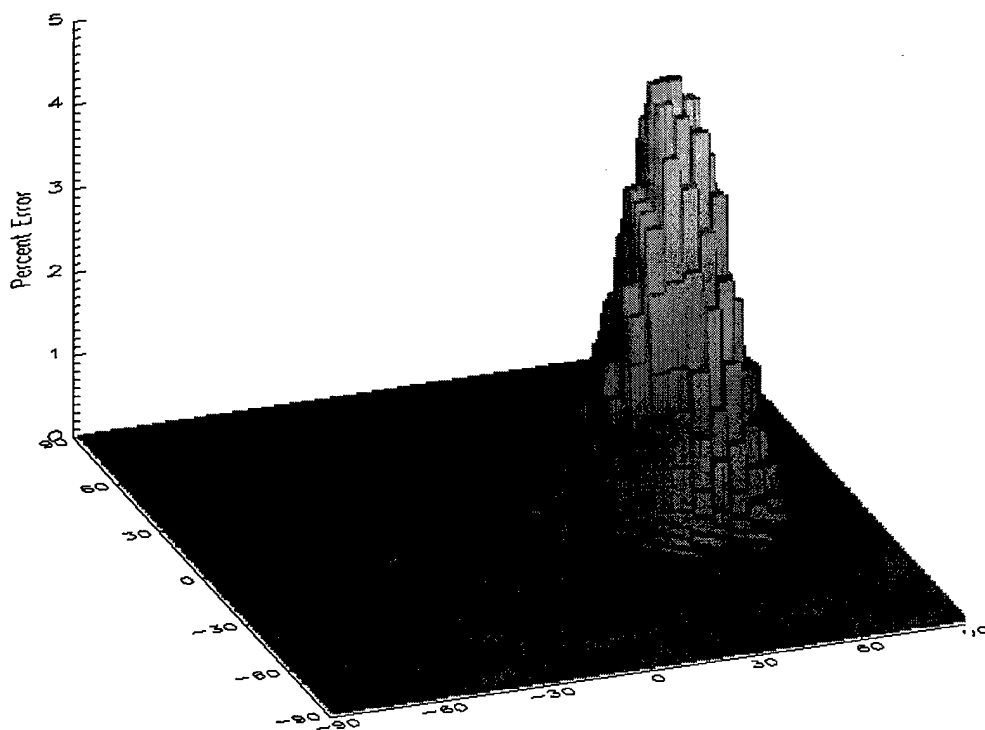


Figure 31: A 3-D view of Figure 30 (d) with the “x” and “y” axis of this plot labeled for theta angles from 0° at the center to 90° at the edges. The + and – signs on the theta angles serve to reference the quadrants of the normally circular plots. The Gaussian like shape of the data is even more apparent here than in Figure 30.

The display in Figure 32 in particular seems to call for two specifications to quantify the percent error: the peak and the full width at half the maximum (FWHM or half-width). The concept of a half-width as applied to the 3-D data, of course, would be better. Once we realize that these “widths” represent solid angles and that the widths can change by changing the input cloud solid angle (i.e. a bigger or smaller clouds), the concept of the half-width applied here requires modification. The

modification that I will employ is to use the ratio of the total solid angle with a percent error greater than half the peak percent error ( $\Omega_{FWHM}$ ) to the solid angle of the cloud that caused the error ( $\Omega_{Cloud}$ ) and call it an “normalized error width ratio” or  $\epsilon_{WR}$ .

$$\epsilon_{WR} = \frac{\Omega_{FWHM}}{\Omega_{Cloud}}$$

EQ 38

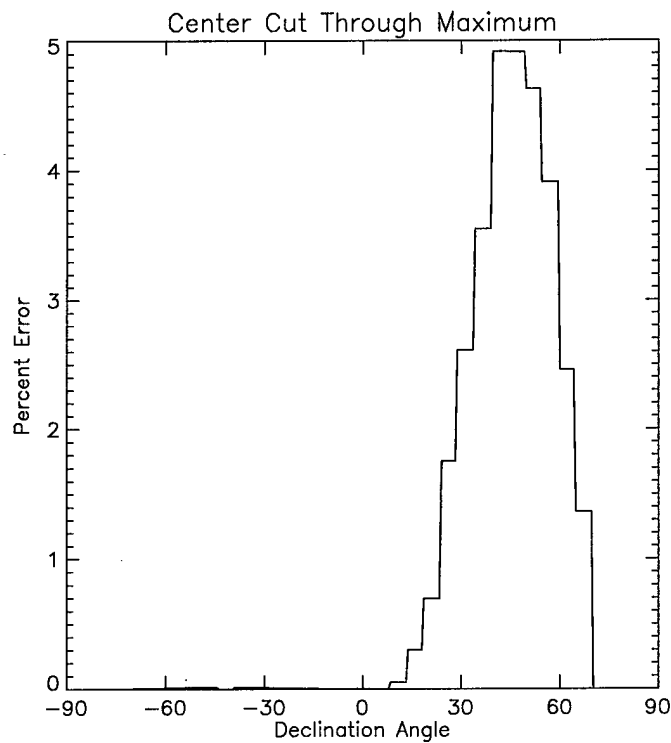


Figure 32: A diameter slice through the center of Figure 30 (d) yields the data plotted here. Both the 5° binning and the Gaussian like shape are apparent. The peak error occurs at a declination angle centered at 41.143° which is the center of the quad opposite the actual cloud. The location is consistent with the reflection angle off of the water surface.

For the Band 8 data shown in Figure 30(d), Figure 31, and Figure 32, the cloud was centered on the quad at 100° azimuth and 41.143° declination angle. It had a solid angle of 0.0051538sr [ $\sin(\theta)d\theta d\phi = \sin(41.143^\circ) \cdot (5.143^\circ) \cdot (5^\circ) \cdot (\pi/180^\circ)^2 = 0.0051538\text{sr}$ ] and the FWHM solid angle of the percent error is 0.174674sr (found by summing the quads with percent error greater than  $\epsilon_{\text{peak}}/2$ ) which yields a normalized error width ratio of  $\epsilon_{\text{WR}} = 33.892$ . The peak error,  $\epsilon_{\text{peak}}$ , is 4.912% in that band.

### **Affect on the SeaWiFS Calculations**

Now that we have our quality parameters, we can take the next step by employing some of the SeaWiFS algorithms. We first use EQ 27 to convert the radiances to reflectances and then EQ 29 to remove the Rayleigh component (if the wind speed is below 9m/sec, we don't need to worry about the whitecap component according to Gordon, 1997). With the reflectance values, we can determine the ratio for  $\rho(765\text{nm})$  and  $\rho(865\text{nm})$  and the error in that ratio due to the presence of the clouds. For this example, the peak error in the ratio between  $\rho(765\text{nm})$  and  $\rho(865\text{nm})$  is approximately 1.24% (negatively) with a normalized error width ratio of 31.6.

That error will cause an error in the atmospheric subtraction. Unfortunately, all that we can predict is that the error will most likely underestimate the chlorophyll levels. The fact that the peak error is negative means that the Band7 to Band 8 ratio is less when the cloud is present than it is when the cloud is not present (i.e. the white cloud introduces a flatter spectrum). If that is true, the lower ratio will, in turn, yield a flatter  $\epsilon$  using EQ 30. The flatter  $\epsilon$  will result in values of  $\rho_a(490\text{nm}) + \rho_{ra}(490\text{nm})$  and



$\rho_a(555\text{nm}) + \rho_{ra}(555\text{nm})$  that are too low with a larger error at 490nm than at 555nm. Taking this to the next step,  $\rho_w(490\text{nm})$  and  $\rho_w(555\text{nm})$  will be too large with, again, more error in  $\rho_w(490\text{nm})$  than  $\rho_w(555\text{nm})$ . Thus, the ratio for  $\rho_w(490\text{nm})/\rho_w(555\text{nm})$  will be too large and the chlorophyll content calculated using EQ 33 will be less than the true value. Without the actual data used to derive the atmospheric subtraction routines, we cannot determine exactly how much of an underestimate is calculated. That step is left for further study.

We can, however, analyze the effect of the water leaving reflectance ratio for bands 3 and 5. We do this by assuming that the exact atmosphere can be subtracted and then using the  $\rho_w(490\text{nm})$  and  $\rho_w(555\text{nm})$  as calculated by HydroMod for the analysis. Doing so yields a peak error in  $\rho_w(490\text{nm})/\rho_w(555\text{nm})$  of 3.49% and a normalized error width ratio of 30.82. Both of these error plots can be found in Figure 33.

The error in the derived chlorophyll content strictly due to the error in  $\rho_w(490\text{nm})/\rho_w(555\text{nm})$  of 3.49% is directly calculable. The scenario used chlorophyll content of  $10\mu\text{g/l}$  along with some suspended minerals and dissolved organic matter. The original SeaWiFS algorithm, EQ 31, calculates the chlorophyll content of the baseline (cloudless) scene to be around  $11\mu\text{g/l}$  and the new algorithm, EQ 33, computes the chlorophyll content to be around  $5.8\mu\text{g/l}$ . The difference in the predicted chlorophyll content in the direction of the peak error is  $1.44\mu\text{g/l}$  between the cloud and

no cloud case for the old algorithm and only 0.47 for the new algorithm. Both of these values predicted lower chlorophyll with the cloud than without a cloud.

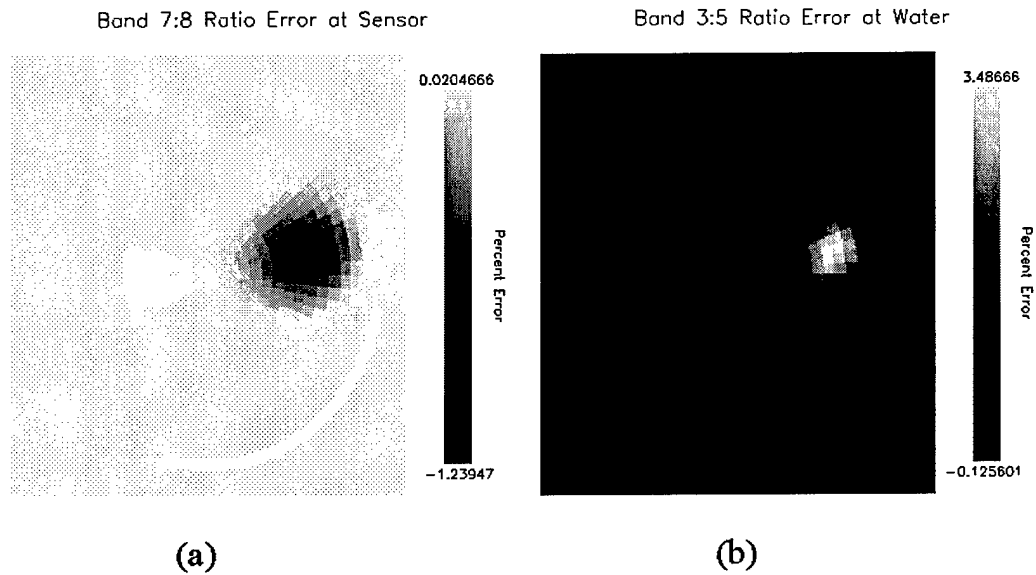


Figure 33: The error in the ratio between  $\rho_t(765)$  and  $\rho_t(865)$  (a) and between  $\rho_w(490)$  and  $\rho_w(555)$  (b) is illustrated. Note that the error in (a) has a negative “peak” due to a flatter spectrum caused by the cloud while the error in (b) has a positive peak. The ultimate impact on the derived chlorophyll content is unknown for (a) other than the tendency to underestimate the chlorophyll. For (b), the impact on the chlorophyll content is calculatable and in this case will also under-estimate the chlorophyll content.

The two most important parameters for the cloud impact are the error in the ratio for  $\rho_t(765\text{nm})$  to  $\rho_t(865\text{nm})$  and error in the ratio of  $\rho_w(490\text{nm})$  to  $\rho_w(555\text{nm})$ . Using the same scenario and changing the brightness of the single cloud yields a series of peak errors and normalized error width ratios. The peaks are plotted in

Figure 34. The normalized error width ratios were all nearly identical around a value of 31.

As expected, as the brightness of the cloud increases, the percent error also increases. The white cloud causes the ratios of both the top of the atmosphere bands 7 and 8 and the water leaving bands 3 and 5 to move closer to 1:1 (white). However, in the Figure 34(a), the original Band 7/8 ratio was greater than 1:1 and the white cloud decreased the ratio. In Figure 34(b), the original Band 3/5 ratio was less than 1:1 and the white cloud increased the ratio.

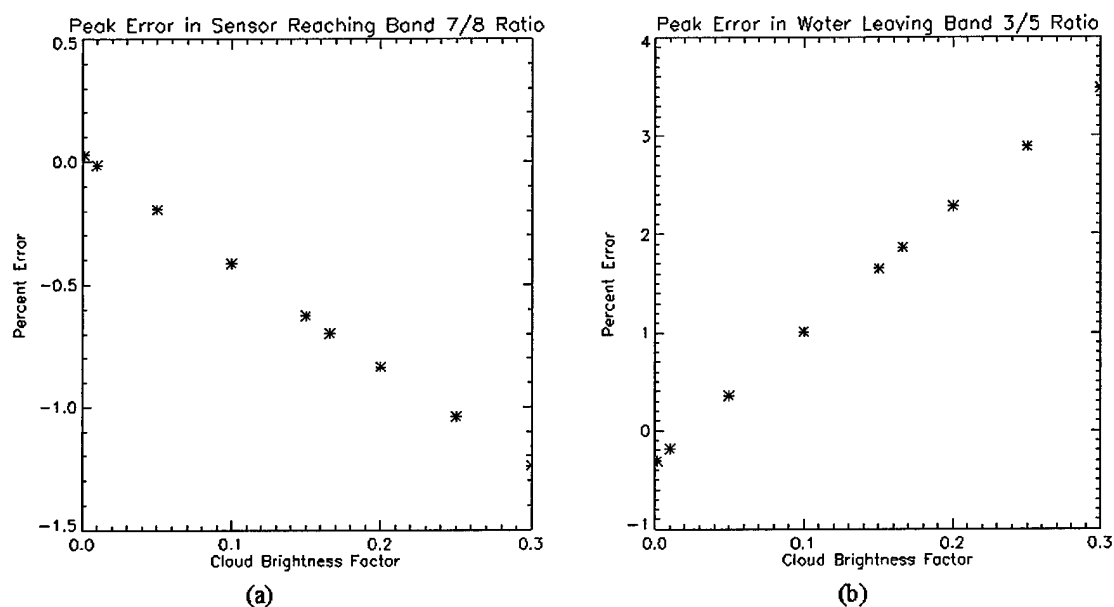


Figure 34: Change in peak percent error for varying cloud brightness levels. (a) is for the peak error in the ratio between the band 7 reflectance and the band 8 reflectance at the top of the atmosphere. In (b), the water leaving reflectance components for bands 3 and 5 were used. These are the important ratios for determination of the chlorophyll content using the SeaWiFS algorithms.

## Cloud Location Affects

Moving the single cloud with a fixed brightness level will allow the normalized error width ratio to vary. Specifically, using a bright cloud with a brightness factor of 0.30 and moving it radially from the end cap to the horizon yields the data in Figure 35.

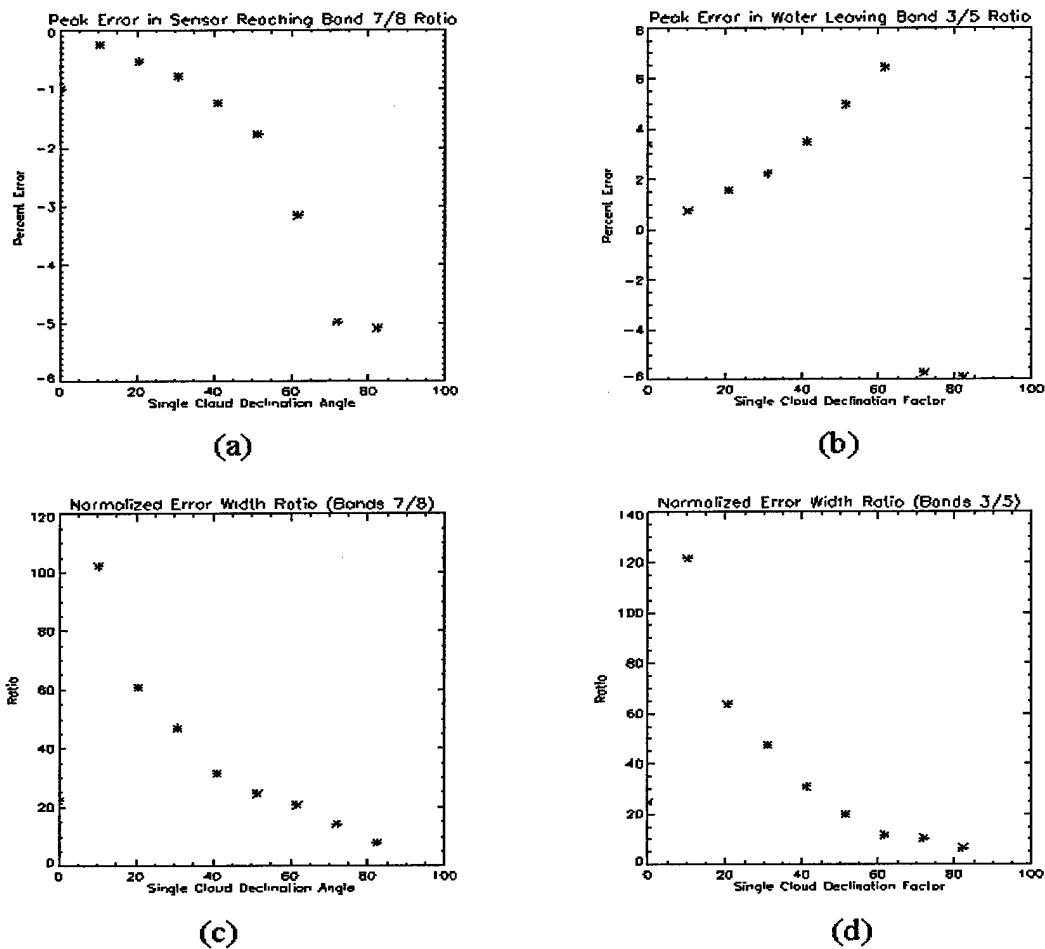


Figure 35: Effect of changing the cloud declination angle (and therefore the solid angle size of the cloud) is shown. The peak error curves of (a) for the sensor reaching Band 7 to Band 8 ratio and (b) for the water leaving Band 3 to Band 5 ratio cutoff above 70° due to the inability of remote sensors to view at higher angles. (That is, since the sensors cannot view at those angles, the HydroMod calculations do not consider them and any data outside of the 70° mark is erroneous.) Also note that the endcap cloud is fairly large, but most of the light from that cloud will enter the water and not reflect.

The Fresnel reflection coefficient increases with increasing incidence angle as in Figure 22. The increase in surface reflectance yields an increase in the error rate as the cloud's declination angle increases. The normalized error width ratio, however, decreases with increasing declination angle because the solid angle of the quad containing the cloud increases.

Note that the drastic changes in error rates beyond the 70° point are geometry artifacts only. Since remote-sensing systems cannot view a point on the water surface at such high declination angles, HydroMod does not account for upwelled radiance in that zone. The result is that any analysis outside of the 70° declination angle barrier is meaningless as is the drastic change artifacts illustrated in Figure 35.

Several other series of runs were accomplished moving the single cloud to various locations around the hemisphere with very predictable results using the data already presented. As the cloud moved, the peak error maintained a position 180° in azimuth away from the cloud at the same declination angle. The normalized error width ratios were comparable to those given in Figure 35 at the corresponding declination angle locations for the cloud. Other than that short summary, those data will not be presented here.

### **Introducing a Cloudbank**

The next phase of the analysis is to increase the physical size of the cloud. The input cloud sky illustrated in Figure 36 was used for a series of runs similar to the

single cloud case discussed. The single cloudbank of Figure 36 is also a slightly more realistic scenario.

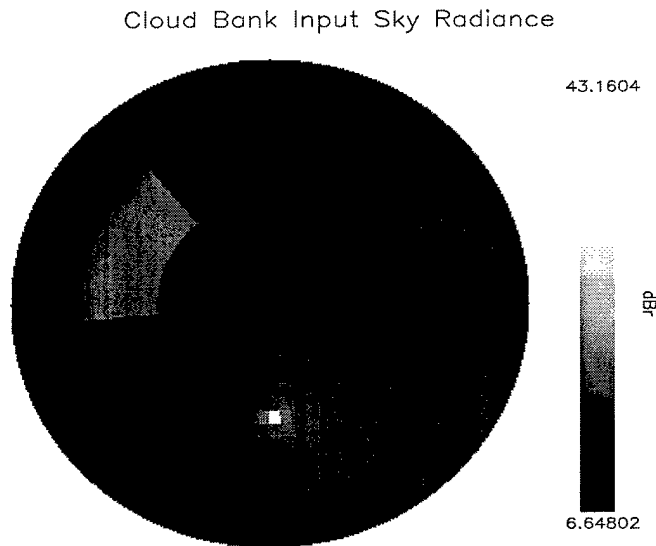


Figure 36: Cloud Bank Input Sky Data. A single cloud bank centered roughly at  $45^\circ$  declination angle between  $45^\circ$  and  $90^\circ$  in azimuth was used for input. The size of the cloud did not change for a series of data acquisitions that varied the brightness level and the cloud/(cloud+sky) ratio. The cloud shown above has a brightness scale factor of 0.075 and the displayed data are for  $\lambda=555\text{nm}$ .

A similar series of data acquisition runs were accomplished with the cloudbank as was with the single cloud. The solid angle of the cloudbank was approximately  $0.334\text{sr}$ . The normalized error width ratio stayed between 1.0 and 3.0 for cloud brightness factors between 0.3 and 0.0 (a cloud brightness factor of 0.0 equates to no radiance from the direction of the cloud reaching the water surface; i.e. a very black cloud). The error peaks for the two main parameters are shown in Figure 37.

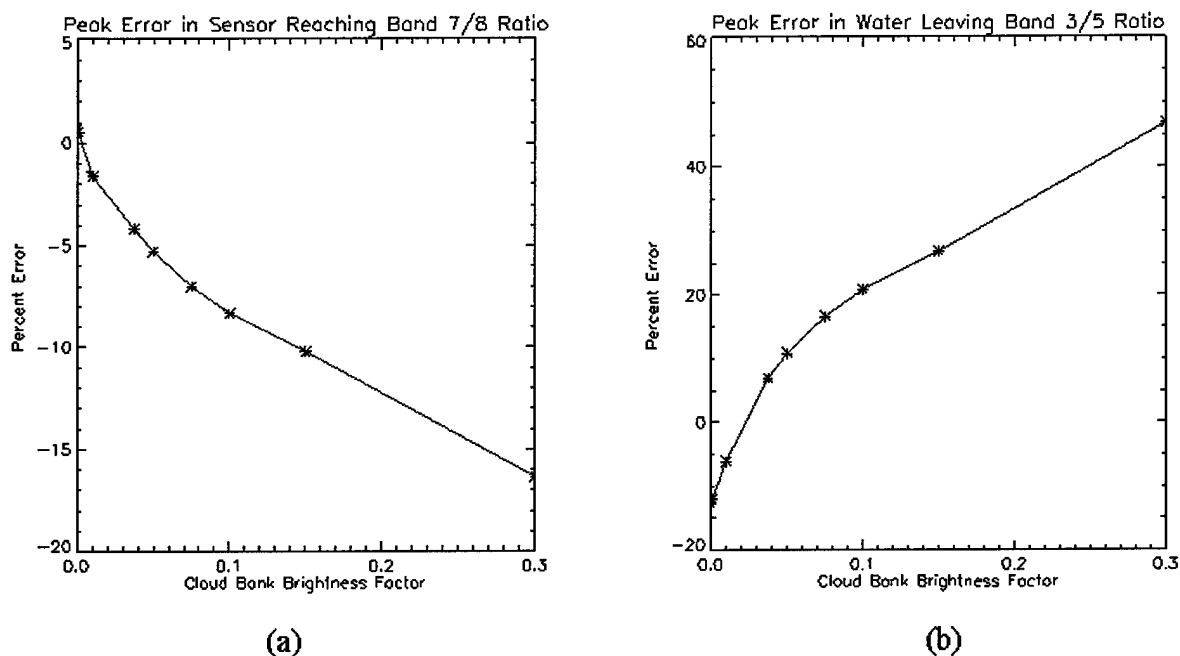


Figure 37: Percent Error for the Two Main Quality Parameters. The peak errors for the sensor reaching Band 7/8 ratio and the water leaving Band 3/5 ratio (b) are plotted as a function of the cloud bank brightness factor. These errors can be quite large for spatially large cloudbanks. The normalized error width ratio for all of these errors ranged from 1.0 to 3.0. The solid angle of the cloud causing the errors was approximately 0.334 sr.

The error in the water leaving radiance of the Band 3/5 ratio is quite high. Even for moderate clouds, the errors can be over 10%. The affect of these errors on the chlorophyll levels on an error percentage basis is even more extreme as illustrated in Figure 38. The data plotted there show that the percent error in the chlorophyll calculations can be over 50% for even moderately bright clouds. With darker clouds, the amount of chlorophyll will be overestimated as illustrated by a negative error rate.

The calculated chlorophyll levels for this case are plotted in Figure 39. Here we see that the original SeaWiFS algorithm would have reported a fairly accurate

10.14 $\mu\text{g/l}$  if no clouds were present, but the new algorithm computes only 5.55 $\mu\text{g/l}$  for the baseline level. The suspended minerals and dissolved organic material cause underestimated chlorophyll levels even without clouds (assuming perfect atmospheric

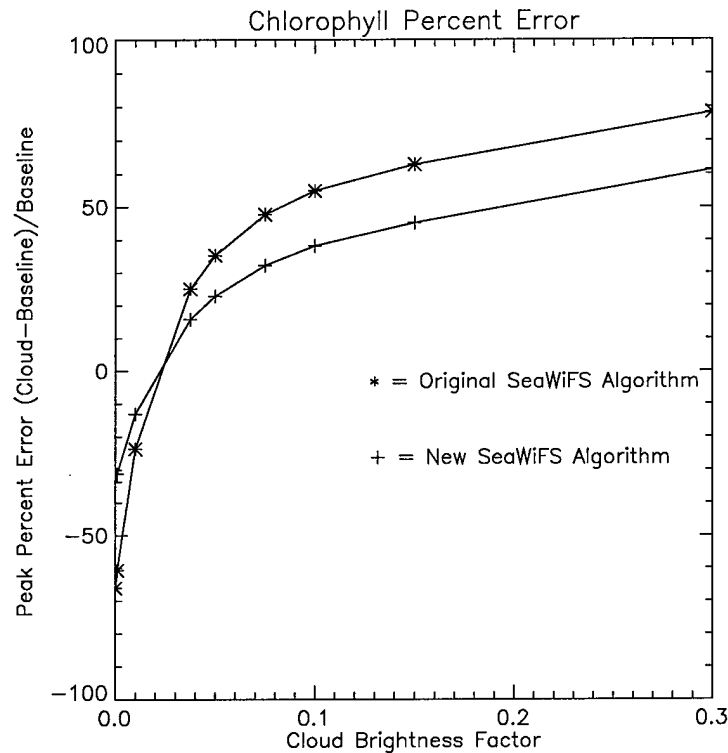


Figure 38: Peak Percent Error on the Chlorophyll content calculated using the original SeaWiFS algorithm (\*) and the new SeaWiFS algorithm (+). Errors as high as 50% for moderate clouds are predicted. The peak error occurs in the azimuth direction 180° away from the cloud at the same declination angle.

subtraction). The affect of the clouds will tend to further lower the estimate. The final analysis plot for these data is the difference in the chlorophyll level calculated with the cloud present less the chlorophyll level calculated without the cloud present. The difference data are plotted in Figure 40.



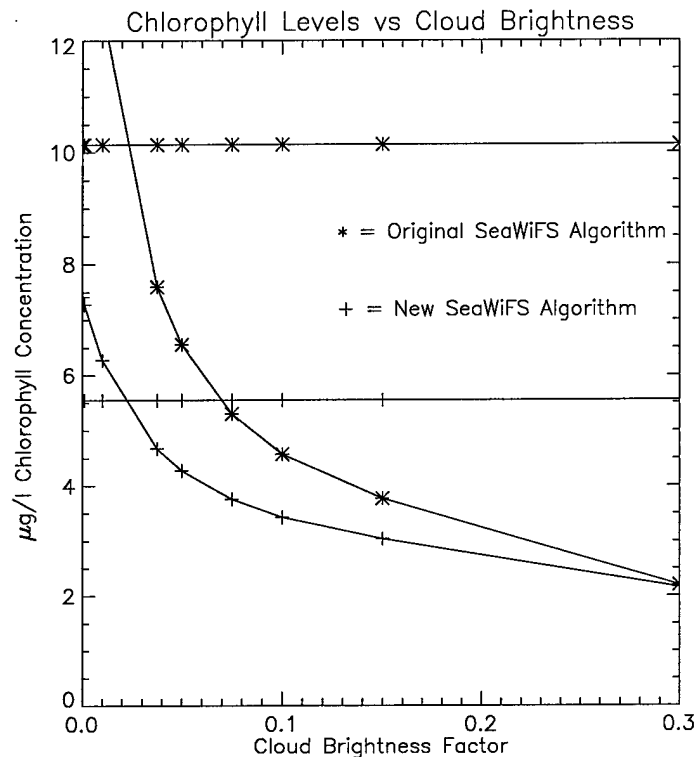


Figure 39: Calculated chlorophyll levels using the original SeaWiFS algorithm (\*) and the new SeaWiFS algorithm (+). The original algorithm would have been fairly close to the actual chlorophyll level of  $10\mu\text{g/l}$ , but the new algorithm underestimates the level. The effects of the clouds tends to reduce the estimate even further.

With Figure 40 it is easy to see that the chlorophyll levels predicted with clouds in the vicinity can be higher or lower than the level predicted without the clouds. For darker clouds and a true chlorophyll level of  $10\mu\text{g/l}$ , the cloud will induce an overestimate. Brighter clouds at the same true chlorophyll level will induce an underestimate.

The values calculated in Figure 38 and Figure 40 represent error of cloud versus no clouds and NOT cloud case versus true levels. The errors plotted and analyzed here represent the cloud impact only; referencing the cloud impact to the true levels would confuse the impact due to the SM and DOM with the cloud results.

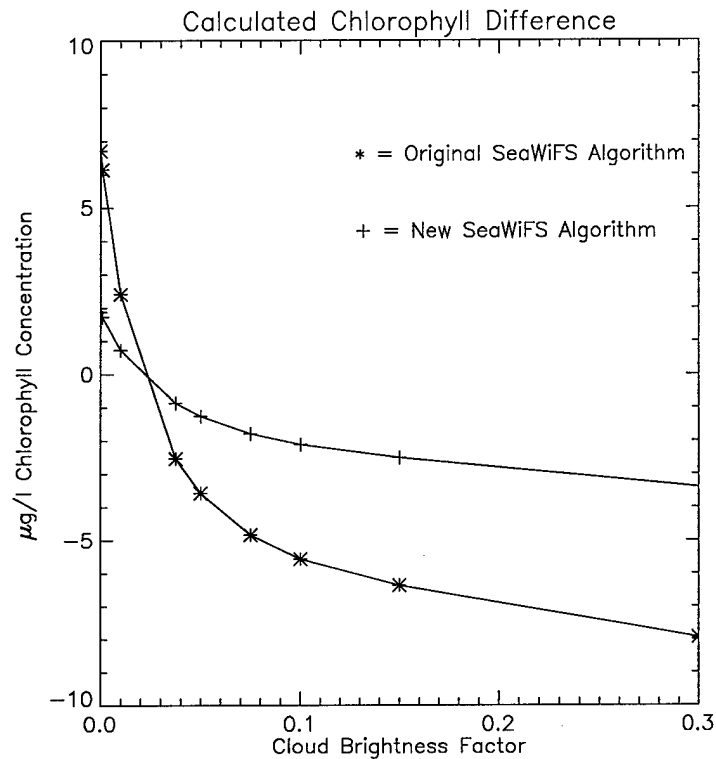


Figure 40: Calculated chlorophyll differences between the cloud case and the no cloud case using the original (\*) and the new (+) SeaWiFS algorithms

The next step is to look at cloud density levels. While doing that, I want to show the affect of continually darkening clouds. Instead of plotting cloud brightness factors ranging from 0.3 to 0.0, we'll reduce the range to 0.15 to 0.0 to see some of the effects at very dark cloud brightness levels.

### Cloud Density Level Impact

With this series of data acquisition runs, the cloud density changed from quads with 100% clouds to quads with 50% cloud and 50% sky to quads with 25% clouds and 75% sky. The cloud brightness factors were left intact, but the predominance of data

presented here are for the lower brightness factors to show the aforementioned affects at darker cloud regions.

Refer to Figure 41 which shows the three cloud/(cloud+sky) density levels plotted as the error in the Band 7/8 ratio at the sensor versus the cloud brightness factor. We see from these data that the denser clouds always have more error than the less dense clouds.

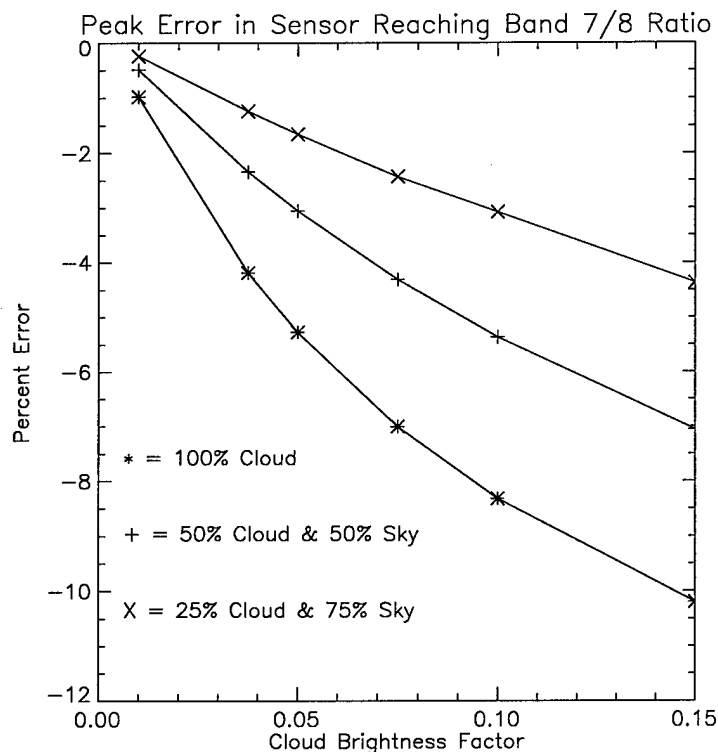


Figure 41: Peak Error in the sensor reaching reflectance Band 7/8 ratio values for varying cloud brightness levels and different cloud densities. There is more error in the Band 7/8 ratio at all brightness factors for denser clouds than for thinner clouds. The three scenarios plotted here are for a cloud representing 100% of each of the quads, 50% of each of the quads, and 25% of each of the quads in the cloud sector displayed in Figure 36

The same type of phenomenon occurs with the water leaving Band 3/5 ratio error as shown in Figure 42. Here we see that the error caused by the cloud cross the zero point somewhere between a brightness factor of 0.05 and 0.01. For clouds brighter than a factor of 0.05, the denser clouds clearly have a larger positive percent error in the Band 3/5 water leaving reflectance ratio. This results in an underestimate of the chlorophyll content using both of the SeaWiFS algorithms (see Figure 43 and Figure 44).

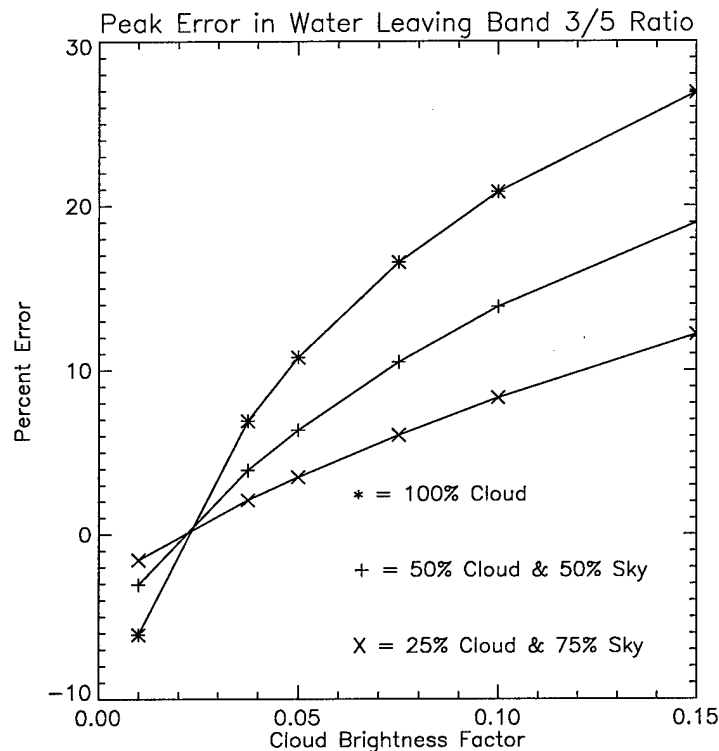


Figure 42: Peak Error in the water leaving Band 3/5 Ratio for varying cloud brightness levels for different cloud densities. The cross over between brightness factors of 0.05 and 0.01 occurs at the point where the cloud reflected component is on the same order of magnitude as the water leaving component. In is also where the calculated chlorophyll levels are inflated using either the original SeaWiFS algorithm (see Figure 43) or the new SeaWiFS algorithm (see Figure 44).

However, somewhere between a cloud brightness factor of 0.05 and 0.01, the calculated chlorophyll content using either the original SeaWiFS algorithm (see Figure 43) or the new SeaWiFS algorithm (see Figure 44) is actually overestimated given the cloud bank and water parameters in the scenario.

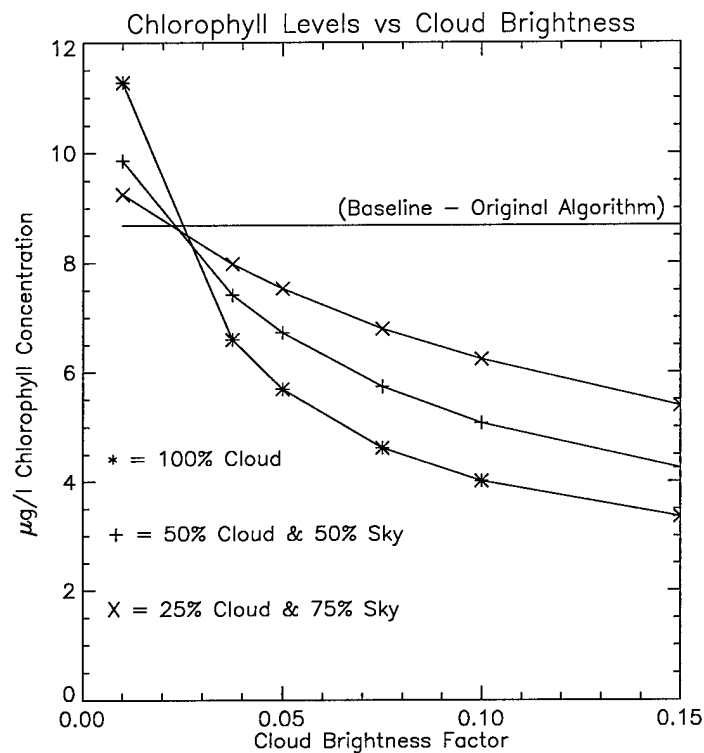


Figure 43: Changes in the Chlorophyll level for the varying cloud brightness for different cloud densities. These calculations were made using the original SeaWiFS algorithm. In most cases, the cloud density level that is higher results in a larger underestimate of the chlorophyll content, but in some limited cases, the chlorophyll content is overestimated.

### The Wind Speed Impact

With that anomaly exposed, we can turn to the impact of varying wind speeds on the important parameters and derived chlorophyll content. The following data represent several data acquisition runs at varying wind speeds and cloudbank

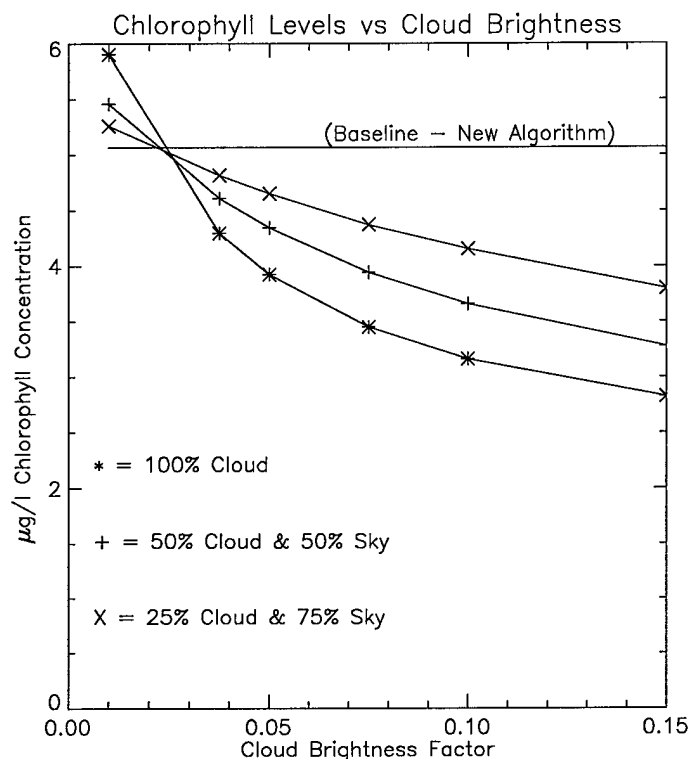


Figure 44: Changes in the Chlorophyll level for the varying cloud brightness for different cloud densities. These calculations were made using the new SeaWiFS algorithm. In most cases, the cloud density level that is higher results in a larger underestimate of the chlorophyll content, but in some limited cases, the chlorophyll content is overestimated.

brightness factors. The cloudbank used in this set of runs was slightly different than in previous data runs. The cloudbank was smaller (spatially) and closer to the endcap quad. Four (and sometimes five) cloud brightness levels were used at wind speeds varying from 0.0m/sec to 10.0 m/sec in 1.0m/sec steps.

Referring to Figure 45, we see little variation in the peak error of the sensor reaching Band 7/8 ratio for wind speeds above 3m/sec or so; certainly, the cloud brightness level seems to have more impact.

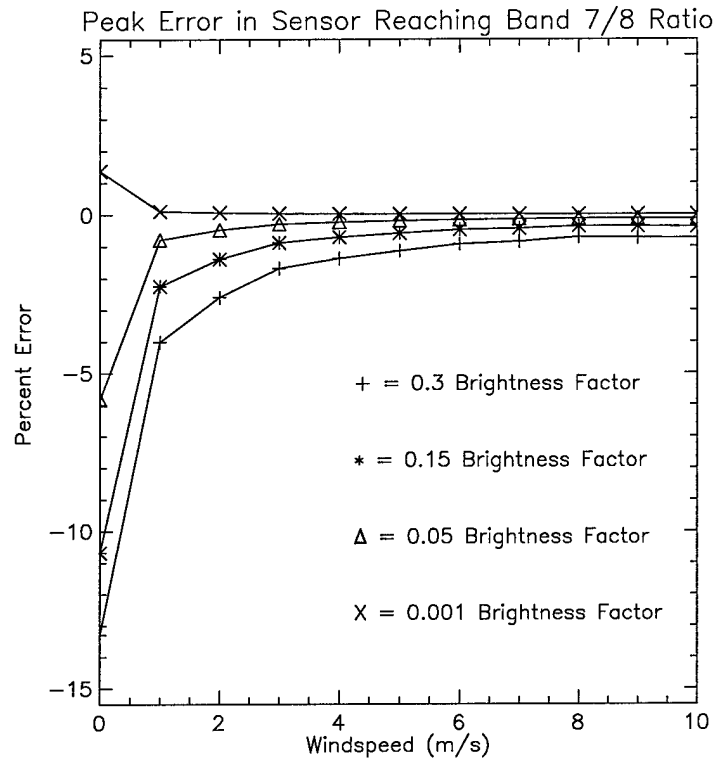


Figure 45: Percent error in Band 7/8 ratio with respect to wind speed for different brightness factor levels.

However, below 3m/sec, the variation in the peak error due to wind speed accelerates to extreme values. Further, we can see in both Figure 45 and Figure 46 that dark cloud affects and bright cloud affects diverge. In Figure 46 the impact of wind speed on the water leaving Band 3/5 ratio is plotted for cloud brightness factor levels ranging from 0.3 to 0.001. Here again, the variation with wind speed is minimal above 3m/sec or so and the variation accelerates for lower wind speeds. One saving grace for the very large errors below 1m/sec is that they correspond to very low normalized error width ratios (close to 1.0).

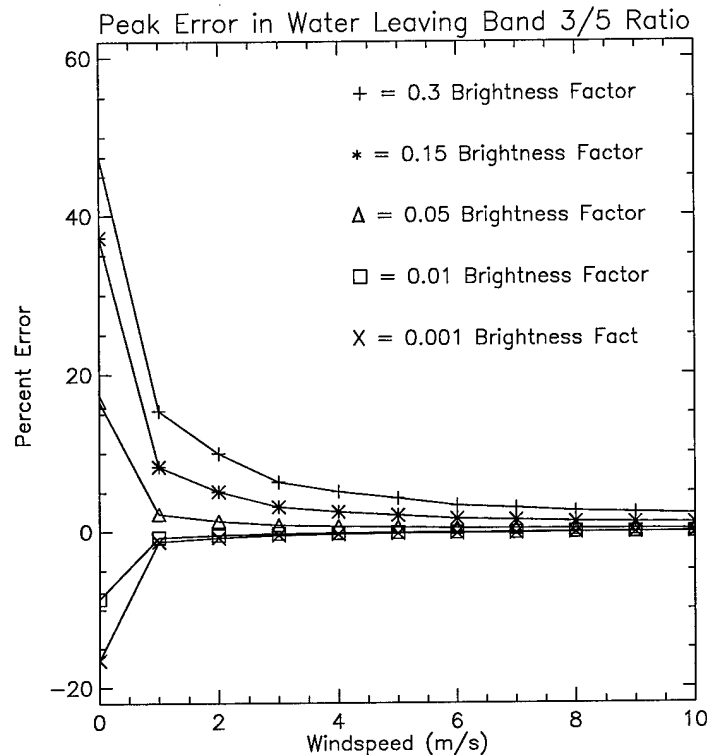


Figure 46: Percent Error in the Band 3/5 ratio as a function of wind speed at different cloud brightness factor levels

That is very intuitive. At very low wind speeds, there are very little surface waves and most of the cloud radiance reflects specularly into one quad (or at least a very limited set of quads). Since all of that radiance will reflect into one direction (tempered by Fresnel's reflection coefficient) we would expect to see a large error in a very few directions, and minimal error elsewhere.

Extending that same argument, we would expect the opposite for larger winds: minimal error spread over a larger spatial extent. Figure 47 clearly shows the increase in the normalized error width ratio with increasing wind speed (i.e. the radiance from the cloud is spread due to the increasing surface waves).



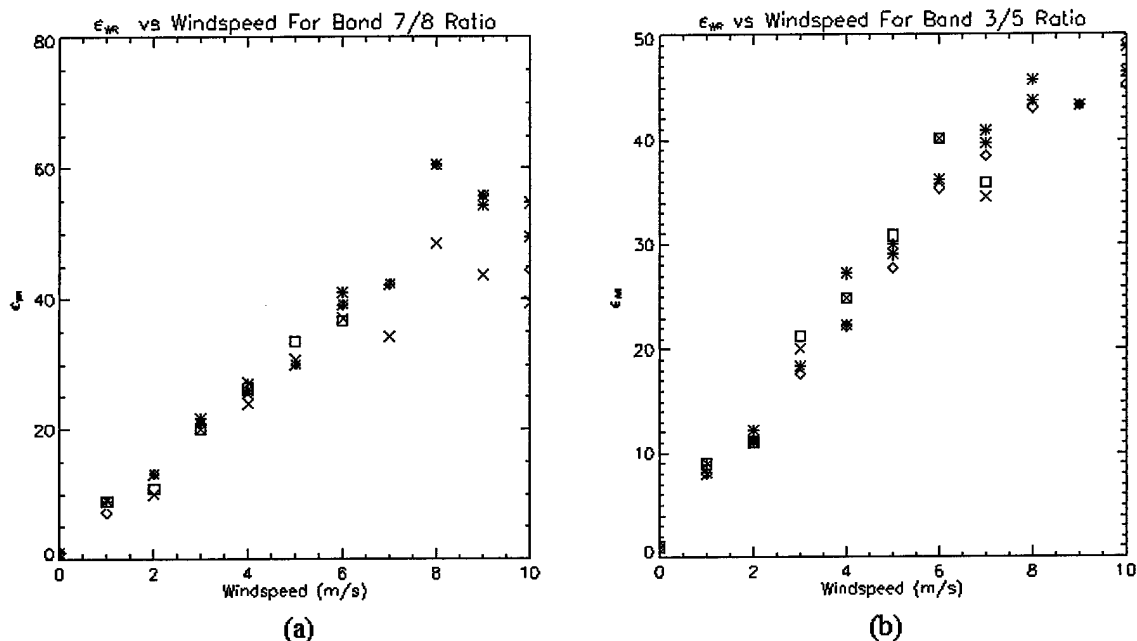


Figure 47: Normalized Error Width Ratio for the error in both the Bands 7/8 ratio at the sensor and the water leaving Band 3/5 ratio. Note the increase with wind speed indicative of the spread in the wave facet slope probability density function.

Note that from wind speeds of roughly 5m/sec to 10m/sec, the normalized error width ratio doubles. That means that twice the solid angle has an error value of at least half the peak error value. Yet, the peak error values for both the sensor reaching Band 7/8 ratio and the water leaving Band 3/5 ratio (Figure 45 and Figure 46 respectively) show very little change between wind speeds of 5m/sec and 10m/sec.

Finally, the chlorophyll content that would be calculated given perfect atmospheric subtraction is given in Figure 48 (a) for the original SeaWiFS algorithm and Figure 48 (b) for the new algorithm. In almost all cases, the chlorophyll content is underestimated from the no cloud case (solid lines).

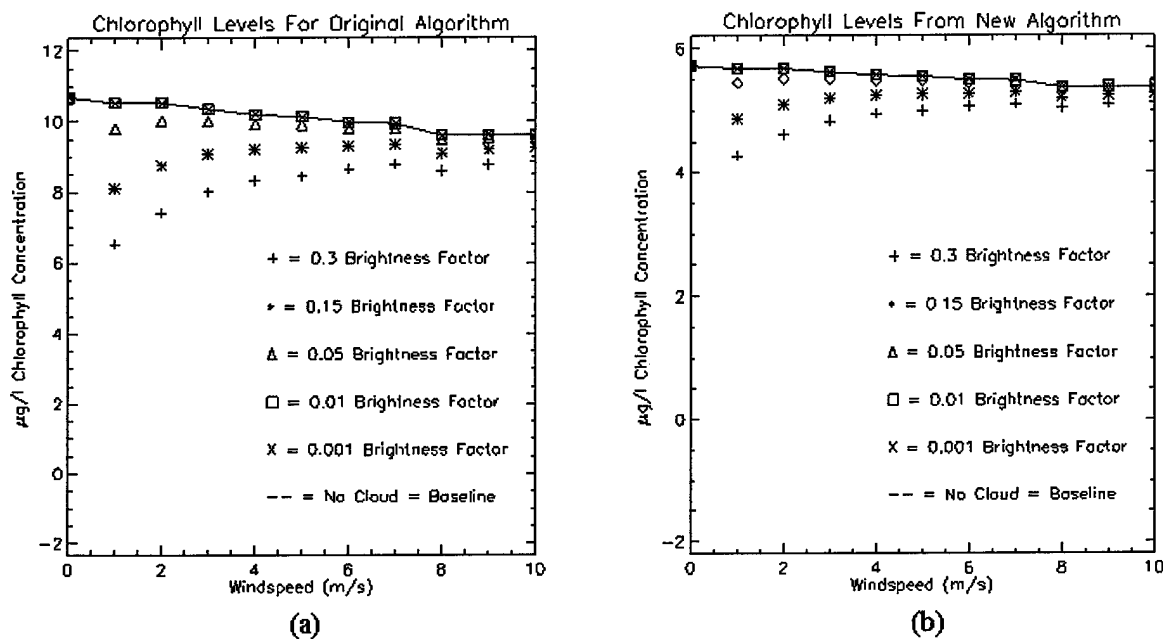


Figure 48: Calculated Chlorophyll levels using the original (a) SeaWiFS algorithm and the new (b) SeaWiFS algorithm for wind speeds ranging from 0.0m/sec and 10.0m/sec and cloud brightness factors ranging from 0.3 to 0.001. The solid line is the no cloud or baseline that each of the SeaWiFS algorithms would calculate in the absence of clouds.

Further, in almost all cases, the chlorophyll content is underestimated from the true value as well. In fact, the new SeaWiFS algorithm underestimates the chlorophyll content in this scenario 100% of the time by at least 4  $\mu\text{g/l}$  which is 40% of the true simulated value.

### The Impact With Respect to Water Quality

A few limited runs using different water quality parameters were performed. Specifically, pure water, moderately clear water (4  $\mu\text{g/l}$  chlorophyll concentration, 2g/m<sup>3</sup> of suspended mineral concentration, and 1g/m<sup>3</sup> of DOM), and more turbid water

(10 $\mu$ g/l chlorophyll concentration, 12g/m<sup>3</sup> of suspended mineral concentration, and 4g/m<sup>3</sup> of DOM) cases were used. The results of the peak error as a function of cloud brightness are presented in Figure 49 for the  $\rho_t(765\text{nm})/\rho_t(865\text{nm})$  and  $\rho_w(490\text{nm})/\rho_w(555\text{nm})$  error parameters.

We see that the affect of the cloud on the two error parameters is a function of what is in the water. High DOM, chlorophyll, and SM will allow the clouds to have a higher impact evidenced by the larger error values in both the water leaving Band 3/5 ratio (as high as 40% error) and the sensor reaching Band 7/8 ratio. Since the cloud impact for high DOM and SM levels is to overestimate the chlorophyll and the high

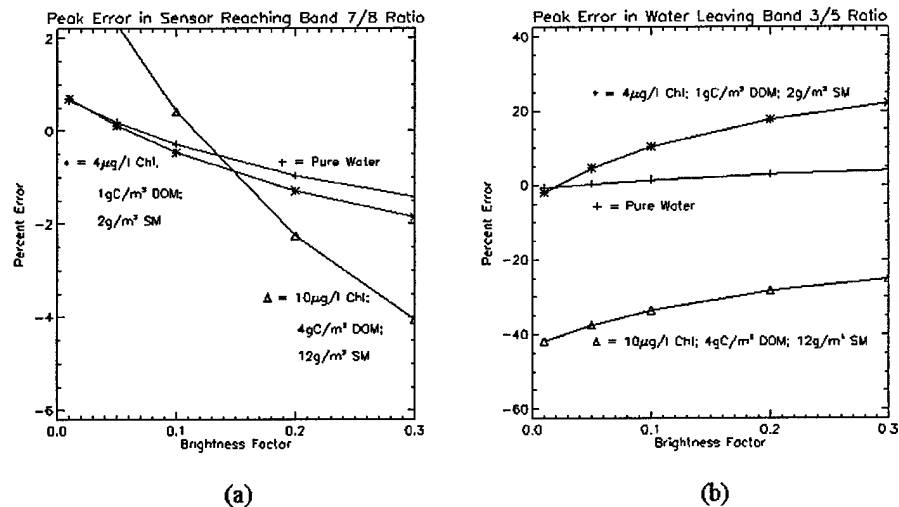


Figure 49: Percent Error both the sensor reaching Band 7/8 ratio and the water leaving Band 3/5 ratio for pure water, semi-clean water, and more turbid water. The pure water (+) is the least affected by the clouds; the semi-clean water (\*) had 4 $\mu$ g/l of chlorophyll, 2g/m<sup>3</sup> of suspended material, and 1gC/m<sup>3</sup> of dissolved organic matter. Higher levels of SM (12g/m<sup>3</sup>) and DOM (4gC/m<sup>3</sup>) are found in the third data set ( $\Delta$ ) (along with 10 $\mu$ g/l of chlorophyll) to allow the clouds to have a higher impact on the percent error for both the ratio parameters.

DOM and SM themselves cause an underestimate in the true chlorophyll levels (if the atmosphere is determined and correctly subtracted) then the errors may cancel each other out. That conclusion is drawn from Figure 50.

The baseline calculated chlorophyll content for the three cases are plotted in Figure 50 with solid lines and the appropriate symbols representing the case. The impact of the cloud for each of the cases is also plotted without the solid line. For the pure water case, the cloud had such a minimal impact on the calculation, that the two lines (+) nearly overlay. The water with higher levels of chlorophyll, DOM, and SM ( $\Delta$ ) shows the largest difference in the calculated chlorophyll content between the baseline and the cloud impacting data. However, both the original SeaWiFS algorithm and the new SeaWiFS algorithm underestimated the true levels (baseline) for the more turbid water. For the moderately clean water, both SeaWiFS algorithms were fairly close to the true levels, but the original algorithm caused an overestimate. The clouds served to lower the chlorophyll estimates in both algorithms for the moderately clear water.

However, we still have the matter of subtracting out the atmospheric affects and the data show much larger Band7/8 ratios for the water with higher levels of SM and DOM. In the earlier analysis and throughout the literature review presented earlier, we determined that more SM in the water would negate the assumption of  $\rho_w(765\text{nm})$  and  $\rho_w(865\text{nm})$  equal to zero. In my error analysis presented here, I'm removing that error from consideration by comparing the cloud data to the data

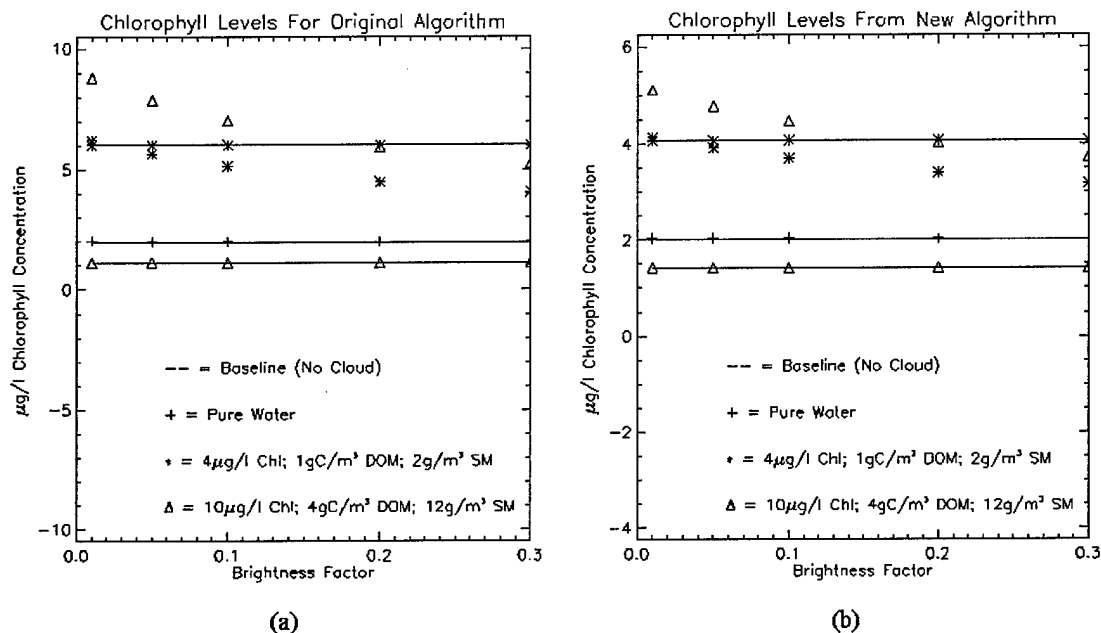


Figure 50: Calculated chlorophyll content for the three water cases used in Figure 49. To make these calculations, the assumption is made that the exact atmosphere can be removed to get to the water leaving radiance (and reflectance) values. We see from these data that the higher levels of SM, DOM, and Chlorophyll ( $\Delta$ ) allow the clouds to impact the estimates more than the lower levels.

without a cloud. The fact that the baseline (the data without a cloud) has non-zero  $\rho_w(765\text{nm})$  and  $\rho_w(865\text{nm})$  is not considered as part of the cloud impact study. I will address that later in a limited sense (see "SM Or Clouds" on page 125).

Another limited case was run with a single cloud brightness factor (0.20) and several levels of chlorophyll content. Chlorophyll levels from  $20\mu\text{g/l}$  to  $0\mu\text{g/l}$  with a low DOM level of  $1.0\text{gC/m}^3$  and a low SM level of  $0.1\text{g/m}^3$  were used. The results are plotted in Figure 51 and Figure 52.

In Figure 51 we see the error in the Band 7/8 ratio at the sensor and the water leaving Band 3/5 ratio can get quite high on a percent error basis. However, in Figure 52 we see that that does not greatly impact the actual chlorophyll calculations. Note

that in Figure 52(b) the new SeaWiFS algorithm quite accurately predicts the true chlorophyll level in the no-cloud case. That conclusion is reasonable considering that the algorithms were derived for Case I waters and the water used in this scenario is roughly Case I.

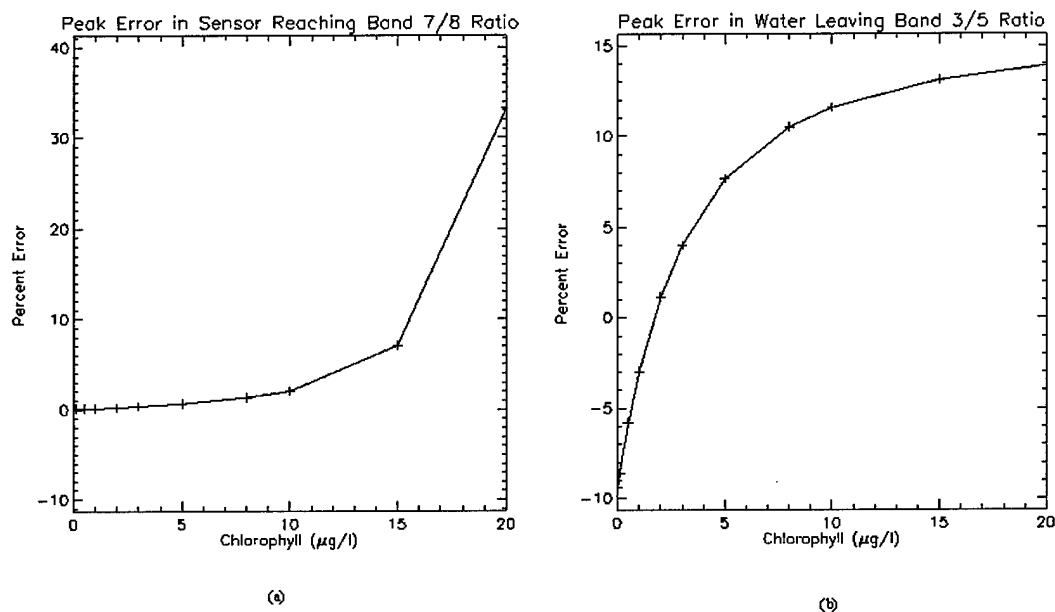


Figure 51: Percent Error for the Band 7/8 ratio (at the sensor) and the Band 3/5 ratio (at the water surface. These apparently large errors caused by the cloud imply an under estimation of chlorophyll if the error is positive and an over estimation if the error is negative. However, when the actual ratios are used to calculate the chlorophyll levels, we see very little error in the final result.

### The Impact With Respect to Atmosphere Model

The final impact area concerns varying the atmospheric aerosols. For this analysis, I used several MODTRAN generated atmospheres and varied the cloud brightness factor. The error in the Band 7/8 ratio at the sensor and error in the water

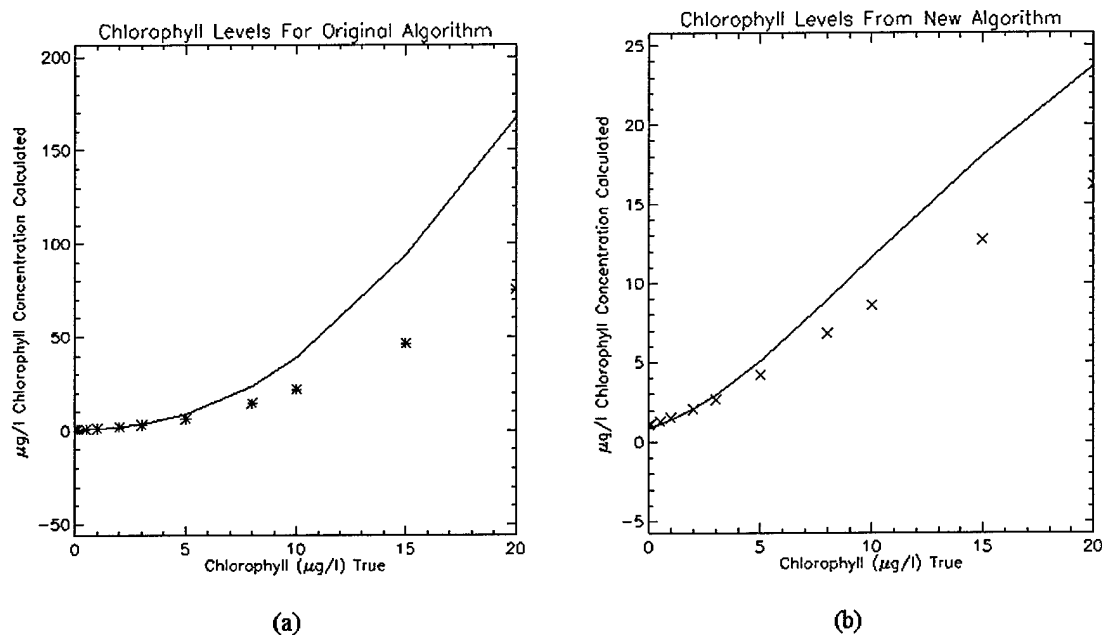


Figure 52: Calculated Chlorophyll content using the original (a) and the new (b) SeaWiFS algorithms. Given the errors plotted in Figure 51, we might expect larger error here. That is not the case for these relatively clean waters. (DOM=1.0gC/m<sup>3</sup> and SM=0.1g/m<sup>3</sup>). The maximum miss-calculation is 1.4  $\mu\text{g/l}$  in the original algorithm and 0.12 in the new algorithm. (NOTE: The data and the words don't match—I'm double checking which is wrong and which is right)

leaving Band 3/5 ratio are shown in Figure 53 for five IHAZE values. The cloud used for the data in Figure 53 occupied a solid angle of 0.083 sr beginning at a 10° declination angle and extending from 45° azimuth to 90° azimuth with a brightness factor ranging from 0.3 to 0.01. We expect to view the largest impact due to this cloud between 10° and 30° in declination angle and between 225° and 270° in azimuth. That expectation is met.

The atmospheres used to generate the data in Figure 53 differed only in the MODTRAN "IHAZE" parameter. Three IHAZE values were for fairly clear conditions and two represented hazier conditions (5km visibility). The three clear atmospheres

used an IHAZE value of 1 which equates to a rural extinction with 23 Km visibility, an IHAZE value of 4 which equates to a Maritime extinction with 23 KM visibility, and an IHAZE value of 6 which equates to a tropospheric extinction with 50 Km visibility. The two hazier atmospheres used an IHAZE of 2 which equates to a rural

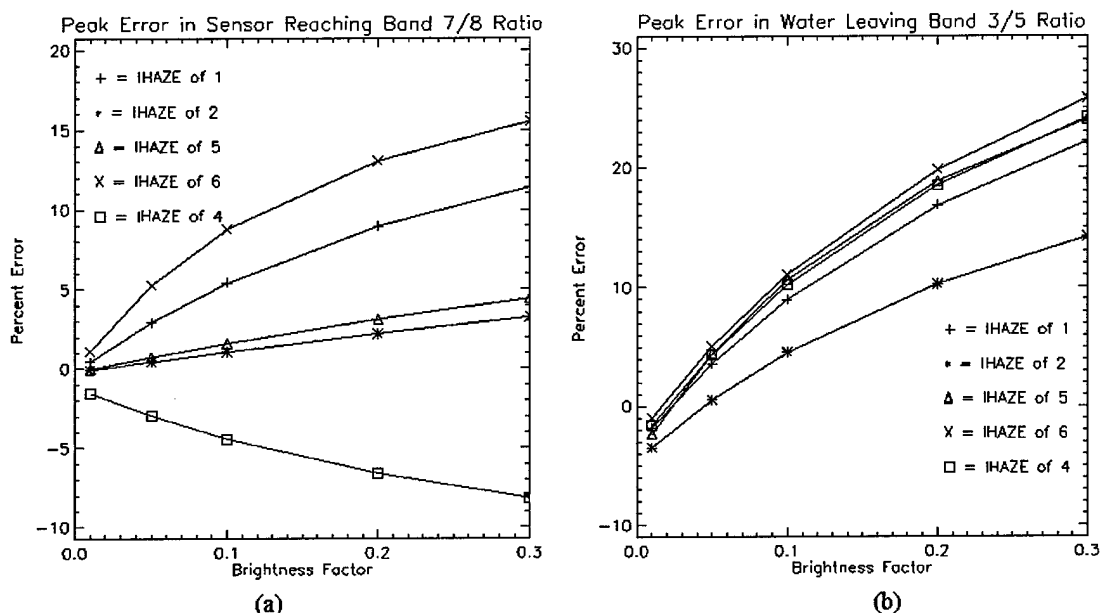


Figure 53: The sensor Reaching Band 7/8 ratio error and Water Leaving Band 3/5 Ratio Error. The cloud occupied a solid angle of 0.083 sr beginning at 10° declination angle and extending from 45° azimuth to 90° azimuth. The largest impact due to the cloud is between 10° and 30° in declination angle and between 225° and 270° in azimuth as expected. The four curves in each of (a) and (b) represent four different IHAZE parameters. An IHAZE of 1 (+) represents a rural extinction with 23Km visibility. An IHAZE of 2 (\*) represents a rural extinction with 5Km visibility. An IHAZE of 4 (□) represents a Maritime extinction with 23 KM visibility. An IHAZE of 5 (Δ) represents an urban extinction with 5Km visibility. Finally, an IHAZE of 6 (X) represents a tropospheric extinction with 50Km visibility. In (a) the two hazier atmospheres (IHAZE of 2 and 5) show less impact due to the cloud on the ratio between bands 7 and 8 at the sensor than do the clearer atmospheres (IHAZE 1, 4, and 6). No such separation is apparent in the water-leaving Band 3/5 ratio data found in (b).

extinction with 5km visibility and an IHAZE of 5 which equates to an urban extinction with 5km visibility. The two hazier atmospheres allow the cloud to impact the sensor reaching Band 7/8 ratio much less than the two clear atmospheres as seen in Figure 53(a). This results from lower transmission coefficients and higher overall



upwelled radiance from the hazier atmospheres. Even though the cloud has less impact, the atmosphere itself more than compensates because there is more of it to remove.

That means that even though I've shown that there is less error in the parameter used to determine the amount of atmosphere to subtract [via  $\rho_a(490\text{nm}) + \rho_{Ra}(490\text{nm})$  and  $\rho_a(555\text{nm}) + \rho_{Ra}(555\text{nm})$ ], there is still more overall atmosphere. Secondly, with the upwelled radiance occupying a larger share of the total sensor reaching radiance, the error in chlorophyll content determination generated by the incorrect Band 7/8 ratio is still unknown. Therefore, we can not conclude that a cloud in the hazier atmosphere will have less impact nor can we conclude that it will have more impact.

We can, however, proceed as before and assume that the correct atmosphere was subtracted in each case and assess the impact on the water leaving Band 3/5 ratio as in Figure 53(b). Here we see no specific distinction between the hazier atmospheres and the clear atmospheres. These error rates equate to chlorophyll content as calculated and displayed in Figure 54(a) and (b).

The water leaving Band 3/5 ratio error is generally positive for all four atmospheres used for Figure 54 which equates to, again, an underestimate of the chlorophyll content. That conclusion is supported by the data in Figure 54 for both the original SeaWiFS algorithm (a) and the new SeaWiFS algorithm (b). Note again

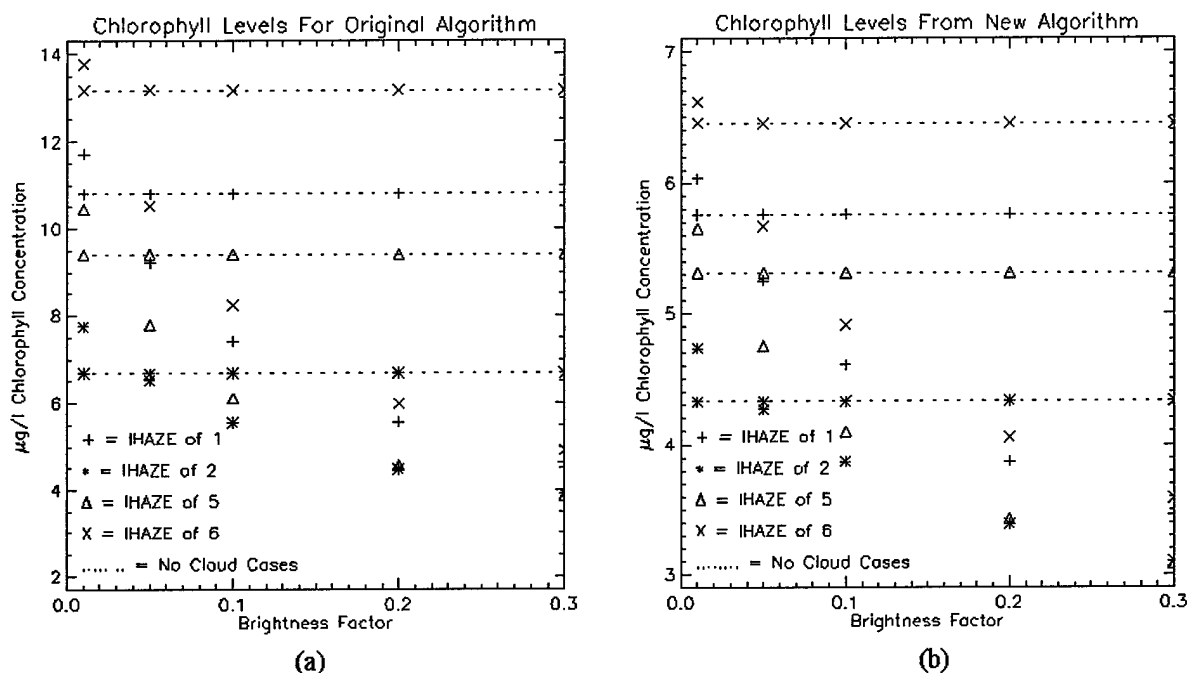


Figure 54: The Calculated Chlorophyll Content with Varying Atmospheres. The chlorophyll content that would be calculated from the Band 3/5 ratios in Figure 53(b) is plotted for both the original SeaWiFS algorithm (a) and the new SeaWiFS algorithm (b). The different atmospheres represent four different MODTRAN IHAZE parameters. An IHAZE of 1 (+) represents a rural extinction with 23Km visibility. An IHAZE of 2 (\*) represents a rural extinction with 5Km visibility. An IHAZE of 5 (Δ) represents an urban extinction with 5Km visibility. Finally, an IHAZE of 6 (X) represents a tropospheric extinction with 50Km visibility. In (a) the two hazier atmospheres (IHAZE of 2 and 5) show less impact due to the cloud on the ratio between bands 7 and 8 at the sensor than do the clearer atmospheres (IHAZE of 1 and 6).

that even without the clouds, the chlorophyll content is underestimated from the true content (10µg/l) in all cases using the new algorithm. The original algorithm would sometimes overestimate and sometimes underestimate the chlorophyll without the cloud impact. (The clearer atmospheres induced an overestimate and the hazier atmospheres induce an underestimate.)

## SM Or Clouds

The data review and cloud impact analyses are complete. The major question that remains to be answered is: "Which is a bigger problem, suspended minerals or clouds?" With the existence of the end-to-end radiative transfer tool created here, we can try to answer this question.

Using the current algorithms, the ultimate impact comparison would be in calculated chlorophyll content versus changes in "normal" SM concentrations and "normal" clouds for different levels of chlorophyll. Using this method we could easily compare the chlorophyll estimates with the "true" values to derive the impact. However, we expect that suspended minerals will have the largest impact on the atmospheric subtraction routines and the empirical database for those routines is not available. The first attempt, then, failed due to the lack of the database. My second attempt at the comparison met with more disastrous results.

Without the atmospheric subtraction database I could not use the current algorithm, so I reverted to the older CZCS algorithms. With anything in the water other than 0.25  $\mu\text{g/l}$  of chlorophyll or less this method failed miserably and it was not possible to answer the SM versus clouds question. Attempt number three fared much better.

The sensor reaching Band 7/8 ratios and the water leaving Band 3/5 ratios themselves can be compared. (Comparing the error rates would not be helpful in this case. Only the actual ratios will help answer the question.) As SM concentrations

change and as cloud brightness factors change, the two key ratios will change. The highest change will provide the highest impact. Though this method seems to imply that a series of derivatives should be used, I did not compute them. However, we can still answer the questions using the ratios and the apparent derivatives as in Figure 55.

In Figure 55 I've plotted the means of the two key ratios for chlorophyll content of  $1.0\mu\text{g/l}$  at several SM concentrations (0, 1, 5, 10, and  $15\text{ g/m}^3$ ) and four cloud brightness factors: baseline (i.e. no cloud); 0.2; 0.1; and 0.05. The means were computed for two sections. In (a) and (b) the means are over all directions outside of the sun glint and cloud glint regions and in (c) and (d) the means are over the cloud glint region alone.

We can see from these data that outside of the cloud specular region, (a) and (b) in Figure 55, the largest changes occur when the suspended minerals change. In Figure 55(a), the sensor-reaching Band 7/8 ratio change is relatively constant over the range of SM concentrations used no matter what the cloud brightness factor was. However, in Figure 55(b) we see that the water leaving Band 3/5 ratio has the largest change for low SM concentrations and minimal changes once the concentration is above  $1.0\text{g/m}^3$  or so. Again, these changes are roughly the same for all of the cloud brightness values used.

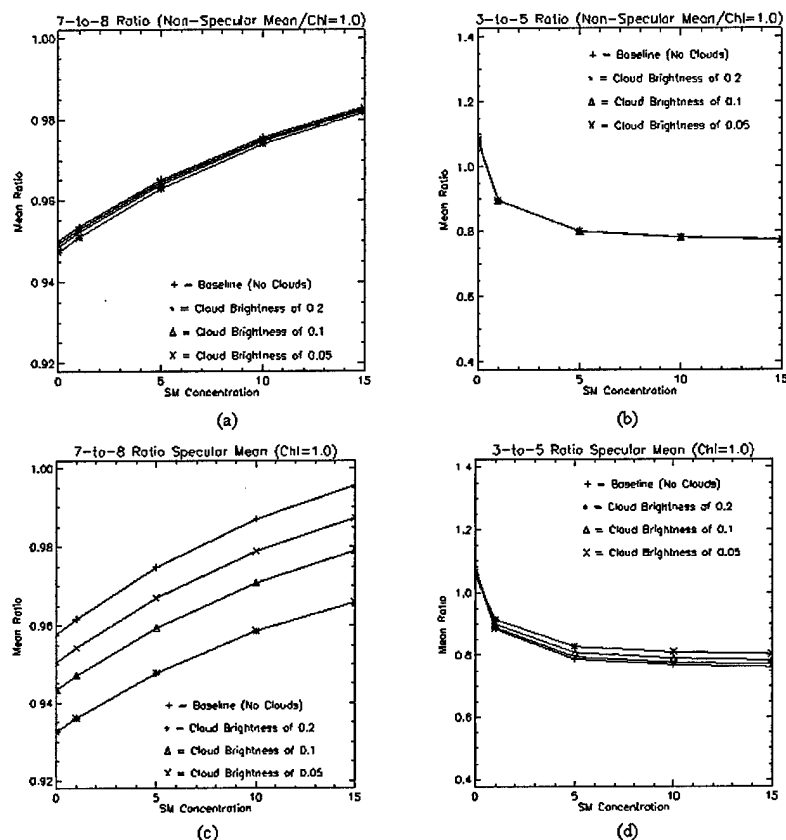


Figure 55: Suspended Mineral and Cloud Changes at a Chlorophyll level of 1.0 µg/l. The means of the two key ratios for chlorophyll content of 1.0µg/l at several SM concentrations (0, 1, 5, 10, and 15 g/m³) and four cloud brightness factors: baseline (i.e. no cloud); 0.2; 0.1; and 0.05. The means were computed for two sections. In (a) and (b) the means are over all directions outside of the sun glint and cloud glint regions and in (c) and (d) the means are over the cloud glint region alone.

In Figure 55(c) and (d), that is not the case. In the cloud specular region, the cloud could impact the two key ratios as much or more than the suspended minerals. In fact, above 5 g/m³, the largest variation in the water leaving Band 3/5 ratio comes from the changes in the cloud brightness factor. (As the SM concentration rises from 5g/m³ to 15g/m³ the water leaving Band 3/5 ratio stays nearly constant. Yet, over the same range, as the cloud brightness factor changes, large changes occur in the water

leaving Band 3/5 ratio.) Similar data and results are obtained for chlorophyll levels of 0.1 $\mu$ g/l and 10.0 $\mu$ g/l and at different levels of DOM concentration.

These results are consistent with the cloud analysis performed here and the SM studies in the literature. Bukata (1997) has indicated that any appreciable concentrations will greatly impact the water's chromaticity (and, thus, the ratios of the volume reflectance for two different wavelengths). He further states that after the initial fast changes, the chromatic behavior asymptotically approaches a constant value. Such a behavior is found in Figure 55(b) and (d).

### **Summary of Results**

With the exception of the one section on varying water conditions, all of the analysis used nominal Lake Ontario waters of 10  $\mu$ g/l of chlorophyll content, 2 .0gC/m<sup>3</sup> of Dissolved Organic Matter, and 6.0g/m<sup>3</sup> of Suspended Materials. Also, Maritime, Rural, Urban, and Tropospheric aerosol extinctions were used with visibilities ranging from 5 km to 50km. Cloud impacts were derived for varying the cloud brightness factor, the cloud location, the cloud to cloud+sky ratio, the shape of the clouds, the water conditions, the wind speed, and the atmospheric aerosol IHAZE parameter.

We showed that varying the cloud brightness factor impacts both of the key SeaWiFS parameters, the sensor reaching  $\rho_t(765\text{nm})/\rho_t(865\text{nm})$  and the water leaving  $\rho_w(490\text{nm})/\rho_w(555\text{nm})$ . However, the impact was localized to the viewing angle 180° in azimuth away from the cloud at roughly the same declination angle. The only

spread outside that quad (parameterized with the normalized error width ratio) was due to the surface wave orientation changes with wind speed. The overall affect of the white clouds was to underestimate the chlorophyll content for the water conditions used.

The location of a single cloud affects the estimated chlorophyll content similarly, but the larger Fresnel reflectance (i.e. cloud glint) of high declination angle clouds cause a larger impact. Further affects were shown in the normalized error width ratio. With the quad partitioning used by HydroMod, larger declination angles would necessarily have larger solid angles and a correspondingly smaller  $\epsilon_{WR}$ .

The size of the cloud was shown to effect the peak error in both  $\rho_t(765nm)/\rho_t(865nm)$  and  $\rho_w(490nm)/\rho_w(555nm)$ . Larger clouds provide correspondingly more radiance to the water surface and affect the error parameters similarly. Larger cloudbanks also helped keep the normalized error width ratio close to 1.0.

Wind speed was shown to affect both the peak errors and the normalized error width ratio. As the wind speed increased, the peak error decreased slightly and spread to more quads. This was evidenced as a steadily increasing normalized error width ratio. The peak error did not decrease at the same rate as  $\epsilon_{WR}$  increased for any of the cloud brightness factors shown. The exception to that conclusion is at very low wind speeds (less than 2m/sec). In that case, the peak decreased rapidly from the

specular case (0m/sec and  $\epsilon_{WR}=1.0$ ) to cases similar to the PDF's given by Cox and Munk in EQ 5.

The analysis carried further than just the impact on the key parameters,  $\rho_t(765nm)/\rho_t(865nm)$  and  $\rho_w(490nm)/\rho_w(555nm)$ , and into the actual calculation of the chlorophyll content using both the original SeaWiFS algorithm (EQ 31) and the new SeaWiFS algorithm (EQ 33). In all of those calculations, perfect atmospheric subtraction is assumed. In almost all of those chlorophyll predictions, the impact of the clouds is to underestimate the chlorophyll content.

The water content was also changed and the brightness factor variation was presented. For clearer water, the overestimate of chlorophyll caused by the cloud was evident. For less clear water, the reverse was true.

Finally, different atmospheres were selected and the affects on the key parameters were derived. It was demonstrated that hazy atmospheres have less error in the  $\rho_t(765nm)/\rho_t(865nm)$  atmospheric correction parameter, but they also have more atmosphere for which to correct. The hazier atmospheres also resulted in an underestimate of the chlorophyll content using  $\rho_w(490nm)/\rho_w(555nm)$ ; this was consistent with normal results using a clear atmosphere with the standard water conditions.



## **Operational Impact of Results**

Future algorithms for monitoring water quality parameters via remote sensing may wish to consider the impact of clouds on the remotely sensed data. From the results and cloud impact analysis performed and presented here, we can determine some of the operational considerations that should be included in those future algorithms.

I've shown in the analysis that the clouds' specular direction is the direction of peak error due to clouds. Further, the "width" of the error depends on wind speed and, to a lesser extent, on the clouds' declination angle. Therefore, operationally we may want to look for clouds in the scene that are at or near the specular direction of the sensor's look angle. The term "near" would be largely a function of the wind speed. Outside of the specular direction and "near" the specular direction, the cloud impact seems to be minimal. Also, the amount of impact (other than direction) is not affected by the wind speed for speeds greater than about 2m/sec.

Since the cloud brightness factor plays a large roll in the cloud impact, a method is required to determine that relative factor at the point of interest on the water surface. This method would most likely account for the sun and cloud location, the type of cloud in question, the size and shape of the cloud, and the number of clouds in the scene. A (currently non-existing) database of cloud brightness factors with respect to those variables is required to derive such a method.

Another operational impact concerns the atmosphere itself. The wide variation in impact due to the changes in IHAZE parameters suggests separate atmospheric correction algorithms for different operational regimes. That is, over the Laurentian Great Lakes we would never have a Maritime atmosphere (since it contains a salt content) so why use an algorithm that was derived primarily for the Maritime conditions? A new algorithm (or perhaps the same algorithm with different parameters) is required to take advantage of this non-Maritime fact.

The atmosphere and its subtraction from the data remain the key component in monitoring the water quality parameters. As such, most of the effort should be spent in this area. A new algorithm specifically derived for use over the Laurentian Great Lakes would be a major step in improving the estimates of water quality parameters. The specular region once again is the only area of concern when correcting for clouds as part of the atmospheric subtraction routines. Once the atmospheric component is correctly removed from the data, the water leaving component can be effectively addressed.

Specifically, new algorithms are again required for deriving the water quality parameters in the presence of high suspended mineral concentrations. (In fact, they are required in the presence of *any* suspended mineral concentrations.) The same applies for higher chlorophyll concentrations; however, the new SeaWiFS algorithm is much better than the original SeaWiFS algorithm. It was also shown that the higher concentrations of suspended minerals and/or chlorophyll will impact the key ratios

much more than clouds for directions other than near the cloud specular direction. Since that can be a larger number of directions (depending on the amount of cloud cover and the wind speed), more accurate algorithms are needed. Further, even near the specular direction the algorithms need to work for the higher concentrations before we even consider the clouds.

Therefore, operationally we need to worry about and correct for clouds at or near the specular direction only and only after better atmospheric correction algorithms and better water-quality-parameter-algorithms are created. HydroMod can help create such algorithms.



## *Chapter 6*

### **CONCLUSIONS**

#### **Summary of Contributions**

The major contributions from this work to the field of remote sensing over water include:

1. The creation of the entire end-to-end model;
2. The incorporation of a realistic cloud model in the study of radiative transfer over water; and
3. The characterization of the impact of clouds to the radiance reaching the SeaWiFS sensor along with the derived chlorophyll content.

HydroMod, the end-to-end radiative transfer model created for this study, is an extremely valuable tool for developing and evaluating algorithms for retrieval of water parameters. Even for a cloud free sky, such a model has not been reported in the literature. This report does not cover HydroMod in and of itself. Appendix I contains a Users Manual for HydroMod and Appendix II contains some additional information concerning HydroMod. All of the decisions and conclusion drawn in the body of this work were incorporated into HydroMod as part of the end to end model. (Other items,

such as radiance sources internal to the water body were also included in HydroMod, but were not discussed here.)

MODTRAN has become the industry standard for many atmospheric and/or land based radiative transfer derivations due to its accuracy. However, using MODTRAN to provide the input to an underwater module is unique. Further, using the MODTRAN radiance values along with the Cox and Munk water surface orientation to get the true downward radiance distribution below the surface,  $L_{\lambda}^{\downarrow}(\theta, \phi)$ , allows accuracy that is rarely achieved for such a complex problem. The model is very valuable if it were only used to study water quality algorithms or water quality detection schemes. Adding cloud inputs makes the model even more valuable.

The cloud model is both simple and elegant. Instead of endeavoring to accurately model these complex and nebulous blobs of water and ice, calculate a BDRF, determine the total input radiance from all directions, and then calculate the radiance to the point of interest, we chose to simply model the radiance to the point of interest. The key bit of good luck with the cloud model is that the spectral response curves for all of the MODTRAN generated clouds were extremely similar. Instead of having a family of cloud spectral response curves, a single curve could be used. HydroMod, however, allows for that curve to be changed at the users' discretion. This allows the advantage of

being able to model an exact scene using spectralradiometer measurements from the true clouds in the vicinity. Without the cloud model, the cloud impact analysis could not have been completed.

The cloud impact analysis is required so that we may know when and how clouds impact (or could impact) the conclusions drawn from the remotely sensed data. The failures noted in the introduction concerning SeaWiFS calculated chlorophyll levels (i.e. the reason that generated the requirement to study the impact of clouds) tended to be when SeaWiFS predicted too much chlorophyll. However, one of the main findings here is that for most normal Lake Ontario waters, the impact of clouds should be a lower chlorophyll prediction. The main exception to that finding occurs in the presence of hazier atmospheres.

A full summary of all of the results from the cloud impact study can be found at the end of that chapter.

### **Recommendations**

Though all requirements set forth in the proposal were met (and exceeded in most cases), there are some other areas of interest that should be pursued. Many such recommended pursuits center on the use and future improvements for HydroMod.

Other recommendations are in the area of further cloud impact studies and SeaWiFS chlorophyll content derivations and failures.

With the remote sensing over water end-to-end radiative transfer tool in hand, we can begin to build large databases of look up tables for various water and atmospheric conditions. This will most likely occur. However, we could take full advantage of the linearity of the results by using a "sky" input of only a single component from one declination angle. A series of these single cases for each declination angle is required. For the HydroMod high-resolution data, there are 18 declination angles to consider; in the low-resolution mode there are 10. Using the results of each one of these 10 (or 18) cases, we can artificially create the results from any sky input. Linearly scaling, rotating, and summing copies of results from the original 10 (or 18) runs can do this.

I highly recommend performing a few simple test cases that include all of the functionality of HydroMod. There will be some cases where it works very well and exact results are obtained. Yet, there may be some cases (like when using radiance sources internal to the water body as a possibility) that are not practical.

Another set of look up tables can be generated that uses only the total absorption coefficient and total scattering coefficient as variables. From this set of look up tables, whenever chlorophyll, DOM, and SM concentrations and cross sectional data are selected, a new set of look up tables can be easily generated. When using this recommendation, we need to note three caveats: (1) that it would not apply



if internal sources were included; (2) it only applies if the bottom is not a factor; and (3) the water body is assumed homogeneous. A major advantage to this approach is that the data do not need to be run spectrally. The spectral content only applies when we use an absorption or scattering cross section. That means that the spectral character comes out when generating the specific results for the selected concentrations and cross sections.

If HydroMod is going to be around for a long time, I recommend vectorizing the Hydrolight Fortran code to speed up processing. We could also replace the method used for the Riccati equation integration; the Hydrolight method of a fourth order Runge-Kutta algorithm is the normally recommended method for solving differential equations, but simpler and faster methods are available that should provide just as much accuracy a lot faster. (Since the attenuation and scattering of light underwater are well-behaved smooth functions, we shouldn't need the fourth order Runge-Kutta method used by Hydrolight.)

Concerning further analysis of the cloud impact study, the next phase should be to clean up some of the missing components. For instance, more analysis should be done with different atmospheres and different water content with the goal of creating new and improved algorithms for use over the Great Lakes and/or coastal regions. The limited range presented here was both more than originally planned and far from completing the whole job. It did, however, point to the need for more work in those areas.

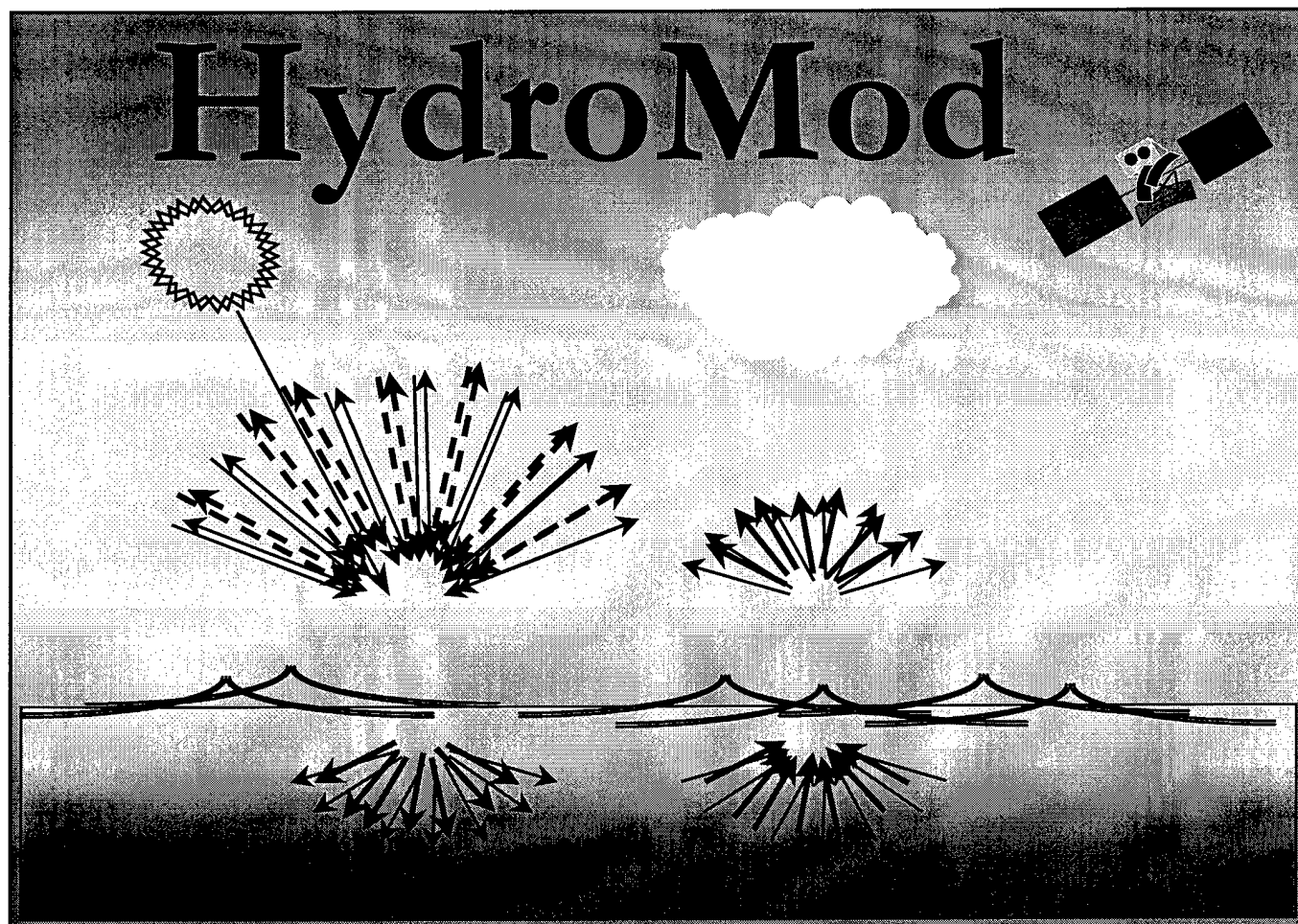
Notwithstanding the need for the improved algorithms, correcting for the cloud impact on the chlorophyll content can be attacked starting now. All of the tools are in place to perform the required analysis. However, based on the results here and until we get more data from different water content and different atmospheres, there may not be a need to correct the SeaWiFS algorithms. We may be trading one bad estimate for another bad estimate.

## **APPENDIX I**

### **A HydroMod Users Manual**



DIGITAL IMAGING AND REMOTE SENSING GROUP  
Carlson Center for Imaging Sciences, Rochester Institute of  
Technology



A Remote Sensing Water Quality Tool  
HydroMod Version 1.0

# Users Manual

Ronald R. Fairbanks; Dr John R. Schott Advisor



## Acknowledgements

Many people helped in the creation of HydroMod and I would be remiss if I did not acknowledge the efforts by these individuals. I must say up front, however, that any errors in the code and/or illogical processes that HydroMod undertakes are solely my responsibility. I started with excellent industry standard codes in MODTRAN and Hydrolight, and I received some excellent advice and comments. Manipulating that code and implementing that advice, however, are where all of the illogic and outright errors (though minimal and minor) lie and I hold only myself accountable for all of that.

Dr. John Schott is my principal advisor and the driving source behind the creation of HydroMod. It was his idea and it was under his direction that the code took shape. Dr. Anthony Vodacek supplied many comments, goals, and advice for manipulation of the underwater portion of the code. Dr. Vodacek also supplied the original Hydrolight 3.0 code that I started with. The rest of my dissertation committee, Dr. Harvey Rhody and Dr. John Waud, also supplied several meaningful comments and advice along the way.

Scott Brown supplied several MODTRAN tips and tricks and generously allowed me to bounce ideas and thoughts off of him before I implemented them in the code. Capt Erich Hernandez-Baquero was a tremendous help in the code validation process. Erich always seemed to have the right question for me to attack and he helped exercise HydroMod in the early stages. 1Lt Niki Wilson was also an early participant and helped convert HydroMod to the original UNIX versions. Mary Ellen Miller was the first actual user of HydroMod other than me. She was and still is the main guinea pig and by asking questions and finding some of those errors or illogical processes she has been a great help.

The original code that I started with includes MODTRAN and Hydrolight, but it also contains some portions of IDL code written by Julia Barsi. She writes good code and I used her same logic in several routines. The list of MODTRAN authors is long; I'll simply say thanks for creating, supplying, and continually updating MODTRAN to the Air Force Laboratory at Hanscom AFB (AFRL/VS). That thanks goes out especially to Jim Chetwynd, Mike Hoke, and Gail Anderson. Dr. Curtis Mobley wrote the Hydrolight code and I am deeply indebted to him for making the code available for educational purposes. Combining Hydrolight and his book, *Light and Water*, to help explain what the code is calculating, Dr. Mobley supplied me with almost all of the information that I needed for the underwater portion of HydroMod.

The biggest contributors gave no advice and only minimal comments, only full support and a lot of love. The support provided by my wife, Tina, and my children, Alex and Joshua, was indispensable. The working weekends, long days, and many evenings take their toll. Families as loving and as strong as mine help each other survive and thrive and I am truly blessed.





# Table of Contents

<b>Chapter 1: Introduction</b>	<b>149</b>
<i>System Requirements</i>	<i>150</i>
<i>Installing HydroMod</i>	<i>151</i>
<i>Existing Look Up Tables</i>	<i>153</i>
<i>Theory of Operation</i>	<i>154</i>
 <b>Chapter 2: Running HydroMod</b>	 <b>159</b>
<i>Collecting HydroMod Input</i>	<i>159</i>
<i>Begin Execution</i>	<i>179</i>
<i>HydroMod Output</i>	<i>185</i>
 <b>Chapter 3: Outside of HydroMod</b>	 <b>189</b>
<i>Running H20Code.exe</i>	<i>189</i>
<i>Changing Defaults and Files</i>	<i>192</i>
<i>Creating Look Up Tables Offline</i>	<i>193</i>
<i>HydroMod Output</i>	<i>194</i>
<i>Conclusion</i>	<i>201</i>







## Introduction

*Chapter Synopsis: In this chapter we introduce HydroMod, get it installed on the computer with the correct files in the correct locations, and cover some of the basic theory of operations.*

---

### CHAPTER OUTLINE

---

-  System Requirements
  -  Installing HydroMod
  -  Existing LUTs
  -  Theory of Operation
- 

The name "HydroMod" represents three simultaneous occurrences: (1) it is a water quality ("Hydro") remote sensing model ("Mod"); (2) its main components stem from two pre-existing industry standard codes, Hydrolight and MODTRAN; and (3) its creation involved several modifications ("Mod") to Hydrolight ("Hydro"). The name would have probably been different if the three statements were not simultaneously true. The fact that it is a tool for studying remote sensing of water quality, however, is constant whatever the name happens to be.





And HydroMod is exactly that: a tool for studying the remote sensing of water quality parameters. Fundamentally, we seek to solve the radiative transfer equations in a realistic environment starting from the sun and ending at the remote sensing platform. Operationally, HydroMod uses two premier industry standard codes to actually solve the radiative transfer equations (MODTRAN and Hydrolight). In that sense, HydroMod is an IDL widget (graphical user interface in IDL terms) driven shell that sets up the "realistic" environment under study. The ability to add clouds into our environment has been added outside of the MODTRAN and Hydrolight pre-existing codes as has several data analysis capabilities.

This *Users Manual* will attempt to guide new users through the first few runs of HydroMod. This first chapter, "Introduction", covers the background information needed to install HydroMod and understand what the code is doing. The second chapter, "Running HydroMod", is the bulk of the manual and covers actually running the code. The sections of Chapter 2 cover the user supplied input options and some of the theory behind those options. The third and final

chapter, "*Outside HydroMod*" covers other IDL codes that come with HydroMod for either creating new input files or for using HydroMod output files or other related events. Since HydroMod is written using IDL, the full utility of this image based language is at our disposal; I highly recommend using it to your full potential. Stated another way, don't rely on the IDL code and code fragments supplied with HydroMod for all the data analysis; adventure into IDL along with your imagination and create your own analysis tools.

## System Requirements

HydroMod was created to operate on a MS Windows based PC. However, most of the functionality has also been used on a DEC Alpha Unix based system. At the core, HydroMod is IDL and Fortran 77 and can ultimately be made to work on any system that can use both of those languages. However, the conversion to systems other than MS Windows based PCs is more advanced and is not covered here. If that is your intention, good luck and happy computing. Here we will cover the basic requirements for the core code as supplied in the "standard" distribution.

SYSTEM REQUIREMENTS	
	Pentium or Similar PC
	Windows 95/98/NT
	IDL 5.0 or Newer
	16MB Disk Space

If you have MS Windows 95/98 or MS Windows NT with IDL Version 5.0 or later (through at least 5.2) and at least one hard drive with at least 16MB<sup>1</sup> free disk space, then HydroMod should work on your system. The lowest end system that HydroMod has been demonstrated on is an Intel Pentium 200MHz with 32 MB RAM running Windows 95 and IDL 5.0. It has run well on laptop and desktop systems; Pentium and Pentium II; Windows 95, Windows 98, and Windows NT; and IDL 5.0 and 5.2. It does NOT work with IDL versions prior to 5.0.

---

<sup>1</sup> The 16MB of free disk space is an absolute minimum. The code installation will require only about 5MB of space, but the operation requires unpacking zipped look up tables and creating output files. The smallest of the look up tables and output files would consume the final 11 MB quickly; at least 10 times 16MB or 160MB is recommended as the operational minimum.

## Installing HydroMod

To set up HydroMod for use on a PC, follow these simple steps (the explanation follows the list):

1. **Copy the 'HMDATA' directory and all of its contents to the "C:\\" hard drive on your P.C.** The Fortran 77 based compiled codes will be reading and writing to files that must be contained under the "C:\HMDATA" directory or its subdirectories.
2. **Change the attributes of the above files by removing the READ ONLY option.** Some of these files will be written over during execution of HydroMod. Since these files all come from the CD ROM they are inherently READ ONLY and when HydroMod attempts to write over the files an error will occur.
3. **Copy the contents of the "IDLPros" directory to whatever hard drive directory you want to run HydroMod from.** This directory contains about 35 IDL procedures (and counting) for use by HydroMod and the output associated with HydroMod. It also contains a batch file for the DOS based executable code that runs the underwater module, H2OCode.EXE and, during execution, it will contain the scattering phase function data used by the code. (More information for the scattering phase functions can be found later.)
4. **Obtain a compiled copy of H2OCode.EXE** (which is the modified version of Hydrolight compiled and running on a Windows based PC) **and put it in the directory in #3 above from which you will be running HydroMod.** When I modified Hydrolight 3.0 I didn't think it was right to still call it Hydrolight so out of respect for Dr. Mobley and his original work, I changed the name of the executable code from the modified version to simply "H2OCode.EXE". However, the original copyright most likely still applies (and I've honored it to the fullest extent possible) so you'll need to obtain a copy of the executable H2OCode.EXE under either a new agreement with Dr. Mobley or via the terms and conditions of the original copyright. If you are an RIT user, the program should be included or at least available.

5. **Decide on a directory or directories for the LUTs and make sure that they exist. Put copies of PKZIP.EXE and PKUNZIP.EXE in those directories.** You'll need to get copies of PKZIP.EXE and PKUNZIP.EXE from PKWARE at <http://www.pkware.com> if you do not already have them. I am not allowed to distribute them to you. (Note: If you are an RIT student or faculty/staff member then the disk that contains HydroMod may also contain the PKZIP.EXE and PKUNZIP.EXE)
6. **IF you have room on a hard drive, copy all of the look up tables (LUTs) to the hard drive.** There are LUTs for the sky files and LUTs for the wind roughened sea surface files (more information is available in the next section). You can also use these directly from the CD if you do not have enough room on your hard drive. (You'll still need the directories and PKfiles from step 5 above.)
7. **Start IDL and change directories to the IDLPros directory you copied onto your hard drive.** An alternative is to set your IDL\_Path variable to look in that directory; either way works. To make this easy for me, I created a three line IDL procedure that changes the working directory at execution and then I put it in my IDL library of functions. The three lines are:

```

pro gthm                                ; "GTHM" stands for "Go To HydroMod"
cd, 'd:\HydroMod\IDLPros\'             ; My working HydroMod directory of course
end

```

When I enter IDL and want to run HydroMod, I first type "GTHM" at the prompt and my working directory changes to "D:\HYDROMOD\IDLPROS\".

8. **Type "hydromod" at the IDL prompt to run HydroMod.**

For many users, the program is now running. However, some anomalies that I've come across may occur (and, perhaps, several that I haven't come across.) For instance, a copy of "IDLspawn.PIF" may be needed in the directory from which you are running HydroMod and in the directories containing the look up tables. This seems to be true for some IDL versions prior to 5.2 and at least when using Windows 95. In

at least one case using IDL 5.0 and Windows NT the copies of "IDLSpawn.PIF" were required.

Many errors that can occur in HydroMod do not cause operation to cease. As such, users go blindly forward not knowing that an error occurred and critical files were not created or output was not read, or some spawned process never actually occurred. This happens for multiple reasons. One reason is that IDL widgets are very error friendly and generously allow the error to occur while simply reporting the fact. Another is that spawned processes flash the existence of an error on a DOS window, but the window is closed too fast to be seen. Yet another is that when the compiled Fortran codes hit an error they stop and give control back to the DOS window which promptly closes and returns control back to IDL before users can view what happened. Please be aware of the possibilities.

## Existing Look Up Tables

I've generated at least 75 atmospheric and over 90 wind roughened sea surface look up table files (LUTs) for use in HydroMod. Those were most likely included with this manual and the associated code. Users will eventually generate their own LUTs, but the first few runs will probably be completed using the existing ones.

If the LUTs exist on the hard drive, it is simply a matter of knowing the location and HydroMod can use them. If using a CD ROM, HydroMod can still use them, but the added step of copying the precise LUTs needed to the hard drive is added. The CD ROM method uses more time and less space. The hard drive method uses more space and less time and it is slightly easier; the HydroMod default is to NOT use the CD ROM method so that option needs to be checked each time it is used.

In any event, the files that are already created (and most of those that HydroMod will create) use a specific naming convention that indicates most of the MODTRAN parameters used to generate the file. For instance, one example of a file is:

S40M2S-5C363H1S0V0C00C00V00R000.zip

The name is a series of letters followed by numbers. The letters stand for the variable or parameter that the number represents. In this

example, S40 means that the sun is declined 40° from zenith; M2 means that the MODTRAN "Model" variable was 2 which means that it was a Mid-Latitude Summer atmospheric model. The S-5 represents the surface albedo of the earth and in this case, a -5 means that it is the albedo of the ocean. C363 means that the CO<sub>2</sub> mixing ratio was 363 ppmV; the H1 represents and IHAZE of 1 (rural extinction with 23 Km default visibility.) The next S0 represents the selection for the ISEASN MODTRAN parameter that is 0 in this case. The rest of the letters represent IVULCN (V), ICSTL (C), ICLD (C), VIS (V), and RAINRT (R). All of the files generated to date use a ground altitude of 218 m above sea level; sea level is defined to be the mean radius of the earth. A naming convention in later models may add the "G218" tag to the filenames to indicate the ground altitude.

The existing look-up-tables include sun declination angles of 20°, 30°, 40°, 41°, 50°, 60°, and 70° with various IHAZE parameters and model atmospheres. All of them were generated with multiple scattering turned on using the Isaac's two-stream model (i.e. DISORT was not turned on).

The water surface LUTs have names like:

W0453672.zip

that mean it is for a wind speed (W) of 4.5m/sec (045) with 36 quads in declination angle and 72 quads in azimuth angle(3672). The wind speeds cover 0.0m/sec to 12.5m/sec in 0.5m/sec steps and include other MODTRAN defaults of 4.1m/sec, 6.7m/sec, 6.9m/sec, 7.2m/sec, 10.3m/sec, and 12.3m/sec. Data resolutions include 36x72 quads (high resolution), 20x24 quads (low resolution), and 36x24 quads (medium resolution).

## Theory of Operation

Take a quick look at the front cover of this manual; the picture explains what HydroMod does. HydroMod predicts the radiance in all directions (upward and/or downward hemispheres at a time) using an input set of information for the atmosphere, clouds, wind speed, water, and wavelength bands of interest. The "radiance in all directions" is at the water surface (above and below the surface); at the sensor; at the bottom of the water; and at any specified point within the water body. To explain how this is done within HydroMod, the first thing we need is a method of accounting for the geometry.



HydroMod uses the digitized sphere in Figure 1 to account for the directional information. The sphere shown is partitioned into  $34 \times 72 = 2448$  equiangular plus 2 endcap "quads". Half of these represent the upper hemisphere and half represent the lower hemisphere. In half, the light travels up into quads representing a given azimuthal and declination angular direction and in half the light travels down into quads representing azimuthal and declination angular directions. The spacing for each quad is  $360^\circ/72=5^\circ$  in azimuth and  $180^\circ/35 \cong 5.1429^\circ$  in declination angle. The center for each of the 72 quads adjacent to the endcap is at  $5.1429^\circ$ ; the center for each of the 72 quads in the next ring out is at  $10.286^\circ$ .... Logically, the center for the ring of quads right next to the  $90^\circ$  point is at  $90^\circ - (1/2)(5.1429^\circ) = 17 \times 5.1429 = 87.429^\circ$ .

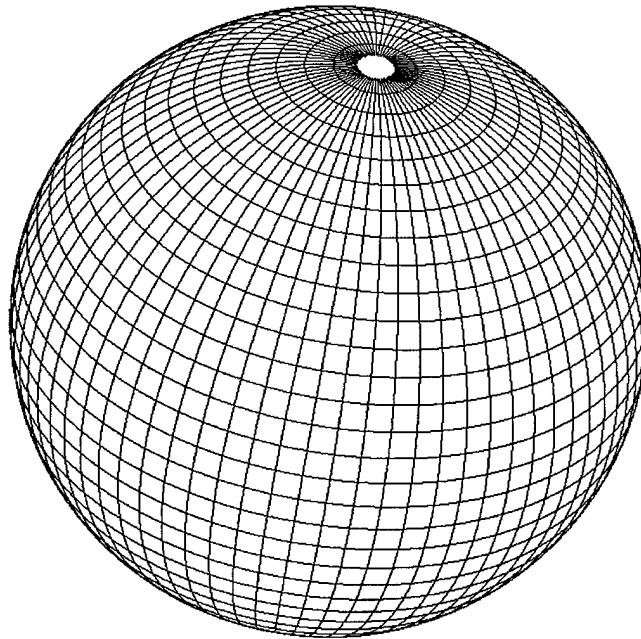


Figure 1: HydroMod's method of spatial accounting is illustrated in this sphere. Each quad, other than the endcap, is a  $5^\circ \times 5^\circ$  solid angle representing the direction from which and into which light travels. Incoming skylight to a point on the water surface, for instance, will come from each quad in the upper hemisphere. Light traveling into the water, then, will be going into each quad in the lower hemisphere.

Now that we have our accounting method, we can begin to talk about the radiance values HydroMod will be using and computing. A radiance value is represented by something like  $+L_{\lambda}^{\downarrow}(\theta, \phi)$  which

represents the spectral ( $\lambda$ ) radiance ( $L$ ) above the water surface (+) heading down ( $\downarrow$ ) from the  $(\theta, \phi)$  direction. Sometimes the vertical point in space or within the water column is also designated as in  ${}^{-}L_{\lambda}^{\uparrow}(z; \theta, \phi)$ . This represents the spectral radiance below the water surface heading up at a depth of  $z$  in the  $(\theta, \phi)$  direction.

The first set of radiance values that HydroMod needs to compute (or find in a LUT) is the input sun and sky radiance,  ${}^{+}L_{\lambda}^{\downarrow}(\theta, \phi)$  for the hemisphere above the water surface. HydroMod does this by *either* finding the set of  ${}^{+}L_{\lambda}^{\downarrow}(\theta, \phi)$  values already existing in a look up table or by running MODTRAN 630 times to generate the  ${}^{+}L_{\lambda}^{\downarrow}(\theta, \phi)$  values needed. These data are then stored in a new look up table. (The 630 comes from using azimuthal angles from  $0^{\circ}$  to  $180^{\circ}$  inclusive in  $5^{\circ}$  steps and declination angles from  $5.1429^{\circ}$  to  $87.429^{\circ}$  inclusive in  $5.1429^{\circ}$  steps plus one endcap:  $630 = 17 \times 37 + 1$ . The full hemisphere is created by noting that the data from using an azimuth angle of  $5^{\circ}$  is the same as the data at an azimuth angle of  $355^{\circ}$ ; the data at  $10^{\circ}$  is the same as the data at  $350^{\circ}$ ; .... This is a true statement as long as the first ( $0^{\circ}$ ) or last ( $180^{\circ}$ ) cut goes through the sun. *For sun azimuthal angles other than  $0^{\circ}$  or  $180^{\circ}$  the full hemisphere is created and rotated to put the sun in the correct location.* )

When running at lower resolution, HydroMod will average the radiance values from appropriate quads to form larger (i.e. lower resolution) quads.

The spectral range on all of the LUTs and all of the  ${}^{+}L_{\lambda}^{\downarrow}(\theta, \phi)$  to this point runs from 290nm to 1000nm in 1nm steps (711 wavelengths). When some subset of that spectral range is needed, say for a 10nm bandwidth from 500nm to 510nm for instance, HydroMod opens the required LUT and extracts the 500nm to 510nm sets of radiance values (11 sets of  $(\theta, \phi)$  pointed radiances) and averages them for the input radiance values.

HydroMod allows for adding clouds to the input hemispherical spectral radiance,  ${}^{+}L_{\lambda}^{\downarrow}(\theta, \phi)$ , at the desired  $(\theta', \phi')$  directions. These clouds will have a spectral character of their own. They will also have an associated brightness level and a given quad may be partially sky and partially cloud so that a cloud to cloud plus sky ratio is also needed. HydroMod allows all of these to vary at the users discretion. It then replaces the radiance from the sky in the  $(\theta', \phi')$  direction with the radiance from the user defined cloud in the  $(\theta', \phi')$  direction. The

number of  $(\theta', \phi')$  directions (quads) that contain clouds is only limited by the number of quads in the hemisphere ( $1225=17 \times 72+1$ ).

At this point, HydroMod hands off the data to a modified version of Hydrolight. (See "Begin Execution" in the next chapter.) The compiled and modified Hydrolight is called H20Code.exe. It performs the radiance transfer through the wind roughened water surface, into and around the water, and back out of the wind roughened surface. The wind roughened surface data, however, comes from another LUT that HydroMod enables based on the selected wind speed and spatial resolution.

Several wind roughened surfaces have been generated and are normally included as zipped LUTs with the code. They are for wind speeds of 0 m/sec to 12.5m/sec in 0.5m/sec steps and for the default wind speeds built into MODTRAN (4.1m/sec, 10.3m/sec, 6.7m/sec,...) for the different atmospheric models. HydroMod will select the correct wind roughened surface, unzip it, and make it ready for H20Code.exe to read and use.

H20Code.exe will also read several other input files. These files give it data on how to run (what wavelengths, output depths, how deep the water is, what is on the bottom...); tell it what is in the water (spectral absorption and scattering coefficients for chlorophyll, Dissolved Organic Matter, and Suspended Minerals); and other important information (internal source data, concentration variation with depth,...)

The final radiance values needed are the upwelled radiance values. These are generally found in the same LUTs as the sky and sun input files. If they need to be generated, another set of MODTRAN runs are required using the MODTRAN sensor in space and looking down at the ground.

We can obtain the total radiance at the sensor by multiplying the correct transmission coefficients (obtained, again, from either MODTRAN or from one of the LUTs) by the sum of the radiance leaving the water and the radiance reflected off of the water and then adding in the upwelled radiance.

## HydroMod USERS MANUAL

For more information on the theory of operation, please see my dissertation<sup>2</sup>.

---

<sup>2</sup> Fairbanks, Ronald R., John Schott, Advisor, "A Characterization of the Impact of Clouds on Remotely Sensed Water Quality", Ph.D. Dissertation, Rochester Institute of Technology, Rochester, NY, August, 1999.

## Running HydroMod

### CHAPTER OUTLINE

<input checked="" type="checkbox"/>	Collect HydroMod Input
<input checked="" type="checkbox"/>	Changing Default File Locations
<input checked="" type="checkbox"/>	Atmospheric Conditions
<input checked="" type="checkbox"/>	Wind Speed
<input checked="" type="checkbox"/>	Resolution
<input checked="" type="checkbox"/>	Adding Clouds
<input checked="" type="checkbox"/>	Water Quality Parameters
<input checked="" type="checkbox"/>	Internal Sources
<input checked="" type="checkbox"/>	Output Depths
<input checked="" type="checkbox"/>	Output Wavelengths
<input checked="" type="checkbox"/>	Begin Execution
<input checked="" type="checkbox"/>	Data Analysis

*Chapter Synopsis: In Chapter 2 we cover how to actually run HydroMod. The IDL widgets and their operation are covered in as much detail as possible to help users set up the required input files. The final two sections simply describe what happens when "Begin Execution" is pressed and what the "Data Analysis" button does.*

The act of running HydroMod involves setting up the environment that we want to simulate, executing the actual number crunching code, and performing analysis of the data. As you will find, most of the data analysis that you will perform will be outside of HydroMod using the included IDL routines and many others that YOU will write to do the specific analysis tasks that you want to do. The first task is collecting the information that we need in order to set up the environment.

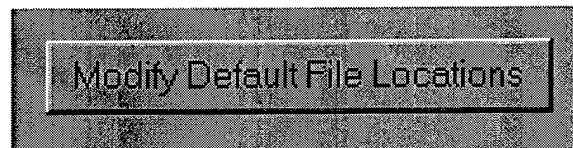
### Collecting HydroMod Input

Both MODTRAN and Hydrolight are very flexible and capable computer codes for radiative transfer in their respective regimes. However, since HydroMod mates these two codes *and adds a cloud modeling capability*, that means that there is a lot of information that HydroMod needs to know in order for it to do its intended job. So let's get to it and decipher what HydroMod needs to know and how it gets to know it. The following sections are titled after the HydroMod functions that they perform.

The HydroMod main screen is not shown; as you read this manual, you may want to have HydroMod running (if possible) so that you can refer to sections that I will describe.

## Changing Default File Locations

This is fairly easy and straightforward. When running on a new computer for the first time, or when changing file locations we need to tell HydroMod where to find information and where to put information. That is what this widget does. It also tells HydroMod to enable running off of the CD ROM when the vast majority of LUTs are located there. To begin, we push this button at the top of the HydroMod main screen



and a new window appears that looks like this:

**Basic Paths for HYDROMOD Input and Output**

Enter Pathname for MODTRAN (Do not forget the final '\')

D:\MODTRAN\Mod3-7\

Enter Pathname for Output Files (Do not forget the final '\')

D:\HydroMod\Output\

☐ Use CDROM for Look Up Tables

Enter Sky Information Pathname on a WRITEABLE Drive (Do not forget the final '\')

D:\HydroMod\LUTs\Atmos\Sun\

Enter Sky LUT Pathname on the CDROM (Do not forget the final '\')

H:\LUTs\Atmos\Sun\

Enter Surface Information Pathname on a WRITEABLE Drive (Do not forget the final '\')

D:\HydroMod\LUTs\Surfaces\

Enter Surface LUT Pathname on the CDROM (Do not forget the final '\')

H:\LUTs\Surfaces\

☐ Set as System Defaults

Using this widget you tell HydroMod where on your computer to find the information it needs to do its job. You can type in the pathname or browse to select the pathname. Note that if you are browsing to select the path, you need to actually select a file in the path in order for HydroMod to recognize it. (There is an easy IDL fix for this clumsiness, but I haven't gotten around to do it.)

Since these are indeed paths, the final “\” is required. The HydroMod IDL code will be adding filenames on the end of these strings so that a file called “MyFile.DAT” in the “C:\DATA\” directory would become a file called “DATAMyFile.DAT” in the “C:\” directory if you do not put the final “\” in the pathname.

If you'll be using the CD-ROM for most of the LUTs, this is where you tell HydroMod to do that. If HydroMod finds the LUT it needs on your CD-ROM, it will copy it to the hard drive location for the particular LUT in question. In the above figure, IF “Use CDROM for Look Up Tables” were checked and IF HydroMod could not find the atmospheric LUT on the hard drive under “D:\Hydromod\LUTs\Atmos\Sun\”, but it could find it under “H:\LUTs\Atmos\Sun\” (where “H:\” is the CD-ROM drive), THEN it would copy the LUT from H:\LUTs\Atmos\Sun\ to D:\Hydromod\LUTs\Atmos\Sun\ and use it from there.

Please note that every HydroMod session that you'll be using the CD-ROM you'll need to open this widget and check off the “Use CDROM for Look Up Tables” box.

## Atmospheric Conditions

Here we give HydroMod all of the information about the atmosphere that it uses to create (or find in a LUT) the  $+L_{\lambda}^{\downarrow}(\theta, \phi)$  radiance distribution. HydroMod gives us three options: Use the same atmosphere as last time; build (or find in a LUT) a new atmosphere; or use a known existing atmosphere. The drop down list selects which option to use.



Note that HydroMod searches in the locations it was told to look (see ***Changing Default File Locations*** above) for LUTs created with the same parameters as those chosen. If it can't find the LUT, then it will create a new one and it tells you that it is going to do that with the statement "HydroMod will create the required atmosphere". If it can find the LUT, then it tells you that as well. In the case above, HydroMod could not find the atmospheric LUT, but it found the wind roughened surface LUT file so the statement "The selected wind roughened surface file exists" appears.

If "Use Known Existing Data File" is selected, the partially obscured filename block is enabled and you can type in a name of a file or "Browse" to find the file. If using this option, it is important that the data file is in the right format. The right format is as follows:

1. It must be a zipped file such as MYSKYDATA.ZIP or, possibly something like S41M2S-5C363H4S0V0C00C00V00R000G080.zip.
2. Within the zipped file must be three (or more, but at least these three—see item 5 of this list.) files with these exact (case insensitive) names: SKYFILES.RAD, SKYFILES.TRN, and SKYFILES.UWR.
3. The SKYFILES.RAD is the radiance distribution file in ascii format. It contains radiance values for 711 wavelengths from an endcap quad plus 629 ( $\theta, \phi$ ) directions at the center of each of the 629 other quads in the quartersphere. (Hold on, this gets even more complicated.) The format of the ascii data file is exactly this:



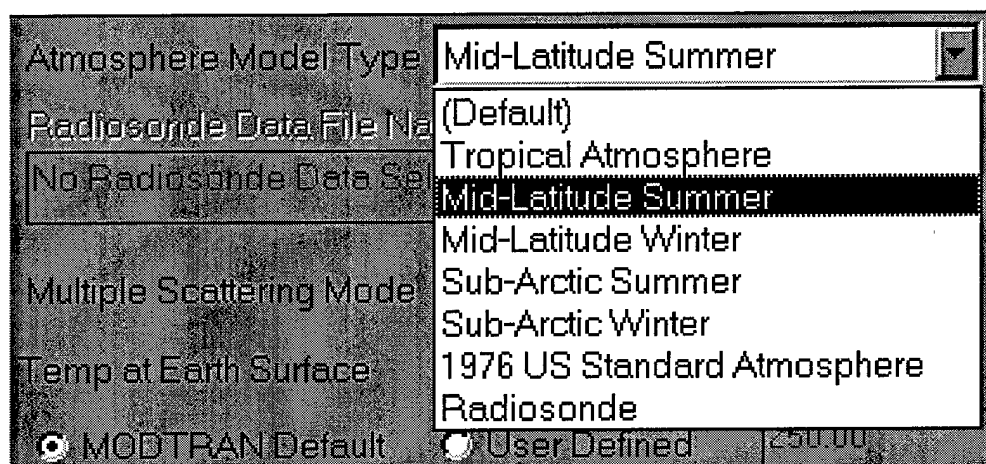
(2F10.4,/(71(10F12.4,/),F12.4,/),37(17(71(10F12.4,/),F12.4,/))). The first two numbers on the first line (2F10.4,/) are the quad partitioning indicators 5.1429 (for  $\theta$ ) and 5.000 (for  $\phi$ ). The next 711 numbers written out 10 per line, (71(10F12.4,/),F12.4,/), is the endcap quad. The final (and largest) block of numbers is the rest of the quarter sphere 37(17(71(10F12.4,/),F12.4,/)) which is 17 declination angles by 37 azimuthal angles by 711 wavelengths. These, again, are 10 per line for 71 lines and then 1 on a line. Here is the key point: for this radiance sky file to be realistic, the sun MUST be located along the  $\theta = 0^\circ$  line because HydroMod is going to unzip it, read it, and fold it over the  $0^\circ$ - $180^\circ$  line to create the entire hemisphere. HydroMod will then rotate that file to put the sun in the desired location.

4. The SKYFILES.TRN and SKYFILES.UWR are respectively the transmission coefficients and the upwelled radiance distribution files in ascii format. The only data actually needed in the SKYFILES.TRN file are the first line and the first 18 (endcap plus 17) declination angle sets of 711 wavelength specific transmission coefficients. Yet, both of these files have the same format as SKYFILES.RAD except the floating point values are store as F10.4, not F12.4. That is, the format is (2F10.4,/(71(10F10.4,/),F10.4,/),37(17(71(10F10.4,/),F10.4,/))) and the values represent the same quads as in SKYFILES.RAD.
5. You may find that most of the LUTs that exist for the skyfiles include three other files called SKYFILES.DEP, SKYFILUW.TRN, and SKYFILUW.DEP. Their format is exactly the same as that used in item #4 above. They contain the optical depth information (\*.DEP) for both the input sky runs and the upwelled radiance runs and the atmospheric transmission data from the upwelled radiance runs. The "UW" indicates the data sets from the upwelled radiance runs. These files are not used and are not needed. However, in the future, the "sensor" might not be in space and the SKYFILUW.TRN should be used in place of the SKYFILES.TRN in item #4. For now, since we have the sensor in space, SKYFILES.TRN should be identical to SKYFILUW.TRN.

That should be enough information for you to build your own sky files off line and still use them in HydroMod if you choose. For most of the runs, you'll be selecting the atmospheric parameters by selecting "Build Specific Atmosphere" from the drop down list.

Doing so, produces a new window full of selections that allow you to create an atmosphere in MODTRAN with MODTRAN styled choices.

That window is too large to display accurately here, but we can go over one element at a time. For instance, in the upper left is a drop down list used to select the model atmosphere to use. In this sample, the HydroMod default Mid-Latitude Summer model is chosen.



Other HydroMod/MODTRAN atmospheric inputs control the temperature and surface albedo of the earth, the CO<sub>2</sub> mixing ratio, the boundary layer aerosol model (IHAZE in MODTRAN-speak), and the visibility. Some values use sliders, some use drop down lists, and in others you can type in the value. (If you type the value in, make sure to use the "enter" key; a few of the values mistakenly require it and I'm not sure if I tracked down all of them for this version of HydroMod.)

Some atmospheric parameter selections become enabled and/or disabled depending upon other selections. For instance, all three sliders shown on the next figure are disabled until a selection is made that enables the slider. In the top slider, the "Temperature at Earth Surface must be "User Defined" before the slider turns on and allows the user to define it. For the Surface Albedo and the CO<sub>2</sub> mixing ratio, the same type of constraints apply.

In that same figure, the visibility block and the coastal influence block are also disabled until the right choices are made in other places.

All of the atmospheric specific inputs are used by HydroMod to set up "card decks" for MODTRAN and then execute MODTRAN to build the sky files required.

[illegible]

Some selections in this atmospheric parameter selection window are not atmosphere specific and will be addressed in more detail in the next few sections. They include the wind speed and the resolution.

## **Wind Speed**

The wind speed is always used to roughen the sea surface. It is also sometimes used by MODTRAN, that is why it is included in the atmospheric window. HydroMod uses the wind speed to determine which wind roughened sea surface to use. The HydroMod default is to use a 5m/sec wind speed (which equates to roughly 18 km/hr or 9.7 knots). Users can select their own wind speed. LUTs exist (and are included) for wind speeds from 0.0m/sec to 12.5m/sec in 0.5m/sec steps. They also exist for wind speeds that match the MODTRAN default wind speeds for the various model atmospheres. If you select a wind speed other than that provided in these look up tables, HydroMod will generate the new wind speed for you. I must point out, however, that that capability has not been tested since it was installed in the very early versions of HydroMod. If it doesn't work let me know.

## **Resolution**

There are three resolutions available for running HydroMod: Low, Medium, and High. The lower the spatial resolution, the faster the water portion of the code will run. The atmospheric LUTs are always created with the highest resolution.

To get to the lower resolution, HydroMod starts with the high-resolution and spatially averages the radiance values. For instance, the low-resolution requires 10 x 24 quads to make up a hemisphere (which equates to roughly 9.5° x 15° quads). The high-resolution requires 18 x 72 quads to do the same thing. HydroMod averages the radiance from all of the high-resolution quads contained in one low-resolution quad and calls that the radiance from the quad. The array size required by

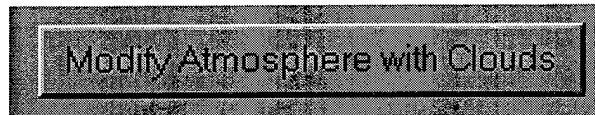
the water portion of the code (and the array size of the output) is only 20x24 for the entire sphere versus 36x72 for the high-resolution mode.

To make the output from the code work the same in the data analysis tools regardless of the resolution, the low-resolution data are re-sampled to "high" resolution. (Obviously, the data are still low-resolution, HydroMod just makes the arrays bigger so that they will work while using the same software routines as for the high-resolution data.

### **Adding Clouds**

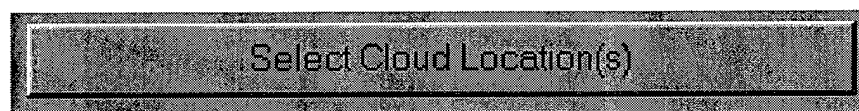
Much has been written about the way HydroMod adds clouds to the scene. You may want to see my dissertation referenced a few pages back for one reference or some of the Power Point presentations included with this users guide for more information.

You may have noticed that when you push this button

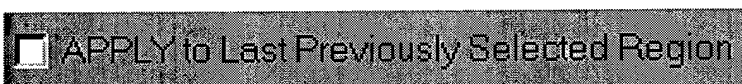


on the main HydroMod screen, the main screen actually goes away and the cloud module comes up. This is the only widget that does that. All of the other sub-windows (modal widgets in IDL-speak) exist on top of the main HydroMod screen except this one. The reason for that is that this widget uses a function built into IDL called CW\_DEFROI.PRO that allows the user to define a region of interest by pointing and clicking. The drawback is that CW\_DEFROI.PRO cannot be called from a modal widget. That is, it cannot exist on top of another main controlling widget. Therefore, the HydroMod main screen shuts off and turns full control over to the cloud module. When the cloud module exits, the main screen is reactivated and the information acquired in the cloud module is made available. I think it works well enough that you may not have even noticed that this happens.

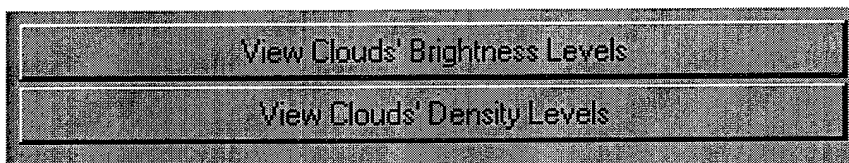
There are four elements that define the cloud(s) we can add to the scene. They are location, spectral response, brightness, and cloud to cloud plus sky ratio. Location is the easiest. By pressing



a new widget activates that allows you to literally point and click the clouds on the screen. (I recommend first turning on the polar overlay and the clear sky radiance display to help select the cloud locations.) These clouds will have the brightness values and the cloud/cloud+sky ratio that are currently selected. However, once located, the cloud brightness and cloud/cloud+sky ratio can be changed for the last set for clouds defined by setting new values and then clicking on



In this way, you can define a bunch of dark clouds, and then some lighter clouds, and then some medium clouds or whatever you want in any location in the hemisphere. In order to view the clouds that you've created click on either one of these



All of the visual information in this widget is only intended to give you a feel for what HydroMod "thinks" the scene looks like. That includes the clear sky radiance overlay. The clear sky radiance overlay is NOT your sky. It is A sky that happens to have the sun in the same place as your sky. The images and displays are created in IDL using a TVSCL routine. One impact of using TVSCL this way is that if you were to "View Clouds' Brightness Levels" and then brighten the last cloud created and view them again, the cloud may not actually appear brighter, instead, the polar overlay scale may appear darker. However, HydroMod stores the brightness values of the clouds appropriately.

The brightness values are actually multipliers used to scale the cloud spectral response file. The spectral response file is a set of data representing the spectral character of the cloud. The spectral character is what makes a white cloud white. The HydroMod default comes from several runs of MODTRAN using the "sensor" just over the clouds and

looking down for bright clouds and up for dark ones. After several runs with different geometry and different MODTRAN clouds and atmospheres, a family of representative curves was generated. It was obvious when looking at these curves that the only thing that varied much at all was the radiance level. The shape of all of the curves was very nearly identical. That led to the method used in HydroMod: a single spectral response file (see figure below) that is scaled by a brightness factor.

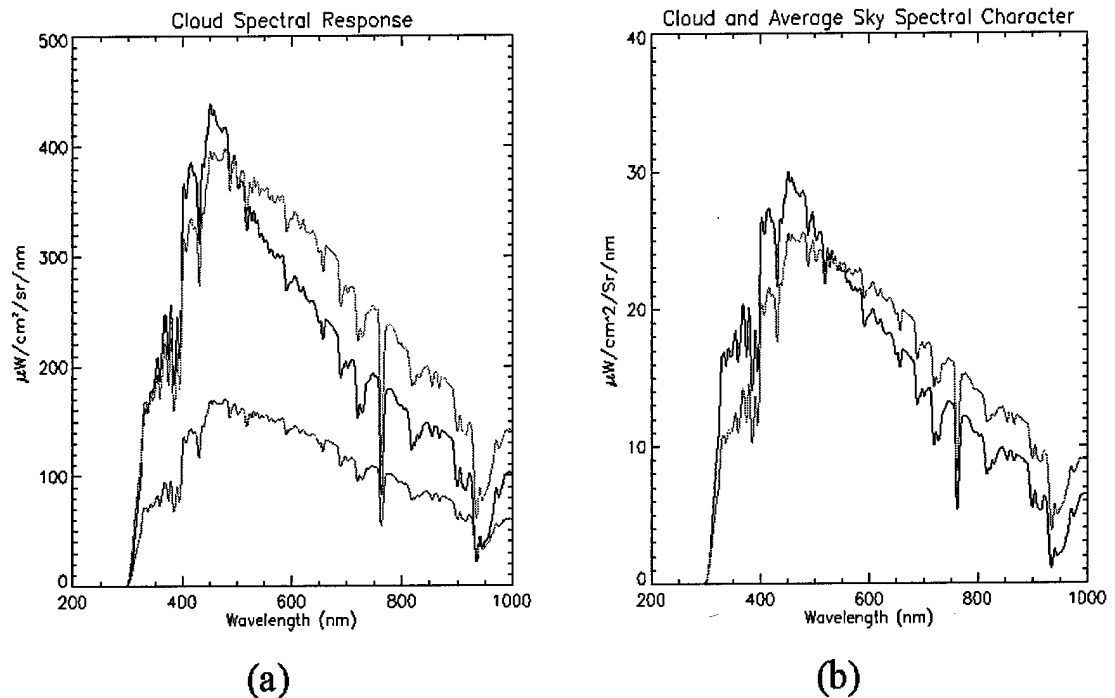


Figure 2: Cloud Spectral Response. The lighter curves in each of (a) and (b) above are HydroMod's default spectral response data for clouds. In (a) we compare the cloud spectral character to the atmospheric radiance forward scattered from the sun. The two scale factors used on the identical cloud spectral files in (a) are 1.0 for the upper cloud curve and 0.30 for the lower cloud curve. In (b), a cloud scale factor of 0.65 was used and the data are compared to the spatially averaged sky radiance for a clear Maritime atmosphere with 23Km visibility.

Using the default spectral response file, a very bright cloud has a brightness scale factor of about 0.3 and a fairly dark cloud has a brightness scale factor of less than 0.02 according to the MODTRAN runs. HydroMod allows you to change this cloud spectral response file by pressing

Change Cloud Spectrum File

near the bottom left section of the window. Doing so, you'll be asked to select a file to use by browsing through the system. If you create your own cloud spectral response file, you'll need to know that the format is 711 lines of ascii data representing the wavelengths 290nm to 1000nm and each data point is an F12.6 format. The format to write the data would be 711(F12.6,/).

The cloud/(cloud+sky) ratio lets you define how much of the quad is cloud and how much is sky; how much is white and how much is blue. Note, however, that if a very large section is selected and defined as, say, 30% cloud, then that means that each and every quad in that sector is 30% cloud and 70% sky. It does not mean just 30% of the sector is clouds (which could have some quads with 100% cloud and some with 0% cloud; if that is what you want, you'll have to define it another way.)

When all of the parameters are selected<sup>3</sup>, HydroMod will multiply the cloud spectral response file by the brightness scale factor and add it (using the correct ratio) to the radiance coming from the correct directions found in the atmospheric LUTs or via the MODTRAN sky input runs. That is, HydroMod combines the white cloud and the blue sky using the defined brightnesses and cloud/(cloud+sky) ratios for each and every point in the high-resolution hemisphere. (The locations in the hemisphere that do not have any clouds defined are by definition 100% sky and 0% cloud.) This becomes the actual sky file used by HydroMod to create the input to the water module.

### Water Quality Parameters

HydroMod assumes that there are four things in the water: pure water, chlorophyll, dissolved organic matter, and suspended minerals. It will internally perform these calculations:

---

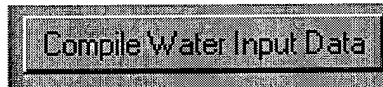
<sup>3</sup> Actually, that is not quite a correct statement. The cloud information is truly stored in a data structure for use later when the user selects "Begin Execution". That way, HydroMod allows the user to change clouds several times in the same run without writing and overwriting files.



$$a(\lambda) = a_w(\lambda) + C_{DOM} a_{DOM}(\lambda) + C_{SM} a_{SM}(\lambda) + C_{chl} a_{chl}(\lambda)$$

$$b(\lambda) = b_w(\lambda) + C_{SM} b_{SM}(\lambda) + C_{chl} b_{chl}(\lambda)$$

We give HydroMod the individual components of the above equation using



and then the boxes similar to

Chlorophyll Absorption Cross Section:	HYDROMOD Default ▾	Concentration (mg/m <sup>3</sup> ) =
Chlorophyll Absorption Cross Section File Name:	10.0000	
c:\hmdata\data\chlorophyll.abs		
Chlorophyll Scattering Cross Section:	HYDROMOD Default ▾	
Chlorophyll Scattering Cross Section File Name:		
c:\hmdata\data\chlorophyll.scf		

The default absorption cross section and scattering cross section data comes primarily from Dr. Robert Bukata's "Optical Properties and Remote Sensing of Inland and Coastal Waters". Some of the data are as he measured for Lake Ontario and some (above 700nm and below 400nm) comes from equations he gives in his book. The default cross sections in HydroMod are given in Figure 3 below.

You can change the default cross sectional data by creating (offline) and then selecting (using the widget above) a file that contains 711 data values, one per line, in an F12.6 format. To change all 7 cross sectional curves you'll need 7 files using the same format. (There are 7 because dissolved organic matter does not scatter and therefore does not have a scattering cross sectional curve associated with it. Pure water, chlorophyll, and suspended minerals have both absorption and scattering cross sectional curves.)

HydroMod uses the concentrations inserted with this widget and the cross section curves to come up with individual absorption and scattering coefficients from the four components of water. HydroMod then writes those eight coefficients, four at a time, into two files: "C:\hmdata\data\absorp.out" for the four absorption coefficients, and "C:\hmdata\data\scatter.out" for the four scattering coefficients (the DOM column will be all zeros). The format for both of these files is (711(4F12.6,/)) with the order of the four columns being water, chlorophyll, DOM, and SM.

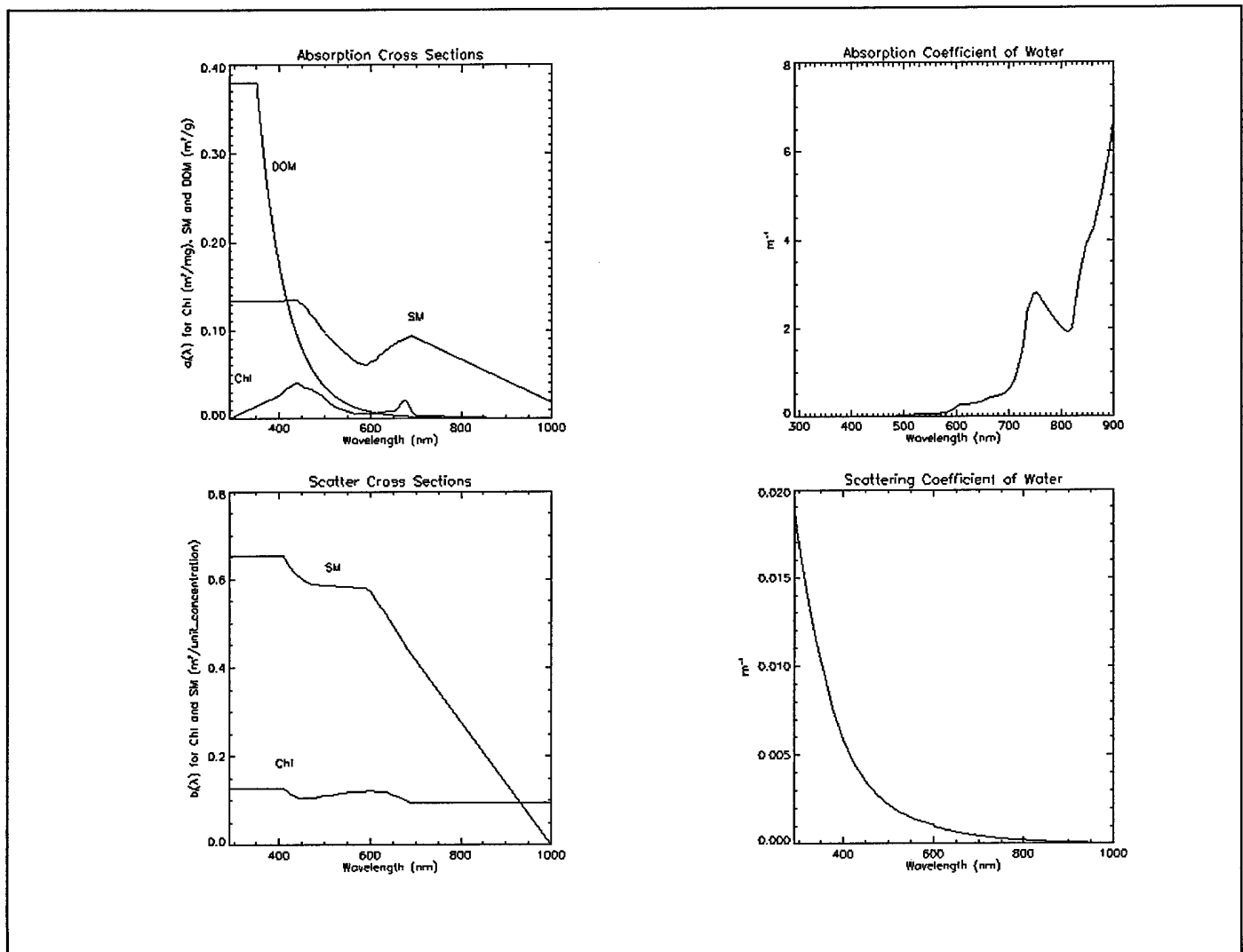


Figure 3: Absorption and Scattering Cross Section Curves. The data from 400nm to 700nm are measured Lake Ontario data from Bukata. Outside of this region the data were "created" from equations given by Bukata with one exception. The absorption by Chlorophyll under 400nm was artificially (and arbitrarily) tapered to zero. The water absorption comes from the literature.

The underwater module of HydroMod is a compiled Fortran program called H2OCode.exe. (Actually, a DOS batch file called H2OCode.BAT runs, but all it does is call H2OCode.exe and then pause so that you can see if any errors occur.) That compiled code was originally the Hydrolight computer code that I modified. When the underwater module runs, it reads the files "C:\hmdata\data\absorp.out" and "C:\hmdata\data\scatter.out" and it uses the information contained there in several ways.

Now that we have our concentrations and our cross sections, we can get a little fancy and vary the concentrations with depth. The blocks similar to this

Suspended Minerals Function of Depth, X

☒ Homogeneous (Constant Concentration)  
☐ Linear Decay -- Enter slope: mX  
☐ Exponential Decay -- Enter Decay Rate:  $\exp(-X/\text{rate})$   
☐ Exp. Peak/Decay --  $c0 + c1 \cdot \exp(-([X - X_{\text{max}}]/\text{rate})^2)$

Slope =	Rate =	c0 =	c1 =	Xmax =
0.000000	0.000000	0.000000	1.000000	0.000000

are used to do that for the three non-water components. The default is for the water to be homogeneous. However, we can have the concentration levels vary with depth, X.

For the linear decay, you enter the slope and HydroMod will change the concentration from a high at the surface using the number you gave it for the concentration down to either a concentration of 0 or to the bottom, whichever occurs first.

The exponential decay will never hit zero, it just keeps getting smaller and smaller. For that you'll enter the rate of decay.

The most likely situation (according to the literature) will be an exponential peak and then decay. The concentration at depth X will be determined within H2OCode.exe as the value of this function times the concentration that you entered for the constituent.

HydroMod performs the tasks in two steps. It first writes out a 3 x 5 array with the 5 parameters for the 3 constituents. (Note that the maximum number of required parameters is four when using the exponential peak and decay: C0, C1, Xmax, and rate; no other selection uses more than four. The fifth element is used to tell H2OCode.exe which type of function to use.) That 3x5 array is written to a file called "C:\hmdata\data\depth.out" with a format of (5(3F12.6,/)) and the order of the columns is chlorophyll, DOM and SM. The second step is for H2OCode.exe to read that file and use the information to vary the concentration with depth.

We also use this widget to define the bottom.

How Deep is the Bottom? (meters) 10.0000

Type of Bottom Boundary: Green Algae

Wavelength Independent Reflectance: 0.000000

The depth and the reflectance of the bottom are required. Otherwise, a default depth of 10m with a bottom of green algae will be used. The bottom must be greater than 0.1m. Keep in mind that the deeper the water, the more calculations will be required and the time to numerically solve the equations increases. Also, the clearer the water the more you'll see the bottom. The bottom selections are available via the drop down list. Green Algae is currently selected in the box above. I recommend not using the infinitely deep selection. I apparently broke that subroutine somehow and I haven't gone back to fix it.

When the "User Supplied Constant Reflectance" is used, the "Wavelength Independent Reflectance" box is enabled and you can enter the bottom reflectance manually. Note that this is a spectrally constant value. Future versions will probably allow users to define their own spectrally varying bottom, but not this one.

### Internal Sources

I'm not going to tell you very much about the internal source terms. The reason is this: if you know enough about the radiative transfer processes to want to modify the internal source terms, then you're probably not reading this section. And, if you *are* reading this section, then you probably don't want to modify the internal source

terms, you just want to use them or understand them. In that case, I refer you to Dr Curtis Mobley's textbook, "Light and Water" for a good discussion on the terms included in HydroMod.

In any event, on the HydroMod main screen pressing

Compile Internal Sources' Input Data

produces the following new widget.

**Internal Source Term Inputs**

**Chlorophyll Fluorescence:** Include as Source with User Supplied Parameters

Chlorophyll Fluorescence Parameters:  
The chlorophyll fluorescence emission function is of the form  $c0 \cdot \exp(-[(Y - Y_{max})/rate]^2)$  where Y is the emission wavelength and c0 includes the quantum efficiency. The parameters to be used are:

c0 = 0.00112900 Ymax = 685.000 Rate = 14.9906

The wavelengths capable of exciting the emission range from MINY to MAXY:

MINY = 370.000 MAXY = 690.000

**DOM Fluorescence:** Include as Source with User Supplied Parameters

DOM Fluorescence Parameters:  
The DOM spectral fluorescence quantum efficiency function follows the form:

$$\eta^F(\lambda' \rightarrow \lambda) = A0(\lambda') \exp \left[ - \frac{\left( \frac{1}{\lambda} - \frac{A1}{\lambda'} - B1 \right)^2}{0.00045700 + B2} \right]$$

The HydroMod Defaults are recommended for A1, A2, B1 and B2.  
The parameters to be used are:

A1 = 0.470000 A2 = 0.407000 B1 = 0.000807700 B2 = -0.00045700

The function A0 can be changed by supplying the name of a file containing the data: c:\hmodata\data\defaults\domfluor.pks Browse

**Raman Scattering:** Include as Source with User Supplied Parameters

Raman Scattering Parameters:  
The Raman Absorption Coefficient is of the form  $A0 \cdot (Y0/Y)^X$  where Y is the excitation wavelength, Y0 is a reference wavelength, A0 is the value at Y=Y0, and X is an exponent. The parameters to be used are:

A0 = 0.000265000 Y0 = 488.000 X = 5.33000

The Raman wavelength redistribution function parameters as given in Mobley's Table 5.3 are used by HydroMod. To Change the default values, Edit file 'C:\HMODATA\DATA\TABLE53.OUT'

**Bioluminescence:** Include as Source with User Supplied Parameters

Bioluminescence Parameters:  
Bioluminescence is modelled as a Gaussian in wavelength with the form  $c0 \cdot \exp(-[(Y - Y_{max})/rate]^2)$  where Y is the luminescence wavelength. The parameters to be used are:

c0 = 4.12000e-006 Ymax = 480.000 Rate = 21.2132

Bioluminescence Depth Parameters:  
The Bioluminescence plume will peak at some depth, ZPEAK. The plume could be concentrated at that depth or it could be nearly depth independent. A LOCALIZATION PARAMETER of 2.0 would concentrate the plume to within 1/2 m depth of ZPEAK; a value of 0.1 would concentrate the plume to within 1/0.1 or 10 m depth of ZPEAK. The parameters to be used are:

ZPEAK = 5.00000 Localization Parameter = 2.00000

Done Cancel

By entering numbers in these blocks (after first selecting "Include as a Source with User Supplied Parameters" from the drop down menus) HydroMod creates four files in the "C:\hmodata\data\" directory called "CHLFluor.out", "DOMFluor.out", "Raman589.out", and "Biolumin.out". H2OCode.exe then reads these files to set up the internal source terms. The HydroMod widget screen itself has a lot of

explanation about the internal sources and the parameters that describe them.

The four created files are all simple coefficients for the equations as listed in the widget. The Fortran code performs those exact equations using the parameters entered (if the internal source is indeed turned on.) H20Code.exe is told which internal sources to use via HMINDAT1.TXT (see page 180); that file will contain four flags telling H20Code.exe which internal sources to turn on and which ones to not turn on.

## Output Depths

Selecting



from the HydroMod main screen produces

HydroMod will provide radiance distribution data in the  $(\theta, \phi)$  directions for the hemispheres above and below the depths entered in this widget. In addition, HydroMod will ALWAYS give the radiance distributions above the water surface, just below the surface, and at the bottom.

The depths entered here must be greater than 0.1m (if non-zero) and less than the depth of the water. You do not need to enter anything. If you do not want to know the light distribution below the surface, you can skip this widget entirely.

If you want to know the light distribution at several depths, you can have HydroMod read in a data file that contains the information. That way you don't have to type them in every time you run HydroMod. The file to be read must be an integer on the first line with an (I4) format followed by the depths, one per line, in (F8.3) format. The integer on the first line is the number of depths to read from the rest of the file. An example file is included as  
C:\HMDATA\DATA\OUTDEPTH.OUT

HydroMod uses this information by including it as part of "C:\hmdata\data\hmindat1.txt" for H2OCode.exe to read. H2OCode.exe then provides the output radiance distributions at those depths. The only quirk here is that HydroMod includes the entered depths and the entered depths plus 5cm to the hmindat1.txt file. The reason for that is that the original Hydrolight code was written to only print out the radiance distributions at every other depth. A closely spaced companion depth is used for other internal calculations (K-functions).

## Wavelengths of Interest

Selecting



from the HydroMod main screen induces



**HydroMod Wavelength Bands Selection**

Enter up to 10 bands (20 wavelength pairs) at right for which you desire a radiance distribution output or select from the options below.

☒ SeaWiFS  
☐ CZCS  
☐ User Defined  
☐ Clear Values  
☐ Read File

(The file may contain up to 71 bands.)

File Name Containing Wavelength Bands:

From Wavelength	<<< Band # >>>	To Wavelength
402.000	<<< Band #1 >>>	422.000
433.000	<<< Band #2 >>>	453.000
480.000	<<< Band #3 >>>	500.000
501.000	<<< Band #4 >>>	519.000
545.000	<<< Band #5 >>>	565.000
660.000	<<< Band #6 >>>	680.000
745.000	<<< Band #7 >>>	785.000
845.000	<<< Band #8 >>>	885.000
0.000000	<<< Band #9 >>>	0.000000
0.000000	<<< Band #10 >>>	0.000000

Here we can enter our wavelength bands of interest. The SeaWiFS and Coastal Zone Color Scanner bands are point and click selectable. The default is to run at the SeaWiFS bands (which are listed above). You can also enter a file that contains up to 71 bands. The file must have an integer (Format=I4) first telling how many wavelengths to read (twice the number of bands) followed by that number of wavelengths, one per line (Format= ##(F8.3,/)).

HydroMod uses this information also in the "hmindat1.txt" file found in the "C:\hmdata\data\" directory to pass the information on to H2OCode.exe. The center of each bandwidth will be used to select the spectral information of interest for the reflecting media inside the water (the bottom, the chlorophyll, DOM, and SM cross sections, ...).

The information is also used by HydroMod to select the sky (and cloud) spectral information and average it over each bandwidth

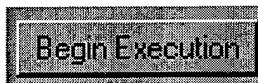


(representing a square wave detector response). This action generates new sky files called HMSKYDAT.RAD, HMSKYDAT.TRN, and HMSKYUWR.RAD. These are the sky input radiance distributions, transmission distributions, and upwelled radiance distributions respectively for each wavelength band of interest.

The LUTs from which the data come from to generate these three files is high spatial ( $\sim 5.143^\circ \times 5^\circ$ ) and high spectral (290nm to 100nm in 1nm steps) resolution data. HydroMod re-samples the data using averaging spectrally based on the bandwidths and spatially if necessary to lower the resolution. However, the HMSKYDAT.TRN file is not spatially averaged. It contains 18 values for each wavelength band of interest. The three files also go through a flip-flop. Hydrolight treats the horizon as the start of the array (element #1 in Fortran) and I created the skies using the horizon as the end of the array (the 17<sup>th</sup> element which is #16 in IDL).

## Begin Execution

Very few calculations and data manipulations occur prior to selecting



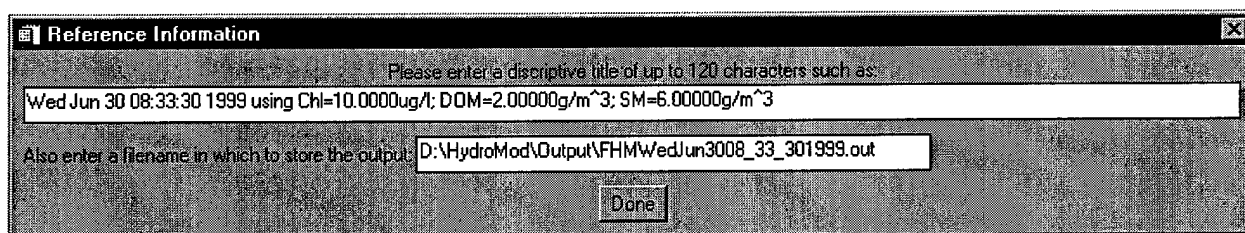
from the main HydroMod screen. However, once that button is selected, a lot happens. LUTs, if they exist, are unzipped; the clouds are added to the clear sky files; the wavelength bands of interest are used to spectrally average the sky data; if other than high resolution is being used, the sky and upwelled radiance data are spatially averaged; data is written to files for H20Code.exe to read; and other things.

The first thing that occurs is that HydroMod checks to see whether the user has selected to "Use a Known Existing Data File" (see page 162) and if so, HydroMod copies that file to where the Sky information is located (selected with the widget on page 160) using the name "NEWFILE.ZIP". That zipped up sky file is then ready to be unzipped.

## Titles and Header Information

HydroMod then asks the user to enter a filename for the output and a one-line header containing information about the run. The

filename will be used after H20Code.exe completes running. The temporary names for the two output files from H20Code.exe are “outputx.txt” (which contains the log information) and “radiance.bin” (which contains the actual data.) After the run, HydroMod will add upwelled radiance and transmission information to the “radiance.bin” and then copy both of the generated files using the user supplied name (the log file has an “\_explanation” tagged onto the name.) But all of that comes later. For now, we use



to enter a filename and the header line of data. The default header line (which is a brand new default header line) tells the day and time and the concentration levels of the three parameters. The default filename has the time and date along with FHM which, for me, stands for “Full HydroMod” run. You can use any name that you want to use.

### HMINDAT1.TXT

The third thing that happens is that HydroMod writes the file “C:\hmdata\hmindat1.txt” which is the main input file for H20Code.exe to read. An example for that file is included here:

```
D:\HydroMod\LUTs\Surfaces\surfts.sda
D:\HydroMod\LUTs\Atmos\Sun\hmskydat.rad
D:\HydroMod\Output\outputx.txt
D:\HydroMod\Output\radiance.bin
HydroMod Run on Tue Jun 29 15:26:12 1999 using default input data.
4
8 0 0 0 0
402.000 422.000 433.000 453.000 480.000 500.000 501.000 519.000 545.000 565.000
660.000 680.000 745.000 785.000 845.000 885.000
3 0.000000
0 8 0.0000 0.0100
4.0000 4.0100
8.0000 8.0100
10.0000 10.0500
```

The first two lines tell H20Code.exe where to find the wind roughened water surface file (which is always named “surfts.sda” in the path where the surface information is contained) and the sky information in the correct format, HMSKYDAT.RAD (see page 179) in the correct path as well. The next two lines tell H20Code.exe where to write the output to.

These lines are almost always the same. However, if you ever wanted to change them manually to have more than one copy of H2OCode.exe running at the same time, you can do that. (I've done that several times and it works well.)

The next line of data is the one-line header information that you just entered and H2OCode.exe will transfer that to the output log file (outputx.txt in this case).

The next line is the number 4. Until future versions of HydroMod come out, this will always be a 4. It tells H2OCode.exe how many "things" are in the water (pure water, chlorophyll, DOM, and SM or four things.)

The next line gives the number of wavelength bands in the run (8 in this case) and four other integers that flag whether to use Bioluminescence, Chlorophyll Fluorescence, DOM Fluorescence, and/or Raman Scattering respectively. If the internal sources are to be included, HydroMod puts a 1 in for that variable.

The next several lines (two in this case) contain the wavelength band information. Each two wavelengths are a band. After the last wavelength, the next line contains the information for the bottom. The 3 in this case flags the use of a Green Bottom and the reflectance value (given here as 0.0000) will not be used. A value of 1 means to use a Lambertian bottom at the constant reflectance value given next (which, again, is 0.0000 for this case); a value of 2 means to use the reflection spectrum of clean coral sand. A 4 means to use brown algae on the bottom and, finally, a 5 means to use red algae.

The next line tells H2OCode.exe that the depths are given as geometric depths and not optical depths. The integer "0" flags that (a "1" would tell H2OCode.exe to use Optical Depths) and the "8" tells H2OCode that output is desired at 8 depths. The depths are for the surface (0.00m and 0.01m), two sets of internal depths (4.0m/4.01m and 8.0m/8.01m) and the bottom (10.0m and 10.05m). The user in this example entered 4.0 and 8.0 and the bottom depth of 10.0 and HydroMod added the 0.01, 4.01, 8.01, 10.05 and the actual surface (0.0). Don't worry about why. It just happens so be aware of it.

At this point, I'll deviate from the tradition step by step approach to describe what HydroMod is doing. There are too many flags and IF THEN type of arrangements to keep them all straight anyway. Let's

just assume, for the moment anyway, that HydroMod keeps all of your choices in mind and does exactly what you tell it to do. With that assumption, we may proceed with three cases: (1) all LUTs that are needed exist; (2) a sky LUT needs to be generated; and/or (3) a wind roughened sea surface needs to be generated. Once we've covered those cases, we may proceed with the rest of the processes that HydroMod performs.

### **All LUTs Exist**

This will hopefully be the most common case. If HydroMod generates an LUT then several hours of computational time are consumed doing so and that is time we could well use for other computations. This is also the point to where we will always end up anyway. Even if HydroMod generates new LUTs, at some point they will exist and we would find ourselves here. So, they exist. Now what?

We'll attack one file type at a time the same way that HydroMod does. The first will be the input sky radiance files.

The sky radiance files are stored in zipped files using PKZIP.EXE (see PKWARE at <http://www.pkware.com> for more information) as incoming radiance, upwelling radiance, and atmospheric transmission distribution files. These files are for the quarter sphere with the sun located along the 0° azimuth line at a declination angle pertinent to the LUT.

In turn, the incoming sky radiance and the upwelling radiance files are opened, read into IDL, manipulated to create the whole hemisphere, rotated to put the sun in the correct azimuthally oriented quad, adjusted for clouds, spectrally averaged to the appropriate bandwidths, spatially averaged to get the correct resolution, and written out to files called HMSKYDAT.RAD and HMSKYUWR.RAD respectively. (Now how's that for a sentence!) If you follow the logic of the code, you'll see exactly those steps (see for instance SKYWRITE.PRO and UWRWRITE.PRO.) Now, don't forget the fact that H20Code.exe wants the horizon to be at the beginning of the array and the IDL portions of the code want the horizon to be at the end of the array. We need to keep that straight as well.

The transmission data is only slightly different. First, clouds do not affect the transmission data. Second, they are not spatially averaged. And third, we only need the data in declination angle space

because all azimuths are redundant. That is, I only need 18 points of transmission data to describe the hemisphere above the water.

To open the water surface LUT, HydroMod uses the wind speed and the resolution to determine which LUT to unzip. Once unzipped, the file is renamed to SURFRTS.SDA and can be quite large (like on the order of 45 MB). The size of the surface LUTs is what generated the need for the zipped and unzipped approach to begin with. Once unzipped and renamed, the file is ready to go. H20Code.exe will read in the data contained in SURFRTS.SDA and use it appropriately.

That is pretty much what happens to enable the input sky radiance, upwelling radiance, wind roughened sea surface, and atmospheric transmission data. We still need to create several other files for H20Code.exe to read that describe the environment, but first let's take a look at what happens if one (or both) of the LUTs do not exist.

### **The Atmospheric LUT Does Not Exist**

The selections made for the atmospheric make-up in the section starting on page 162 will tell HydroMod which LUT to look for. The paths submitted in the "Modify File Locations" widget button from the main screen tell HydroMod where to look. If HydroMod cannot find the right LUT file in the right location, it will go out and create a new one. This section describes how that is done.

HydroMod will call MODTRAN 630 times to create a sky input radiance LUT. It will call MODTRAN another 519 times to create an upwelled radiance file. (The transmission data generated from both of those times should be identical except for the last three declination angles which are missing from the upwelled radiance set.) Both data sets are created in the roughly  $5.143^\circ \times 5^\circ$  quad partitioning described earlier. The sun is placed along the  $0^\circ$  azimuth line and only the quarter sphere is scanned, one quad at a time. Later, when HMSKYDAT.RAD is created, the quarter-sphere is folded into a hemisphere by using some simple facts: With the sun along the  $0^\circ$  azimuth line, the radiance along the  $5^\circ$  azimuth line is the same as the radiance along the  $355^\circ$  azimuth line. This same principle progresses through the radiance along the  $175^\circ$  azimuth line which is the same as the data along the  $185^\circ$  azimuth line.

Once the files are created and stored, HydroMod will zip them up and store the zipped file with the rest of the LUTs.

### **A Wind Roughened Surface LUT Does Not Exist**

If HydroMod cannot find the wind roughened water surface file that gives it the surface transmission and reflectance information, it will create it by using SURFACE.EXE. The only information that is important to the SURFACE.EXE program is the wind speed and the resolution of the data. HydroMod uses SURFACE.EXE by writing the resolution required and the wind speed in question to a file called "C:\HMDATA\DATA\RECORD1.TXT". This file is then read in by SURFACE.EXE and, in a few hours, a new wind roughened sea surface is generated. The SURFACE.EXE code is a MonteCarlo based code that is used to determine what the surface reflectance and transmission coefficients are for the wind roughened sea surface in question. The operation of this code is beyond the scope of this manual. See Dr Curtis Mobley's textbook, *Light and Water* and the raw Fortran code if you want to know more.

### **Other Duties**

HydroMod will perform other duties to get ready for the water code to begin its execution. In particular, it writes the absorption coefficient and scattering coefficient data for the three water contaminants to files called "ABSORP.OUT" and "SCATTER.OUT" respectively. The files have four columns formatted as (711(4F12.6,/)). They represent, in order, pure water, chlorophyll, DOM, and SM. The DOM column exists in the SCATTER.OUT file even though it is a column of zeros. These data are simply the coefficients (selected by you, the user, in the "Compile Water Data") multiplied by the absorption and/or scattering cross sections (also, possibly, selected by you--see the section starting on page 170).

HydroMod also writes out an array of parameters that tell H20Code.exe how to model the chlorophyll, DOM, and SM concentrations as functions of depth. The array is 3x5 and the format is (5(3F12.6,/)) which is 3 columns of 5 elements. The first element in each column tell the type of concentration change with depth (0=homogeneous, 1=linear decay, 2=exponential decay, and 3=exponential peak and then a decay.) Now here, as it turns out, I did something that wasn't all that smart. It works, but if I had the time, I would definitely change this part. I may confuse you here, but re-read

this section a few times and you'll get it. (And when you do get it you'll say, "gosh, that wasn't too smart, why didn't he just...")

Anyway, the IDL code gives you four options for the variation with depth of each of the three parameters: homogeneous, linear decay, exponential decay, and exponential peak and then a decay. The code allows you to change the parameters that describe the change in concentrations with depth. All is well so far. However, the HydroMod defaults are homogeneous concentrations with depth; they are also set as *linear decays with 0 slope*. That might confuse you if you look at DEPTH.OUT and notice the parameters are all pointing toward a linear decay with depth, but a zero slope. (Which, by the way, IS homogeneous.) If you're not confused yet, hang on. If you click on "Homogeneous" in the water parameter selection widget (see page 170), which, by the way, is already selected as the default, then the parameters in DEPTH.OUT will change to truly homogeneous. So, a DEPTH.OUT column with a 0.0 in the first row (OR 1.0 in the first row and 0.0 in the second row) means homogeneous. Lets get just a little more confusing.

In the Fortran code, DEPTH.OUT is read and the parameters are used to select the correct coefficients to fulfill this Fortran statement (for each of the three contaminants):

$$chlz = \min(pk, \max(0.0, c0c + c1c * z + c2c * \exp(-(z - c3c)/c4c) ** c5c)))$$

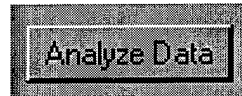
where the min and max statements keep the concentration multiplication parameter between 0.0 and the peak. (The peak, pk, is normally 1.0 unless you've selected "exponential peak and decay". In that case, the multiplication factor is 1.0 at the surface and the peak will be the peak of the exponential function. In the above expression that would be  $c0c + c2c$  (and in the IDL widget on page 173 it would be  $c0c + c1$ ). If I had it to do over again, I would have you input the  $c0c$  through  $c5c$  coefficients in the above equation and make DEPTH.OUT 3x6 and call it done.

## HydroMod Output

HydroMod will provide you with two output files. In reality, you get two copies of each of two files. You'll always get (unless you manually change them in HMINDAT1.TXT) OUTPUTX.TXT and

RADIANCE.BIN which are the log file for the underwater run and the data file respectively. You'll also get copies of these two files using the name that you specified (see the widget on page 180). The log file will have the name along with "\_explanation" appended just prior to the file extension. You can read the log file at your leisure to discover what type of information is contained therein. I'll spend my time on describing the data.

The data file contains all the radiance distribution information from the run. It includes the input sky radiance distribution, the radiance distribution above and below the water surface, reflected off the surface, upwelled, and more. The information is contained spectrally as well. To get to the specifics about that data file look closely at READHMRADFILE.PRO. (If you need to get to the details about the data, then you're capable of deciphering my code. That IDL procedure reads the data files and puts the data into useable format by most of the rest of the data analysis IDL procedures.) A full description of the data file and what it contains is included in the next chapter. For now, we'll stick to the IDL Data Analysis widget that is generated when we select



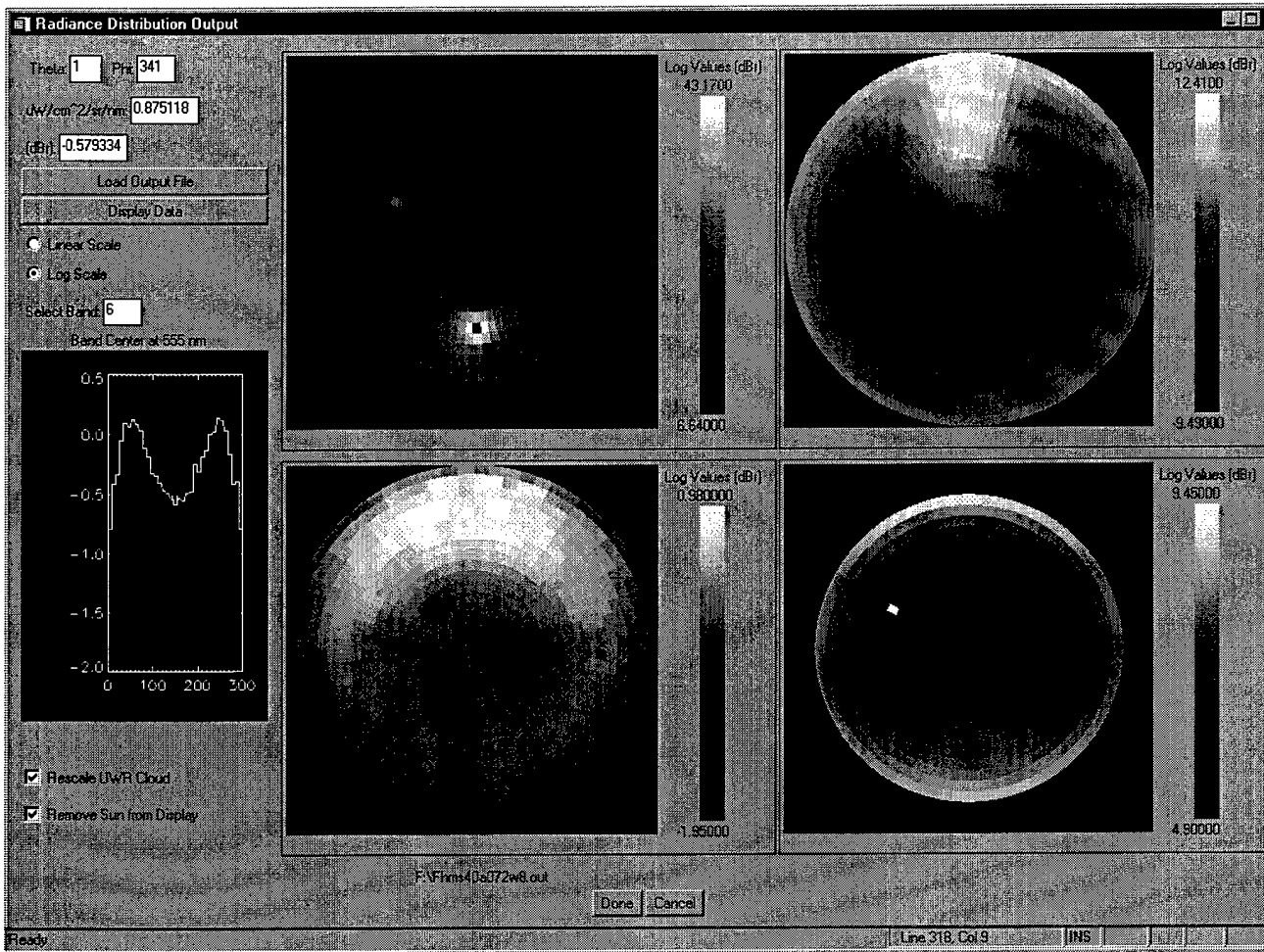
from the main HydroMod screen.

Doing so produces the one and only data analysis widget *inside of HydroMod*. Most of the other data analysis occurs outside of HydroMod by first using READHMRADFILE.PRO and then doing your own thing with the data. See the next chapter and especially page 194.

The one and only data analysis widget inside of HydroMod is meant to allow you to view the data in a quick-look type of format. You get four windows that represent, starting in the upper left and proceeding clockwise, the input sky radiance distribution, the radiance reflected off of the water surface, the radiance that exits the water body (without adding the reflected component), and the upwelling radiance. The fifth window on the widget is a horizontal slice across the radiance distribution that currently contains the mouse pointer at the position of the pointer.

The widget with data loaded and various options checked looks like this:





The data can be plotted in log format (decibels relative to one radiance unit or dBr) or in linear format ( $\mu\text{W}/\text{cm}^2 \cdot \text{sr} \cdot \text{nm}$ ) and several options are available. Here, these data are plotted in log format and the sun has been removed to allow better viewing of the input sky file. Each window has its own scale so don't be confused by the varying brightness levels.

This sky contains one single cloud in the quad centered at about  $41^\circ$  in declination by about  $60^\circ$  in azimuth. That cloud would normally swamp out the upwelled radiance distribution seen in the lower right, but the box in the lower far left that re-scales the cloud is checked. The filename of the data set these data came from is included at the bottom of the widget. In this case, it was F:\FHMS40A072W8.out. Just incase you were wondering, the wind speed was 8m/sec when the data were generated, but you can't tell that from this widget.

The mouse pointer was positioned over the water leaving radiance window near the center of that window. The horizontal slice cut in that fifth window shows the variation with declination angle (roughly, since I may not have had the pointer at the exact center of the displayed data). In fact, I had the pointer at  $\theta=1^\circ$  and  $\phi=341^\circ$  as shown in the very upper left of the widget.

Don't get too dismayed if the listed locations ( $\theta$  and  $\phi$ ) and the data do not exactly seem to correspond. The display is slightly in error by (I think)  $2.5^\circ$  in  $\phi$  (azimuth). The data as input assumes the quads are centered at  $0^\circ, 5^\circ, 10^\circ, \dots$  and these windows think that the  $5^\circ$  points are the edges of the quads. This is another area that can be modified in future versions. (If twelve people weren't already using the code as I type this users manual, I would fix the problems—maybe). In any event, this viewing widget is for quick looks anyway. You will most likely not bet the farm on this widget alone. It is highly recommended that you use the data that you've generated outside of HydroMod.

That seems like a good place to end this section and start talking about things you can (and should) do outside of HydroMod.

## Outside of HydroMod

*Chapter Synopsis: We cover four events that you may want to perform outside of HydroMod. These events are the operation of H20Code.exe, the creation and changing of default files, the creation of new look up tables for the sky radiance distributions, and the analysis of data. The data analysis section (called HydroMod Output) tells you how to read the data that you've created and gives a few examples of what to do with the data and is probably the most important section of this chapter.*

---

### CHAPTER OUTLINE

---

- ☒ Running H20Code.exe
  - ☒ Changing Defaults &  
Files
  - ☒ Generating LUT's
  - ☒ HydroMod Output
  - ☒ Conclusion
- 

**Y**ou can run virtually all aspects of HydroMod outside of HydroMod. You can generate your own sky input and upwelled radiance distributions using MODTRAN or *whatever* method you choose. The H20Code.exe is a compiled Fortran program and will certainly run in any DOS window. You can add the upwelled radiance data and the transmission data to the output files on your own using either the included "ADDUWR.PRO" or similar procedures. You can certainly do all of those things. Normally, however, we'll let HydroMod do it for us. In some cases, however, we do want and need to operate outside of HydroMod. It is for those times that this chapter was created.

### Running H20Code.exe

From time to time you may want to have several copies of H20Code.exe running simultaneously. (For instance, if you want to start several copies running and then go home for the weekend and let the computer work for you. You may also want to let the code run in a DOS window while you still have access to IDL. Also, on UNIX based computers especially, you could easily have several copies running in the background on different machines; running the IDL code in the background is not very easy.) In any event, those times exist so let's see what we need to do to make it happen.

H20Code.exe reads nine fixed files, four semi-permanent files and two other flexible files. (There is a difference between “fixed” and “semi-permanent”. The fixed files have a fixed name but ASCII content that can be easily edited offline if you want. The semi-permanent files are the quad partitioned scattering phase function files and are very difficult to change.) It provides output to two flexible files. We’ll need to take care of all nine inputs and the two outputs. (It turns out that the two output files are easy to take care of with simple name changes, but we’ll cover that in a few minutes.)

### **The Nine Fixed Input Files**

The nine fixed input files include five that tell H20Code.exe all about the radiance sources internal to the water. They are all included c:\hmdata\data\ and are called:

Biolumin.out  
Raman589.out  
ChlFluor.out  
DOMFluor.out  
Table53.out

The nice thing about these files is that all of them are used in the first few minutes of execution and never accessed again. That means that as long as H20Code.exe has finished “initializing” the first time, you can change these files and get ready for the next run.

Three of the other four fixed files tell H20Code.exe about the absorption and scattering coefficients and the variation in concentrations with depth. They are also included in c:\hmdata\data\ and are called:

absorp.out  
scatter.out and  
depth.out

These files are not as nice as the internal source files. Absorp.out and Scatter.out are read each time that the wavelength changes (i.e. for each band). That means that if you change the water parameters, you cannot have multiple copies of H20Code.exe running simultaneously on the same PC. This would be another one of those things to change in a future version.

The final fixed file is HMINDAT1.TXT. (See page 180) That file tells H2OCode.exe most of the basic information that it needs to perform its run. The information includes the filenames of the files that will contain the output data. These names would be one thing for you to change if multiple runs of H2OCode.exe were operating simultaneously.

### **The Two Flexible Input Files**

The names of the files that contain the input sky radiance distribution and the quad partitioned wind roughened sea surface are also included within HMINDAT1.TXT. When I completed several HydroMod runs for my dissertation, often the only thing that changed was the input sky radiance distribution because I was changing clouds. I ran several copies of H2OCode.exe simultaneously (and repeated the process on several machines) by changing only the input sky distribution file. Changing the name of the HMSKYDAT.RAD file in the directory that contains the sky LUTs and then putting that new name into HMINDAT1.TXT in the proper place easily does this.

The other flexible file that H2OCode.exe will read is the quad partitioned wind roughened sea surface file with a default name of SURFRTS.SDA. If you are changing wind speeds and/or resolution while running multiple copies of H2OCode.exe simultaneously, you'll need to change this file and filename.

### **The Two Flexible Output Files**

For all of these situations, you'll also need to change the name of the output files so that two copies of H2OCode.exe aren't over-writing each other. That is the aforementioned easy part about changing the two flexible output files. Inside of HMINDAT1.TXT are listed the names of the two output files: the log file "... \outputx.txt" and the data file "... \radiance.bin". Change this to whatever you want to change them to if you'll be running multiple copies simultaneously.

The final thing you'll need to do is add the upwelled radiance data and the atmospheric transmission data to the output data file (radiance.bin if you don't change the name). These two files (which HydroMod creates and puts in the same path that contains all of your LUTs for the sky) are HMSKYUWR.RAD and HMSKYDAT.TRN respectively. They are simply appended onto the output data file immediately following the last line of data. The format is important, so don't add a line of blank data or you'll mess it up.

One method is to use the included IDL routine called ADDUWR.PRO. The current version will add both the upwelled radiance distribution and the transmission data. Don't be afraid to adjust the IDL procedure to your own needs. When I did all of my data runs for my dissertation, I wrote another IDL procedure that gathered all of the filenames and called ADDUWR.PRO on its own. You may want to do the same type of thing.

### **The Four Semi-Permanent Files**

The scattering phase functions for the particles in the water and for the water itself are already quad partitioned for the three selectable resolutions and stored in C:\HMDATA\DATA\DEFAULTS\ as Phase1Water#### and Phase2Particle#### where #### represents the resolution ( $20 \times 24 = 2024$ ,  $36 \times 24 = 3624$ , and  $36 \times 72 = 3672$ ). In a nutshell, particles in the water have scattering phase functions that are similar enough to define a single scattering phase function for all particles. That is the particle phase function and it is used for chlorophyll and for suspended minerals. The particle phase function is a log different than the pure water scattering phase function. H2OCode.exe reads in a phase function for each of the four water components. (We know that DOM does not scatter, but while it is reading in the data, H2OCode.exe does not know that DOM does not scatter and it wants to have a scattering phase function for it.) HydroMod makes the four phase functions available by selecting the correct two (from Phase1Water#### and Phase2Particle####) and putting copies in the current directory. The copies are called Phase1, Phase2, Phase3, and Phase4 where Phase3 and Phase4 are both copies of Phase2.

Changing the scattering phase functions requires re-compiling the code and running with different options. If you really need to do this, contact me and I'll walk you through it.

### **Changing Defaults and Files**

Once you are proficient at using HydroMod with the current settings you will inevitably want to change some of the default cross sections or other settings. Go for it! That is one of the primary benefits of using IDL and the flexible style that I used in HydroMod. The two types of changes that you may want to make include changing the

internal default selections and changing or creating files that are eventually read into HydroMod.

Many of the defaults are selected inside of the IDL procedure PRELIMINARIES.PRO when the original code structures are created. Go ahead and modify some of those numbers if you wish to change default selections and default values.

For instance, you may find that you are always running with a bottom depth of 20.0m. Instead of opening that widget (see page 174) each time, change the value in PRELIMINARIES.PRO. (That particular one is in the "waterinfo" structure as waterinfo.bottom=10.0; you would change it in the example to waterinfo.bottom=20.0.)

I know that I am advocating multiple versions of the code with that statement, but as long as the defaults are the only thing that you consistently change, then there shouldn't be a problem. However, be very very careful if you share a PC with another HydroMod user!!

The other offline files that you might want to change or create are the absorption and scattering cross section data and files that contain sets of bandwidths over which to operate and depths for the output data. (Look up tables are covered in the next section.) The formats for those files were covered earlier (see page 171, page 177, and page 178). The default cross section files are currently located in c:\hmdata\data\defaults\ as CDOM.ABS, WATER.ABS, CHLOROPHYLL.ABS, SUSMIN.ABS, WATER.SCT, CHLOROPHYLL.SCT, and SUSMIN.SCT.

## Creating Look Up Tables Offline

You can create new sky radiance distributions via ANY method that you choose as long as the format is the same as that given in the section starting on page 162. Allow me to illustrate how extreme that can be: during the code testing phase, I used a sky with zero radiance from all directions except for three "suns" located at specific locations. For testing and understanding, you can be as flexible as you want.

I use MODTRAN and HydroMod will attempt to use MODTRAN as well. (However, I can't distribute MODTRAN and you'll need to obtain a copy of it yourself. That is, unless you are an RIT user; in your case, MODTRAN is available on several RIT computers.) The easy way

to generate a new sky file off line is to use the IDL procedure `STRUCTHMDEF.PRO` to create a "carddeck" as in

```
crdk=structhmdef()
```

The next step would be to change your carddeck parameters however you wish. (Note that as of this writing, using radiosonde data may not work well.) For instance, you might want a CO<sub>2</sub> mixing ration of 380ppmV so you would use a statement like:

```
crdk.c1a.co2mx=380.0
```

which means to change the CO2MX variable on the C1A card of the CRDK carddeck. (If you want to run these sky files offline, I'm assuming you know enough about IDL and MODTRAN to understand what these things mean. If you don't then you're probably pretty upset at me about now.)

The next step is to create the sky by calling MODTRAN 630 times for the input radiance distribution. You can do that with one statement:

```
HMSKYLUT,crdk,modpath,skypath,name,time
```

where CRDK is the carddeck, MODPATH is the path to the location of MODTRAN, SKYPATH is the location that you want to store the output sky file in, NAME is the name to give the outputfile, and TIME just lets you keep track of how long it took. To get the upwelled radiance distribution file, use

```
HMUWRLUT,crdk,modpath,skypath,name,time
```

Both of these commands will give you the transmission information. On a Pentium II 350MHz system, it will take about 14 hrs for the input sky and 11 hours for the upwelled radiance.

## HydroMod Output



**A NOTE ON UNITS**

- 
- ☒ Radiance:  
 $\mu\text{W}/\text{cm}^2 \cdot \text{sr} \cdot \text{nm}$
- 
- ☒ Wavelengths: nm
- 
- ☒ Transmission  
Coefficients: Unitless
- 

Data analysis is a personal thing. What is it that you want to do with the data? I can put it in your hands, but you'll need to use IDL (or whatever language you want) to do things with it. You can read the data outside of HydroMod using the IDL command

`READHMRADFILE, 'f:\myoutput\mydatafile.out', data`

where "f:\myoutput\mydatafile.out" is the name and location of the data file to be read and DATA will contain the data. Actually, DATA is an IDL structure with the following data<sup>4</sup>:

- ☒ Allskyin=fltarr(# of wavelength bands, 17,72) A.K.A. fltarr(#wl,17,72). These data are the sky input radiance distributions for each of the wavelength bands in the HydroMod run.
- ☒ Allecskyin=fltarr(#wl); These data are the sky input radiance from the endcap
- ☒ Allskyref=fltarr(#wl,17,72); These data are the reflected radiance distributions for each of the wavelength bands in the HydroMod run.
- ☒ Allecskyref=fltarr(#wl); These data are the reflected radiance into the endcap direction
- ☒ Allwater=fltarr(#wl,17,72); These data are the water leaving radiance less the reflected radiance distributions for each of the wavelength bands in the HydroMod run.
- ☒ allecwater=fltarr(#wl); These data are the water leaving radiance less the reflected radiance into the endcap direction
- ☒ allskyuwr=fltarr(#wl,17,72); These data are the upwelled radiance distributions for each of the wavelength bands in the HydroMod run.
- ☒ allecskyuwr=fltarr(#wl); These data are the upwelled radiance into the endcap direction for each of the wavelength bands in the HydroMod run

---

<sup>4</sup> All radiance values have units of  $\mu\text{W}/\text{cm}^2 \cdot \text{sr} \cdot \text{nm}$ ; all wavelengths are specified in nm.

- ☑ `radmz=fltarr(#wl, #theta, #phi, #depths)`; this is the upward heading radiance at each of the depths below the surface
- ☑ `radpa` =an array of zeros; forget it.
- ☑ `Radpz=fltarr(#wl, #theta, #phi, #depths)`; this is the downward heading radiance at each of the depths below the surface
- ☑ `rad0pa=fltarr(#wl, #theta, #phi)`; this is the same as `allskyin`
- ☑ `skyin=fltarr(17,72)`; the first wavelength band sky input radiance
- ☑ `skyref=fltarr(17,72)`; the first wavelength band reflected radiance
- ☑ `water=fltarr(17,72)`; the first wavelength band water leaving radiance less the reflected radiance
- ☑ `skyuwr=fltarr(17,72)`; the first wavelength band upwelled radiance
- ☑ `ecskyin`, `ecskyref`, `ecskyuwr`, and `ecwater` the end caps of the above terms
- ☑ `rad0pz=fltarr(#wl, #theta, #phi, #depths)`; this is the downward heading radiance at each of the depths below the surface caused solely by the original direct radiance distribution (no scattering within the water)
- ☑ `imisc=intarr(20)` Twenty integers used in Hydrolight/HydroMod
- ☑ `wave=fltarr(71)`; each of the wavelength band centers in the HydroMod run
- ☑ `trans=fltarr(#wl, #theta)` the transmission coefficients into each of the directions between the water and the space based sensor.

Once you've executed `READHMRADFILE` and you have the data in your hands you can do whatever you want. As I stated earlier, data analysis is very personal. I can give you a few examples of some of the

procedures that I've written for my data analysis (and I've included them and more with the code), but most of the procedures that you will use, you will probably create on your own.

### Offline Sample Data Analysis

Assume for a moment that we've executed READHMRADFILE and we have the data that we want in a structure called DATA. One common procedure that you may want to do is to view the data using HydroMod's standard polar format. This is done in two steps: (1) form the data into the polar format and (2) display the data. Please note that the polar format view is for one wavelength (or band) at a time.

To perform "Step #1: Form the data into the polar format" on, say, the 5<sup>th</sup> band of the input sky radiance, execute the following IDL procedure:

```
VIEWONERADHM,data.allskyin(5,*,*),data.alleskyin(5),newsqr=NS
```

The variable, "NS" now contains a 301x301 array of the polar view of the data in the 5<sup>th</sup> band of DATA.ALLSKYIN. The inputs to VIEWONERADHM are the data array (17x72 or 1x17x72; in this case it is 1x17x72) and the endcap value. There are many keywords that are possible and they include NEWSQR which is set to a named variable to contain the polar formatted array. A full description of VIEWONERADHM follows the full statement:

```
viewoneradhm,radfile,ec,newsqr=newsqr,log=log,uwrflag=uwrflag,w=w,phisqr=phisqr,$
edgecolor=edgecolor,zerorim=zerorim,units=units
```

RADFILE is the 17x72 (or 1x17x72) array to be polar formatted

EC is the endcap of the radfile data

NEWSQR is set to a named variable that will contain the polar formatted array

LOG is a flag that tells whether to use log values or not

UWRFLAG is a flag that signals whether the data are from an Upwelled radiance file or not. If they are indeed UWR data, then we

expect zeros in the array and VIEWONERADHM handles these differently.

W is set to a window number that you want the polar formatted array displayed into using TVPSCALE (W must be greater than 0)

PHISQR is a named variable to contain the phi values around the NEWSQR 301x301 array

EDGECOLOR is the relative color (0 to 255) to make the 301x301 array outside the circular region

ZERORIM is a flag that sets the data outside of the 74° declination quads to the minimum (positive) value inside that ring of quads.

UNITS is a pass through string variable to be used as the units in TVPSCALE if W is set to a value greater than 0

I tried to build a lot of flexibility into VIEWONERADHM. In my analysis, I often sent ratios or differences to be polar formatted as in

```
viewoneradhm, data.allskyref(7,*,*)/data.allskyref(8,*,*),
data.alleskyref(7)/data.alleskyref(8), newsqr=ratio78ref
```

or even

```
viewoneradhm, data.allskyref(7,*,*)/data.allskyref(8,*,*) -
data2.allskyref(7,*,*)/data2.allskyref(8,*,*),
data.alleskyref(7)/data.alleskyref(8) -
data2.alleskyref(7)/data2.alleskyref(8) , newsqr=difratio78ref
```

The first of these statements would polar format the ratio between bands 7 and 8 of the reflected component of the sky input radiance. The second statement would polar format the difference in that same ratio between two different data sets (DATA and DATA2).

One way to view the data you just created is to use TVSCL,NS where NS is the polar formatted data array. I created my own version of TVSCL called TVPSCALE that actually puts a scale on the display. This procedure is accessed with the following command:

```
TVPScale,image,units=units,win=win
```

IMAGE is the 301x301 data array to be displayed

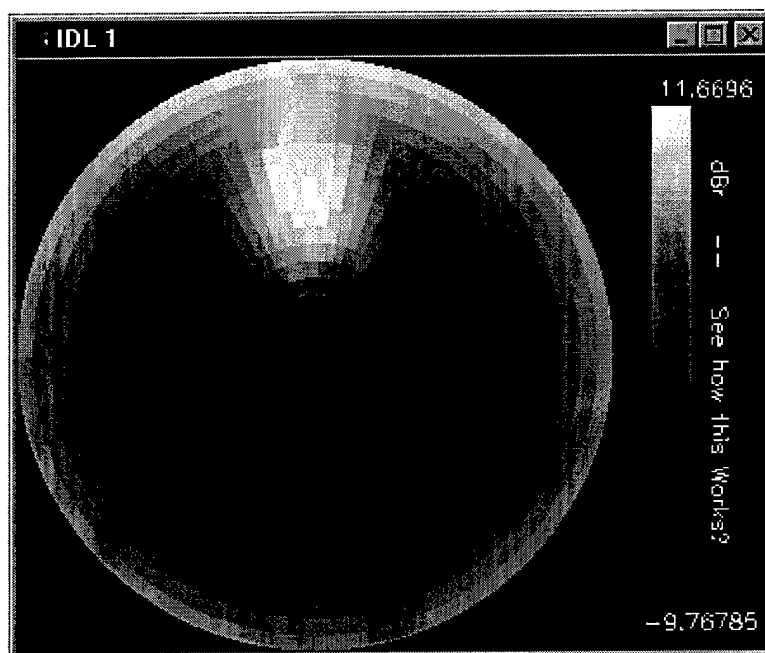
UNITS is a string variable that contains the units to display on the scale. The default is ' $\mu\text{W}/\text{cm}^2/\text{sr}/\text{nm}$ ' which IDL interprets as  $\mu\text{W}/\text{cm}^2/\text{sr}/\text{nm}$ .

WIN is the window display number and must be 1 or greater

Using these statements

```
readhmrادfile,'c:\hmdata\data\defaults\Sample1.out',sample
viewonerادhm,sample.allskyref(5,*,*),sample.alleskyref(5),newsqr=ns
tvpscale,10.*alog10(ns),units='dBr' -- See how this Works?',win=1
```

yields

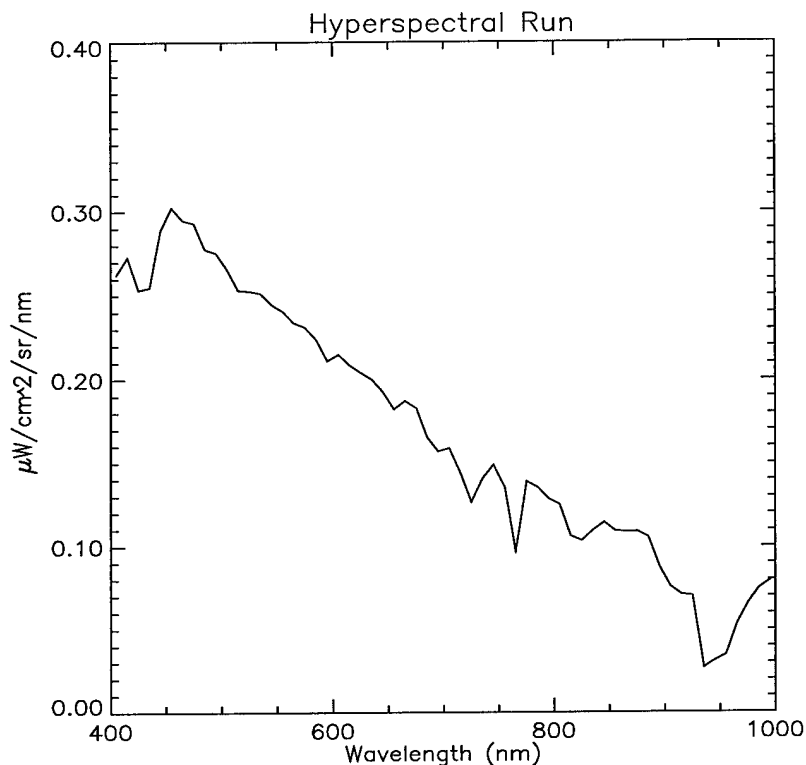


Other data analysis procedures include plotting data versus depth or wavelength. For instance, I've completed a set of hyperspectral runs for data from 400nm to 1000nm in 10nm steps. To get a plot of these data versus wavelength in the direction of the endcap (because that is the easiest) we would execute the following:

```
readhmrادfile,'c:\hmdata\data\defaults\sample2.out',hyper
wl=indgen(60)*10+405
```

```
plot, wl, hyper.alleskyref, title = 'Hyperspectral Run', xtitle='Wavelength
(nm)', ytitle='!71!3W/cm^2/sr/nm', color=0, background=255
```

would produce



Other useful procedures and functions that are included with HydroMod include:

Transmission.pro that applies the transmission coefficients to the data as in

```
result=transmission(data.allskyref+data.allwater,data.trans)
```

and TVPSCALECGM which acts much the same way as the previous TVPSCALE except that this one puts the data in CGM format to a filename that you specify.

## Conclusion

The title of this section should actually be "Beginning" because it is time for you to start using the code and exploring the possibilities. The output data arrays in particular hold a lot of information that YOU need to glean and use to YOUR purposes. I've given you the tool and hopefully a little understanding about the use of the tool, now it is up to you to dig out the information.

If I put anymore words into this conclusion, it would just be dribble so I'll stop. Good Luck!

## **APPENDIX II**

### **HydroMod Additional Information**





# HydroMod Overview

---

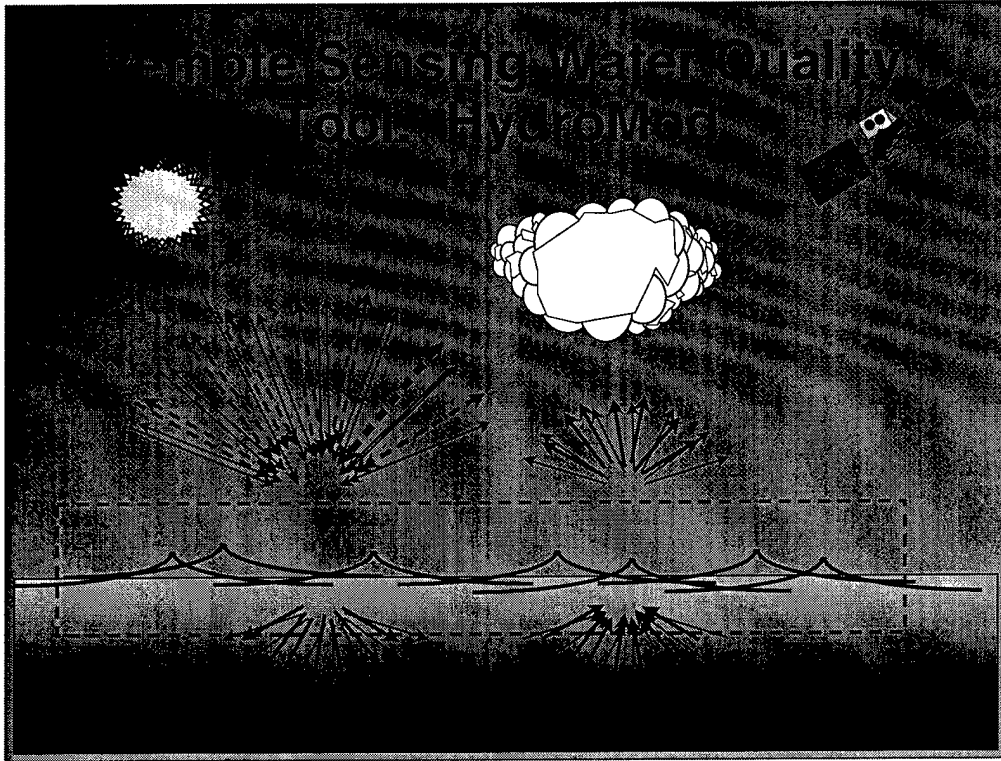
- **Basic Information**
- **Code Capabilities**
  - Confirmation of Expectations
  - Hidden Efficiency
- **Current/Projected Uses**
- **Future Disposition**
- **Summary**

---

8/24/99

Digital Imaging and Remote Sensing Laboratory  
Major Ronald R. Fairbanks, USAF

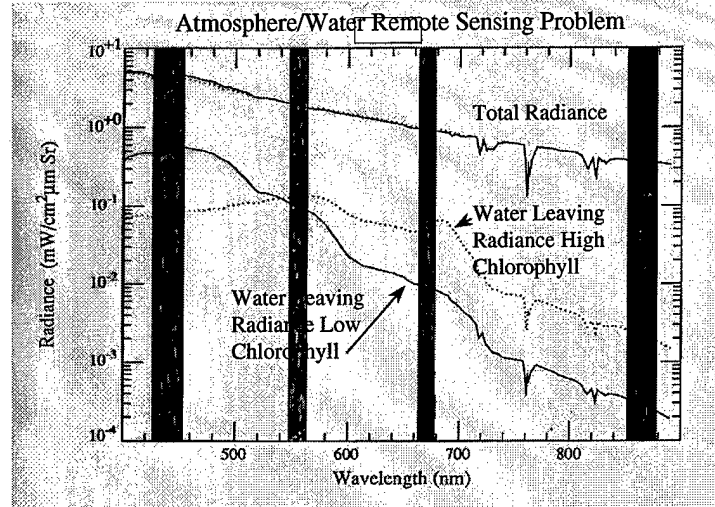
1



This is the overall HydroMod scene showing the radiative transfer areas of interest. Light from the sun interacts with the atmosphere (including clouds) creating a full sky radiance distribution. This light then enters the water through a wind roughened surface. In the water, the next major phase of radiative transfer depends on the parameters of the constituents in the water. Some light exits the water through that same wind roughened surface. Finally, the light exiting the water, combined with the light that reflects off of the water travels back through the atmosphere to the sensor along with the upwelled radiance from the sky.

# One Reason for HydroMod

- Most light at sensor comes from upwelled radiance
- Changes in water constituents yields very small changes in sensor radiance



[http://phyvax.ir.miami.edu:8001/chris/envr\\_optics.html](http://phyvax.ir.miami.edu:8001/chris/envr_optics.html)

8/24/99

Digital Imaging and Remote Sensing Laboratory

Major Ronald R. Fairbanks, USAF

3

Two cases are shown. One with a lot of chlorophyll and one with little chlorophyll. Since upwelled radiance is so high, it is hard to tell the difference at the sensor. Atmospheric subtraction is VERY important for remote sensing over water.

## **Other Reasons for HydroMod**

---

- **Ground Truth Difficult to Obtain**
- **Algorithms Fail Near Coastal Regions**
- **Great Lakes are “Interesting” Environment**
- **Specific Cloud Impact is Unknown**
- **Very Good Main Pieces Exist (Atmosphere and Water) but They are Not Integrated.**

---

8/24/99

Digital Imaging and Remote Sensing Laboratory  
Major Ronald R. Fairbanks, USAF

4

These are some of the other reasons that a good remote sensing water quality computer tool is needed.

# HydroMod Goals and Objectives

---

- **Purpose of Creation:**

- Cloud Impact Study on SeaWiFS
- Accurate Prediction of Water Leaving Radiance
- Enable Atmospheric Impact Studies
- Enable Water Contaminate Impact Studies
- Multiple Remote Sensing Water Studies
- Code is FULLY Operational and Validated for Primary Purpose

- **Future: Integrate to DIRSIG**

---

8/24/99

Major Ronald R. Fairbanks, USAF

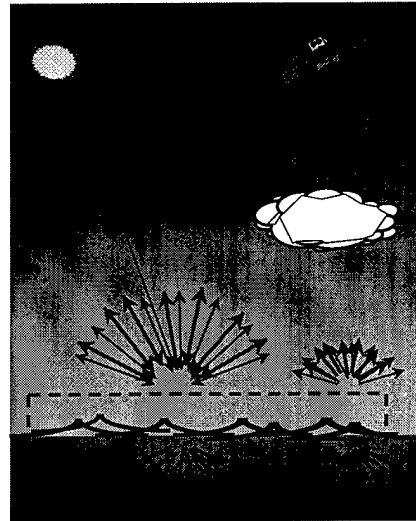
Digital Imaging and Remote Sensing Laboratory

5

These are some of the driving reasons behind my creation of HydroMod when and how I created it. They are also the reasons why RIT's Center for Imaging Science wanted something like HydroMod. Many of HydroMod's capabilities were spawned from these requirements.

# HydroMod Challenge

- **Transitions: Air (down), Clouds, Air/Water (in), Water, Water/Air (out), Air (up)** (Red = MODTRAN // Green = Hydrolight)
- **Calculate, Display, Store Radiance in Each Direction Due to Each Module**
- **Input Parameter Variability Maximized**
  - Atmosphere, Water Column, Clouds, Sensor, ... Fully Variable
  - Contains Defaults for Lake Ontario and SeaWiFS



8/24/99

Major Ronald R. Fairbanks, USAF

Digital Imaging and Remote Sensing Laboratory

6

This is what HydroMod had to do to meet the needs given previously. Two main radiative transfer codes that are nearly industry standards are MODTRAN for atmospheric propagation and radiative transfer and Hydrolight for underwater radiative transfer.

MODTRAN is the creation of the Air Force Laboratories Geophysics group at Hanscom AFB, MA. They also control the distribution of MODTRAN. I used MODTRAN for the downwelled and upwelled radiance portion of HydroMod.

Hydrolight is the creation of Dr. Curtis Mobley currently at Sequoia Scientific Corporation. Dr Mobley controls the distribution of Hydrolight. I used modified versions of Hydrolight 3.0 for the Air/Water interface and the underwater radiative transfer sections of HydroMod.

Other challenges included the requirement to display the radiance distribution caused by each component in the environment and to maintain maximum flexibility of the environmental parameters.

The cloud module is my own creation.

## HydroMod Basic Information

---

- **Mates MODTRAN to Hydrolight\***
  - IDL Widget Driven Shell
  - MODTRAN 3.7 (and 4.0) Unmodified
  - Extensive Hydrolight 3.0 Input/Output Modifications
- **+PLUS+Ability to Add Realistic Clouds to Scene**
- **Meets Calculate/Display/Manipulate Goal**
- **290 nm -1000 nm in 1nm steps**

\*Hydrolight is nearly an industry standard water radiance transfer code created and controlled by Dr. Curtis Mobley currently with Sequoia Scientific. The code employs invariant imbedding techniques to solve the radiative transfer equations. More information can be found in Dr. Mobley's book: Light and Water from Academic Press, 1994.

8/24/99

Digital Imaging and Remote Sensing Laboratory  
Major Ronald R. Fairbanks, USAF

7

From one aspect, HydroMod is just an IDL widget driven shell wrapped around two very capable codes with the ability to add realistic clouds to the scene. I made no modifications to MODTRAN; HydroMod works with either MODTRAN 3.7 or 4.0. I modified Hydrolight to read input files for several water quality parameters and changed some of the output format. Hydrolight also reads the sky radiance data created by MODTRAN via HydroMod.

The ability to add clouds will be covered later.

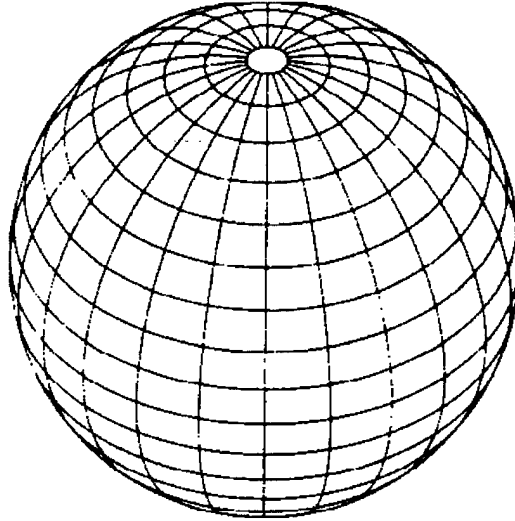
HydroMod meets all the requirements and challenges outlined previously. The wavelength coverage is limited to 290nm-1000nm.



# Quad Partitioning

---

- Pixel Centered Coordinates
- Hemisphere for Sky; Hemisphere for Water
- ~5° x 5° HydroMod Standard Grid (9° x 15° shown)
- End Cap is Special Case



---

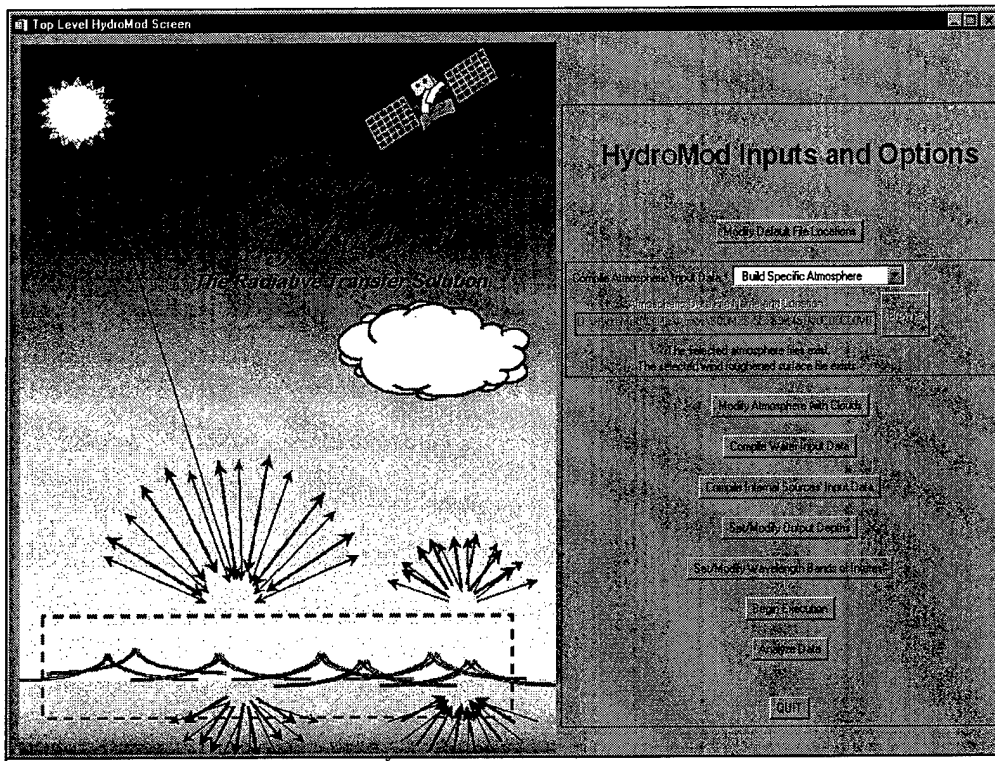
8/24/99

Digital Imaging and Remote Sensing Laboratory  
Major Ronald R. Fairbanks, USAF

8

The quad averaging used in HydroMod is roughly 5 deg x 5 deg. Keep in mind that this remote sensing program has to work with a sphere instead of the normal hemisphere.

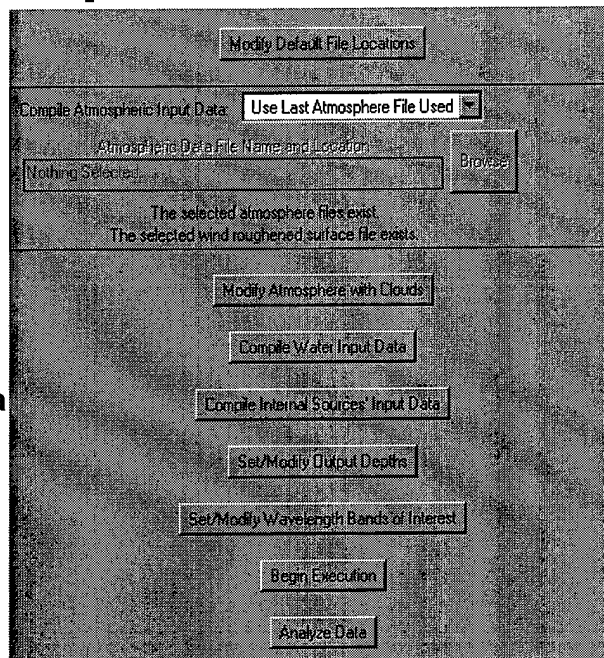
The partitioning of the sphere, other than the size of the quads, came from Dr. Mobley's work and is the same form as Hydrolight 3.0



This is the HydroMod main screen. The buttons on the right are the real meat of the screen and will be viewed enlarged next.

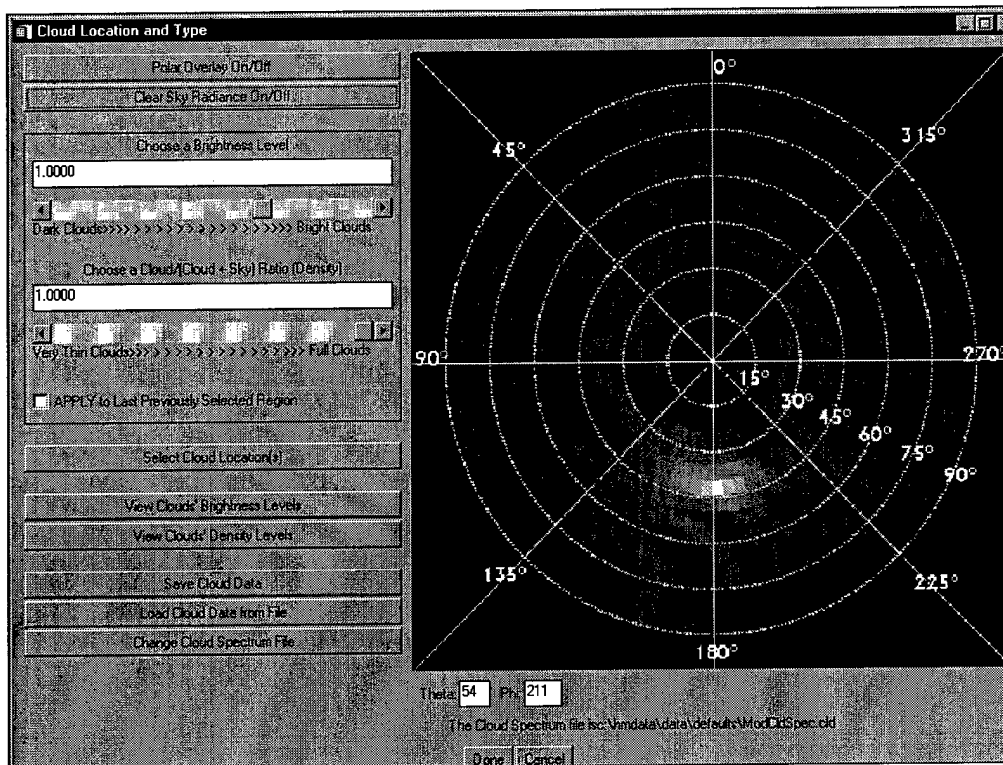
# Code Operation

- **Set Environmental Conditions**
  - IDL Widget Interface
  - Each Button Executes Own Widget
- **Uses Look Up Tables When Possible**
- **HydroMod Creates Data Files for Hydrolight to Read**



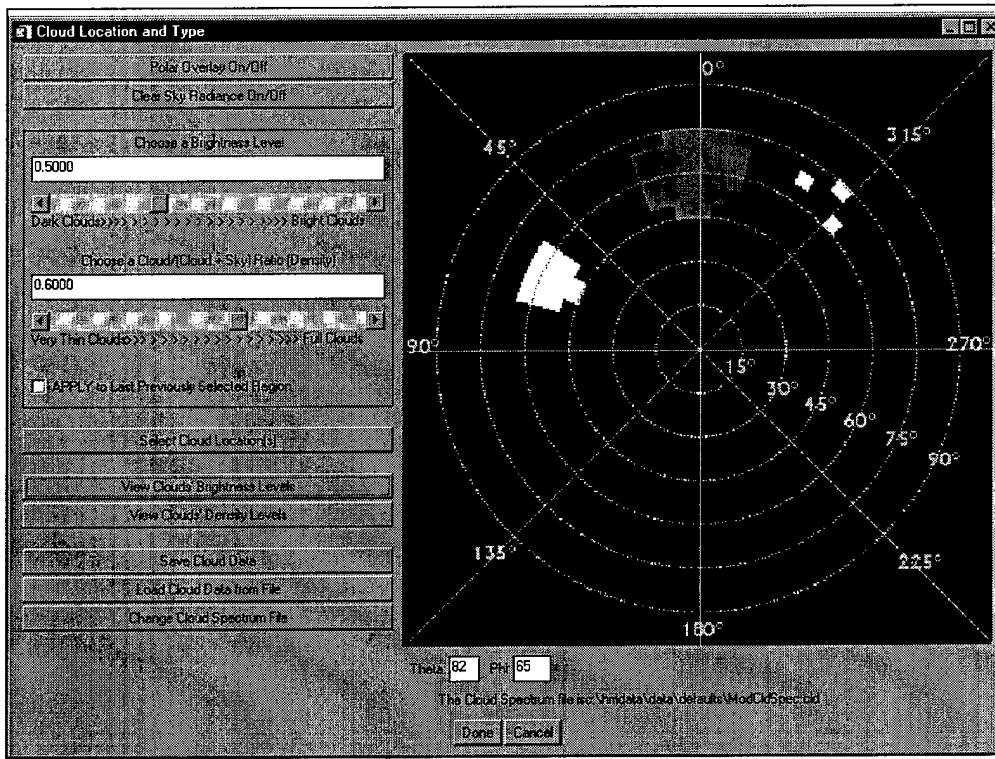
Each button generates its own widget for gleaning input and output information required to build the environment (sky, water, internal sources, clouds, sensor wavelength bands, wind speed,...). HydroMod uses this information to create the files needed by either MODTRAN or Hydrolight. Since most of the time, MODTRAN generated sky files have been generated once before, HydroMod makes extensive use of look-up tables to prevent the need for re-creating the same sky over and over.

For instance, once a sky radiance distribution is created (which takes about 24hrs on a 350MHz Pentium II PC) HydroMod ZIPs the files using PKZIP and stores them for later use. When that same set of sky parameters is chosen again, HydroMod un-ZIPs the file using PKUNZIP and extracts the data it needs. That process takes less than 24 seconds. The same applies to wind roughened sea surface files. To date, over 45 sky files and 36 wind roughened sea surface files are stored as look up tables.



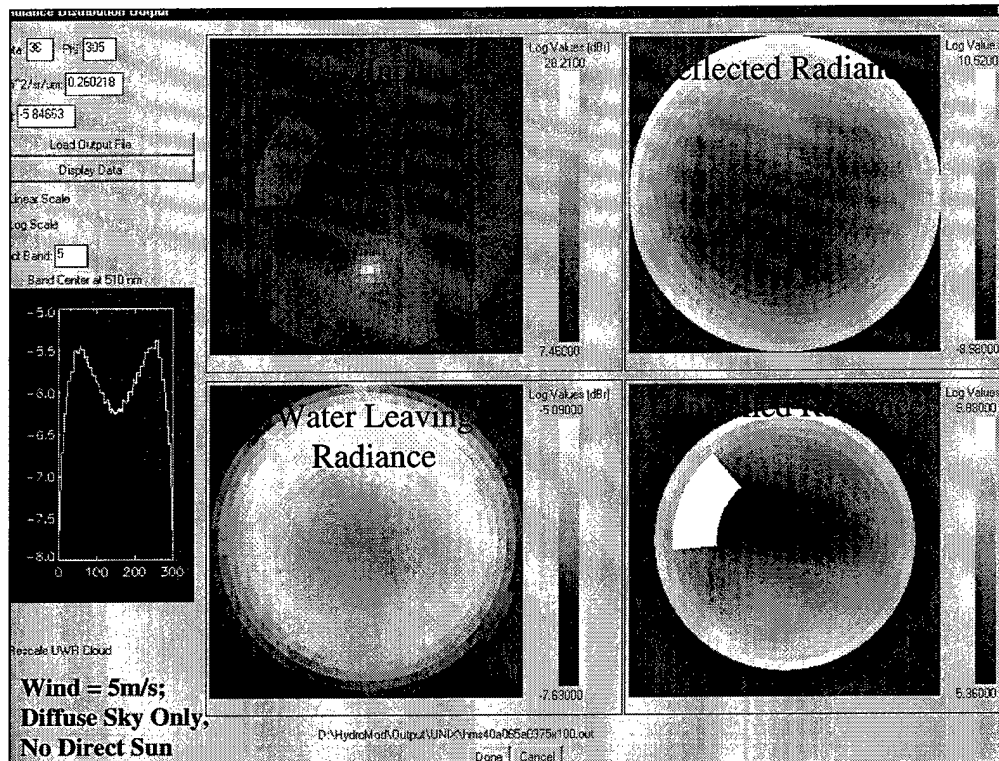
This is the cloud widget. This screen also orients some of the geometry. The center of the polar plot is nadir (or zenith if you prefer, both work) and the outer edge is the horizon. The top is due North and the bottom is South. East and West are arbitrary as long as the user keeps track and is consistent.

With this widget, users select cloud location and size and shape along with a “brightness” value and a “density” value. The brightness is a relative value used to multiply the clouds’ spectral response file by; the density is the cloud to cloud + sky ratio. All of the parameters are variable from cloud to cloud and scene to scene. Once a group of clouds are chosen and set, they can be saved for later retrieval and use on another scenario.



Here is one scene already set. Three lone fairly bright clouds are shown in the North East sky; a larger cloud in the West-North-West has the same brightness. A large cloud bank due North is slightly less bright with a very large cloud bank due East and near the horizon that is very dark

The 5 degree binning can be easily noticed in these plots.



This is one HydroMod output screen. This run was done with only a sky input file; the direct Sun term is not included so that the input sky (and included cloud) could be viewed. The individual darker titles do not appear on a 'normal' HydroMod screen.

The four circular plots are all displayed using a log scale and each have their own scale factors just to the plots' right. The plots represent: Upper left=sky input radiance from the hemisphere; Upper Right=the radiance reflected off the water surface; Lower Left=The water leaving radiance without the reflected term; and Lower Right=the Upwelled radiance. Each plot represents a hemisphere. They are all pixel centered at the point on the water surface that is the center of the remote sensing "pixel".

The plot on the very left is a cut across the Water Leaving Radiance display. During HydroMod operation, that display will change as the mouse pointer changes; it always takes a horizontal cut across the image at the location of the mouse no matter which image the mouse is located in.

Most of the rest of the briefing will be going over these four hemisphere displays to "Confirm Expected Results".

The "dBr" units are for "decibels relative to one radiance unit". The units on Radiance here are actually microWatts per square centimeter per steradian per nanometer.

## Confirmation of Expectations

- Sky 30 - 40 dB down from sun peak
- Total integrated irradiance similar to published values
- MODTRAN Works



8/24/99

Digital Imaging and Remote Sensing Laboratory  
Major Ronald R. Fairbanks, USAF

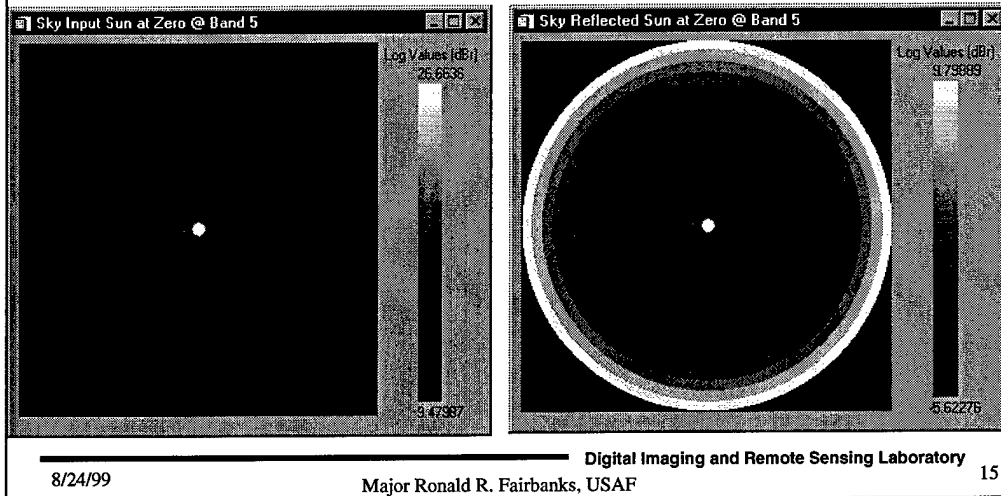
14

Expected results for the sky radiance distribution is a pattern that roughly follows that found by Moon and Spencer back in the 1940's. The less light sky radiance should be about 10-15dB down from the brightest areas of sky radiance. The direct sun term has been removed from the above data so that the display is viewable. Even with the log scale, the direct sun term would be too bright to enable viewing the rest of the sky if it were included.

The bottom line here is that MODTRAN works.

## Reflected Component Confirmation of Expectations

Use a Sun at 0° with no wind and study the reflected radiance



For the reflected component, I used a sun directly overhead and a realistic sky with no wind. I used only the sky scattering terms and the sun direct term is missing here again for viewability. The Sky input radiance distribution is shown on the left. The radiance distribution reflected off the water surface is shown on the right. If we divide the reflected radiance by the sky input radiance, we should get the coefficient of reflectance which is also given by the Fresnel reflectance formula. A line of data from the center radially outward is shown next.

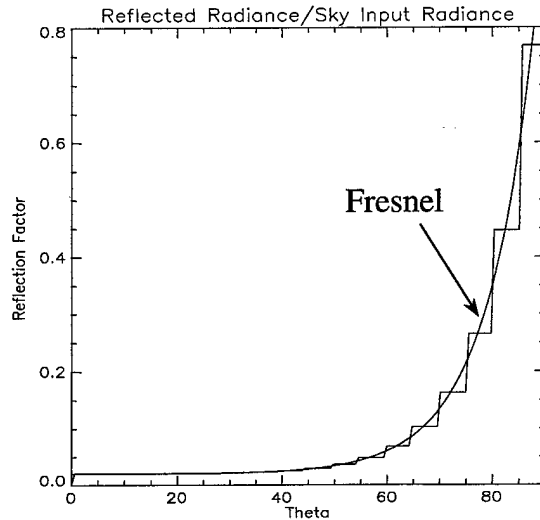


# Fresnel Reflectance Confirmed

- **Fresnel Reflectance formula overlays**

$$\rho = 0.5 \frac{\sin^2(\theta_i - \theta_r)}{\sin^2(\theta_i + \theta_r)} + 0.5 \frac{\tan^2(\theta_i - \theta_r)}{\tan^2(\theta_i + \theta_r)}$$

- **Same at All Bands**
- **Same at Any Sun Location**



8/24/99

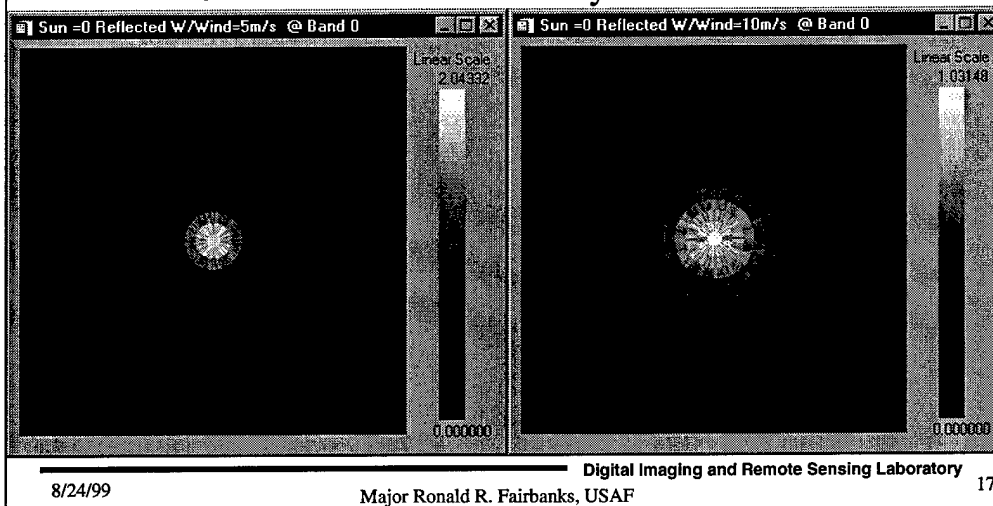
Digital Imaging and Remote Sensing Laboratory  
Major Ronald R. Fairbanks, USAF

16

We see that the reflected component divided by the input radiance component gives us the Fresnel reflectance coefficient as expected. The same is obtained at all bands and at any sun location as long as the wind is zero. As wind increases, the problem changes.

# Wind Affect on Reflected Radiance

Wind Roughened Surface Spreads Reflected Radiance IAW  
Cox and Munk Probability Distribution



These are two reflected radiance distributions from the water surface for wind speeds of 5 and 10 meters per second. In these cases I used only a single input radiance coming straight in from zenith and zero other sky components.

## **Water Leaving Radiance**

### **Confirmation of Expectations**

---

- **Fresnel: More light enters the water from vertical; more light reflects off axis**
- **Law of Refraction: Light exiting the water spreads more as theta increases (max at  $\sim 48^\circ$ )**
- **Scattering Phase Function: Most Light Forward Scatters**
- **Expect Less Light Exiting at Water Center**

---

8/24/99

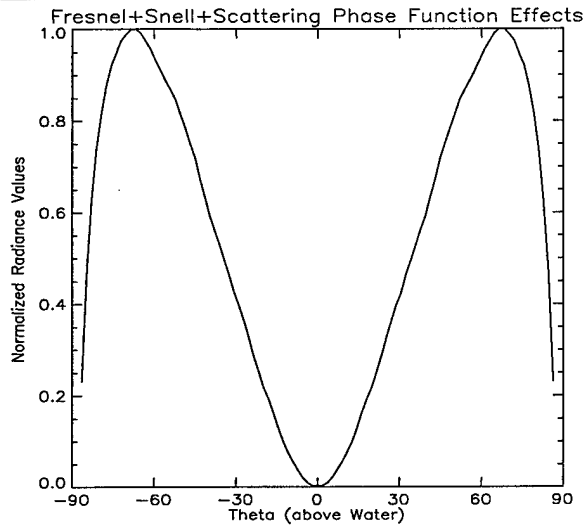
Major Ronald R. Fairbanks, USAF

Digital Imaging and Remote Sensing Laboratory

18

The water leaving component is slightly more complicated. Here we need to combine three affects: Fresnel, Snell, and the scattering phase function. For a single scattering scenario, that simulation was completed and it shows that we should expect less light exiting the water toward the zenith and more light off axis and then tapering off again as we approach the horizon.

# Single Scattering Simulation



- Fresnel + Snell + Phase Function
- Single Scattering Case Only
- Simulation not accurate within 2 degrees of  $0^\circ$  and  $90^\circ$
- All Deep (non-pure) Water Plots Confirm Expectations

8/24/99

Major Ronald R. Fairbanks, USAF

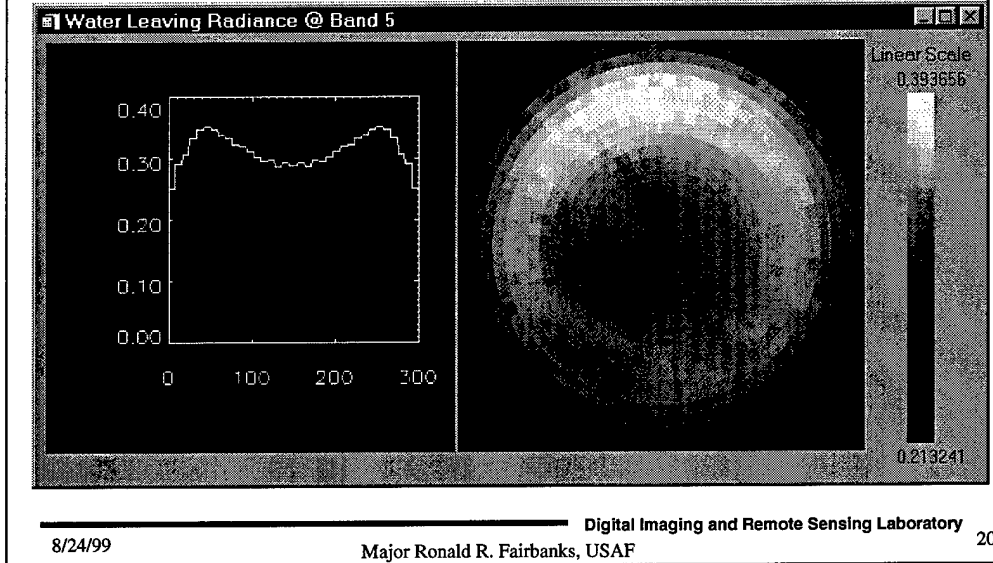
Digital Imaging and Remote Sensing Laboratory

19

This is the normalized outcome from the single scattering simulation. It corresponds to a single radial cut through the center of the water leaving radiance plot. The M shaped curve arises because the scattering phase function is highly peaked in the forward direction (less and less light scatters in scattering directions approaching the complete back-scattering case) combined with Fresnel's reflectance formula (which shows that reflection at the water/air interface increases as you move off axis) and the law of refraction that says that light exiting from off of the vertical will spread into ever increasing solid angles until it hits the maximum at around 48.6 degrees.

# Water Leaving Radiance

## Confirmation of Expectations



This is a typical water leaving radiance plot from HydroMod with a horizontal cut through the center. In this scenario, the sun was placed at 41 degrees due south. You can also notice the slightly brighter area (meaning more light exiting the water) in the Northern section due to the sun in the South and higher "forward" scattering. The curves are not exactly as simulated, but the simulation was an overly simplified case of water radiative transfer.

## Summary of Confirmations

---

- **Additional Confirmations**
  - Changing Depths
  - Changing Water Contamination Concentrations
  - Band Ratios
- **HydroMod met all expectations**

---

8/24/99

Major Ronald R. Fairbanks, USAF

Digital Imaging and Remote Sensing Laboratory

21

Other simulations were ran that helped confirm that the water code was providing correct results. Changing the depth for different bottom reflectances showed the water leaving radiance getting brighter or darker as more water was involved in the radiative transfer exactly as expected. (A very dark bottom would show that the water leaving radiance increased as the water got deeper and a bright bottom shows the water leaving radiance gets darker as the water gets deeper.)

Changing the water contamination levels also showed more or less scattering as the contaminants changed.

HydroMod met all of the expected results.

## **Current Studies**

---

- **Cloud Impact Characterization for SeaWiFS**
  - 90% Complete Data Acquisition
  - SeaWiFS Impacts: Band 7/8 Ratio, Chlorophyll Bands Individually
  - Reflected Radiance Highest Contributor to Error
  - Water Leaving Radiance Smaller Contributor
- **LANDSAT/SeaWiFS Chlorophyll Study**
- **Water Radiance Distribution**
  - Just Beginning
  - Other modules for viewing distributions

---

8/24/99

Digital Imaging and Remote Sensing Laboratory  
Major Ronald R. Fairbanks, USAF

22

These are the current uses of HydroMod. I am nearing completion of my cloud impact study for the SeaWiFS chlorophyll determination. The other studies are in the initial stages.

## **Future: 5 Step Plan to DIRSIG**

---

- **Vectorize Hydrolight Code**
  - Enables Hyperspectral Use
  - Generally Speeds Computations
- **Generate Set Hydrolight Runs for Single Input As Elevation Changes from 0° to 90°**
- **Linear Combination of scaled and rotated single inputs = ANY sky input**
- **Linearly Combine outputs similarly**
- **Mate Process to DIRSIG**

---

8/24/99

Major Ronald R. Fairbanks, USAF

Digital Imaging and Remote Sensing Laboratory

23

Here are the steps that can be taken to integrate HydroMod into DIRSIG. The steps center around using superposition to “build” any sky and then any output through similar combinations of scaled and rotated vector radiances. A big recommendation, however, is to vectorize Hydrolight prior to the DIRSIG integration. Since DIRSIG is hyperspectral by nature, using the current version of Hydrolight may slow the calculations too much.



## **HydroMod Summary**

---

- **HydroMod Fully Functional for Primary Purpose**
- **All Expected Results Confirmed**
- **Currently Used in Three Studies**
- **Flexibility of Code + Variability of Scenarios = Many Possible Studies**
- **DIRSIG Integration steps outlined**

---

8/24/99

Digital Imaging and Remote Sensing Laboratory  
Major Ronald R. Fairbanks, USAF

24

This just summarizes the briefing.

## BIBLIOGRAPHY

Barker, H. W. and J. A. Davies, "Solar radiative fluxes for stochastic, scale-invariant broken cloud fields", *Journal of the Atmospheric Sciences*, Vol. 49, pp. 1115-1126, 1992

Barker, H. W. and J. A. Davies, "Cumulus cloud radiative properties and the characteristic of satellite radiance wavenumber spectra", *Remote Sensing of the Environment*, Vol. 42, pp. 51-64, 1992

Barnes, Robert A., William L. Barnes, Wayne E. Esaias, and Charles R. McClain, "Volume 22, Prelaunch Acceptance Report for the SeaWiFS Radiometer", September 1994

Barnes, Robert A. , Alan W. Holmes, William L. Barnes, Wayne E. Esaias, Charles R. McClain, and Tomas Svitek, "Volume 23, SeaWiFS Pre-launch Radiometric Calibration and Spectral Characterization", October 1994.

Bartlett, Jasmine S., Kenneth J. Voss, Shubha Sathyendranath, and Anthony Vodacek, "Raman scattering by pure water and seawater", *Applied Optics*, Vol.37, No. 15, pp 3324-3332, 20 May 1998.

Bird, R. E., and C. Riordan, "Simple solar spectral model for direct and diffuse irradiance on horizontal and tilted planes at the earth's surface for cloudless atmospheres", *Journal of Climatology and Applied Meteorology*, Vol 25 p 87-97, January 1986.

Bukata, R. P. , J.H. Jerome, J. E. Bruton, and S. C. Jain,, "Nonzero subserface irradiance reflectance at 670nm from Lake Ontario water masses", *Applied Optics*, Vol. 19, pp. 2487-2488, 1980

Bukata, R. P. , J. E. Bruton, J.H. Jerome, S. C. Jain, and H. H. Zwick, "Optical water quality model of Lake Ontario. 1: Determination of the optical cross sections of organic and inorganic particulates in Lake Ontario", *Applied Optics*, Vol. 20, No. 9, pp. 1696-1703, 1 May 1981

Bukata, R. P. , J. E. Bruton, J.H. Jerome, S. C. Jain, and H. H. Zwick, "Optical water quality model of Lake Ontario. 2: Determination of chlorophyll-a and suspended mineral concentrations of natural waters from submersible and low altitude optical sensors", *Applied Optics*, Vol. 20, No. 9, pp. 1704-1714, 1 May 1981

Bukata, Robert P., John H. Jerome, Kirill Ya. Kondratyev, and Dimitry V. Pozdnyakov, "*Optical Properties and Remote Sensing of Inland and Coastal Waters*", New York: CRC Press, ISBN 0-8493-4754-8, 362 pages, 1995.

Bukata, Robert P; John H. Jerome, Kirill Ya Kondratyev, Dimitry V Pozdnyakov, and Alexander A. Kotykhov, "Modelling the radiometric color of inland waters: implications to a) remote sensing and b) limnological color scales", *Journal of Great Lakes research*. Volume 23, Number 3, pp. 254-269, 1997

Bukata, Robert P. and John H. Jerome, "Extracting Concentrations of Water Colorants from Remotely-Sensed Data", presentation to International Association of Great Lakes Research, McMaster University, Hamilton, ON, 19 May 1998. Contact authors at National Water Research Institute, 867 Lakeshore Road, ON L7R 4A6.

Carder, K. L., R.G. Steward, G.R. Harvey, and P.B. Ortner, "Marine humic and fulvic acids: Their effects on remote sensing of chlorophyll-a", *Limnology and Oceanography*, Volume 3, pp. 68-81, January 1989.

Cox, Charles and Walter Munk, "Measurement of the Roughness of the Sea Surface from Photographs of the Sun's Glitter", *Journal of the Optical Society of America*, Vol. 44, No. 11, pp. 838-850, November 1954

Cox, Charles and Walter Munk, "Some Problems in Optical Oceanography", *Journal of Marine Research*, Vol. 14, No. 1, pp. 63-78, 1955

Cox, Charles and Walter Munk, "Slopes of the Sea Surface Deduced from Photographs of Sun Glitter", *Bulletin Scripps Institute of Oceanography of the University of California*, Vol. 6, No. 6, pp. 401-488, 1956

Duntley, Seibert Q., "Measurements of the Distribution of Water Wave Slopes", *Journal of the Optical Society of America*, Vol 44(7), pp. 574-575, July, 1954.

Duntley, Seibert Q., "Light in the sea", *Journal of the Optical Society of America*, Vol 53, pp. 214-233, February, 1963

Gordon, Howard R., Otis B. Brown, and Michael M. Jacobs, "Computed relationships between the inherent and apparent optical properties of a flat homogeneous ocean", *Applied Optics* Vol. 14 No.2, pp. 417 - 427, February 1975.

Gordon, Howard R., Menghua Wang, "Retrieval of water-leaving radiance and aerosol optical thickness over the oceans with SeaWiFS: a preliminary algorithm", *Applied Optics* Vol. 33 No.3, pp. 443 - 452, January 1994.

Gordon, Howard R., "Atmospheric correction of ocean color imagery in the Earth Observing System era", *Journal of Geophysical Research*, Vol. 102, No. D14, pp. 17,081 - 17,106, July 27, 1997

Gregg, Watson W. and K. L. Carder, "A simple spectral solar irradiance model for cloudless maritime atmospheres", *Limnology and Oceanography*, Vol 35, No. 8, pp 1657-1675, December 1990.

Jerlov, N.G., "*Marine Optics, Elsevier Oceanography Series 14*", Elsevier Publishing Co., Amsterdam, 231 pp. 1976.

Jerome, J. H., R. P. Bukata, and J. E. Burton, "Utilizing the components of vector irradiance to estimate the scalar irradiance in natural waters", *Applied Optics* Vol. 27, No. 19, pp. 4012-4018, 1 October 1988

Jerome, J. H., R. P. Bukata, and J. R. Miller, "Remote sensing reflectance and its relationship to optical properties of natural waters", *International Journal of Remote Sensing* pp. 3135-3155, Taylor and Francis Ltd., November 1996.

Kattawar, George W. and Charles N. Adams, "Errors induced when polarization is neglected in radiance calculations for an atmosphere-ocean system", *SPIE Vol. 1749 "Optics of the Air-Sea Interface"*, 1992

Khristoforov, G. N., A. S. Zapevalov, and M.V. Babi, "Statistical Characteristics of Sea Surface Slopes at Different Wind Speeds", *Oceanology*, Vol. 32, No. 3, pp. 300-304, 1992

Kirk, John T.O. "Dependence of relationship between inherent and apparent optical properties of water on solar altitude", *Limnology and Oceanography* Vol. 29 (2), pp. 350-356, 1991

Kirk, John T.O. "Volume scattering function, average cosines and the underwater light field", *Limnology and Oceanography* Vol. 36 (3), pp. 455-467, 1991

Kneizys, F. X., E.P. Shettle, W. O. Gallery, J.H. Chetwynd, Jr., L.W. Abreu, J.E.A. Selby, R.W. Fenn, and R.A. McClatchey, "Atmospheric Transmittance/Radiance: Computer Code LOWTRAN 5", AFGL-TR-80-0067, Air Force Geophysics Laboratory, Hanscom AFB, MA, Optical Physics Division Project 7670, 21 February 1980.

Leckner, B. "The spectral distribution of solar radiation at the earth's surface—elements of a model", *Solar Energy*, Vol 20, pages 143-150, January 1978

Maffione, R.A. 1997. "Theoretical developments on the optical properties of highly turbid waters", to be published in *Limnology and Oceanography*.

Maffione, R.A., and D.R. Dana 1997. "Instruments and methods for measuring the backward-scattering coefficient of ocean waters", to be published in *Applied Optics*

McClain, Charles R., Kevin Arrigo, Wayne E. Esaias, Michael Darzi, Frederick S. Patt, Robert H. Evans, James W. Brown, Christopher W. Brown, Robert A. Barnes, and Lakshmi Kumar, "Volume 28, SeaWiFS Algorithms, Part 1", SeaWiFS Technical Report Series edited by Stanford B. Hooker, Elaine R. Firestone, and James G. Acker. NASA Technical Memorandum 104566, Vol 28, 38 pages plus color plates, June 1995.

Maul, G. A., "Introduction to Satellite Oceanography", Martinus Nijhoff Publishers, Dordrecht, The Netherlands, ISBN 90-247-3096-1, 606 pages, 1985

Mobley, Curtis D. "Light and Water: Radiative Transfer in Natural Waters", Boston, Academic Press, ISBN 0-12-502750-8, 592 pages, 1994

Mobley, Curtis D. "Hydrolight 3.0 User's Guide", SRI International, SRI Project Number 5632 Final Report, Office of Naval Research Contract number N00014-94-C-0062, Menlo Park, CA, 65 pages, March 1995

Mobley, Curtis D., HYDROLIGHT Fortran Computer Code, Version 3.1, March 1995.

Mobley, Curtis D. "Hydrolight 3.1 User's Guide", SRI International, SRI Project Number 6583 Final Report, Office of Naval Research Contract number N00014-95-C-0238, Menlo Park, CA, 65 pages, April 1996

Morel, Andre and Bernard Gentili, "Diffuse reflectance of oceanic waters. II. Bidirectional Aspects", *Applied Optics*, Vol. 32, No. 33, pp. 6864-6879, 20 November 1993

Moon, Parry and Domina Spencer, "Illumination from a Non-Uniform Sky", *Illuminating Engineering*, Vol 37, pp 707-726, December 1942

Pegau, W.S., J.S. Cleveland, W. Doss, C.D. Kennedy, R.A. Maffione, J.L. Mueller, R. Stone, C.C. Trees, A.D. Weidemann, W.H. Wells, and J.R.V. Zaneveld, 1995. "A comparison of methods for the measurement of the absorption coefficient in natural waters", *Journal of Geophysics Research*, Vol 100, pp. 13,201-13,220,.

Plass, Gilbert N. and George Kattawar, "Monte Carlo Calculations of Light Scattering from Clouds", *Applied Optics*, Vol. 7, No. 3, pp. 415-419, March 1968

Plass, Gilbert N. and George Kattawar, "Radiative Transfer in an Atmosphere-Ocean System", *Applied Optics*, Vol. 8, No. 2, pp. 455-466, February 1969

Preisendorfer, R. W. "Hydrologic Optics" in six volumes: *Volume 1: Introduction*, 218 pages, (NTIS PB-259 793/8ST); *Volume 2: Foundations*, 400 pages, (NTIS PB-259 794/6ST); *Volume 3: Solutions*, 246 pages, (NTIS PB-259 795/3ST); *Volume 4: Imbeddings*, 207 pages, (NTIS PB-259 796/1ST); *Volume 5: Properties*, 296 pages, (NTIS PB-259 797/9ST); *Volume 6: Surfaces*, 390 pages, (NTIS PB-268 704/4ST); Pacific Marine Environmental Laboratory/NOAA, Seattle, WA, via National Technical Information Services, 1976.

Preisendorfer, R. W. and C. D. Mobley, "Direct and inverse irradiance models in hydrologic optics", *Limnology and Oceanography*, Vol 29(5), pp 903-929, September, 1984.

Preisendorfer, R. W. and C. D. Mobley, "Albedos and glitter patterns of a wind roughened sea surface", *Journal of Physical Oceanography*, Vol 16(7), pp 1293-1316, July, 1986.

Quan, Xiaohong and Edward S. Fry, "Empirical equation for the index of refraction of seawater", *Applied Optics*, Vol 34, No. 18, pp 3477-3480, 20 June 1995.

Schott, John R., "Remote Sensing The Image Chain Approach", New York: Oxford University Press, ISBN 0-19-508726-7, 394 pages, 1997.

Schott, John R., Anthony Vodacek, Harvey Rhody, and John Waud, Verbal direction from the Dissertation Research Committee at the Proposal Presentation, Rochester Institute of Technology, Rochester, New York, October, 1998.

Selby, J.E.A. and R.A. McClatchey, "Atmospheric Transmittance from 0.25 to 28.5  $\mu\text{m}$ : Computer Code LOWTRAN 2", AFCRL-TR-72-0745, AD 763 721, Air Force Geophysics Laboratory, Hanscom AFB, MA, 1972.

Várnai, Tamás, and Roger Davies, "A Monte Carlo Model To Calculate Shortwave Radiative Transfer in Inhomogeneous Atmospheres Version 1.0", Institute of Atmospheric Physics, University of Arizona, Internal Document (*To be published*), 28 pages, January 1998

Várnai, Tamás, and Roger Davies, "Effects of cloud heterogeneities on shortwave radiation. Part II: Comparison of cloud top variability and internal heterogeneity", Institute of Atmospheric Physics, University of Arizona, Internal Document (*Submitted to the Journal of the Atmospheric Sciences*), 35 pages, March 1998

Wolfe, W. L., "Properties of optical materials", Chapter 7 in *Handbook of Optics*, W.G. Driscoll and W. Vaughan, Editors, McGraw-Hill, New York, 1978.

Wyatt, C. L. "Radiometric Calibration: Theory and Methods", Boston, Academic Press, 200 pages, 1978.

